JAERI-M
84-223

CHARACTERISTICS OF LOWER PLENUM INJECTION REFLOOD TESTS IN SCTF CORE-I

December 1984

Makoto SOBAJIMA, Takamichi IWAMURA, Akira OHNUKI, Yutaka ABE,
Yukio SUDO, Masahiro OSAKABE, Hiromichi ADACHI

日本原子力研究所
Japan Atomic Energy Research Institute

JAERI-Mレポートは，日本原子力研究所が不定期に公刊している研究報告書です。
入手の問合わせは，日本原子力研究所技術情報部情報資料課（〒319-11茨城県那珂郡東海村）あて，お申しこしください。なお，このほかに財団法人原子力弘済会資料センター（〒319-11茨城県那珂郡東海村日本原子力研究所内）で複写による実費頒布をおこなっております。

JAERI-M reports are issued irregularly.
Inquiries about availability of the reports should be addressed to Information Division Department of Technical Information, Japan Atomic Energy Research Institute, Tokai-mura, Naka-gun, Ibaraki-ken 319-11, Japan.

編集兼発行　日本原子力研究所
印　　刷　㈱高野高速印刷

JAERI－M 84－223

Characteristics of Lower Plenum Injection Reflood Tests in SCTF Core-I

Makoto SOBAJIMA, Takamichi IWAMURA, Yutaka ABE, Akira OHNUKI
Yukio SUDO, Masahiro OSAKABE, and Hiromichi ADACHI

Department of Nuclear Safety Research
Tokai Research Establishment, JAERI

(Received November 7, 1984)

Large Scale Reflood Test Program is being performed to study on the end of blowdown, refill and reflood process in loss-of-coolant accident of a PWR in cooperation among Japan, USA and FRG since 1976. The Slab Core Test Program is a part of the Large Scale Reflood Test Program together with the Cylindrical Core Test Program and the major purpose is to investigate the two dimensional thermo-hydrodynamic behavior in the core and the effect of fluid communication between the core and the upper plenum on the reflood phenomena.

In the first lower plenum injection gravity reflood test, the effect of downcomer which was excluded from the forced feed reflood test was investigated. As the water accumulation in the downcomer exceeds that in the core, the core inlet flow rate increased and slightly better core cooling than the forced feed reflood case was observed at the lower core; however overall cooling behavior was similar. In the test for studying the characteristies of low injection rate and its effect on the cooling of the blockage part, poor cooling of the core and a quench delay above the blockage was observed. As for the comparison of system characteristies with FCECHT-SEASET, though overall similarity was obtained, some two dimensionality dominated in SCTF test and a difference in quench characteristics from that in total blockage case was exhibited.

Keywords : Reactor Safety, Reflooding, Core Cooling, LOCA, ECCS, Blockage, Lower Plenum Injection, Gravity Feed, Quench, Refill, PWR

The work was performed under contract with the Atomic Energy Bureau of Science and Technology Agency of Japan.

JAERI－M 84－223

平板炉心試験装置第一次炉心における下部プレナム注入冠水試験の特性

日本原子力研究所東海研究所安全工学部
傍島　眞・岩村公道・阿部　豊・大貫　晃
数土幸夫・刑部真弘・安達公道

（１９８４年１１月７日受理）

加圧水型炉における冷却材喪失事故のブローダウン終期からリフィル，再冠水過程について調べる目的で大型再冠水試験計画が，日・米・西独の協力のもとに実施されている。

平板炉心試験は円筒炉心試験と共に大型再冠水試験計画の一翼をなし，炉心の２次元熱流体挙動と再冠水現象における炉心と上部プレナムとの流体の相互作用を研究の主目的としている。

下部プレナム注入の重力冠水試験では，まず強制冠水試験には含まれていないダウンカマの影響を調べた。ダウンカマへの蓄水が炉心部の蓄水を上回るにつれ炉心入口流量が増え，強制冠水より炉心下部の冷却がやや良くなるというわずかな相違はあったが，全体的な冷却挙動は類似していた。次に低速冠水の特性とブロッケージ部の冷却への影響を調べた試験では，通常冠水速度の試験より全体的に冷却が悪く，ブロッケージ上部のクエンチ遅れが観測された。ＦＬＥＣＨＴ－ＳＥＡＳＥＴ試験との特性比較の試験では，総観的に類似性が見られたものの，平板炉心の温度分布等には２次元性が存在し，また全面ブロッケージのクエンチ特性とは異る特性を示した。

本報告書は電源開発促進対策特別会計法に基づき，科学技術庁からの受託によって行った研究の成果である。

Contents

目　　次

1. Introduction

Large Scale Reflood Test Program is being performed to experimentally study the thermo-hydraulic phenomena during the end of blowdown, refill and reflood procers in loss-of-coolant accidents of a PWR. The slab core test facility (SCTF) is one of the facility in the program for investigating two dimensional thermo-hydraulic behavior. Many test run have been performed so far. The present report describes evaluated results of three lower plenum injection tests performed with SCTF. The three lower plenum injection gravity feed reflood tests were conducted to clarify the downcomer effect and other parameter effects after a series of forced feed reflood tests with blocked downcomer condition. They are classified as transition from forced feed separate effects tests to cold leg injection loop effect tests.

One of the three tests, Test S1-12 (Run 518) is compared with Test S1-01 (Run 507), the base case of the forced feed tests having similar test conditions. The difference is additional ECC injection rate for Test S1-12 to fill also the downcomer space at the equivalent velocity to the liquid level velocity in the core and baffle space.

Another Test S1-22 (Run 532), is to examine coolability of blockage section mainly for relatively low and constant reflood velocity. Other thermo-hydraulic effects of low reflood velocity on rod temperature, quench velocity and water accumulation in the core, the upper plenum and the hot leg are also evaluated.

One more lower plenum injection test, Test S1-13 (Run 519) is compared with a FLECHT-SEASET test[7] having similar boundary conditions in order to examine typicality of the facilities and thermo-hydraulic phenomena including channel blockage effect for relatively high reflood velocity.

Brief description of the facility and instruments is given in Appendix. More detailed information of them is available in the references. Some selected data of the present three tests are attached in the Appendix.

2. Test Sequence and Test Conditions

2.1 Test Sequence

Three tests, Test S1-12, S1-13 and S1-22 were performed with the lower plenum injection and connected downcomer conditions so as to add downcomer effect to the previous series of forced feed reflood tests in which the downcomer was blocked at the bottom with an isolation plate. The vent line connecting the upper plenum with the downcomer was fully open for Test S1-12 and S1-13 and closed for Test S1-22.

For starting the tests, the pressure vessel and loop components including containment tanks-I and II were heated up by steam injection and pressurized up to the specified system pressure of the test run. In the next step, small power was provided to the core so as to adjust the initial maximum rod surface temperature to 523 K (250°C).

Cold water initially existing in the accumulator (Acc) injection piping was purged out through the lower plenum drain of the pressure vessel by Acc water of the specified temperature. Then, saturated water for the system pressure which was made up in the saturated water tank was supplied in the lower plenum up to 1.37 m (for Test S1-12) or 1.67 m (for Test S1-13 and S1-22) from the bottom of the vessel.

Core heating was then initiated with the specified power after the small ramp time of about 6 seconds. When four rod surface temperature exceeded a preset value, a signal for power trip and injection start was generated. After holding constant for 5 seconds, the power moved to decay heat simulation for the decay power after BOCREC (bottom-of-core recovery) time which is supposed in the tests to be 30 seconds of reactor LOCA transient. The decay curve is based on "ANS standard + Actinides + Delayed neutron effect for voided core".

By this time, Acc flow rate (except in Test S1-22) was fully developed to the pre-adjusted value and rod surface temperatures are estimated to be 973 K (700°C) for Test S1-12 and S1-22 and 1087 K (814°C) for Test S1-13 which temperature was equivalent to the FLECHT-SEASET test in stored heat in a rod.

At 20 seconds after the initiation of the Acc injection, the injection rate was reduced to that for LPCI system by switching to a pump injection for Test S1-12 and S1-13. For Test S1-22, however, the injection rate was only of LPCI from the beginning and constant to the end.

Pressure in the containment tank-II was controlled during the tests with a blow-off valve as constant as possible.

2.2 Test Conditions

Table 2-1 through 2-3 give major test conditions of each gravity feed lower plenum injection test and a comparable test such as forced feed test or a counterpart FLECHT-SEASET gravity feed test. For the FLECHT-SEASET test, the comparison of design conditions is also given in the table.

The electric power given to each bundle for the Test S1-12 and S1-22 (and Test S1-13) is

887 (1316) kW/bundle for Bundle 1 and 2

944 (1400) kW/bundle for Bundle 3 and 4

900 (1200) kW/bundle for Bundle 5 and 6

815 (1200) kW/bundle for Bundle 7 and 8

This radial bundle power distribution simulates one in a typical PWR. The power for Bundle 5 and 6 in Test S1-13, however, is exceptionally too small because of limitation in the power source. Required power for the simulation was 1335 kW instead of 1200 kW.

The core inlet subcooling in Test S1-12 and S1-22 was unavoidable in the adopted test procedure mentioned in the previous section because of natural heat loss from the ECC water delivery pipe. Besides that, increase of saturation temperature due to increase of system pressure is taken into account for the subcooling estimation. The maximum core inlet subcooling time also can vary for these reasons.

3. Test Results Comparison

3.1 Gravity and Forced Feed Tests

Characteristics of a lower plenum injection gravity feed test with a connected downcomer condition was examined by comparison with data of a forced feed test with isolated downcomer condition.

3.1.1 Fluid flow behavior

Since the additional injection rate in Test S1-12 to the rate in S1-01 was simply scaled on the base of flow area ratio for the added downcomer, the actual core and baffle inlet flow rate became a little different from that in S1-01 as shown in Fig. 3.1. The dotted line in the figure was obtained by subtracting the water accumulation rate in the downcomer from the lower plenum injection rate. For S1-01, the lower plenum injection rate is equal to the core and baffle flow rate. As the core has flow-in resistance and causes evapolation, the inflow in S1-12 tend to become small for the period of large accumulator injection rate. In the later period, however, the water loss in the core due to evaporation and carryover is compensated by the water fed from the downcomer. Thus, the inflow rate becomes larger than the area scaled rate which corresponds to the flow rate in S1-01.

The core inlet subcooling in Test S1-12 and S1-22 was unavoidable in the adopted test procedure mentioned in the previous section because of natural heat loss from the ECC water delivery pipe. Besides that, increase of saturation temperature due to increase of system pressure is taken into account for the subcooling estimation. The maximum core inlet subcooling time also can vary for these reasons.

3. Test Results Comparison

3.1 Gravity and Forced Feed Tests

Characteristics of a lower plenum injection gravity feed test with a connected downcomer condition was examined by comparison with data of a forced feed test with isolated downcomer condition.

3.1.1 Fluid flow behavior

Since the additional injection rate in Test S1-12 to the rate in S1-01 was simply scaled on the base of flow area ratio for the added downcomer, the actual core and baffle inlet flow rate became a little different from that in S1-01 as shown in Fig. 3.1. The dotted line in the figure was obtained by subtracting the water accumulation rate in the downcomer from the lower plenum injection rate. For S1-01, the lower plenum injection rate is equal to the core and baffle flow rate. As the core has flow-in resistance and causes evapolation, the inflow in S1-12 tend to become small for the period of large accumulator injection rate. In the later period, however, the water loss in the core due to evaporation and carryover is compensated by the water fed from the downcomer. Thus, the inflow rate becomes larger than the area scaled rate which corresponds to the flow rate in S1-01.

The downcomer liquid level is compared with core water head in Fig. 3.2. The core water head is measured from 1.58 m height in the vessel whereas the downcomer liquid level is from 0 m height and the increase rate in the downcomer is recognized to be larger than in the core. The difference of core water head between Test S1-12 and Test S1-01, however, is quite small in spite of the downcomer volume effect. Remarkable point is that the core inflow was not prevented much by the evaporation pressurization effect during the whole Acc injection period of the gravity feed test. The reason of similar water heads is regarded that excess flow into the core tends to be carried over and not to stay in the core. When the downcomer liquid level became full and started to overflow after 300 seconds, oscillation is seen both in the downcomer and in the core. This period is enlarged in Fig. 3.3. It is clear from the figure that there is a phase shift of approximately 90 degrees in which the downcomer has the delay. The mechanism of this level oscillation is not yet certain: however, the small intact loop flow due to open vent line seems to be related as shown in later figures.

The carryover water out of the core partly accumulate in the upper plenum as shown in Fig. 3.4. As can be compared, the gravity feed test, S1-12 has higher accumulation rate in the upper plenum despite of the similarity in the core water accumulation. This is regarded because the inflow rate and resultant carryover rate are higher in Test S1-12 as discussed before. The saturation of the liquid level after 300 s should indicate overflow to the hot leg of which bottom elevation is 1.05 m above the upper core support plate. Therefore, the average void fractions for the collapsed level of 0.75 m and 0.60 m are calculated as 0.29 and 0.43, respectively.

The difference in carryover rates also appeared in the hot leg liquid level as in Fig. 3.5. The onset of liquid accumulation in the hot leg inlet section is much earlier and the liquid level is higher than the forced feed test, S1-01.

The differential pressure across vent valve line was very small in Test S1-12 as compared in Fig. 3.6, because the gate valve attached on the line in place of actual vent valve was not closed before the test.

This influenced the flow rate in the intact loop and thus, pressure loss across it was as small as shown in Fig. 3.7. The rest of the steam should have passed the vent line from the upper head to the downcomer. However, the merged flow at the broken cold leg of vessel side seems to be similar as seen in Fig. 3.8 of differential pressure. The differential pressure at the broken cold leg separator side is also given in Fig. 3.9.

3.1.2 Core thermal behavior

As discussed in the previous section, the fluid behavior on the whole is quite similar between the two tests except the small difference in the core inflow and outflow rates. The consequent core thermal behavior was also compared with each other.

Horizontal cross flow in the core appears in differential pressure measurement across bundles at some elevations. The behavior of them is also quite similar between the two tests as is compared in Figs. 3.10 and 3.11.

Figure 3.12 and 3.13 are typical rod temperatures in which slight difference of turnaround temperatures is observed, while the quench temperatures and times are the same. These characteristics were

statisticaly examined as shown in Figs. 3.14 through 3.16. A general trend in the turnaround temperature is that Test S1-12 showed a little lower one at low elevation points but a little higher one at high elevation points than Test S1-01. On the other hand, quench temperatures and times are quite equal just as repeatability tests.[5]

3.1.3 Summary

(1) The lower plenum injection gravity feed test showed a little larger core inflow and outflow than the corresponding forced feed test. This excess outflow resulted in larger water accumulation in the upper plenum and the hot leg.

(2) Opening of vent line in the gravity feed test led to small differential pressure between upper head and downcomer and small intact loop flow.

(3) Core thermal behavior was slightly different in turnaround temperatures from that of the forced feed test but not different in quench temperatures and quench times.

3.2 Low Constant Gravity Feed Rate Test

Since ECC injection rate is normally changed from Acc rate to LPCI rate at about 15 s after the initiation of reflood, Test S1-22 performed with a constant injection rate of only LPCI will clarify the effect of lacking Acc by comparison with a forced feed test with switching from Acc to LPCI. Test S1-05 was chosen for this comparison. Test S1-12 with Acc injection and larger LPCI injection rate and open vent line condition in the previous section can also be referred to.

3.2.1 Fluid flow behavior

The comparison between injection rate into the lower plenum and flow rate into the core and the baffle region is given in Fig. 3.17 together with the reference test, S1-05. The core and baffle inflow rate is smaller for initial 170 s in S1-22 than in S1-05 due to steam binding effect. However, it gets larger after that time as the downcomer water head developes.

Downcomer liquid level in Test S1-22, shown in Fig. 3.18 rizes much slower than in Test S1-12, and never reaches the overflow level owing to lack of initial Acc injection inspite of the closed vent line condition. Consequently, the core water head also increases slowly and is always lower than Test S1-05 as well as S1-12.

System pressure response is also slow as shown in Fig. 3.19, since the initial steam generation in the core is small because of short reflood length. The peak of the pressure comes in the latter half of the quenching process.

Water accumulation in the upper plenum is extremely small for all bundle regions as is shown in Fig. 3.20. If this figure is compared with Fig. 3.4 for the tests with higher LPCI rate, it is clear that the accumulation rate in the upper plenum is proportional to LPCI rate both in forced feed tests and gravity feed tests. The accumulation rate seems also to be dominated by the core steam generation rate, as the liquid level rizes more rapidly after the core is fully quenched.

The steam flow in the cold legs are compared with those in Test S1-05 in Fig. 3.21. The behavior of peaking is just as of pressure and the peak values at different times are quite equal to each other. On the other hand, the differential pressure in the intact cold leg is higher in S1-22 than in S1-5 as shown in Fig. 3.22 because the

pressure is also higher at the peak time of the steam flow.

3.2.2 Core thermal behavior

Figure 3.23 is an example of rod temperature comparison. The turnaround temperatures became much higher than in Test S1-05 because of the smaller core water accumulation rate and the quench times resultantly became much later. These characteristics statistically examined are shown in Fig. 3.24 through 3.27. The turnaround temperatures are generally much higher except for the lowest elevation points. And the higher the elevation, the larger the temprature difference between S1-22 and S1-05 except for the highest elevation points. The quench time has similar tendency. The scattering of data for elevations 9 and 10, however, is very wide and random due to irregular fall back cooling.

3.2.3 Blockage effect on cooling

The effect of low reflooding velocity on cooling of channel flow blockage region is one of great interests in Test S1-22. Since Bundles 3 and 4 have coplaner blockage sleeves of 60% blockage fraction at the middle height of all heated rods, this region usually has peculiar cooling and quenching behavior. It is already known that quenching is expedited in the region above the blockage, when reflood velocity is relatively high.

The reflood velocity of the present Test S1-22 varies between 1.0 $\sim$ 1.8 cm/s depending on the time, if the inflow rate of core and baffle in Fig. 3.17 is divided by the flow area of them. Quench propagation envelope for normal bundles 5 and 6 and blockage bundles 3 and 4 are compared in Figs. 3.28 $\sim$ 3.31. In the normal bundles, the bottom-up quench propagates smoothly till it meets the top-down quench.

However, in the blockage bundles, the quench time scatters at above the blockage elevation because of peculiarity in cooling. This delay or promotion can be compared with the time given by extrapolation of the quench envelope from the lower elevation in the bundle on the average, taking the difference from the neighbouring bundles into account. Figure 3.32 shows the distribution of this delay in quench time for temperature measurement locations below and above the blockage sleeve. It is clear from this figure that the quench delay for low reflood velocity occurs just above the blockage elevation. For comparison, an example of quench promotion for high reflood velocity is given in Fig. 3.33. This test has a rapid time variation of the reflood velocity due to switching from Acc to LPCI, whereas Test S1-22 in Fig. 3.32 has only slow variation in the small velocity range. To examine the dependency of the quench delay on the reflood velocity variation, two other gravity feed tests S1-12 and S1-13 were plotted as shown in Figs. 3.34 and 3.35. These results obviously show that rods adjacent to non-heated rods or wall tend to quench earlier than the other rods on the average in any case; however, the quench delay on the whole is generally large in low reflood velocity cases except S1-13 in which oscillation in reflood flow was observed.

The effect of blockage on the peak clad temperatures were also checked. However, the difference of the peak clad temperatures around the blockage between blockage bundle and normal bundle is not noticeable. Figures 3.36 and 3.37 are examples of the temperature distirbution variation with time in Test S1-22. These do not seem to indicate higher temperature due to blockage when the power distribution across bundles is taken into account.

The peak temperature at the Bundle 5 side of Bundle 4 seems due to local peculiarity like bend of the bundle rods.

3.2.4 Summary

(1) Low constant gravity feed rate without Acc period resulted in slow increase of steam generation and system pressure because of slow core cooling. Water accumulation in the core and the upper plenum was relatively small.

(2) The turnaround temprature of rods became much higher at middle to upper core than in tests with higher injection rate. The quench time resultantly delayed much.

(3) Low reflood velocity delays the quench of the region just above blockage location for some tens seconds, whereas high reflood velocity promotes it. This effect for approximately 60% blockage fraction is, however, very small and peak clad temperature or heat transfer rate does not show apparent change due to blockage.

3.3 Comparison with FLECHT-SEASET Test

As discussed in the previous chapter there are some differences in design between SCTF and FLECHT-SEASET with 21 rod bundle blockage core such as rod diameter, peaking factor, core bypass (baffle) region and hot leg height as well as their scales. On the other hand, the differences in test conditions are the injected coolant temperature, initial core temperature distribution and the pressure transient of the containment tanks.

3.3.1 Fluid flow behavior

Since the respose of the pressure control valve on the containment tank of SCTF is not so quick and there is a flow resistance in the broken loop, the upper plenum pressure increased rapidly at the beginning of reflood as compared with the FLECHT-SEASET data[8] in Fig. 3.38. The water heads in the core and downcomer are compared between the two tests in Figs. 3.39 and 3.40, respectively in which initial values are adjusted. The core water head transients are similar to each other, whereas the downcomer water head in SCTF represented by a line with circle recovers more rapidly. The reason of this difference is that the upper plenum water was extracted in the SEASET test whereas it accumulated in the plenum quite well in the SCTF test. Considering that the vent line connecting the upper plenum with the downcomer in the SCTF test was open, we should have equality between the sum of upper plenum and core water heads and the downcomer water head. And they are equal for the most part. In the SEASET test, the core water head comes up with the downcomer water head in the end.

The initial oscillation in the figures are examined for the SCTF data by comparing the phase and magnitudes between the core and the downcomer (Fig. 3.41). It is found that the oscillations in the pressure differences are in-phase and proportional in magnitudes to each other. Since the pressure difference indicates the sum of water head, friction loss and acceleration which has opposite sign to the water head for downcomer, the peak points indicates minimum water head. For the core pressure difference, however, the acceleration due to violent vaporization get stronger as more water flows in until the inflow is prevented. Thus, the in-phase oscillation is regarded as a U-tube type level oscillation brought about by the fast reflood flow. Although similar oscillation

is seen in the SEASET data, the detail of the phase data is not available at present.

In accordance with the initial steam generation and accompanying carryover flow, the pressure loss downstream of the upper plenum becomes its maximum for the SEASET test in which the upper plenum water is extracted, whereas the upper plenum water head in SCTF formes peak as shown in Figs. 3.42 and 3.43.

3.3.2 Core thermal behavior

The heating power of a rod before the initiation of the reflood is lower in the FLECHT-SEASET test than in the SCTF test. Therefore, the temperature gradient before the reflood start is gentler in the SEASET test as seen in Figs. 3.44 through 3.47. Some of temperatures at the reflood start do not coinside because the total stored heats in a rod were adjusted to be the same in different axial peaking factor conditions. At any rate, all the temperatures begin to decrease immediately after the reflood start and quench at relatively early time because of fast reflood velocity. The behavior of peak temperature and quenching for each elevation are compared generally in Figs. 3.48 and 3.49, respectively. The peak temperature distribution in SCTF has a skew in which upper half has higher temperature and wider scattering. The skew is probably because the bulk steam temperature during the heat up period can become higher in the upper part of the core due to natural convection. The spread data in the upper part is also seen in the SEASET data.[7]

The quench times for below the blockage are quite similar between the two facilities tests: however, much wider spread for above the blockage is seen in the FLECHT-SEASET core. The SCTF data have

both promotion and delay of quench as already discussed in Section 3.2.3, whereas the SEASET data show only promotion and earlier quench in general than the SCTF data. This can be regarded because the SCTF blockage bundles allow bypass flow in the neighbouring unblocked bundles while the SEASET core for the present test is totally blocked and forces droplet atomization. This difference is the very effect of facility scaling and partial blockage configuration of SCTF.

3.3.3 Two dimensionality in SCTF

Since the SCTF test has the radial power distribution in which Bundles 3 and 4 are the highest and Bundles 7 and 8 are the lowest, rod temperature distribution of the similar shape is observed as shown in Figs. 3.50 and 3.51. It is also seen that peripheral bundles 7 and 8 quench earlier than the other bundles.

As the result of two dimensional (slab) core configuration, cross flow occurs at each core elevation. The horizontal pressure difference measurement between Bundles 5 and 8 (Fig. 3.52) exhibits positive (from 5 to 8) or negative (from 8 to 5) flow depending on the elevations and time. When the middle elevation is almost quenched the pressure difference near the middle elevation turns from positive to negative. This flow direction change corresponds the time when the differential pressures across end box tie plates 7 and 8 decrease (Fig. 3.53) and the upper plenum liquid levels above bundles 7 and 8 begins to increase more dominantly than the others. This sequence suggests fall back flow in the peripheral region and resultant cross flow in the core from the periphery (7 and 8) to the center (1 and 2).

3.3.4 Summary

(1) Overall reflood behavior was similar in the SCTF test to the corresponding FLECHT-SEASET test. Major difference of fluid behavior in SCTF from FLECHT-SEASET is that water accumulation in the downcomer in accordance with the upper plenum was seen dominantly in SCTF.

(2) A U-tube type oscillation of water level in the downcomer and core was observed in SCTF and FLECHT-SEASET showed a similar oscillation.

(3) Quench promotion in SCTF blockage bundles is not so dominant as in FLECHT-SEASET which may have better cooling owing to fluid atomization at above the blockage and SCTF exhibits even quench delay at above the blockage owing to flow bypass in the neighbouring bundles.

(4) Two dimensional thermo-hydraulic behavior such as cross flow in the core, local fall back flow and skewed upper plenum water distribution is observed in SCTF, which has closer scale to a PWR.

4. Conclusions

Three kinds of lower plenum injection gravity feed tests were examined through comparison with forced feed tests under isolated downcomer condition or a FLECHT-SEASET test. The following facts were clarified.

(1) A gravity feed test with flow area scaled injection rate for an forced feed test showed excess inflow and outflow of core and slight difference in turnaround temperatures compared with the forced feed test. However, the difference in cooling was small as a whole.

3.3.4 Summary

(1) Overall reflood behavior was similar in the SCTF test to the corresponding FLECHT-SEASET test. Major difference of fluid behavior in SCTF from FLECHT-SEASET is that water accumulation in the downcomer in accordance with the upper plenum was seen dominantly in SCTF.

(2) A U-tube type oscillation of water level in the downcomer and core was observed in SCTF and FLECHT-SEASET showed a similar oscillation.

(3) Quench promotion in SCTF blockage bundles is not so dominant as in FLECHT-SEASET which may have better cooling owing to fluid atomization at above the blockage and SCTF exhibits even quench delay at above the blockage owing to flow bypass in the neighbouring bundles.

(4) Two dimensional thermo-hydraulic behavior such as cross flow in the core, local fall back flow and skewed upper plenum water distribution is observed in SCTF, which has closer scale to a PWR.

4. Conclusions

Three kinds of lower plenum injection gravity feed tests were examined through comparison with forced feed tests under isolated downcomer condition or a FLECHT-SEASET test. The following facts were clarified.

(1) A gravity feed test with flow area scaled injection rate for an forced feed test showed excess inflow and outflow of core and slight difference in turnaround temperatures compared with the forced feed test. However, the difference in cooling was small as a whole.

(2) A low constant gravity feed rate test showed slow core cooling and small water accumulation in the upper plenum. The slow reflooding delays quenching of the region above blockage location but does not affect peak clad temperature apparently.

(3) Although overall behaviors of SCTF data and FLECHT-SEASET data were similar, some differences were observed. Such differences as core water accumulation rate, cooling of the region above blockage and two dimensional flow are essentially dependent on facility design differences or operation condition differences. SCTF with larger scale is considered to have closer simulation of a PWR.

Acknowledgement

The authors are much indebted to Dr. M. Nozawa, Dr. S. Katsuragi, Dr. M. Hirata, Dr. K. Hirano, and Dr. Y. Murao, for their guidance and encouragement for this program.

They would like to express their appreciation to Messrs. T. Iguchi, J. Sugimoto, H. Akimoto and T. Okubo for their useful discussions, to Messrs. Y. Fukaya, T. Oyama, T. Wakabayashi, Y. Niitsuma, T. Chiba, T. Matsumoto, K. Komori and H. Sonobe, for their excellent operation of the test facility and to Mr. D. H. Miyasaki, resident engineer from USNRC for his devoted help.

(2) A low constant gravity feed rate test showed slow core cooling and small water accumulation in the upper plenum. The slow reflooding delays quenching of the region above blockage location but does not affect peak clad temperature apparently.

(3) Although overall behaviors of SCTF data and FLECHT-SEASET data were similar, some differences were observed. Such differences as core water accumulation rate, cooling of the region above blockage and two dimensional flow are essentially dependent on facility design differences or operation condition differences. SCTF with larger scale is considered to have closer simulation of a PWR.

Acknowledgement

The authors are much indebted to Dr. M. Nozawa, Dr. S. Katsuragi, Dr. M. Hirata, Dr. K. Hirano, and Dr. Y. Murao, for their guidance and encouragement for this program.

They would like to express their appreciation to Messrs. T. Iguchi, J. Sugimoto, H. Akimoto and T. Okubo for their useful discussions, to Messrs. Y. Fukaya, T. Oyama, T. Wakabayashi, Y. Niitsuma, T. Chiba, T. Matsumoto, K. Komori and H. Sonobe, for their excellent operation of the test facility and to Mr. D. H. Miyasaki, resident engineer from USNRC for his devoted help.

References

(1) H. Adachi, et al., Design of Slab Core Test Facility (SCTF) in Large Scale Reflood Test Program, Part I: Core-I, JAERI-M 83-080 (1983)

(2) H. Adachi, et al., System Pressure Effects on Reflooding Phenomena Observed in the SCTF Core-I Forced Flooding Tests, JAERI-M 83-079 (1983)

(3) T. Iwamura, et al., Effects of Core Inlet Water Subcooling on Reflooding Phenomena under Forced Flooding in SCTF Core-I Tests, JAERI-M 83-122 (1983)

(4) Y. Sudo, et al., Effect of Upper Plenum Water Accumulation on Reflooding Phenomena under Forced Flooding in SCTF Core-I Tests, JAERI-M 83-114 (1983)

(5) M. Sobajima, et al., Examination of Repeatability in Reflood Phenomena under Forced Flooding in SCTF Core-I Tests, JAERI-M 83-237 (1984)

(6) T. Iwamura, et al., Core Thermal Behavior under Forced-Feed Flooding, in SCTF Core-I Tests, to be published

(7) M.J. Loftus, et al., PWR FLECHT SEASET 21-Rod Bundle Flow Blockage Task Data and Analysis Report, NUREG/CR-2444 (1982)

(8) L.E. Hochreiter, Personal communication.

(9) T. Iwamura, et al. Effect of Upper Plenum Injection on Thermo-hydrodynamic Behavior under Refill and Reflood Pahases of a PWR-LOCA, JAERI-M 84-221 (1984)

Table 2-1 Test conditions of two comparable tests

	Test S1-12(Run518)	Test S1-01(Run507)
Test Type	Gravity feed: L.P. injection	Forced feed: L.P. injection
Vent line	open	close
Initial Pressure (Core Center)	0.20 MPa	0.198 MPa
Pressure (containment-II)	0.20 MPa(initial) 0.23 MPa(max.)	0.195 MPa(initial) 0.218 MPa(max.)
Max. core temp. (at BOCREC)	973 K(nominal)	973 K(nominal)
Power holding after ACC inj.	5 s	5 s
ACC inj. rate	27 kg/s	21 kg/s
LPCI inj. rate	14 kg/s	11 kg/s
Max. core inlet subcooling	20 K	15.5 K

Table 2-2 Test conditions of two comparable low reflooding rate tests

	Test S1-22(Run532)	Test S1-05(Run511)
Test Type	Gravity feed: L.P. injection	Forced feed: L.P. injection
Vent line	close	close
Initial pressure (core center)	0.20 MPa	0.20 MPa
Pressure (Containment-II)	0.20 MPa(initial) 0.217 MPa(max.)	0.20 MPa(Initial) 0.218 MPa(max.)
Max. core temp. (at BOCREC)	973 K(nominal)	973 K(Nominal)
Power holindg after ACC inj.	5 s	5 s
ACC inj. rate	replaced by LPCI	25 kg/s
LPCI inj. rate	8.0 kg/s	6.2 kg/s
Max. core inlet subcooling	14 K	14.6 K

Table 2-3 SCTF/FLECHT-SEASET Counterpart Test

Items	SCTF	FLECHT -SEASET	Ratio
Design conditions			
Number of rods	2048	21	97.5
Heater rod diameter (mm)	10.7	9.5	1.13
Heater rod insulator	MgO	BN	——
Axial peaking factor	1.40	1.66	0.843
Blockage ratio: local (%)	60	61.3	∿1
Core bypass area (m^2)	0.1	None	-
Downcomer area (m^2)	0.121	0.218×10^{-2}	101
Core fluid area (m^2)	0.312	0.198×10^{-2}	158
Hot leg height above UCSP (m)	1.05	0.2	5.2
Test conditions	S1-13	43716C	
Pressure U.P. (max)(MPa)	0.28(0.39)	0.28	1(1.4)
Initial peak clad T (°C)	832	871	0.955
Initial wall temp. max (°C)	460	500	-
Initial peak rod power (kW/m)	2.29	2.3	∿1
Total power at time 0 (kW)	10230	105	97.4
Flow rate of Acc (kg/s)	100	0.83	120
Corresponding reflood V(cm/s)	19.8	20.0	∿1
Flow rate of LPCI (kg/s)	10.2	095	108
Corresponding reflood V(cm/s)	2.0	2.3	0.87
Coolant temperature (°C)	80	51.7	-

Table 3-1 Chronology of events in the two comparable tests

	Test S1-12(Run518)	Test S1-01(Run507)
Core power on	-108 s	-107 s
ACC inj. initiation	-11	-10
Core power decay initiation	-5	-5
BOCREC	0	0
Max. ECC inj. rate	2 (29 kg/s)	-
Switch ACC to LPCI	12	10
Max. Cont-II pressure	22 (0.23 MPa)	20 (0.218 MPa)
Max. core temp.	43 (1033 K)	33 (1012 K)
Max. core pressure	52 (0.26 MPa)	48 (0.263 MPa)
Max. core inlet subcooling	92 (10 K)	53 (15.5 K)
Whole core quenched	290	292

Table 3-2 Chronology of events in the two low reflooding rate tests

	Test S1-22(Run532)	Test S1-05(Run511)
Core power on	-108 s	-101 s
ACC inj. initiation	-11 (LPCI)	-6
Core power decay initiation	-6	-1
BOCREC	0	0
Switch ACC to LPCI	none	14
Max. Cont-II pressure	20 (0.217 MPa)	20 (0.217 MPa)
Max. core temp.	132 (1206 K)	64 (1014 K)
Max. core pressure	202 (0.252 MPa)	17 (0.257 MPa)
Max. core inlet subcooling	202 (14 K)	200 (14.6)
Whole core quenched	437	333

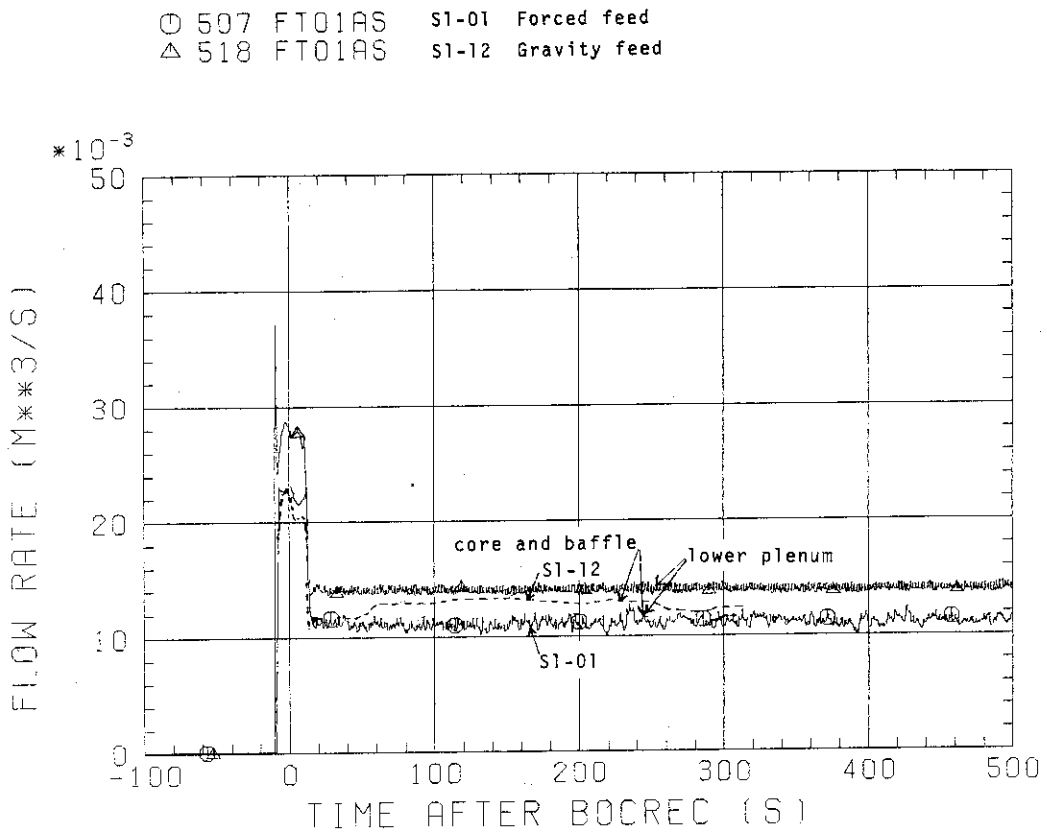

Fig. 3.1 ECC flow rate into lower plenum and flow rate into core and baffle region

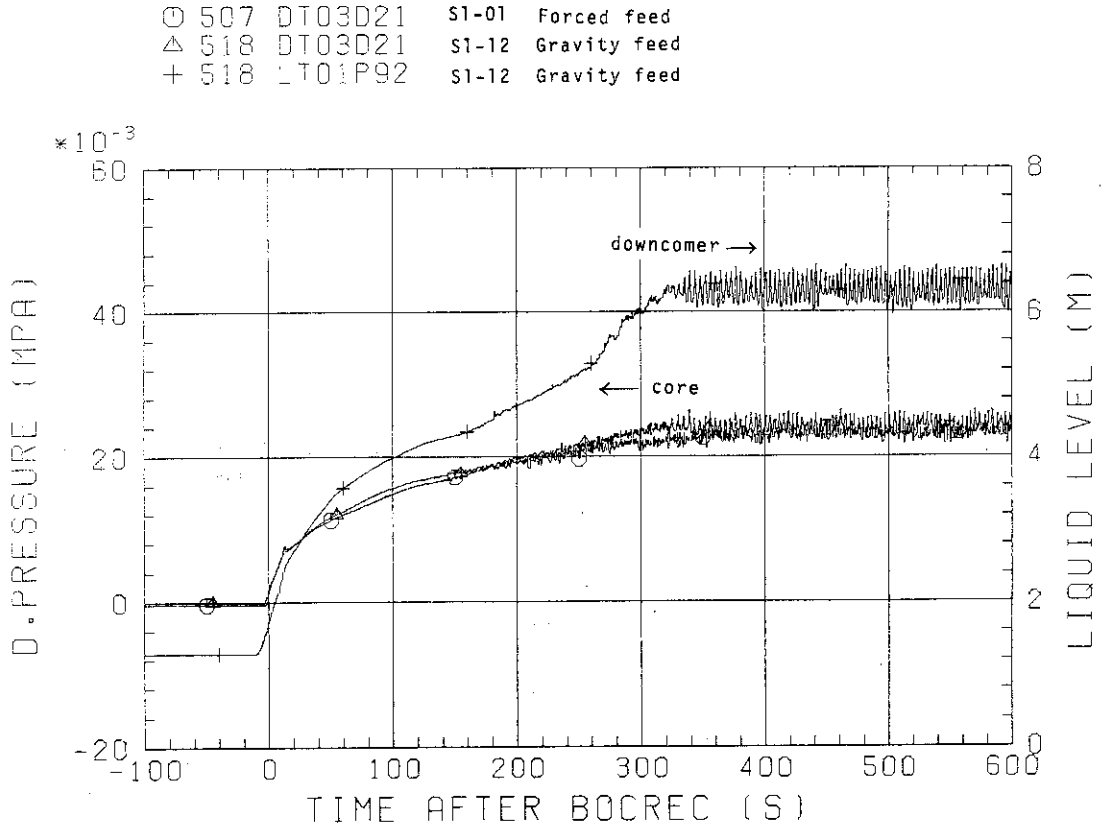

Fig. 3.2 Core full height DP and downcomer liquid level

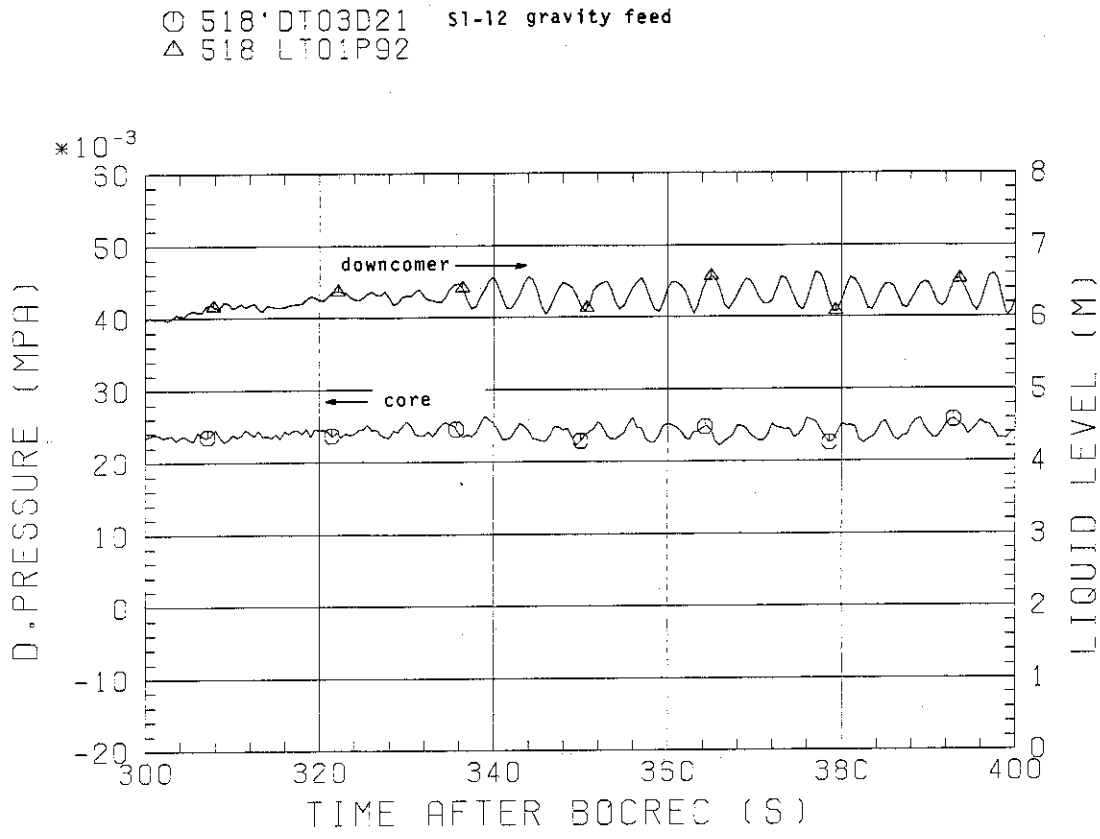

Fig. 3.3 Core full height DP and downcomer liquid level

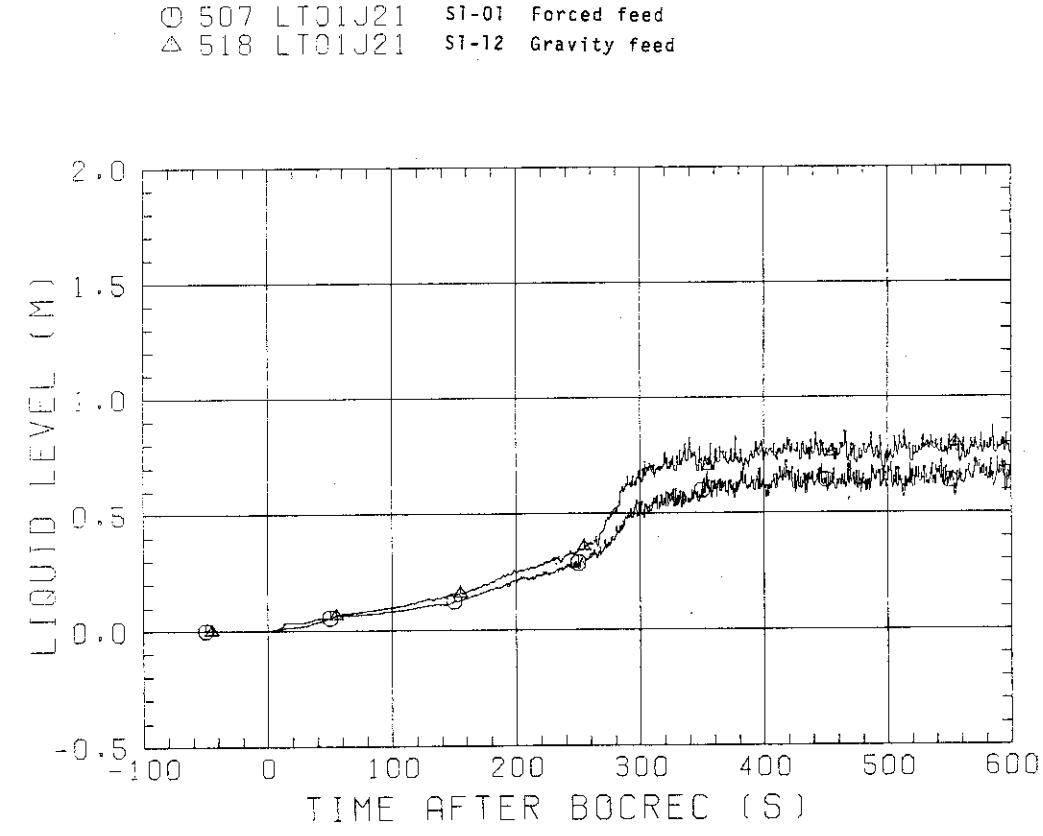

Fig. 3.4 Liquid level in upper plenum above bundle 2

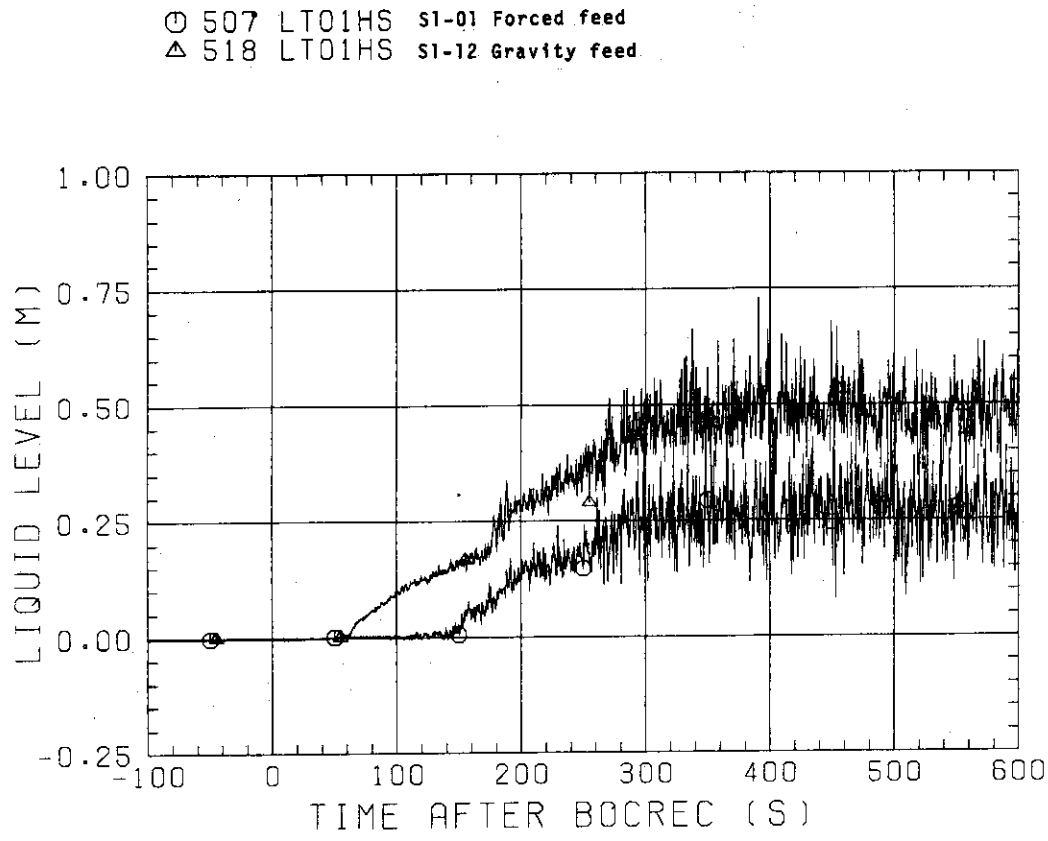

Fig. 3.5 Liquid level in hot leg inlet

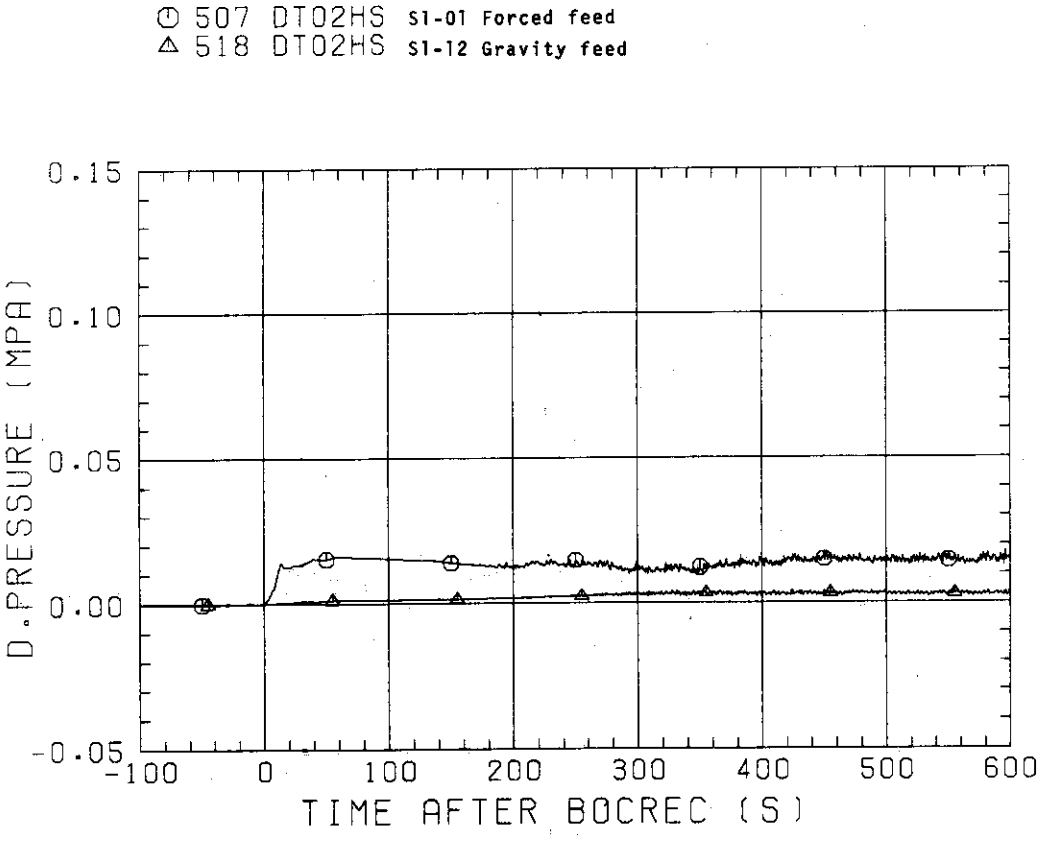

Fig. 3.6 DP across vent valve

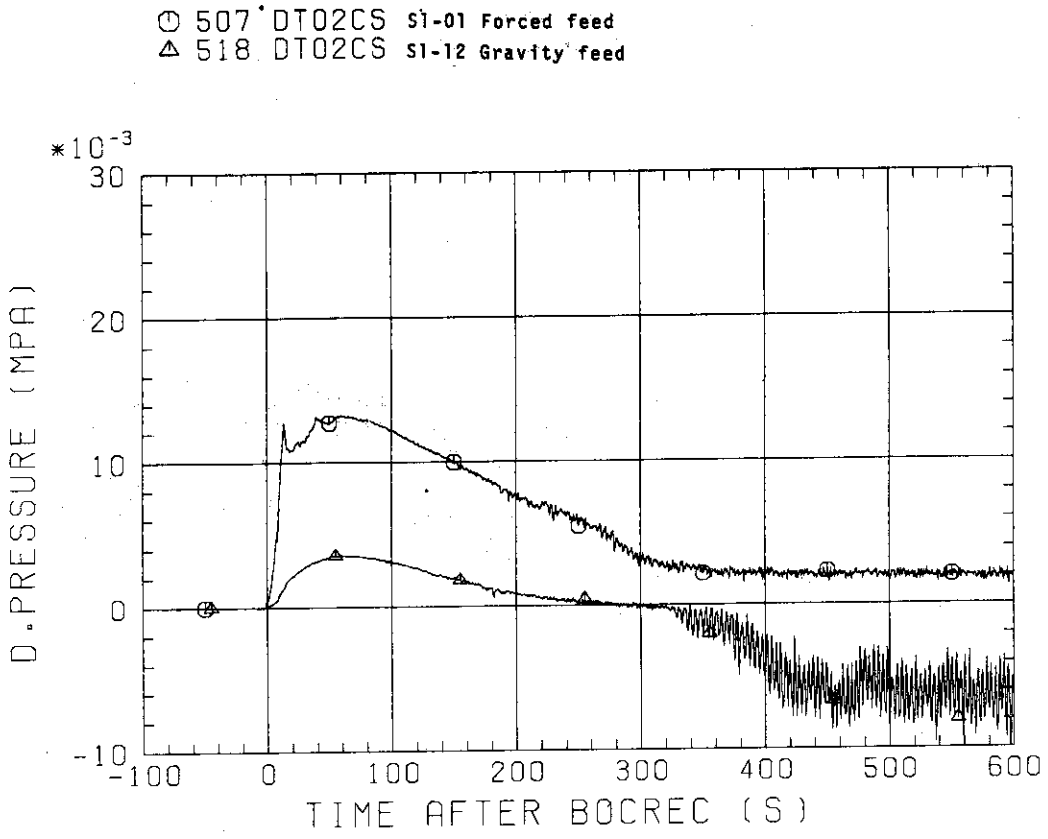

Fig. 3.7 DP across intact cold leg.

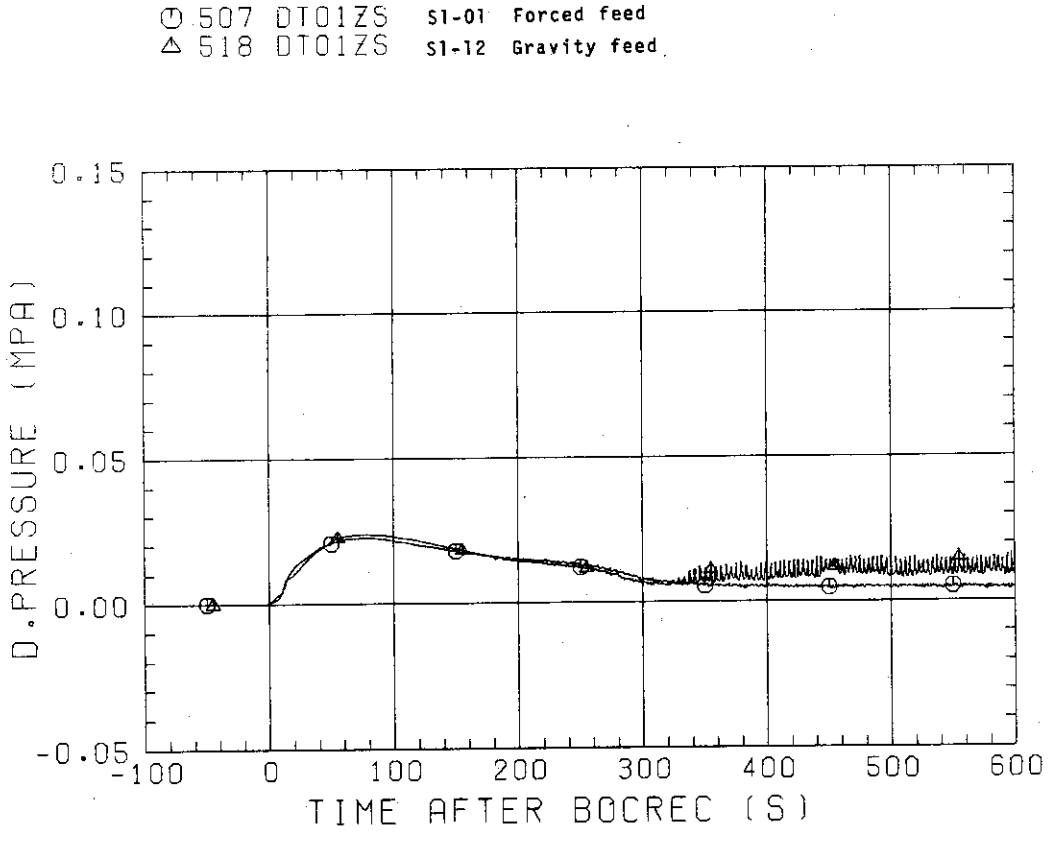

Fig. 3.8 DP in broken cold leg downcomer side

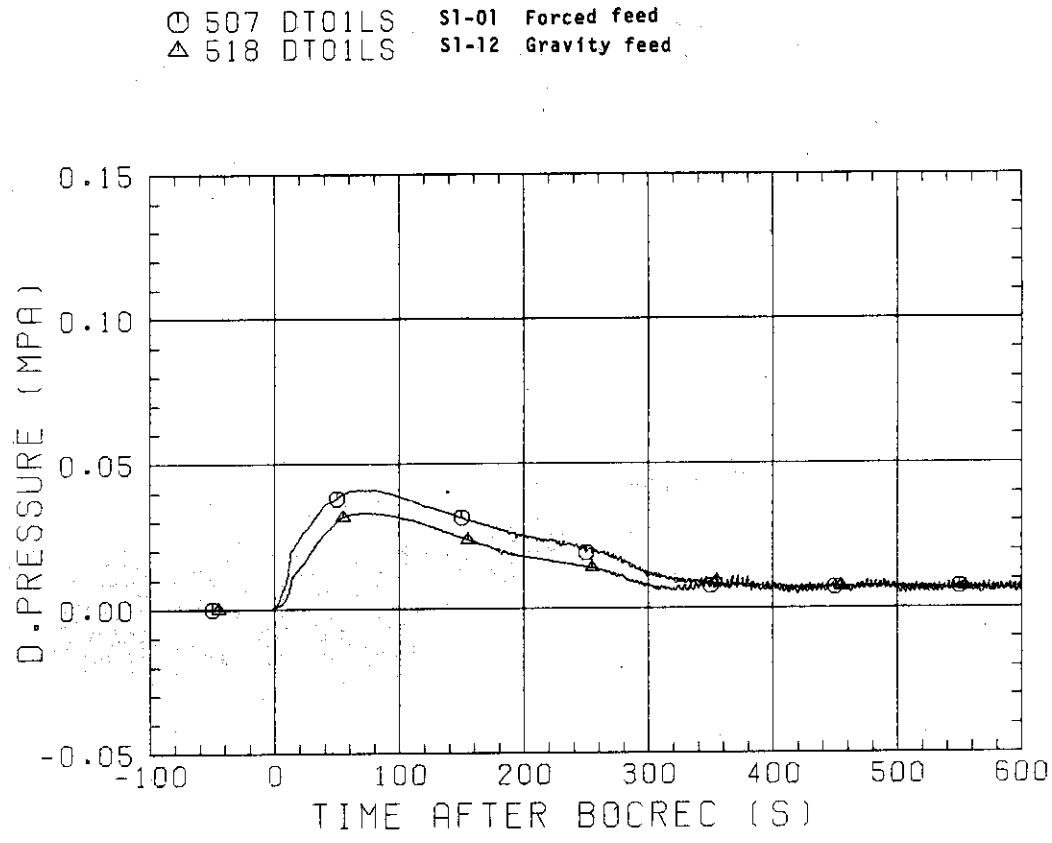

Fig. 3.9 DP across broken cold leg orifice

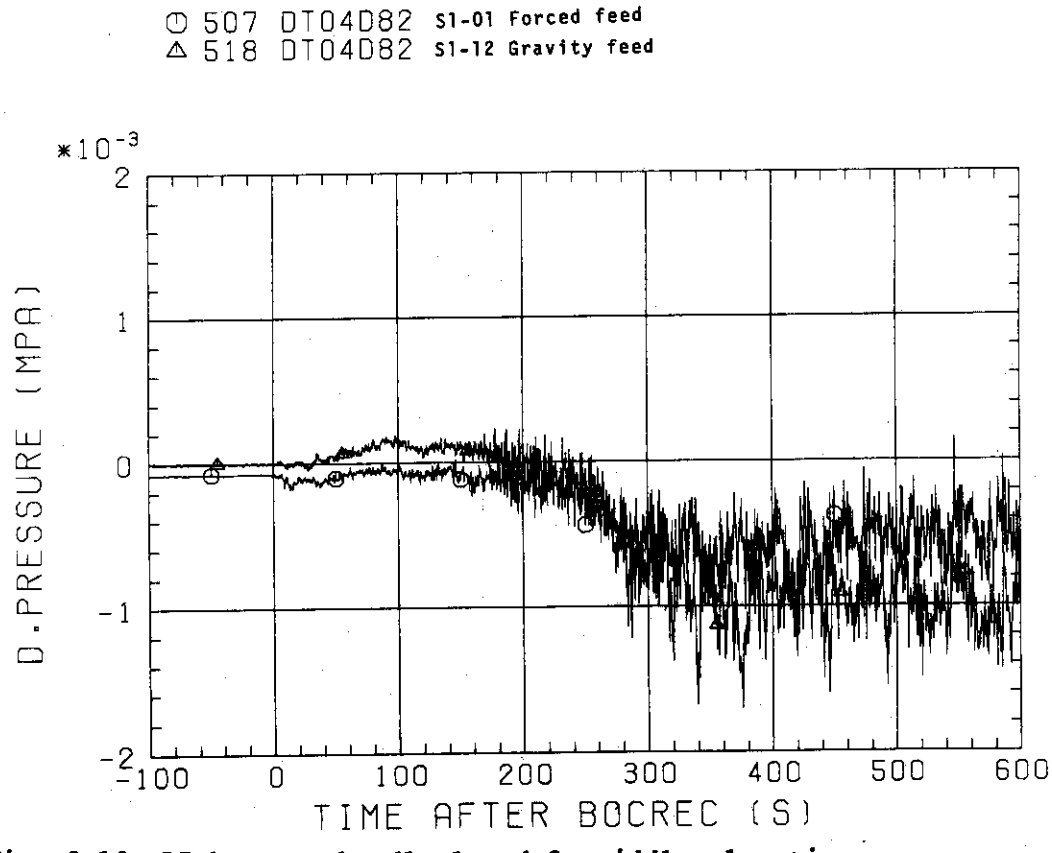

Fig. 3.10 DP between bundle 1 and 8, middle elevation.

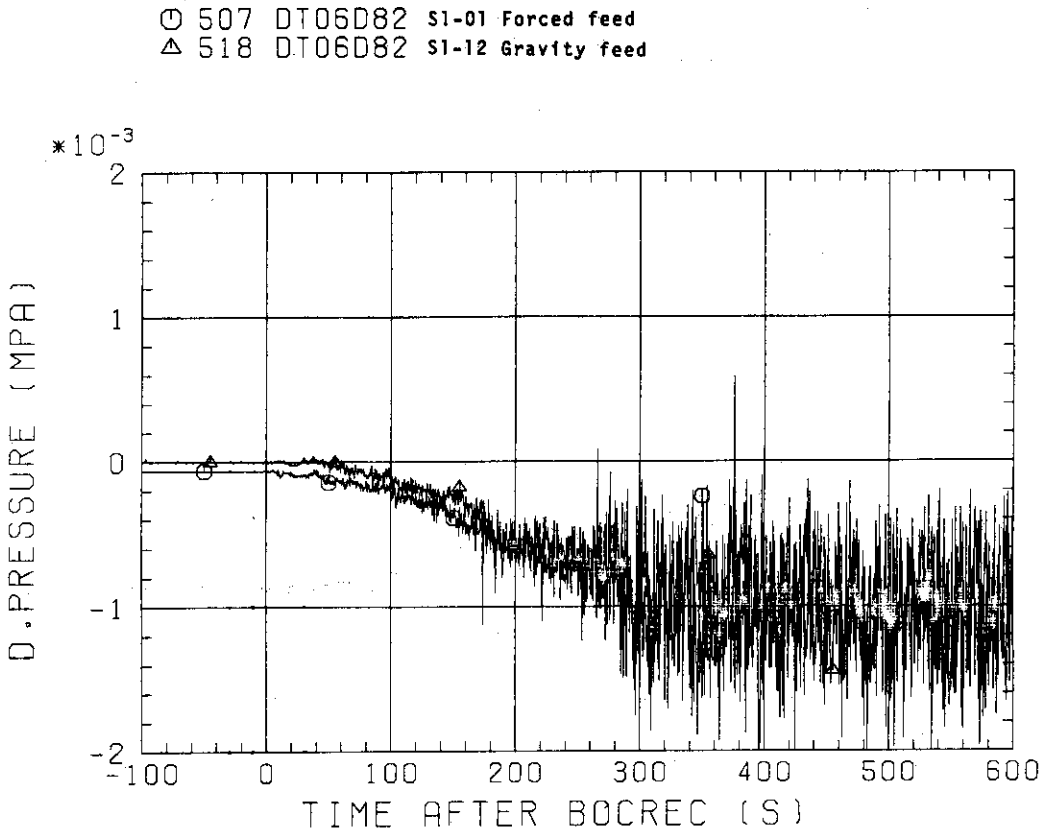

Fig. 3.11 DP between bundle 1 and 8, high elevation.

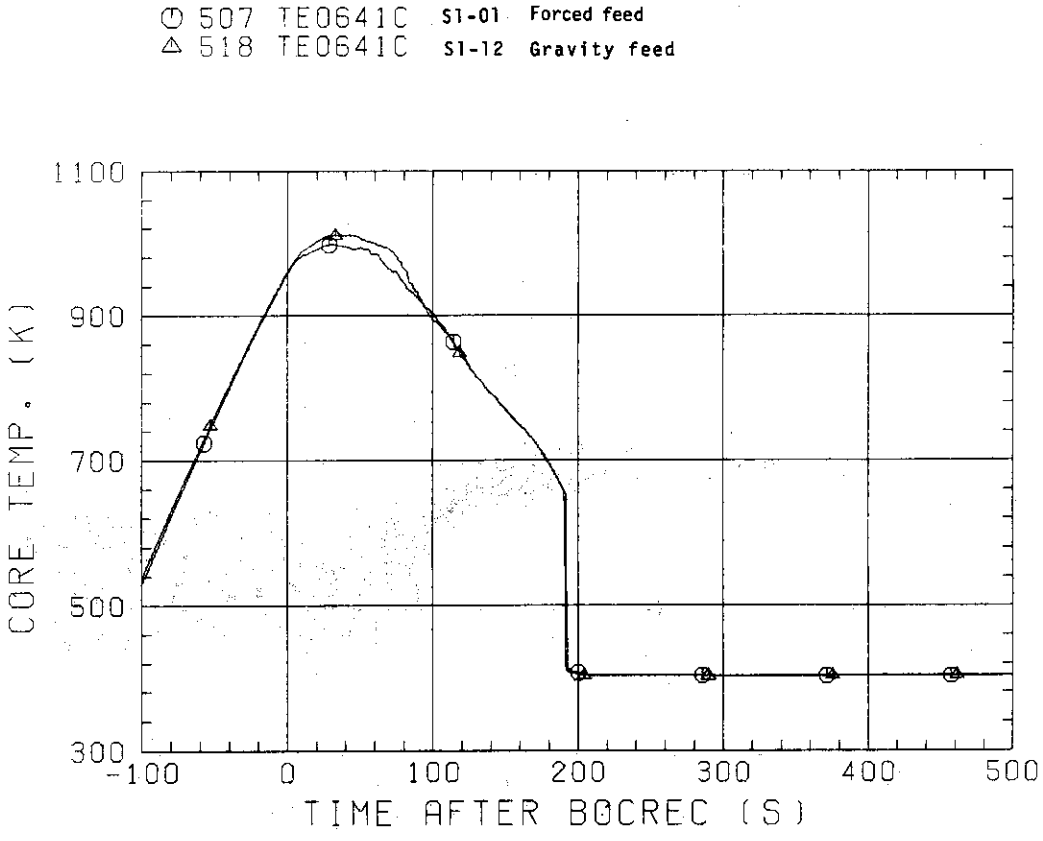

Fig. 3.12 Clad temperature, bundle 4,1905 mm el.

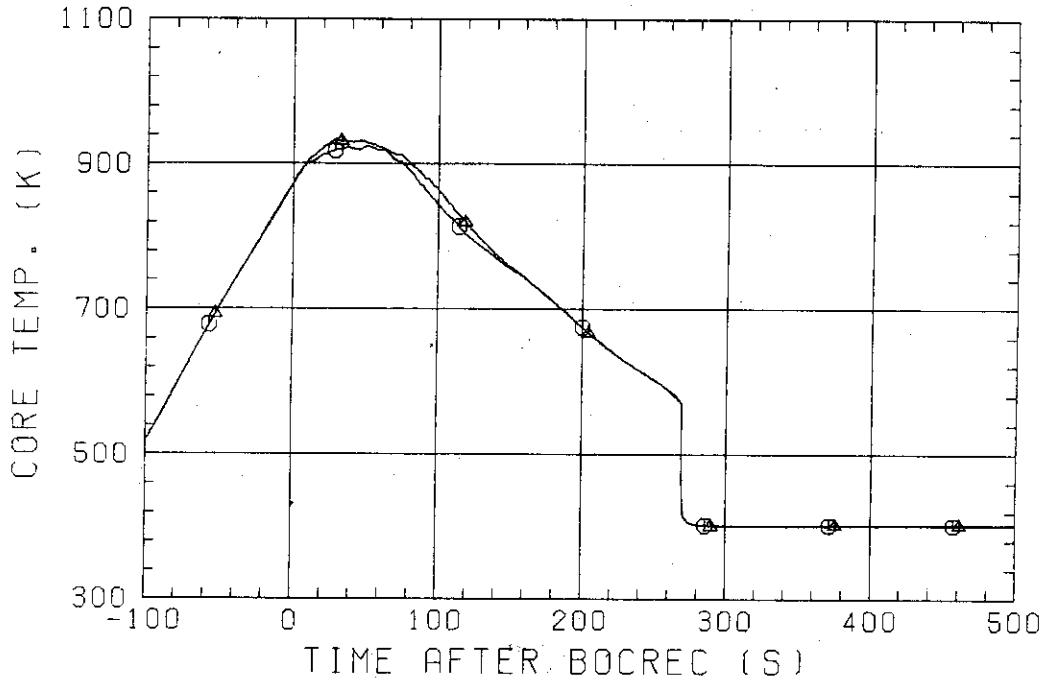

Fig. 3.13 Clad temperature, bundle 4,2760 mm el.

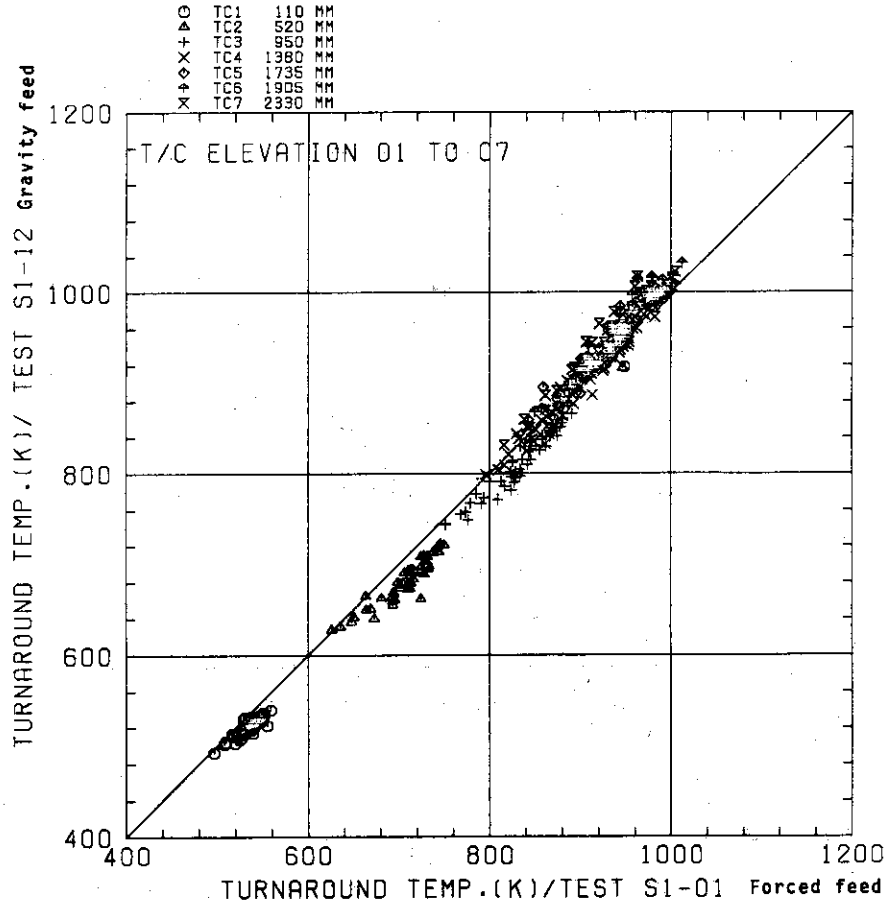

Fig. 3.14 Similarity in turnaround temperture

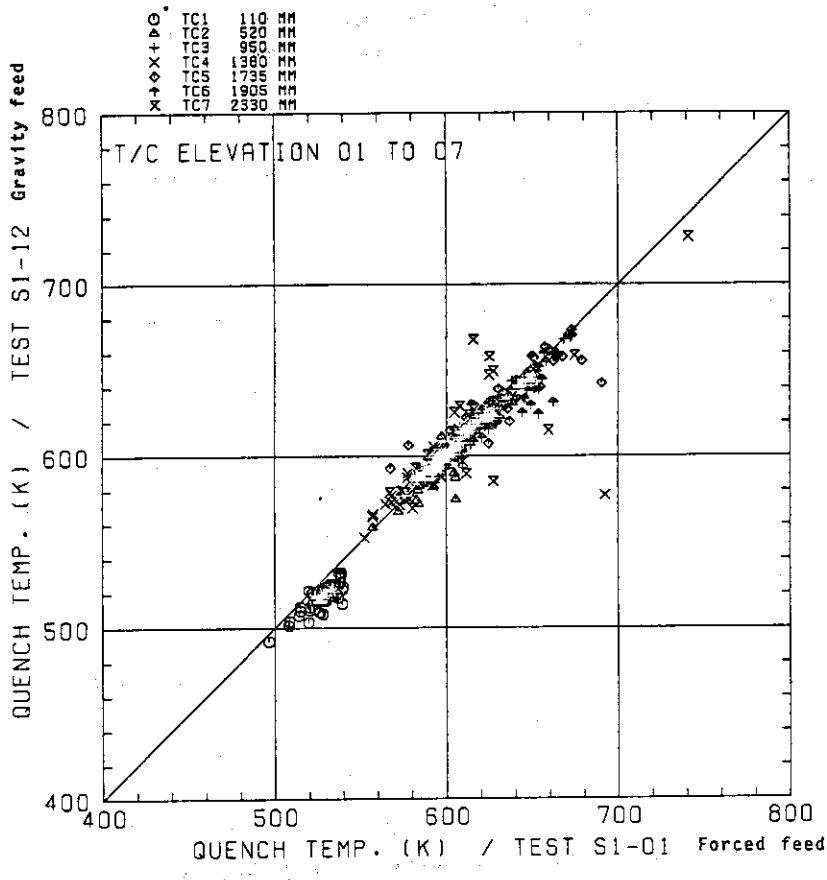

Fig. 3.15 Similarity in quench temperature

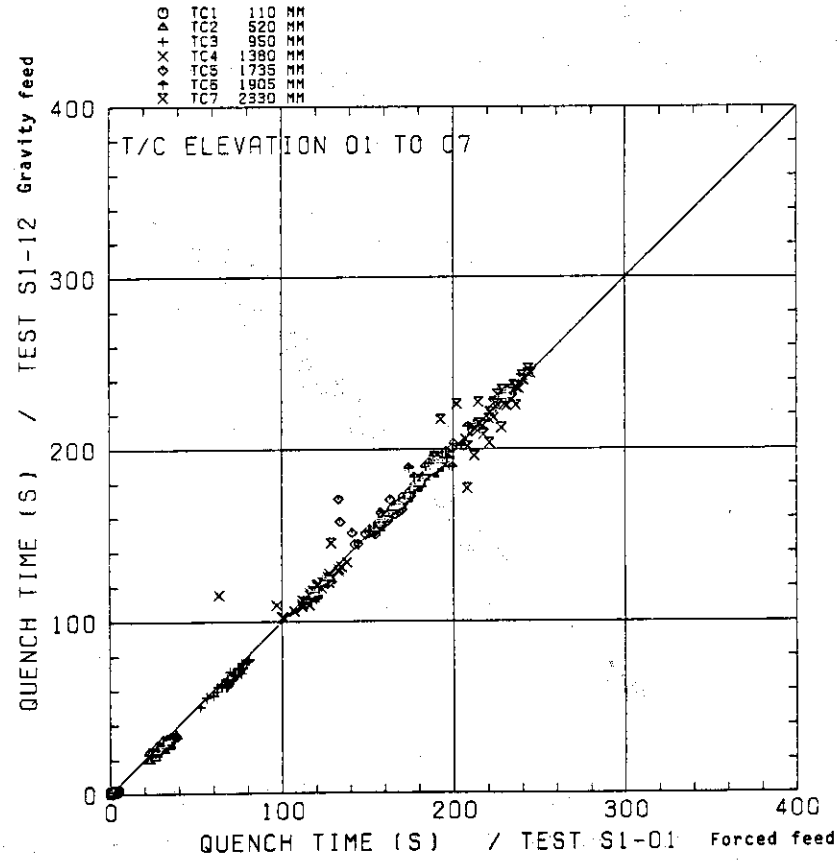

Fig. 3.16 Similarity in quench time

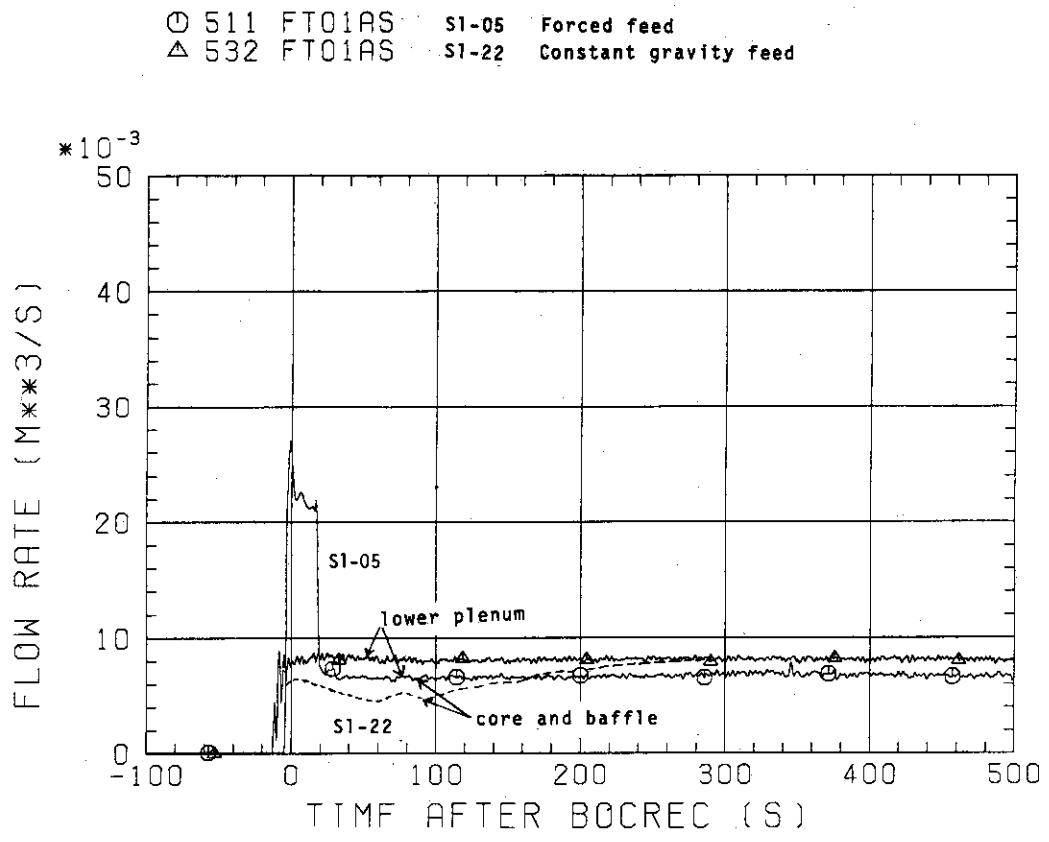

Fig. 3.17 ECC flow rate into lower plenum and flow rate into core and baffle region

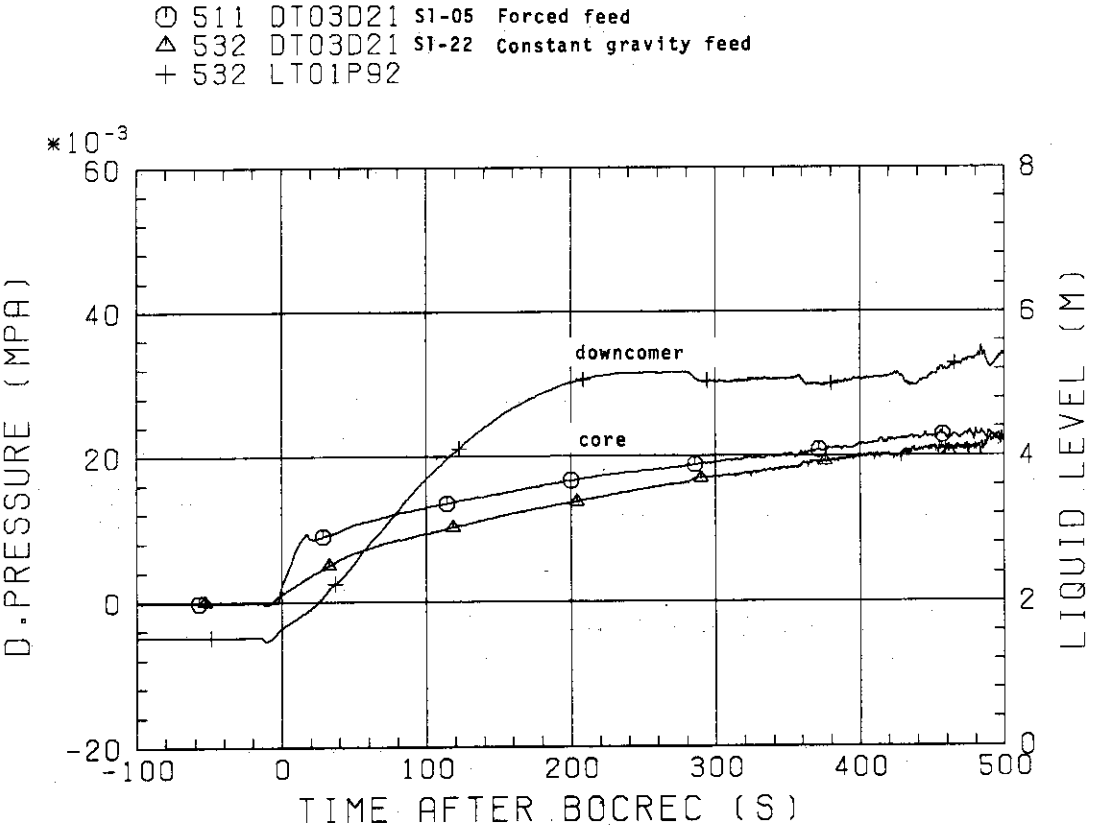

Fig. 3.18 Core full height DP and downcomer liquid level

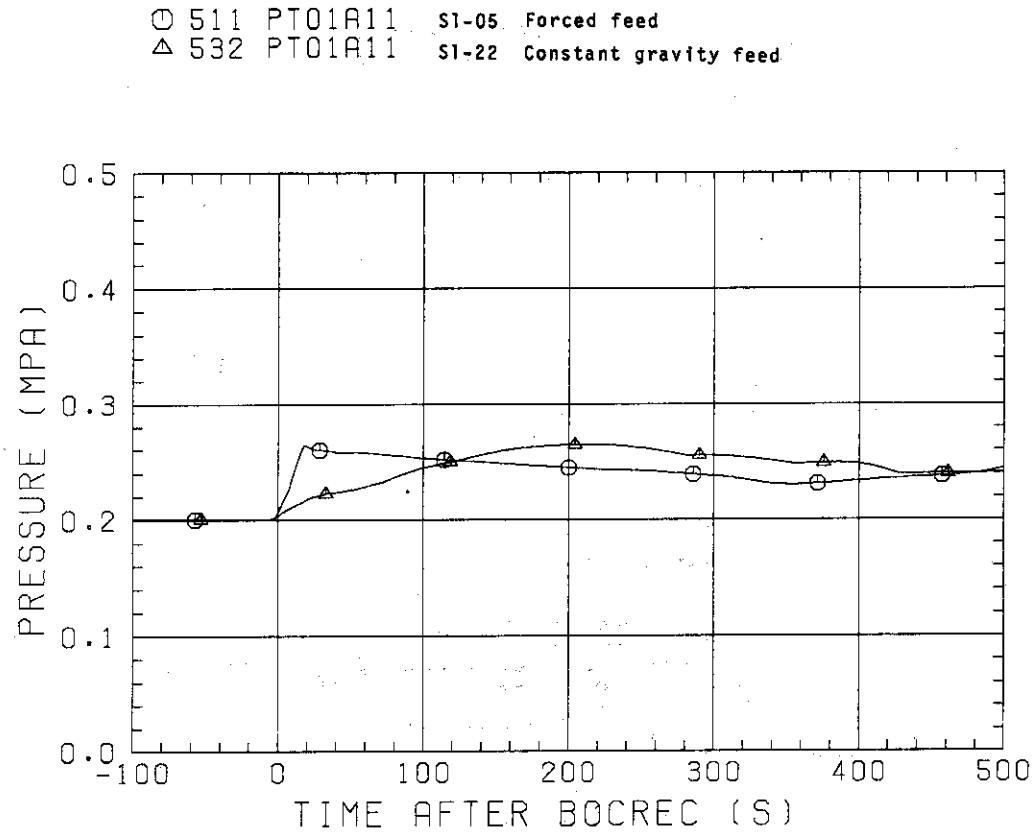

Fig. 3.19 Pressure in lower plenum

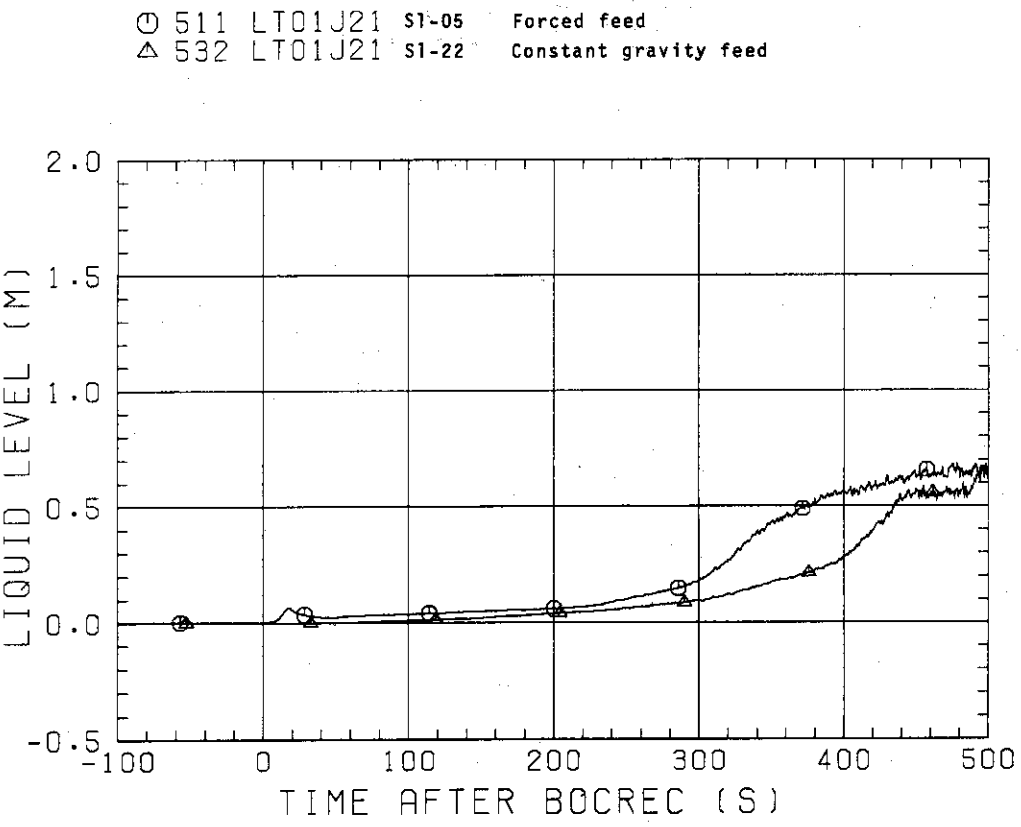

Fig. 3.20 Liquid level in upper plenum above bundle 2

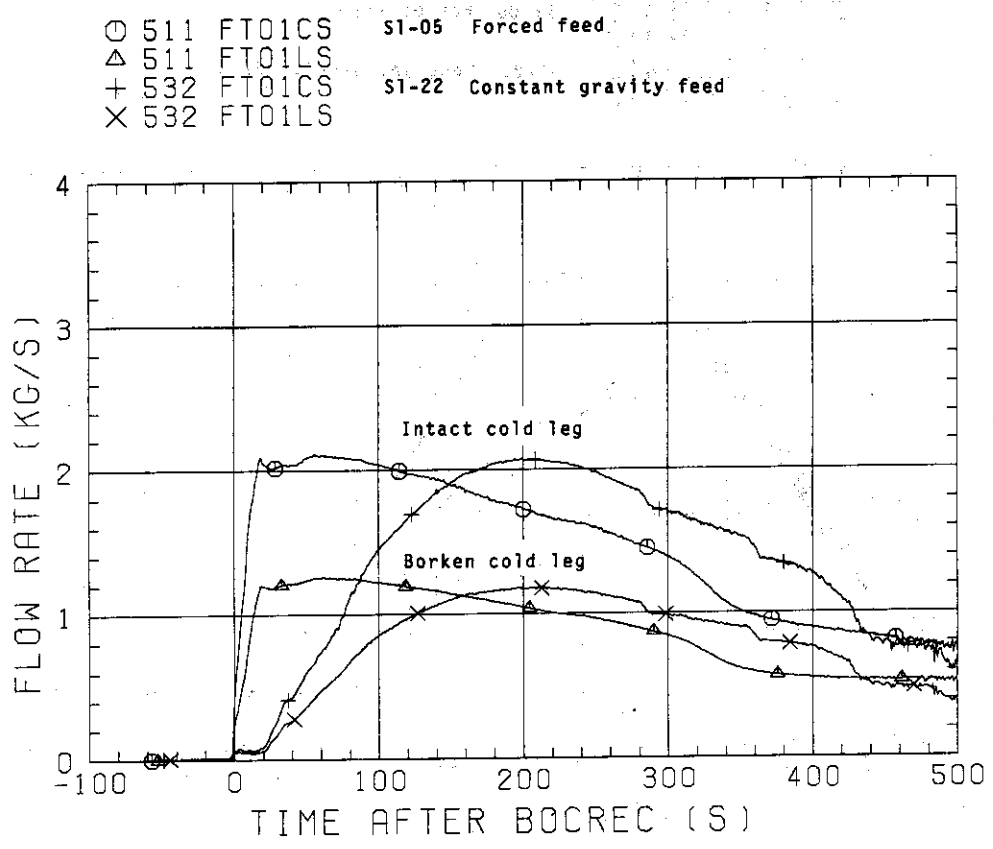

Fig. 3.21 Flow rate in intact cold leg and broken cold leg s/w separator side

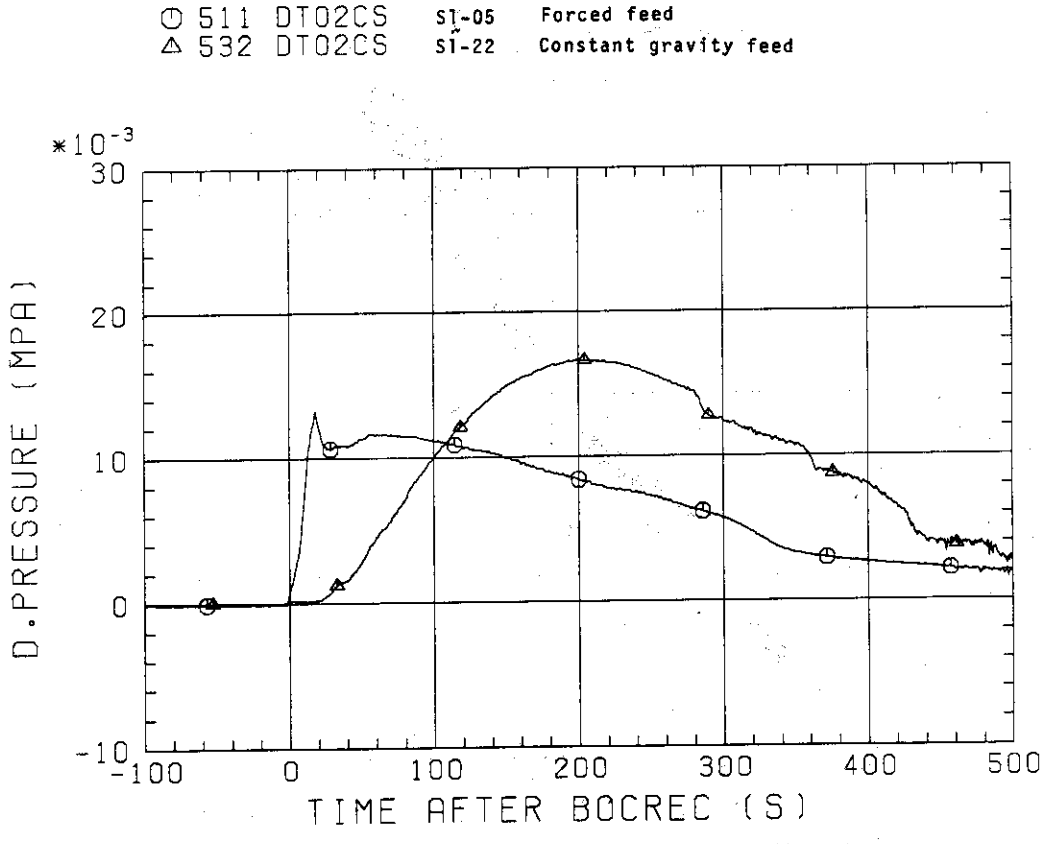

Fig. 3.22 DP across intact cold leg

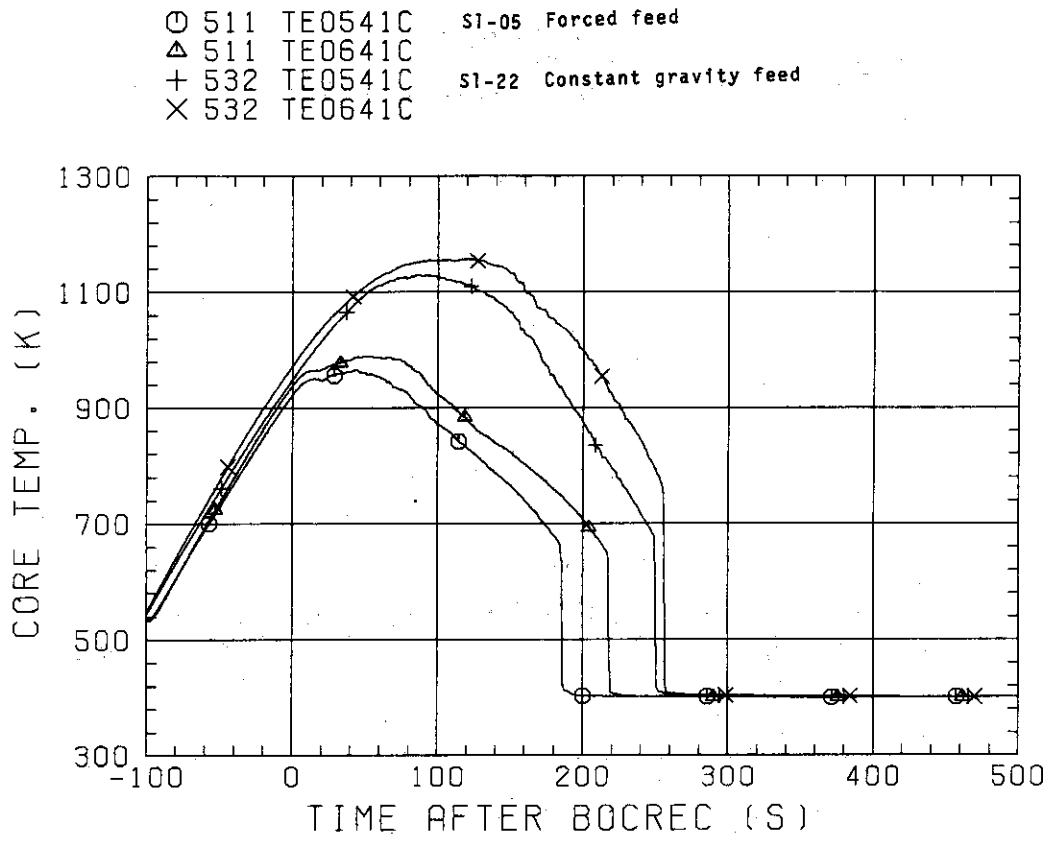

Fig. 3.23 Clad temperature, bundle 4, 1735 mm el. and 1905 mm el.

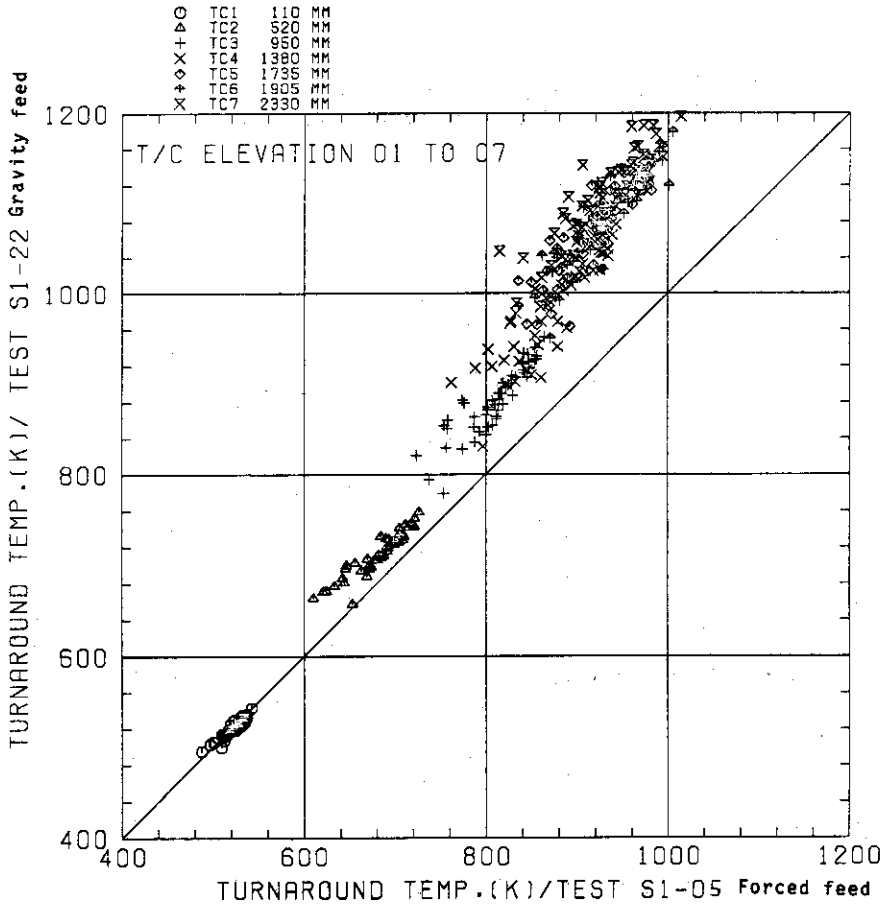

Fig. 3.24 Comparison of turnaround temperature

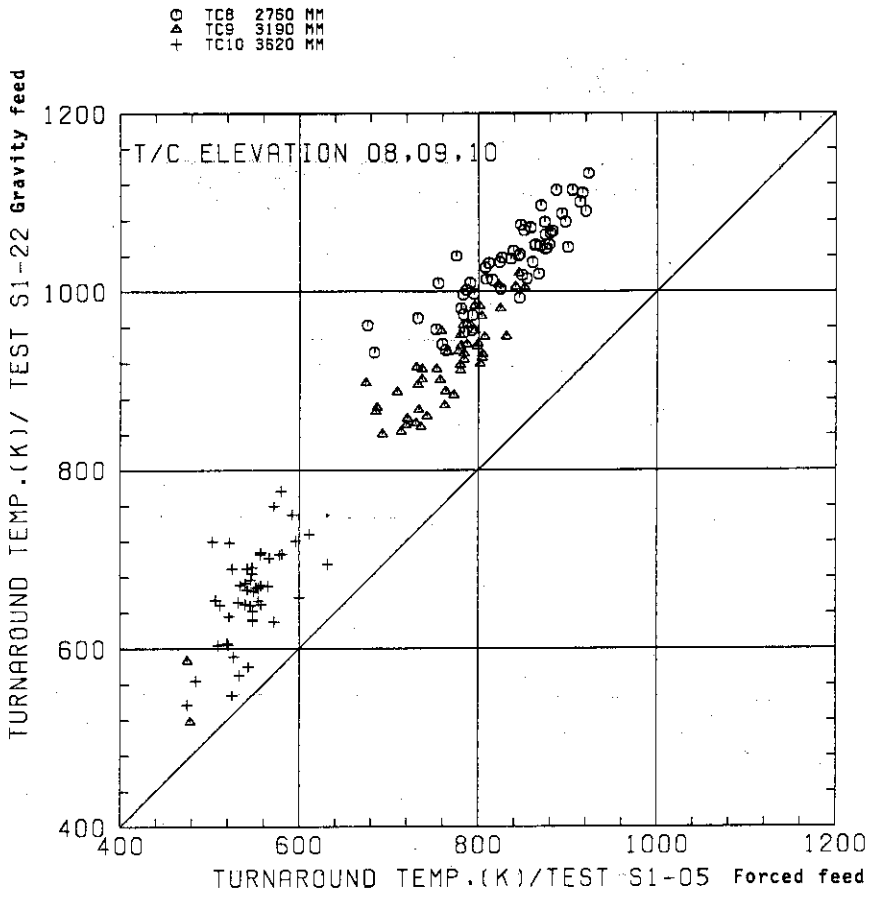

Fig. 3.25 Comparison of turnaround temperature

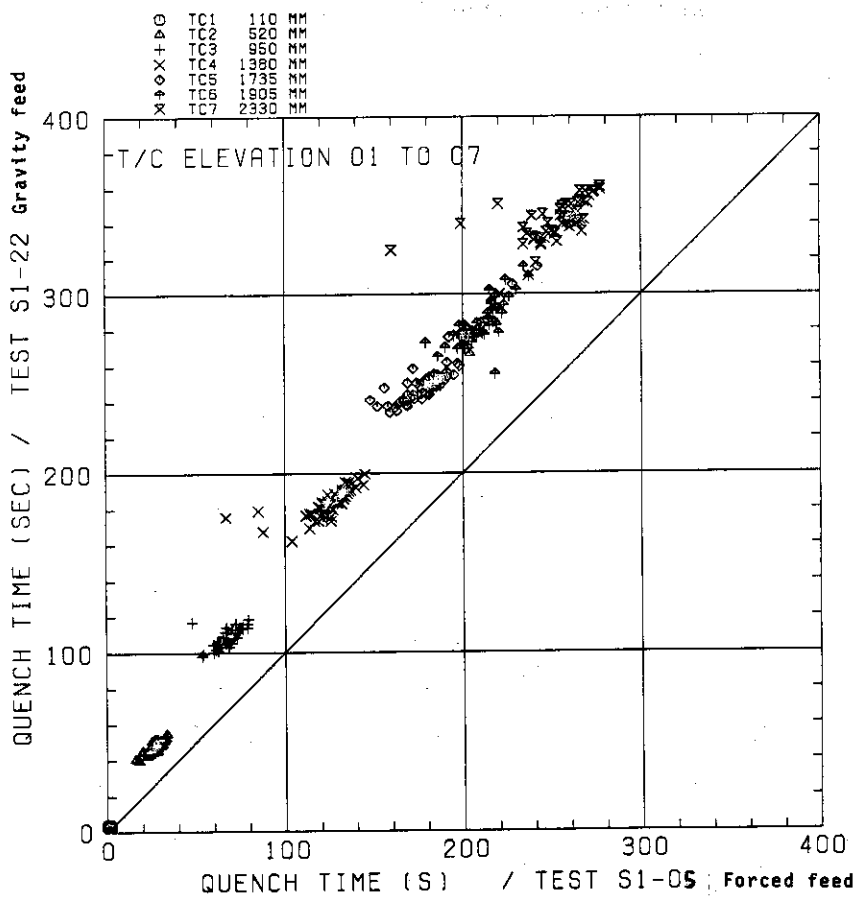

Fig. 3.26 Comparison of quench time

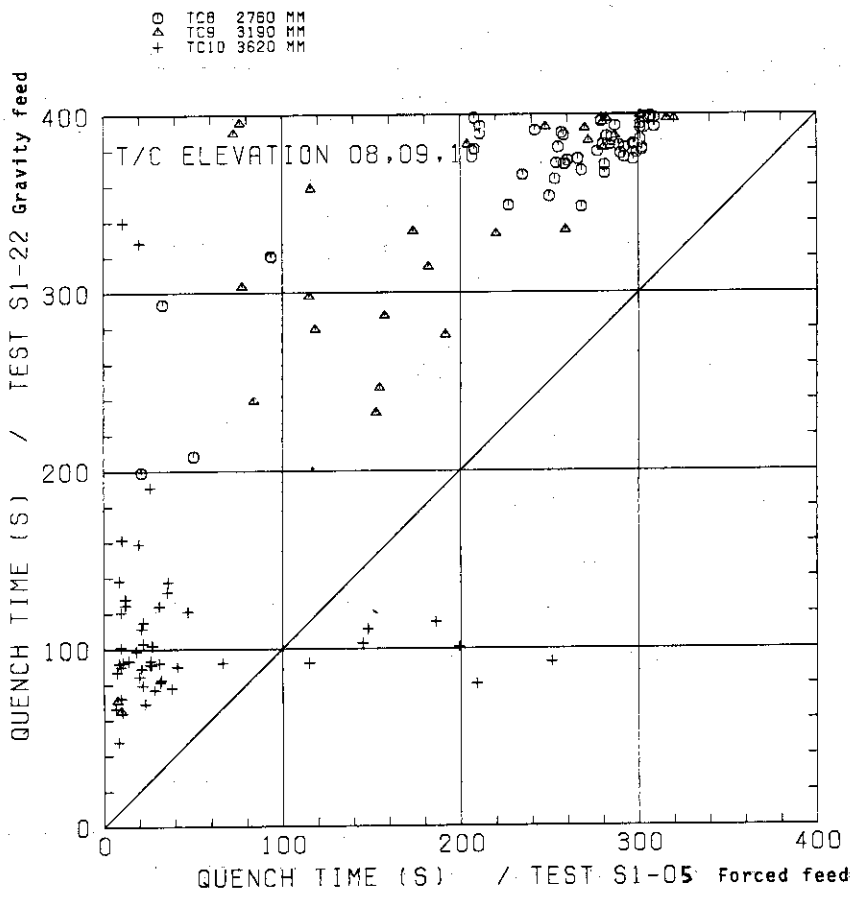

Fig. 3.27 Comparison of quench time

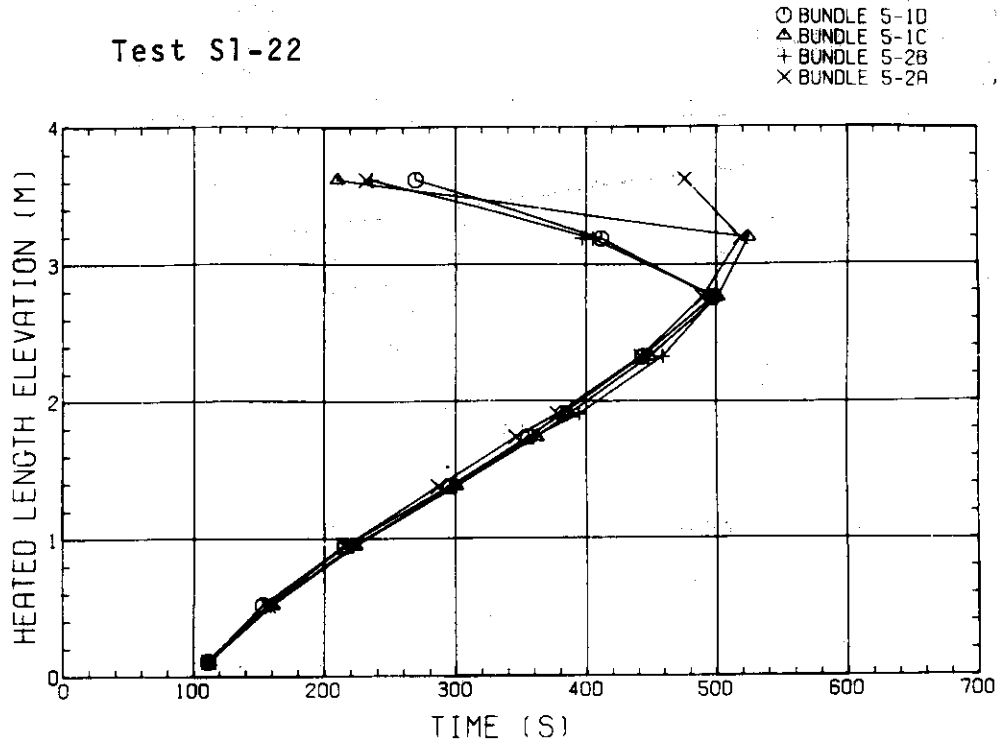

Fig. 3.28 QUENCH ENVELOPE OF BUNDLE 5
(PARALLEL TO WALLS) - See Fig. A-12

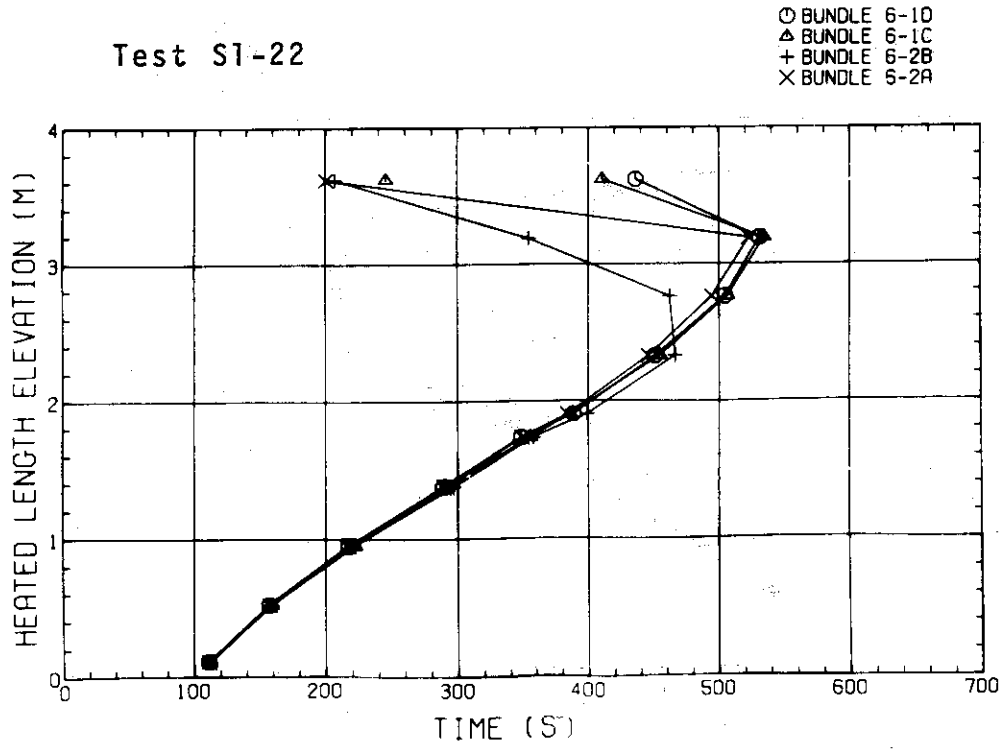

Fig. 3.29 QUENCH ENVELOPE OF BUNDLE 6
(PARALLEL TO WALLS)

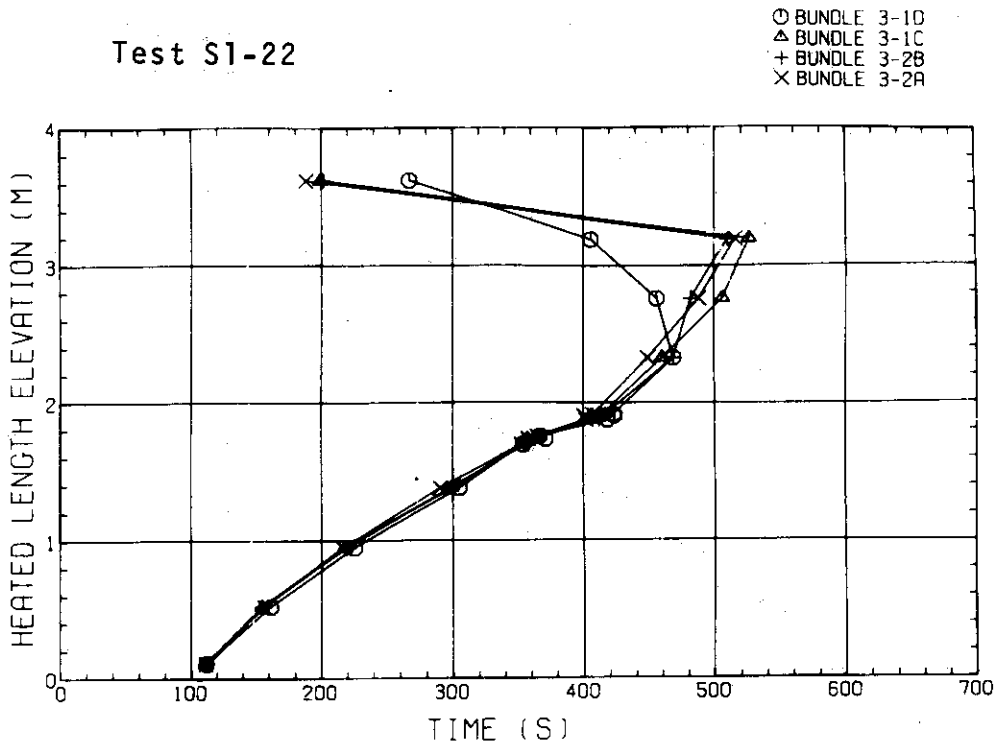

Fig. 3.30 QUENCH ENVELOPE OF BUNDLE 3
(PARALLEL TO WALLS)

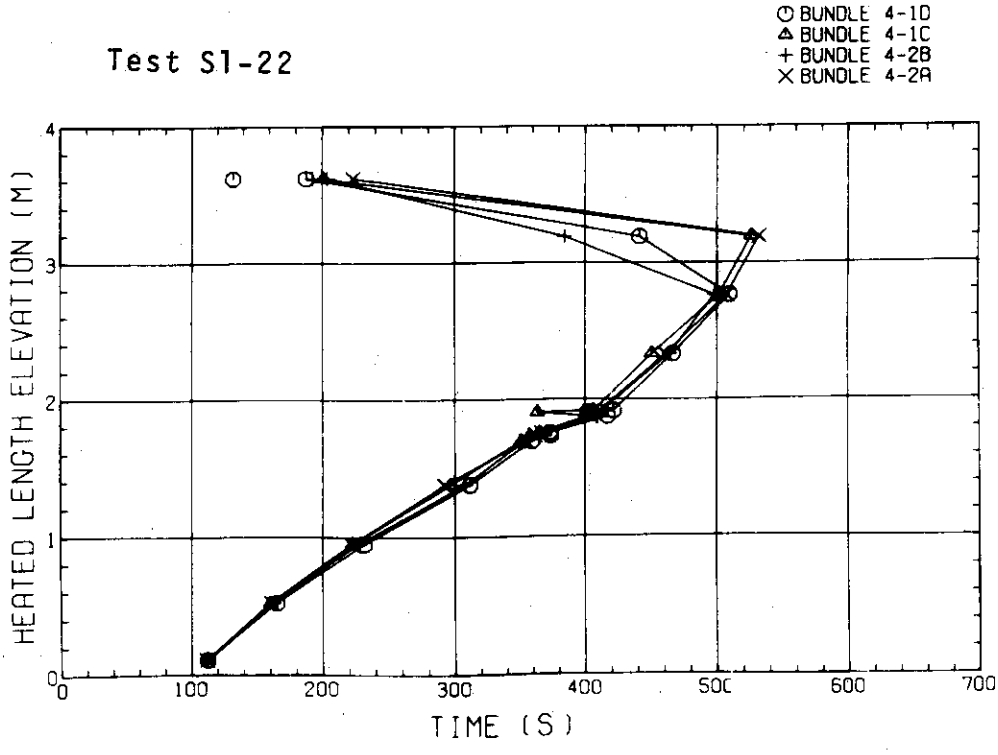

Fig. 3.31 QUENCH ENVELOPE OF BUNDLE 4
(PARALLEL TO WALLS)

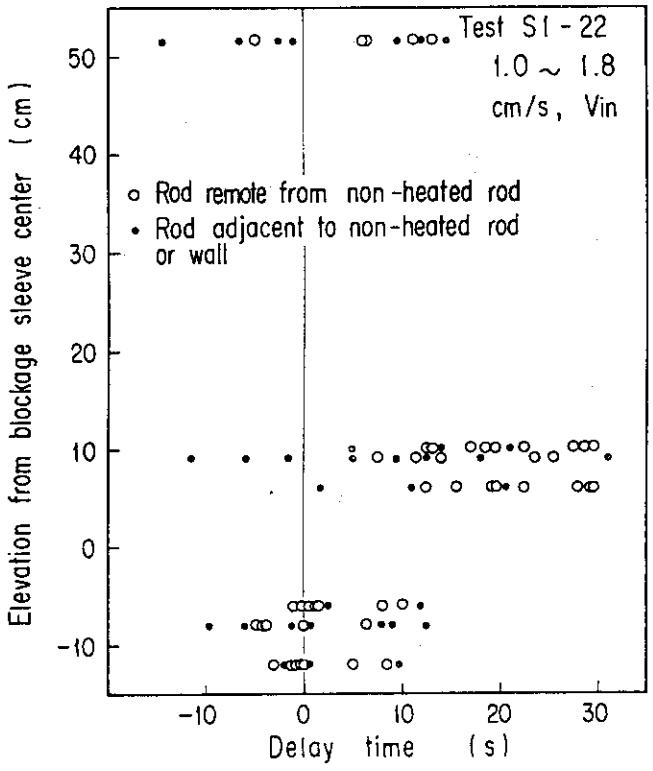

Fig. 3.32 Rod quench delay due to blockage in low ECC flow test

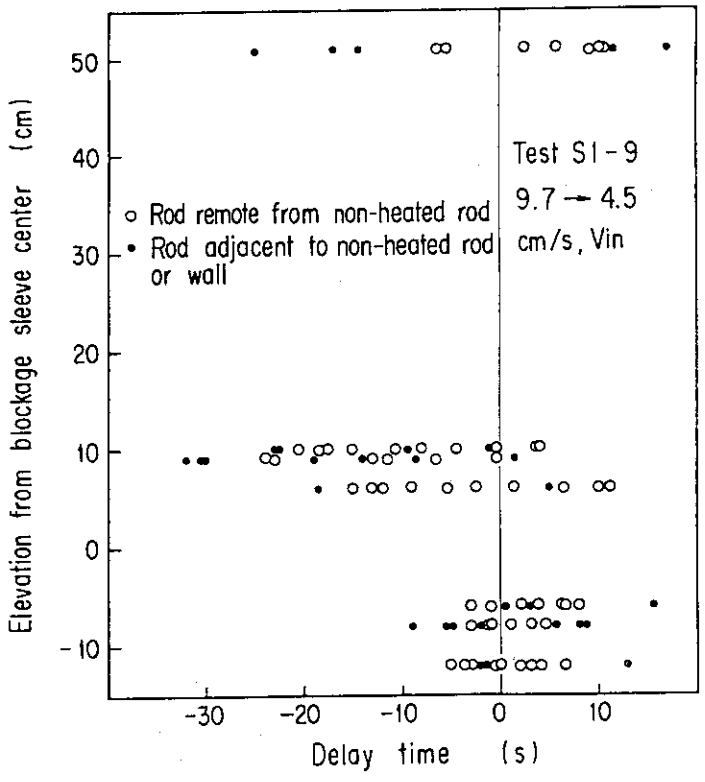

Fig. 3.33 Rod quench delay due to blockage in high ECC flow test

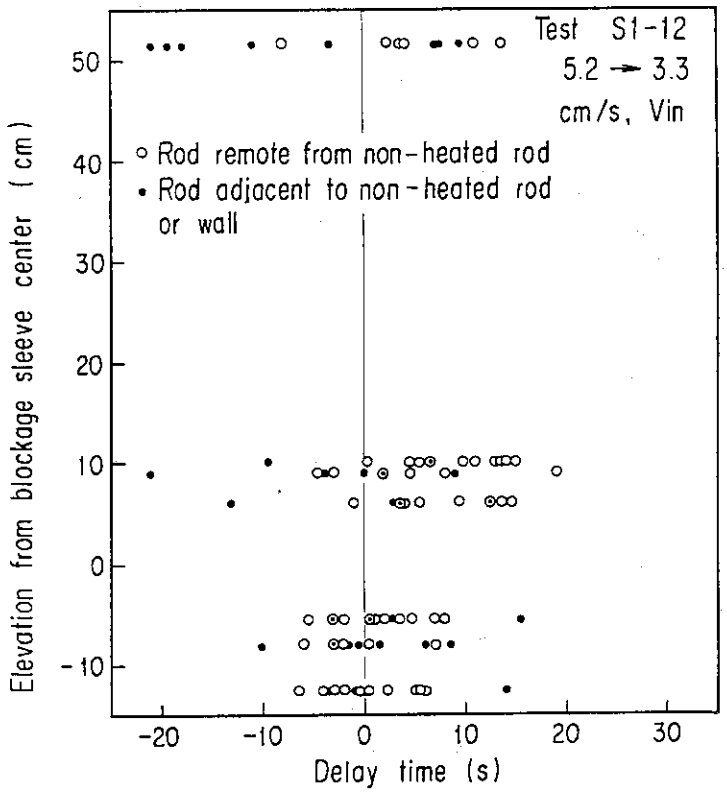

Fig. 3.34 Rod quench delay due to blockage in reference case of gravity feed test

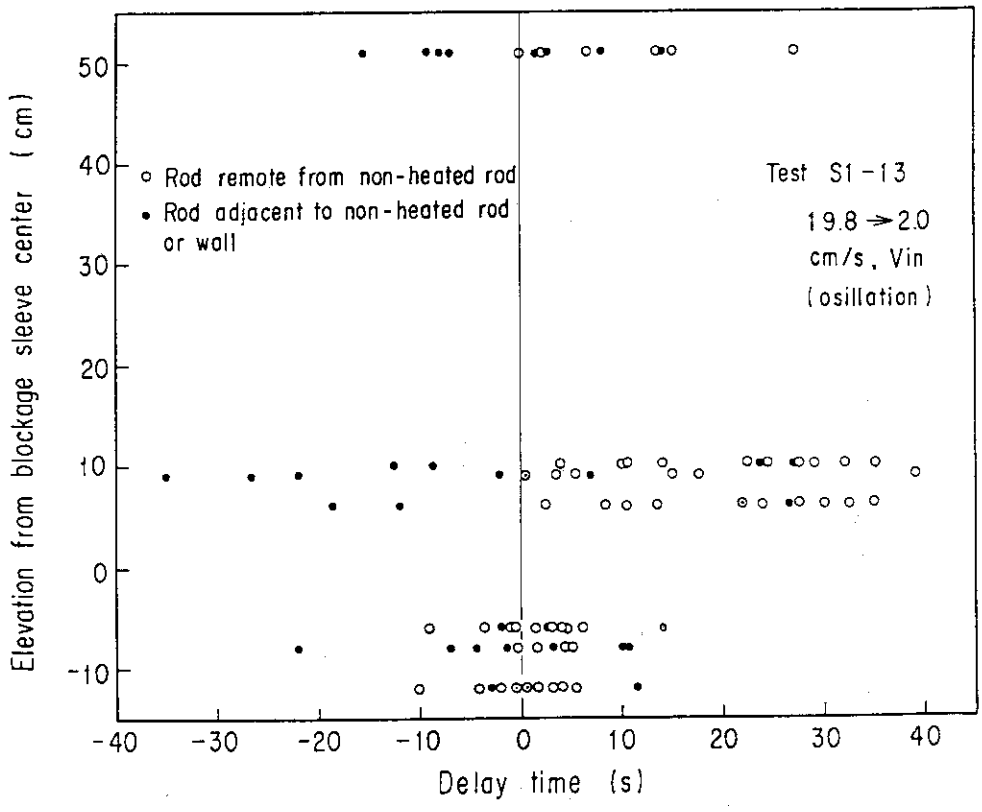

Fig. 3.35 Rod quench delay due to blockage in high Acc flow test

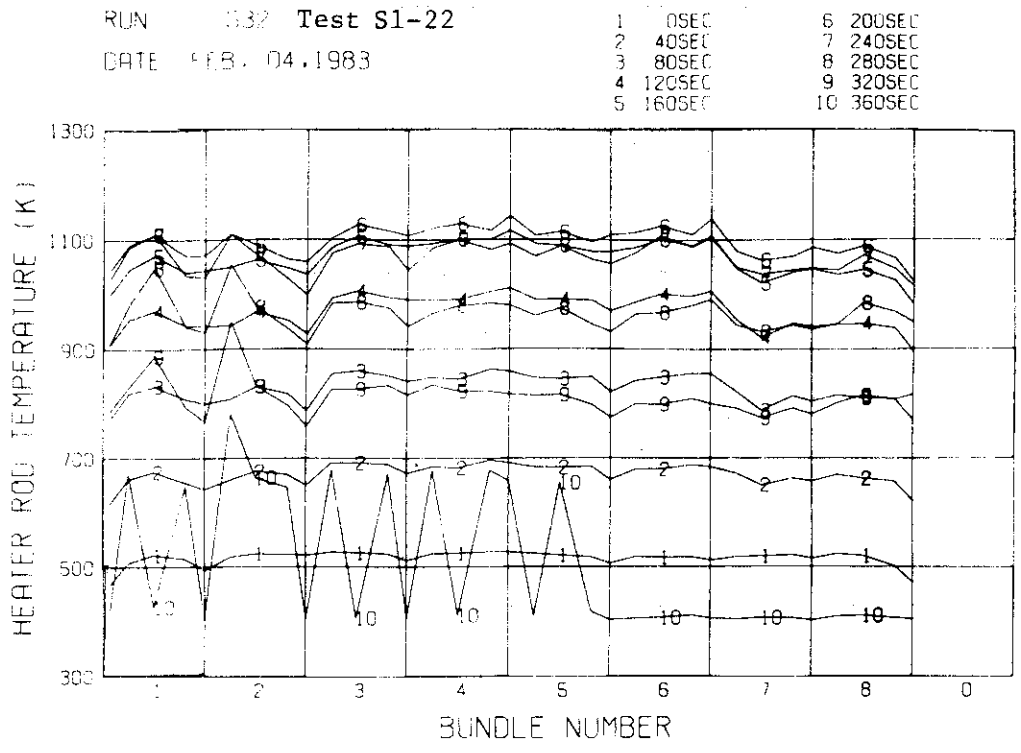

Fig. 3.36 HORIZONTAL CORE TEMPERATURE DISTRIBUTION ON VERTICAL MID PLANE (05 - 1.735M HEIGHT)

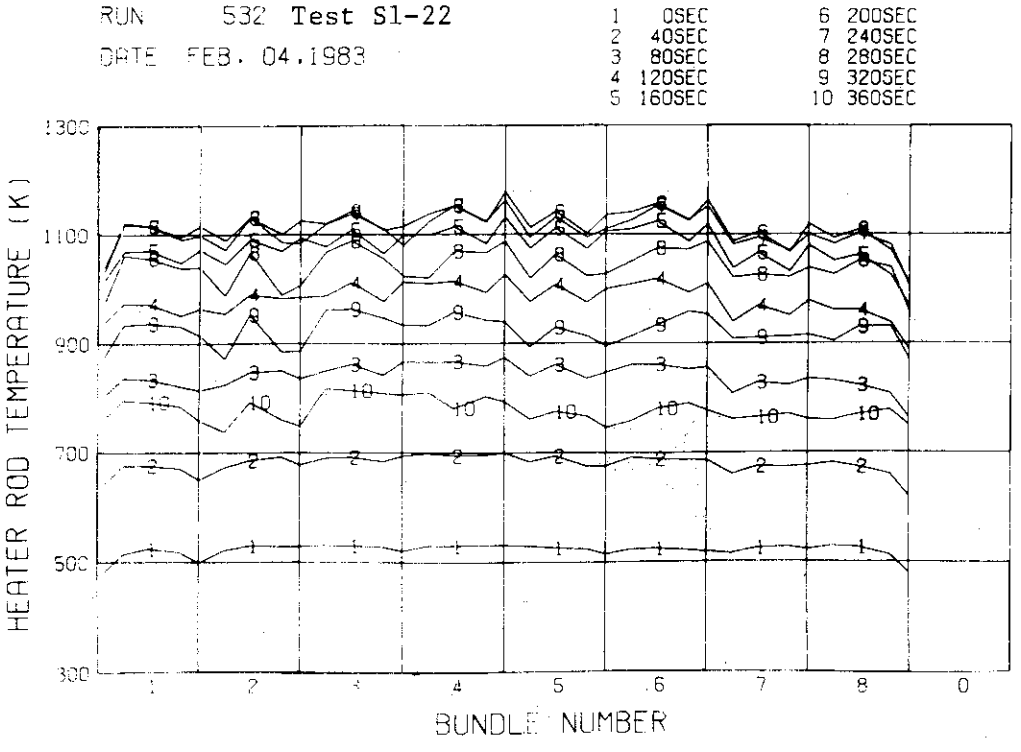

Fig. 3.37 HORIZONTAL CORE TEMPERATURE DISTRIBUTION ON VERTICAL MID PLANE (06 - 1.905M HEIGHT)

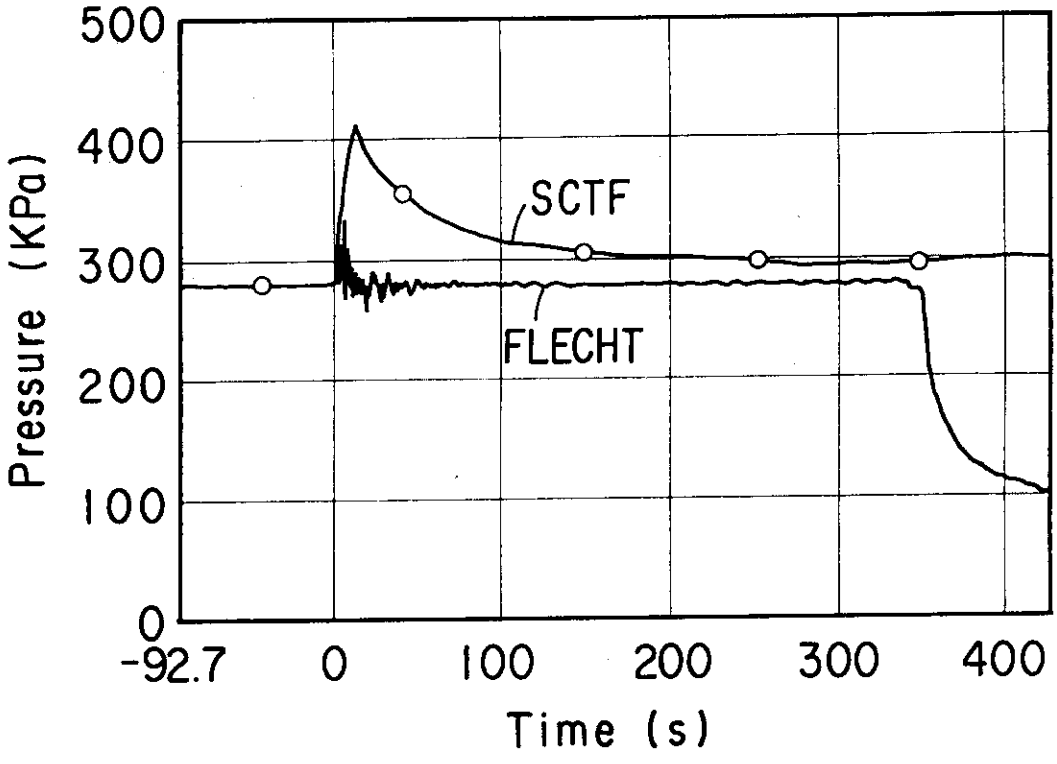

Fig. 3.38 Upper plenum pressure

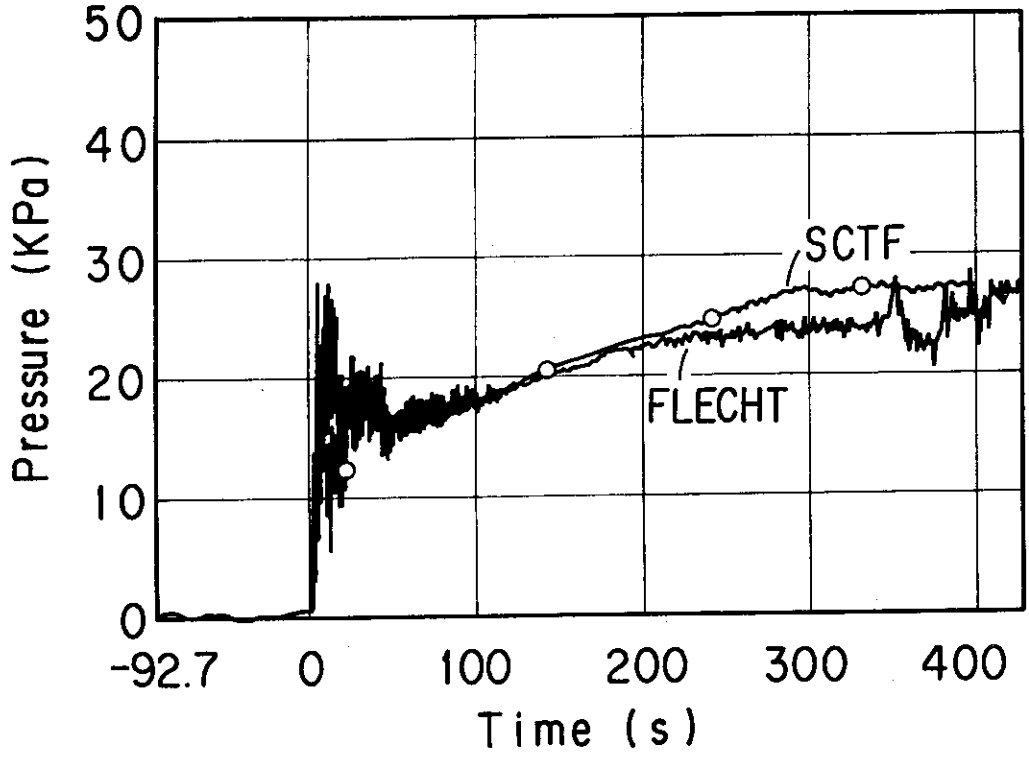

Fig. 3.39 Core full height DP

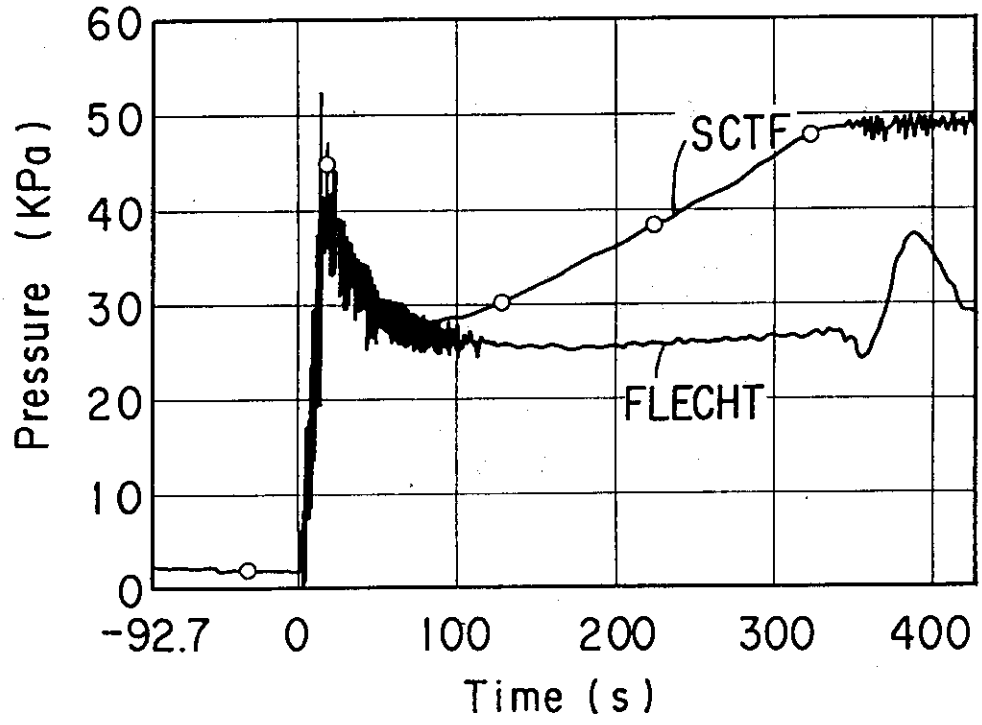

Fig. 3.40 Downcomer DP

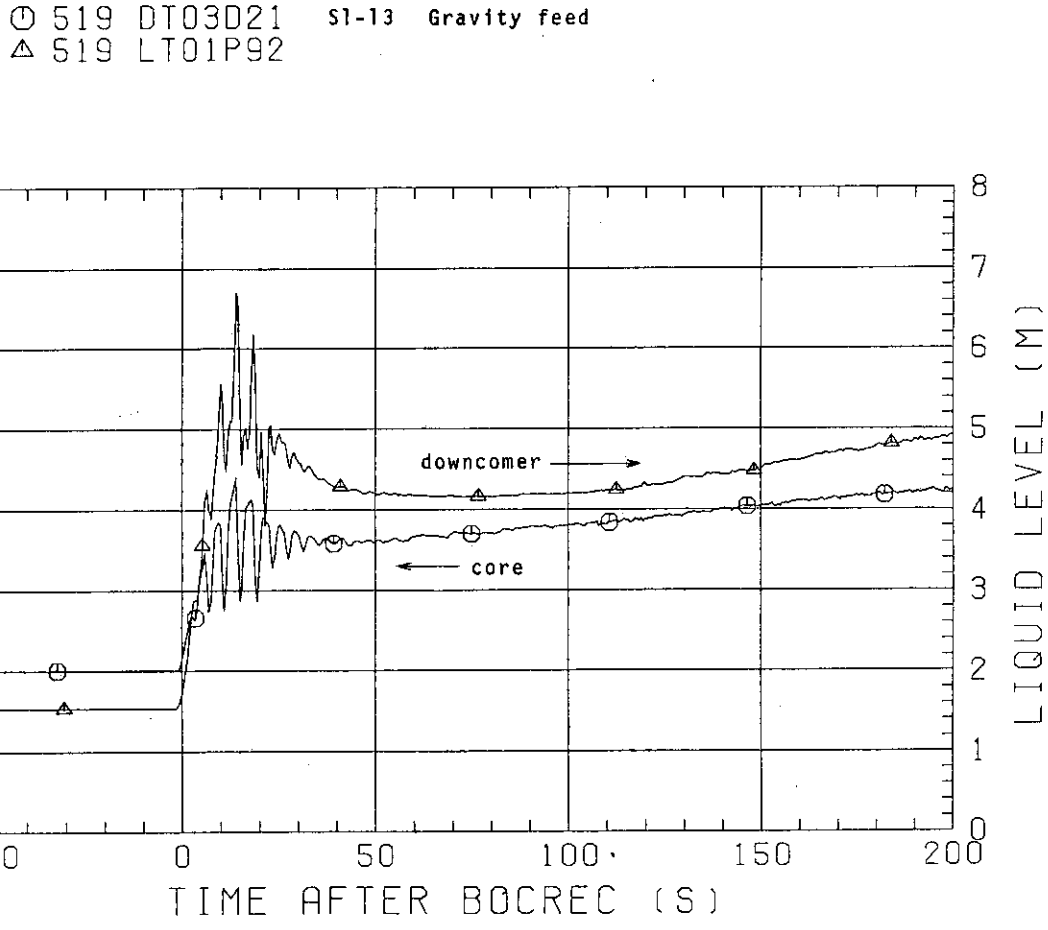

Fig. 3.41 Core full height DP and downcomer liquid level

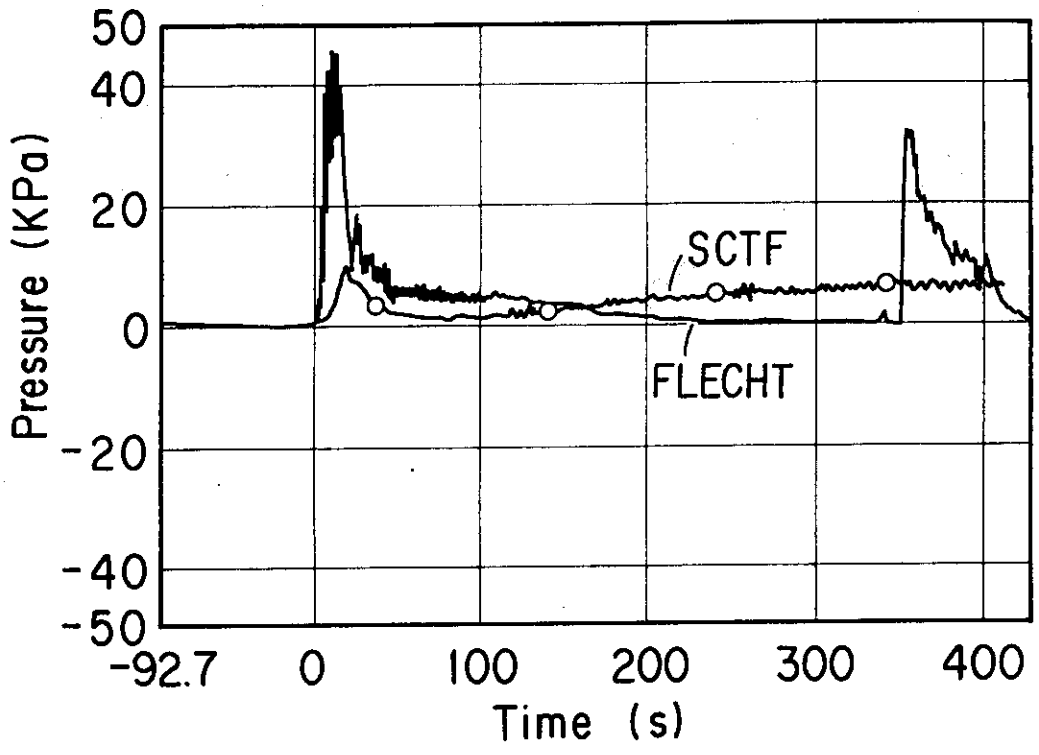

Fig. 3.42 DP, upper plenum - steam separator

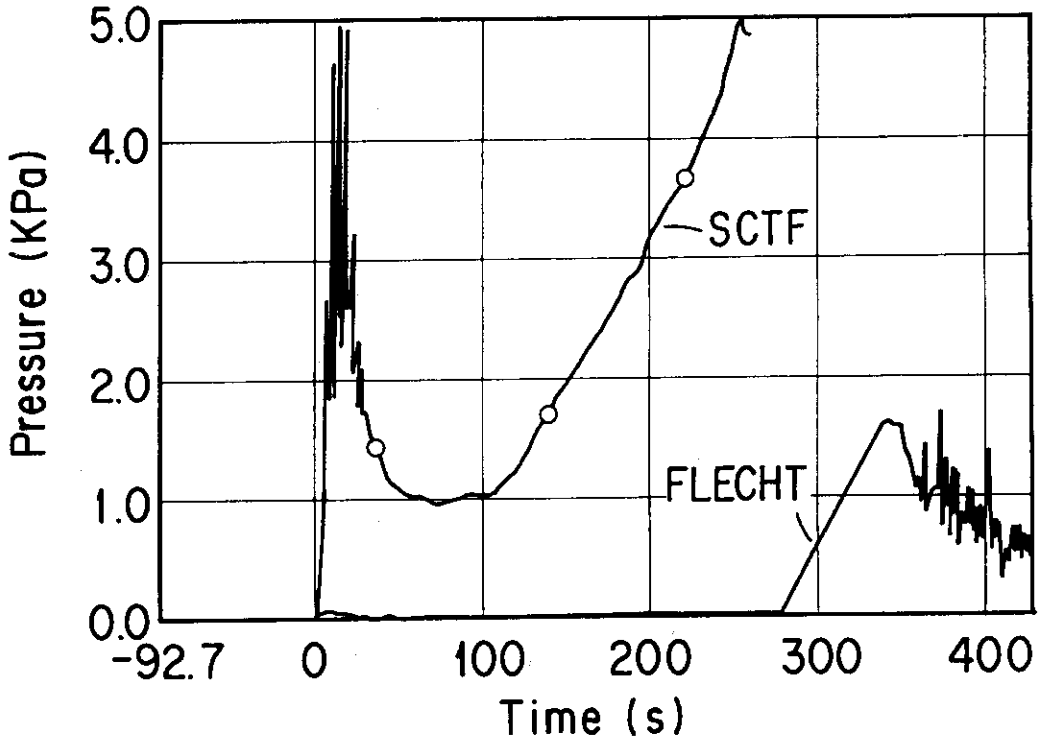

Fig. 3.43 Upper plenum DP

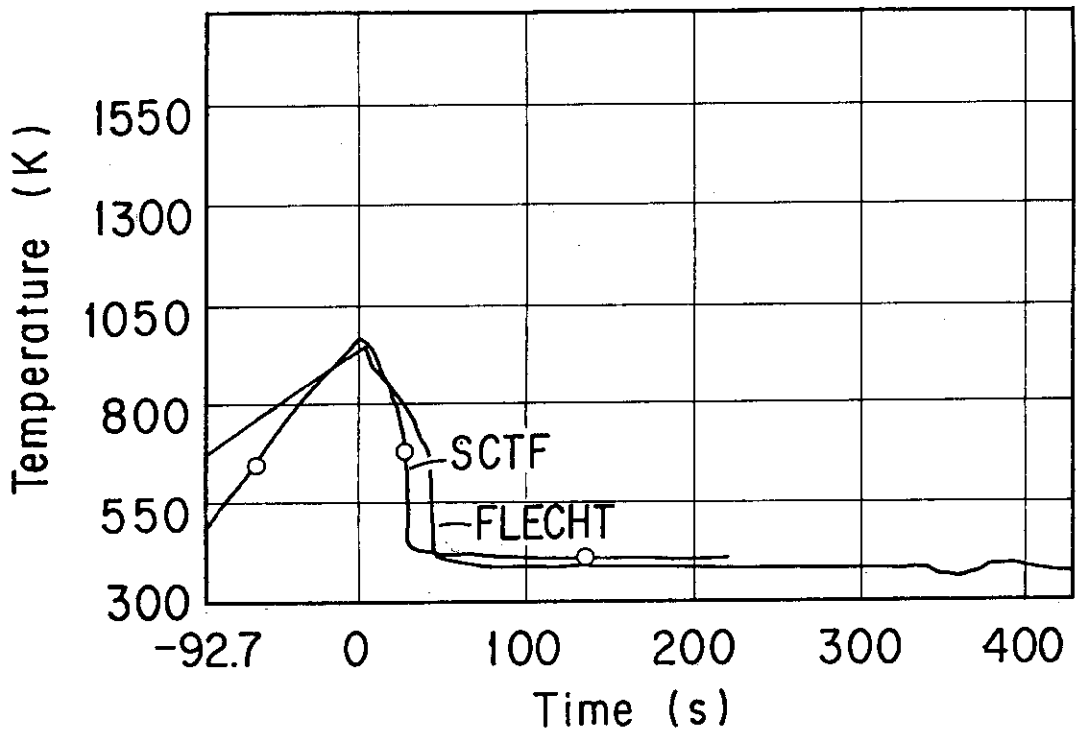

Fig. 3.44 Rod temperature at lower core (~ 0.9 m)

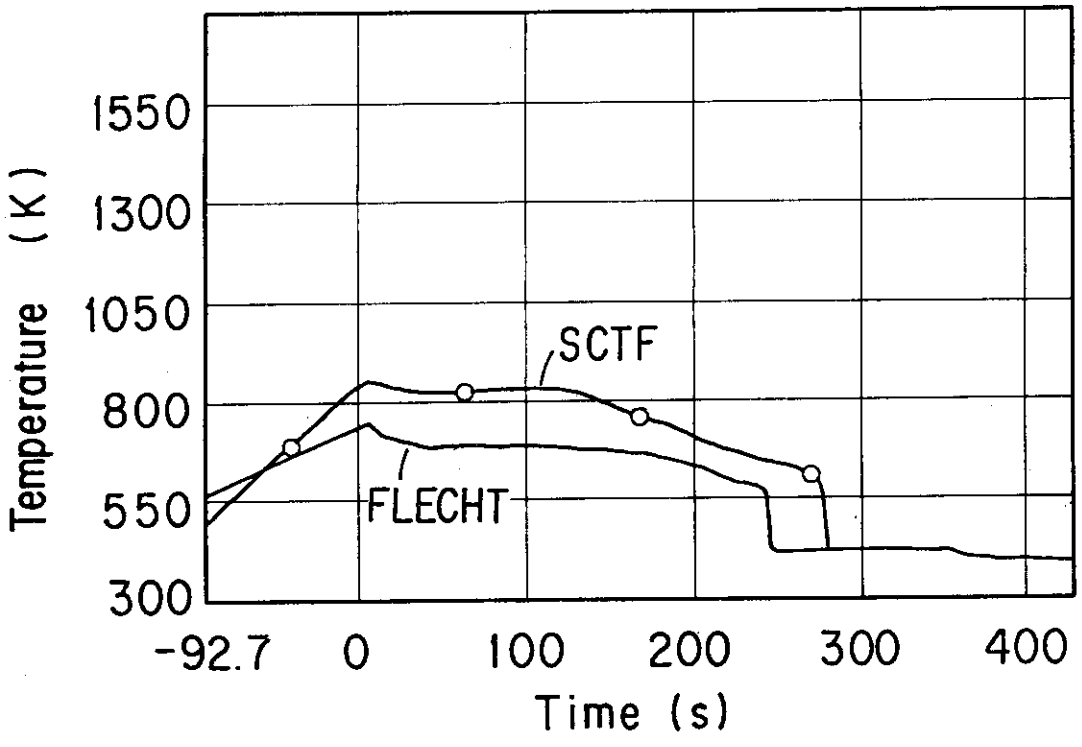

Fig. 3.45 Rod temperature at upper core (~ 3.1 m)

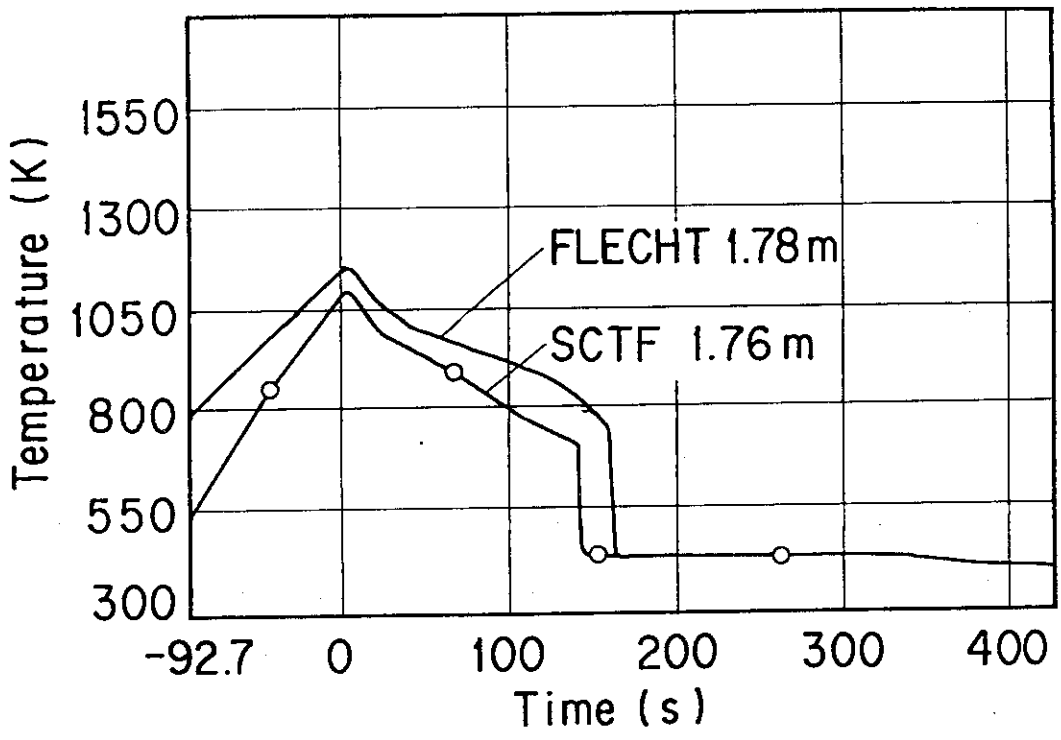

Fig. 3.46 Rod temperature just below the blockage

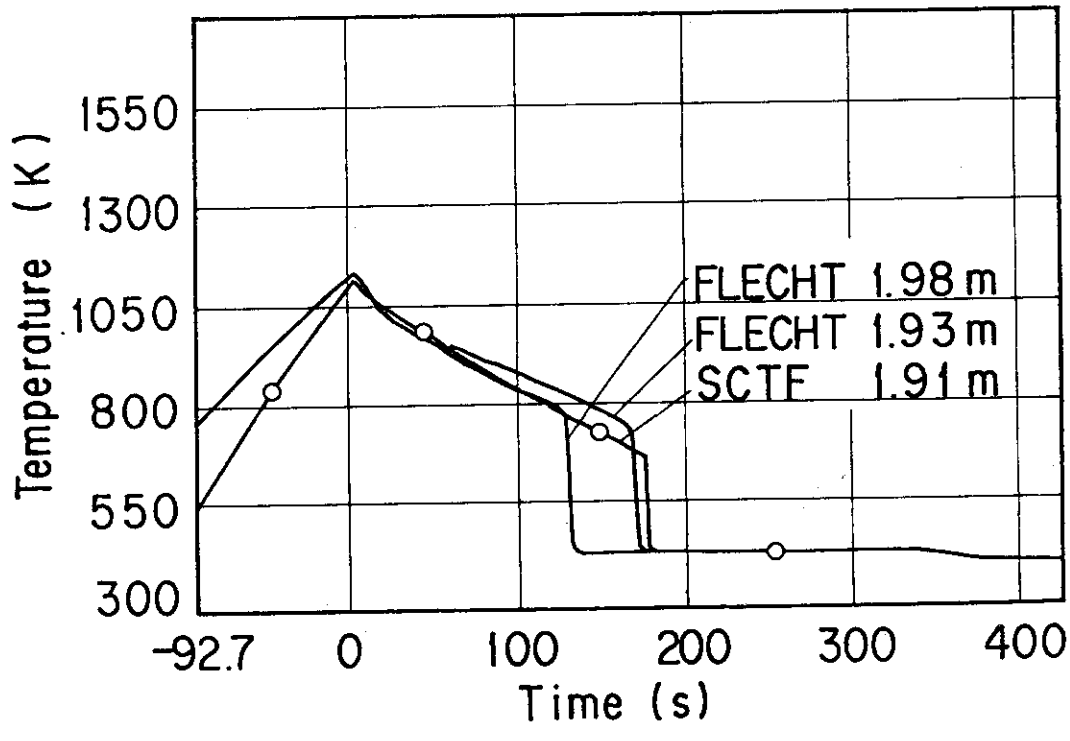

Fig. 3.47 Rod temperature just above the blockage

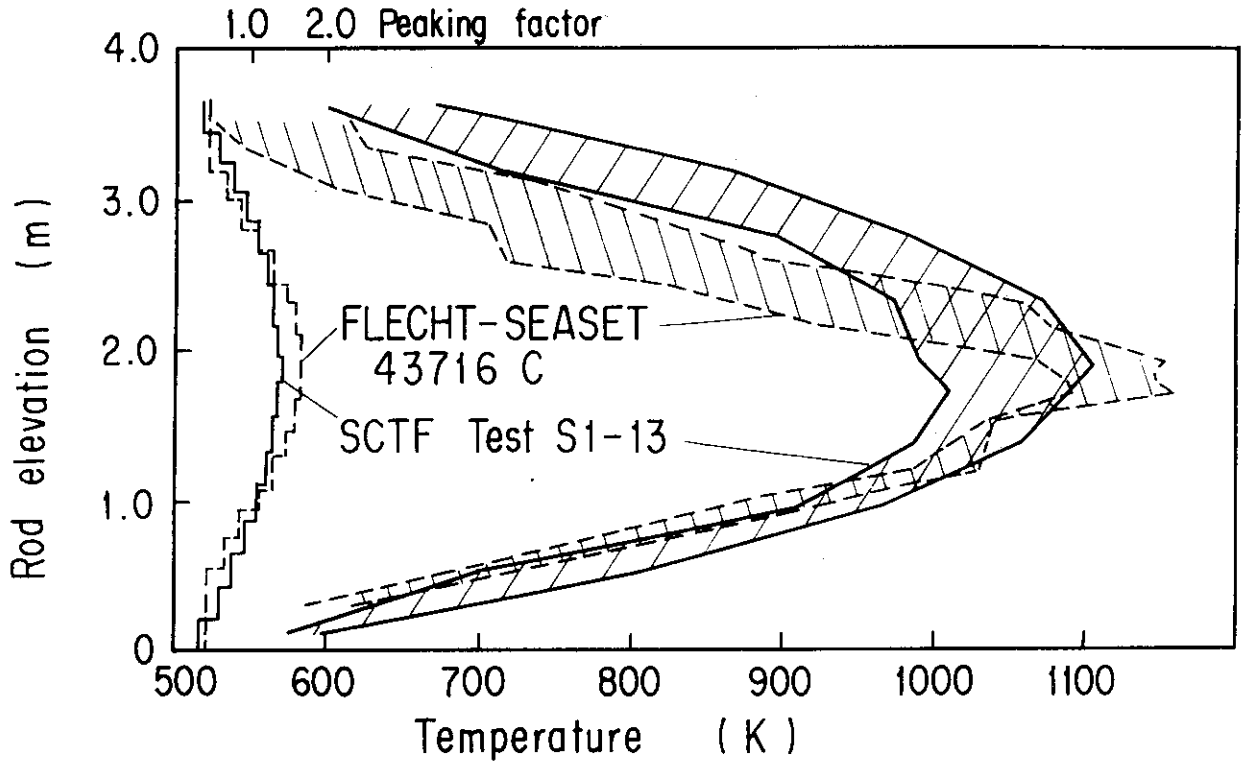

Fig. 3.48 Peak temperature distribution comparison for blockage bundle

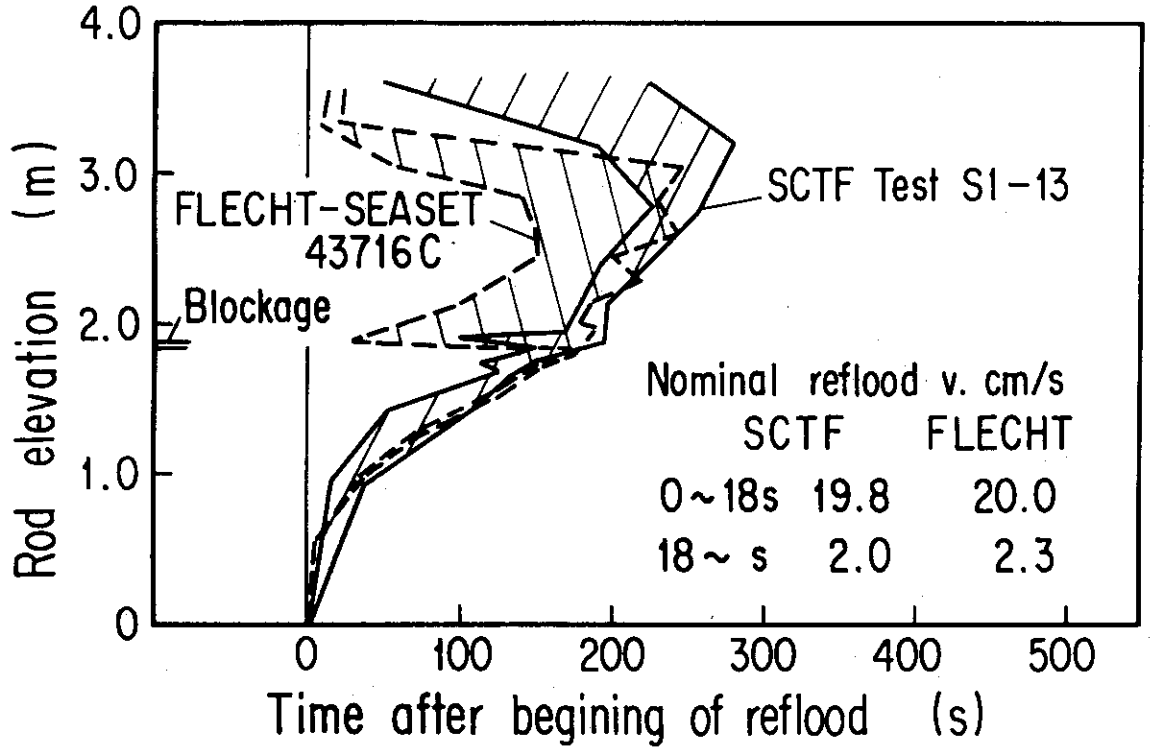

Fig. 3.49 Quench envelope comparison for blockage bundle in gravity feed tests

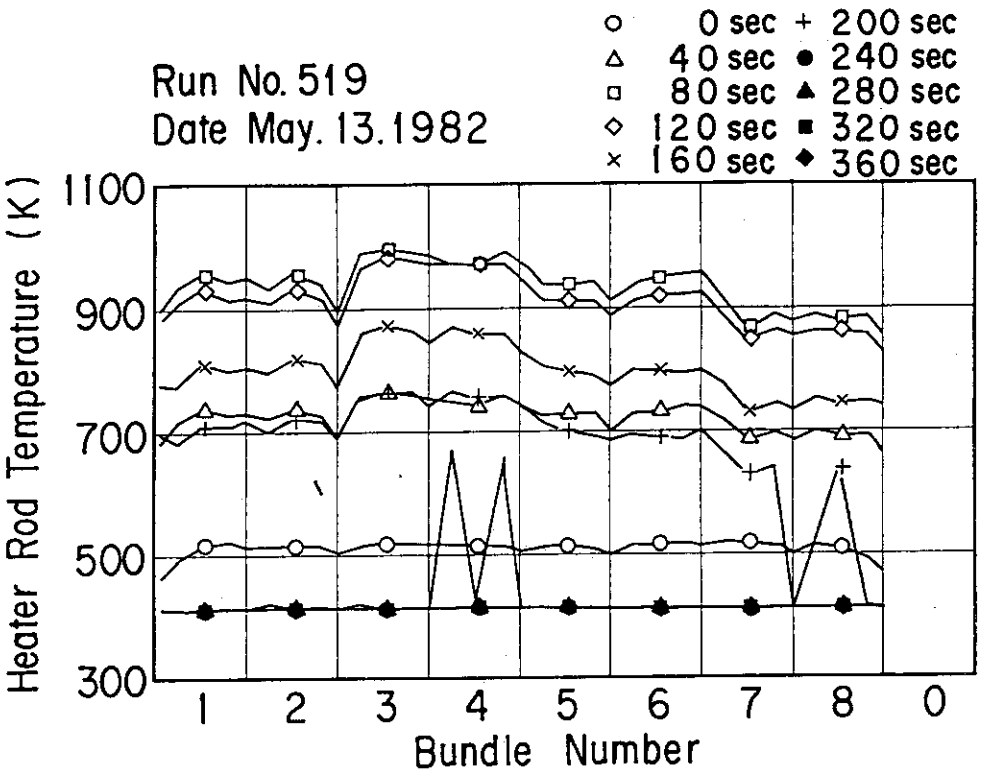

Fig. 3.50 Horizontal Core Temperature Distribution on Vertical Mid Plane (05 - 1.735 m Height)

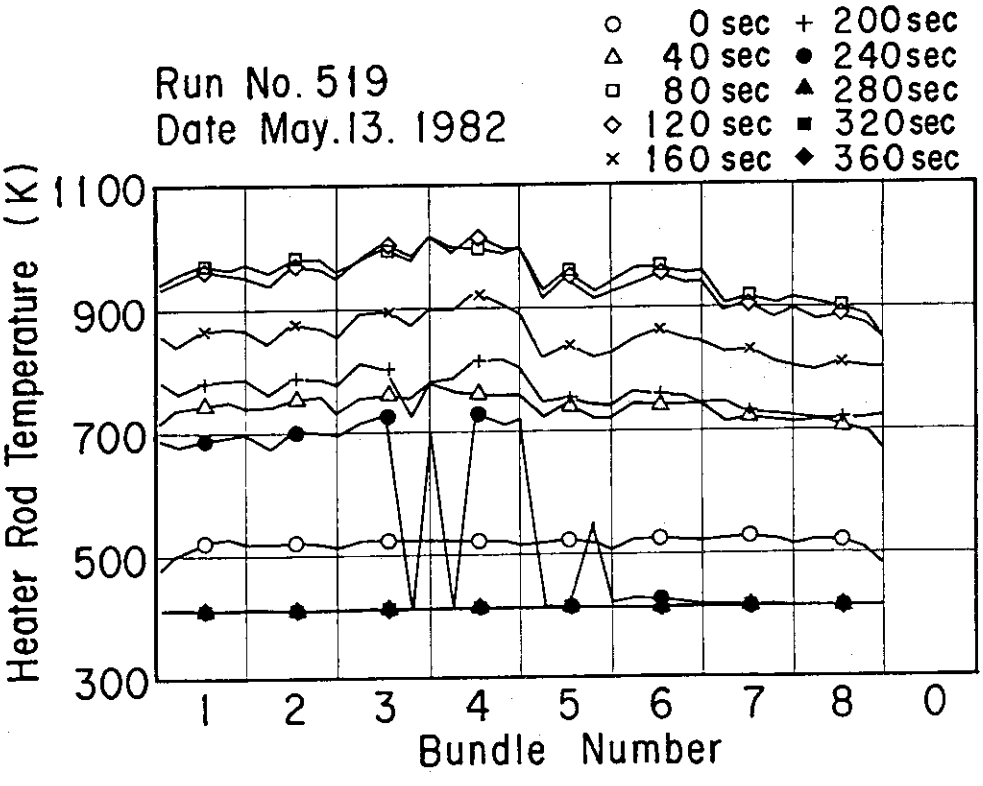

Fig. 3.51 Horizontal Core Temperature Distribution on Vertical Mid Plane (06 - 1.905 m Height)

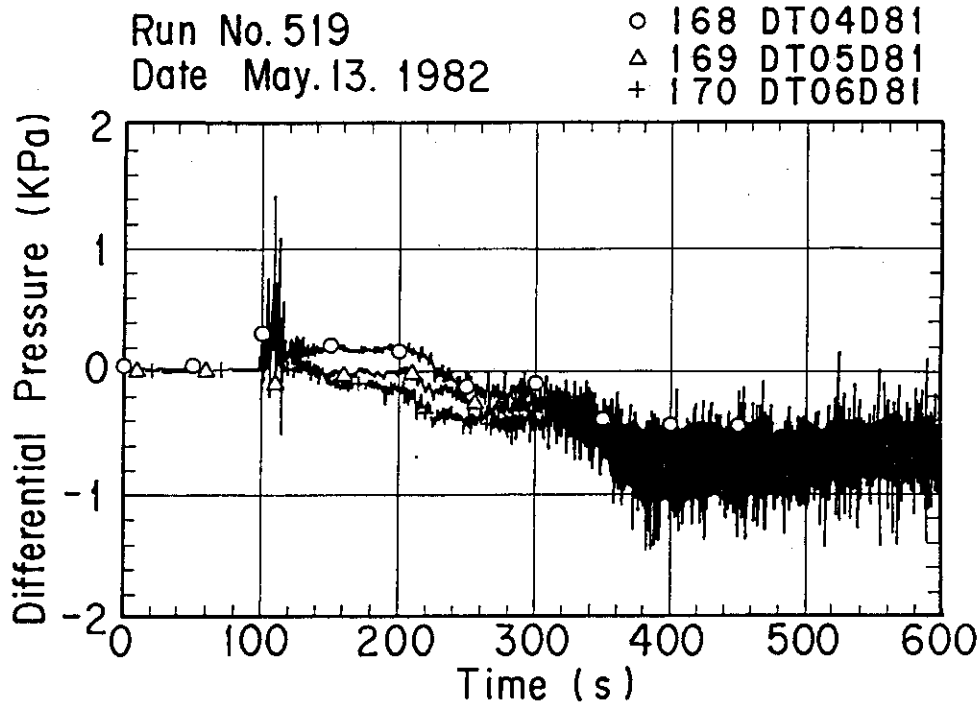

Fig. 3.52 Differential Pressure, Horizontal, Bundle 5 - 8 (04 - below Spacer 4, 05 - below Spacer 6, 06 - below End Box)

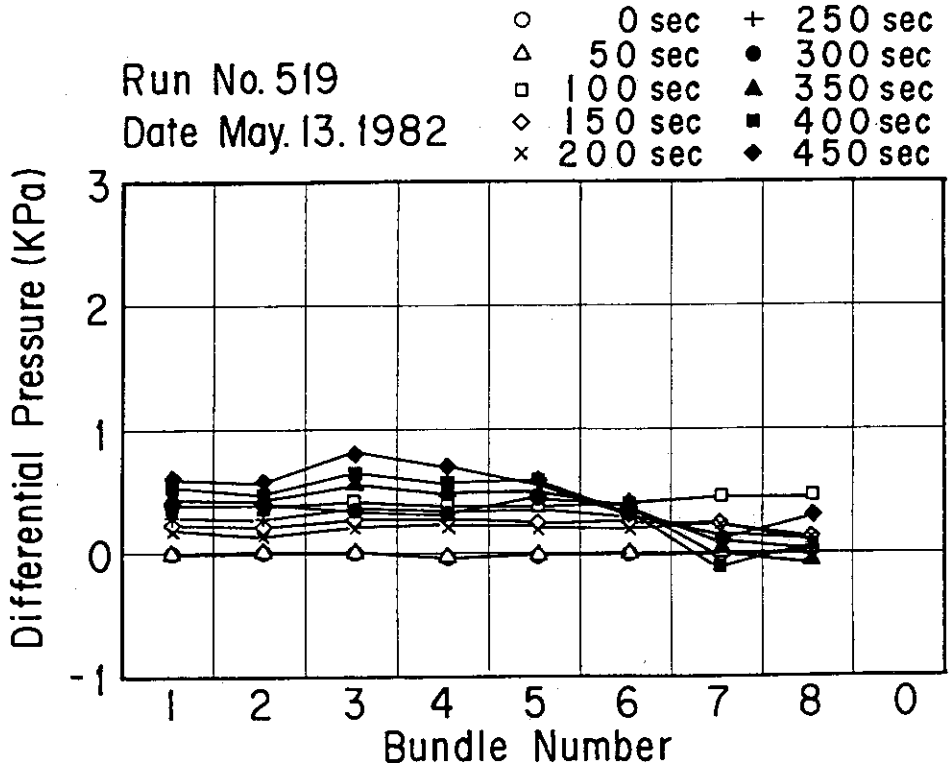

Fig. 3.53 Horizontal Distribution of Differential Pressure across End Box Tie Plate

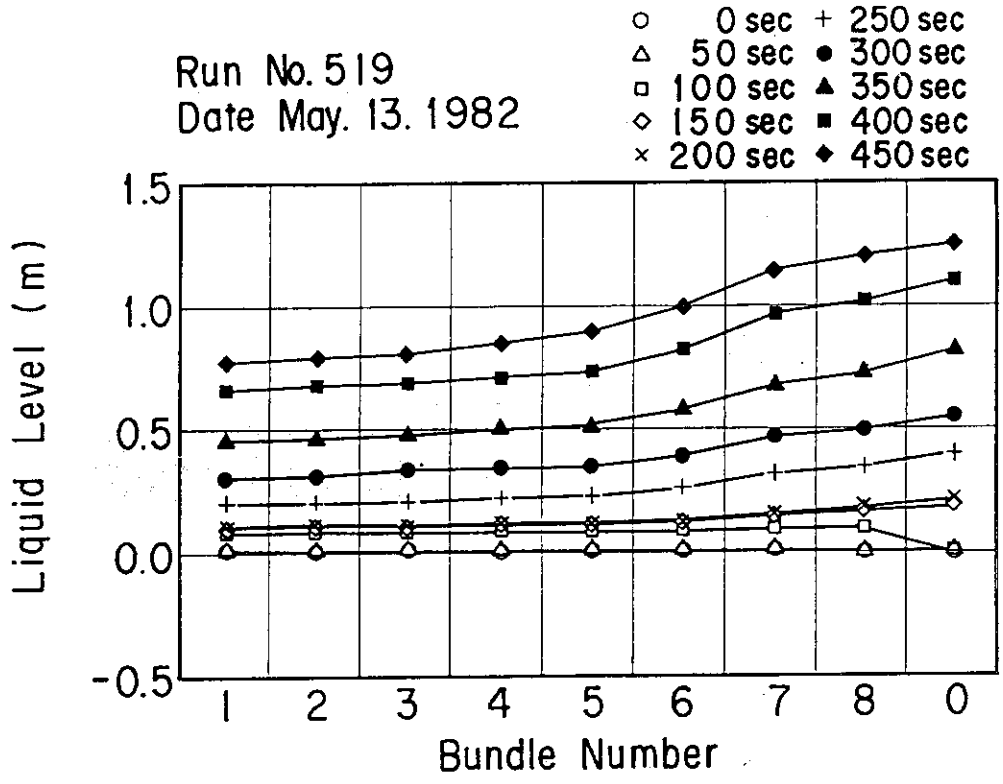

Fig. 3.54 Liquid Level Distribution above UCSP

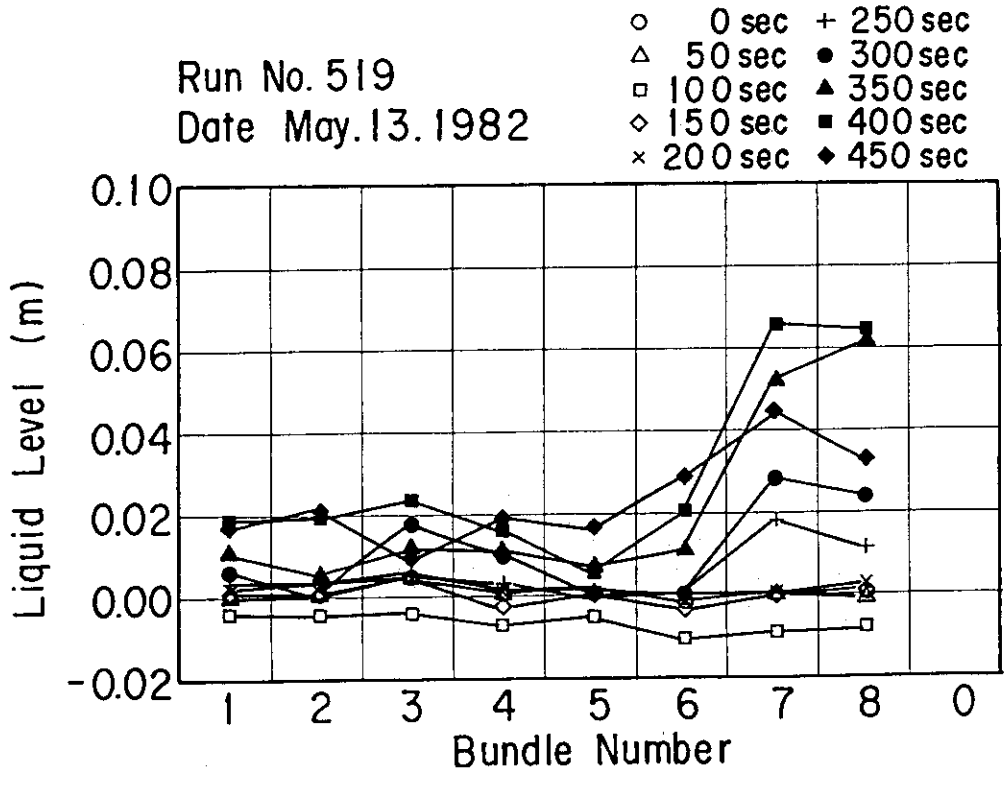

Fig. 3.55 Liquid Level Distribution above End Box Tie Plate

Appendix 1 Slab Core Test Facility (SCTF) Core-I

A.1 Test Facility

The Slab Core Test Facility[1] was designed under the following design philosophy and design criteria:

a. Design Philosophy

(1) The facility should provide the capability to study the two-dimensional, thermohydraulic behavior and core flow within the reactor vessel especially due to the radial power distribution during the end of blowdown, refill and reflood phases of a simulated LOCA for a pressurized water reactor.

(2) To properly simulate the core heat transfer and hydrodynamics, a special emphasis is put on the proper simulation of the components in the pressure vessel. Provided as the components in the pressure vessels are a simulated core, downcomer, core baffle region, lower plenum, upper plenum and upper head. On the other hand, simplified primary coolant loops are provided. Provided as the primary coolant loops are a hot leg, an intact cold leg, broken cold legs and a steam/water separator. The objective of the steam/water separator is to measure the flow rate of carryover water coming out of the upper plenum through the hot leg.

b. Design Criteria

(1) The reference reactor for simulation to the SCTF is the Trojan reactor in the United States which is a four loop 3300 MWt PWR. The Ooi reactor, etc. in Japan are also referred which are of similar type to the Trojan reactor.

(2) A full scale radial and axial section of a pressurized water reactor is provided as a simulated core of the SCTF with single bundle width.

(3) The simulated core consists of 8 bundles arranged in a row. Each bundle has electrically heated rods simulating fuel rods and non-heated rod with 16×16 array.

(4) The flow area and fluid volume of components are scaled down based on the core flow area scaling.

(5) To properly simulate the flow behavior of carryover water and entrainment, the elevations of hot leg and cold legs are designed so as to be the same as the PWRs as much as possible.

(6) The honeycomb structure is used as the side walls which accomodate

the slab core, the upper plenum and the upper part of lower plenum, so as to minimize the effect of walls on the disturbance of the core heat transfer and hydrodynamics.

(7) To investigate the effect of flow resistance in the primary loops are provided the orifices of which dimension is changeable.

(8) The maximum allowable temperature of the simulated fuel rods is 1900°C and the maximum allowable pressure of the facility is 6 kg/cm^2 absolute.

(9) The facility is provided with a hot leg equivalent to four actual hot legs connecting the upper plenum and the steam/water separator, an intact cold leg equivalent to three actual intact cold legs connecting the steam/water separator and the downcomer and two broken cold legs, one is for the steam/water separator side and the other for the pressure vessel side.

(10) The ECCS consists of an Acc, a LPCI and a combined injection systems.

(11) ECC water injection ports are the cold leg, hot leg, upper plenum, downcomer, lower plenum and above the upper core support plate. These portions are to be chosen according to the objective of the test.

(12) For better simulation of lower plenum flow resistance, simulated fuel rods do not penetrate through the bottom plate of the lower plenum but terminate below the bottom of the core.

(13) For measurements in the pressure vessel including core measurements, the feature of the slab geometry of the pressure vessel is utilized as much as possible. Design and arrangement of the instruments are done so as to be able to carry out installation,calibration and removal of the instruments.

(14) View windows are provided where flow pattern recognition is important. The locations are, the interface between the core and the upper plenum, hot leg, pressure vessel side broken cold leg and the downcomer.

(15) The blocked bundle test is carried out in Core-I in order to investigate the effect of the ballooned fuel rods, and the unblocked normal bundle test for the Core-II and -III.

(16) Simulated types of break are cold leg break and hot leg break.

(17) The components and systems such as the containment tanks and ECC water supply system in the CCTF are shared with the SCTF to the maximum extent.

The overall schematic diagram of the SCTF is shown in Fig.A-1. The principal dimensions of the facility is shown in Table A-1, and the comparison of dimensions between the SCTF and the referred PWR is shown in Fig.A-2.

A.1.1 Pressure Vessel and Internals

The pressure vessel is of slab geometry as shown in Fig.A-3. The height of the components in the pressure vessel is almost the same as the reference reactor's, and the flow area and the fluid volume of each component are scaled down based on the nominal core flow area scaling.

The core consists of 8 bundles in a row and each bundles include simulated fuel rods and non-heated rods with 16 × 16 array. The core arrangement for the SCTF Core-I is shown in Fig.A-4, which includes 6 normal bundles and 2 blocked bundles. The core is enveloped by the honeycomb thermal insulator which is attached on the barrel.

The downcomer is located at one end of the pressure vessel which corresponds to the periphery of the actual PWR. The core baffle region is, on the other hand, located between the core and the downcomer. For better understanding, the cross section of the pressure vessel at the elevation of midplane of the core is shown in Fig.A-5.

The design of upper plenum internals is based on that of the new Westinghouse 17 × 17 array fuel assemblies. The internals consist of control rod guide tubes, support columns, orifice plates and open holes and this arrangement is shown in Fig.A-6. The radius of each internal is scaled down by factor 8/15 from that of an actual reactor. Flow resistance baffles are inserted into the guide tubes. The elevation and the configuration of baffle plates are shown in Figs.A-7 and A-8.

The height of the hot leg and cold legs are designed as close to the actual PWR as possible. However, in order to avoid the interference of the nozzles in the downcomer, the height of nozzles for the broken cold leg and the intact cold leg are shifted down compared to that of the hot leg as shown in Fig.A-3.

A.1.2 Heater Rod Assembly

The heater rod assembly for the SCTF Core-I consists of 8 bundles arranged in a row. These bundles are composed of 6 normal unblocked bundles which are located at the 1st, 2nd and 5th to 8th bundles and 2 blocked bundles which are 3rd and 4th bundles as shown in Fig.A-4.

Each bundle has 234 electrically heated rods and 22 non-heated rods. The dimensions of the heater rods are based on a 15 × 15 fuel rod bundle, and the heated length and the outer diameter of each heater rod are 3.66 m and 10.7 mm, respectively. A heater rod consists of a nichrome heater element, magnesium oxide (MgO) and Nichrofer-7216 sheath (equialent to Inconel 600). The sheath wall thickness is about 1.0 mm and is thicker than the actual fuel cladding because of the requirements for thermocouple installation. The heating element is a helical coil and has a 17 step chopped cosine axial power profile as shown in Fig.A-9. The peaking factor is 1.4.

Non-heated rods are either stainless steel pipes or solid rods of 13.8 mm O.D. The heater rods and non-heated rods are fixed at the top of the core allowing the rods to move downward when the thermal expansion occurs. In Fig.A-10 the axial position where blockage sleeves for simulating the ballooned fuel rod are equipped is shown. The blockage sleeves consist of three types of sleeve, one is used for the rods at the corner adjacent to the adjacent blocked bundle, another for the rods adjacent to the side walls and the third for the rods except for the periphery of the blocked bundle. These are named A, B and C respectively in the Fig.A-11 and the configurations for these are shown in Fig.A-12.

For better simulation for flow resistance in the lower plenum,the simulated rods do not penetrate through the bottom plate of the lower plenum as shown in Fig.A-10.

A.1.3 Primary Loops and ECCS.

Primary loops consist of a hot leg equivalent to the four actual hot legs, a steam/water separator for measuring the flow rate of carry over water, an intact cold leg equivalent to the three actual intact loops, a broken cold leg on the pressure vessel side and a broken cold leg on the steam water separator side. These two broken cold legs are connected with two containment tanks through break valves, respectively. The arrangement of the primary loops is shown in Fig.A-13. The flow area of each loop is scaled down based on the core flow area scaling. It should be emphasized that the cross section of the hot leg is an elongated circle to realize the proper flow pattern in the hot leg. The steam/water separator has a steam generator inlet plenum simulator to realize the flow characteristics of carryover water. The cross section of the hot leg and the configuration of the steam generator inlet plenum simulator

are shown in Fig.A-14.

A pump simulator and a loop seal part are provided for the intact cold leg. The arrangement of the intact cold leg is shown in Fig.A-15. The pump simulator consists of the casing and duct simulators and an orifice plate as shown in Fig.A-16. The loop resistance is adjusted with the orifice plates attached to the broken cold legs, the intact cold leg and the pump simulator.

In principle, ECCS consists of an accumulator and a low pressure injection system. The injection port is located as already described in the design criteria. Besides, the UCSP extraction system is provided and the UCSP water injection and extraction systems will be used for combined injection tests.

A.1.4 Containment Tanks and Auxiliary System

Two containment tanks are provided to the SCTF. The containment tank-I is connected with the downcomer through the pressure vessel side broken cold leg and the containment tank-II is connected with the steam/water separator through the steam/water separator side broken cold leg. Especially in the containment tank-I, carryover water from the downcomer is measured by phase separation. These containment tanks and auxiliary system such as a pressurizer for injecting water from the Acc tank, etc. are shared with the CCTF.

A.2 Instrumentation

The instrumentation in the SCTF has been provided both by JAERI and the USNRC. The JAERI-provided instrumentation includes the measurement of temperatures, pressures, differential pressures, liquid levels, flow velocities, and heating powers. The USNRC has provided film probes, impedance probes, string probes, liquid level detectors (LLDs), fluid distribution grids (FDGs), turbine meters, drag disks, γ-densitometers, spool pieces and video optical probes. The measurement items of the JAERI- and USNRC-provided instruments are listed in Tables A-2 and A-3, respectively. Detailed information on the instrumentation of the SCTF is available in reference (1).

Table A-1 Principal Dimensions of Test Facility

1. Core Dimension	
(1) Quantity of Bundle	8 Bundles
(2) Bundle Array	1 × 8
(3) Bundle Pitch	230 mm
(4) Rod Array in a Bundle	16 × 16
(5) Rod Pitch in a Bundle	14.3 mm
(6) Quantity of Heater Rod in a Bundle	234 rods
(7) Quantity of Non-Heated Rod in a Bundle	22 rods
(8) Total Quantity of Heater Rods	234 × 8 = 1872 rods
(9) Total Quantity of Non-Heated Rods	22 × 8 = 176 rods
(10) Effective Heated Length of Heater Rod	3660 mm
(11) Diameter of Heater Rod	10.7 mm
(12) Diameter of Non-Heateed Rod	13.8 mm
2. Flow Area & Fluid Volume	
(1) Core Flow Area* (nominal)	0.227 m^2
(2) Core Fluid Volume	0.92 m^3
(3) Baffle Region Flow Area	0.10 m^2
(4) Baffle Region Fluid Volume	0.36 m^3
(5) Downcomer Flow Area	0.121 m^2
(6) Upper Annulus Flow Area	0.158 m^2
(7) Upper Plenum Horizontal Flow Area	0.525 m^2
(8) Upper Plenum Fluid Volume	1.16 m^2
(9) Upper Head Fluid Volume	0.86 m^3
(10) Lower Plenum Fluid Volume	1.38 m^3
(11) Steam Generator Inlet Plenum Simulator Flow Area	0.626 m^2
(12) Steam Generator Inlet Plenum Simulator Fluid Volume	0.931 m^3
(13) Steam Water Separator Fluid Volume	5.3 m^3
(14) Flow Area at the Top Plate of Steam Generator Inlet Plenum Simulator	0.195 m^2
(15) Hot Leg Flow Area	0.0826 m^2
(16) Intact Cold Leg Flow Area (Diameter = 297.9 mm)	0.0697 m^2
(17) Broken Cold Leg Flow Area (Diameter = 151.0 mm)	0.0179 m^2

* Flow area in the core is 0.35 m^2, including the excess flow area of gaps between the bundle and the surface of thermal insulator and between the core barrel and the pressure vessel wall.

(18) Containment Tank I Fluid Volume	30 m^3
(19) Containment Tank II Fluid Volume	50 m^3

3. Elevation & Height

(1) Top Surface of Upper Core Support Plate (UCSP)	0 mm
(2) Bottom Surface of UCSP	-76 mm
(3) Top of the Effective Heated Length of Heater Rod	-393 mm
(4) Bottom of the Skirt in the Lower Plenum	-5270 mm
(5) Bottom of Intact Cold Leg	+724 mm
(6) Bottom of Hot Leg	+1050 mm
(7) Top of Upper Plenum	+2200 mm
(8) Bottom of Steam Generator Inlet Plenum Simulator	+1933 mm
(9) Centerline of Loop Seal Bottom	-2281 mm
(10) Bottom Surface of End Box	- 185.1 mm
(11) Top of the Upper Annulus	+2234 mm
(12) Height of Steam Generator Inlet Plenum Simulator	1595 mm
(13) Height of Loop Seal	3140 mm
(14) Inner Height of Hot Leg Pipe	737 mm
(15) Bottom of Lower Plenum	-5770 mm
(16) Top of Upper Head	+2887 mm

TABLE A-2 Description of Tag-ID Number (In-Core)

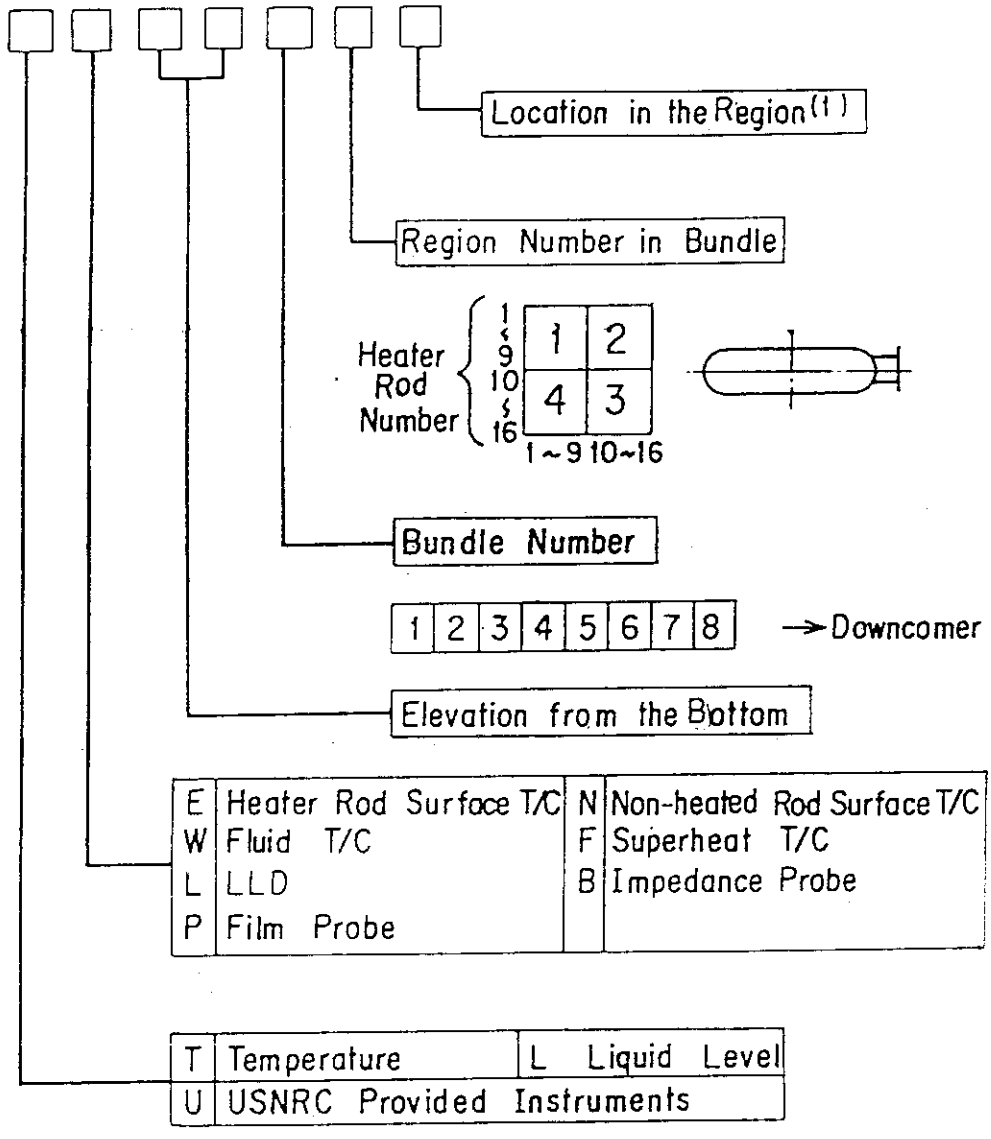

Note : (1) for Heater Rod T/C

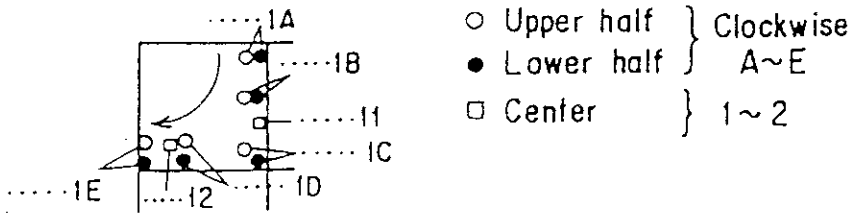

TABLE A-3 Description of Tag-ID Number
(Pressure Vessel Except Core)

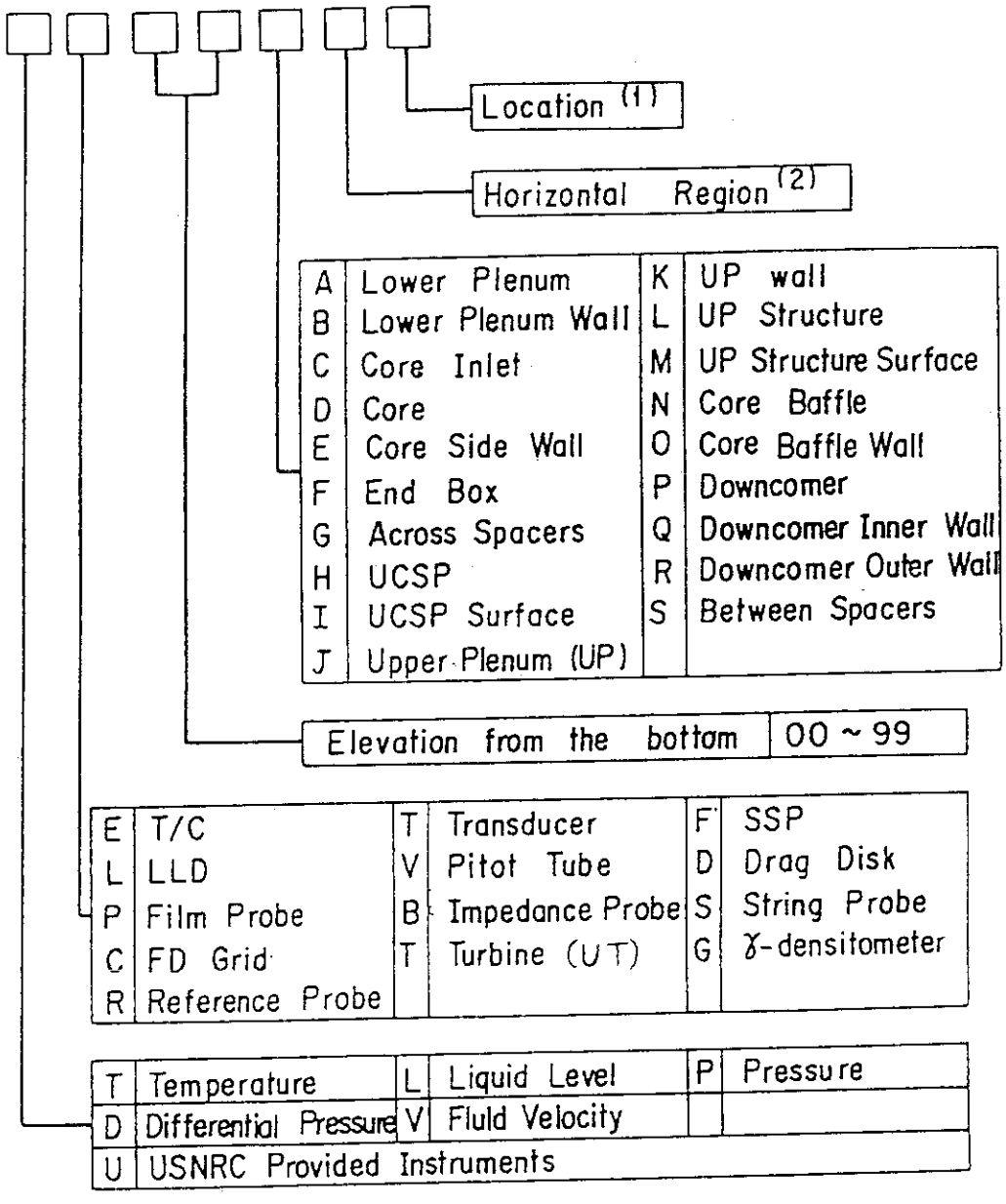

Note

(1)

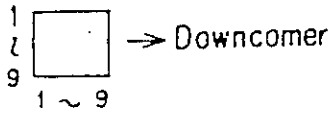

(2)

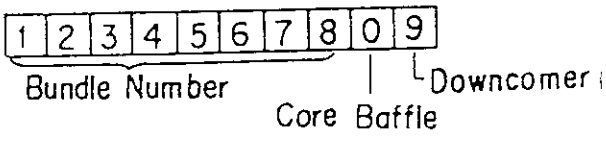

TABLE A-4 Description of Tag-ID Number
(Except Pressure Vessel)

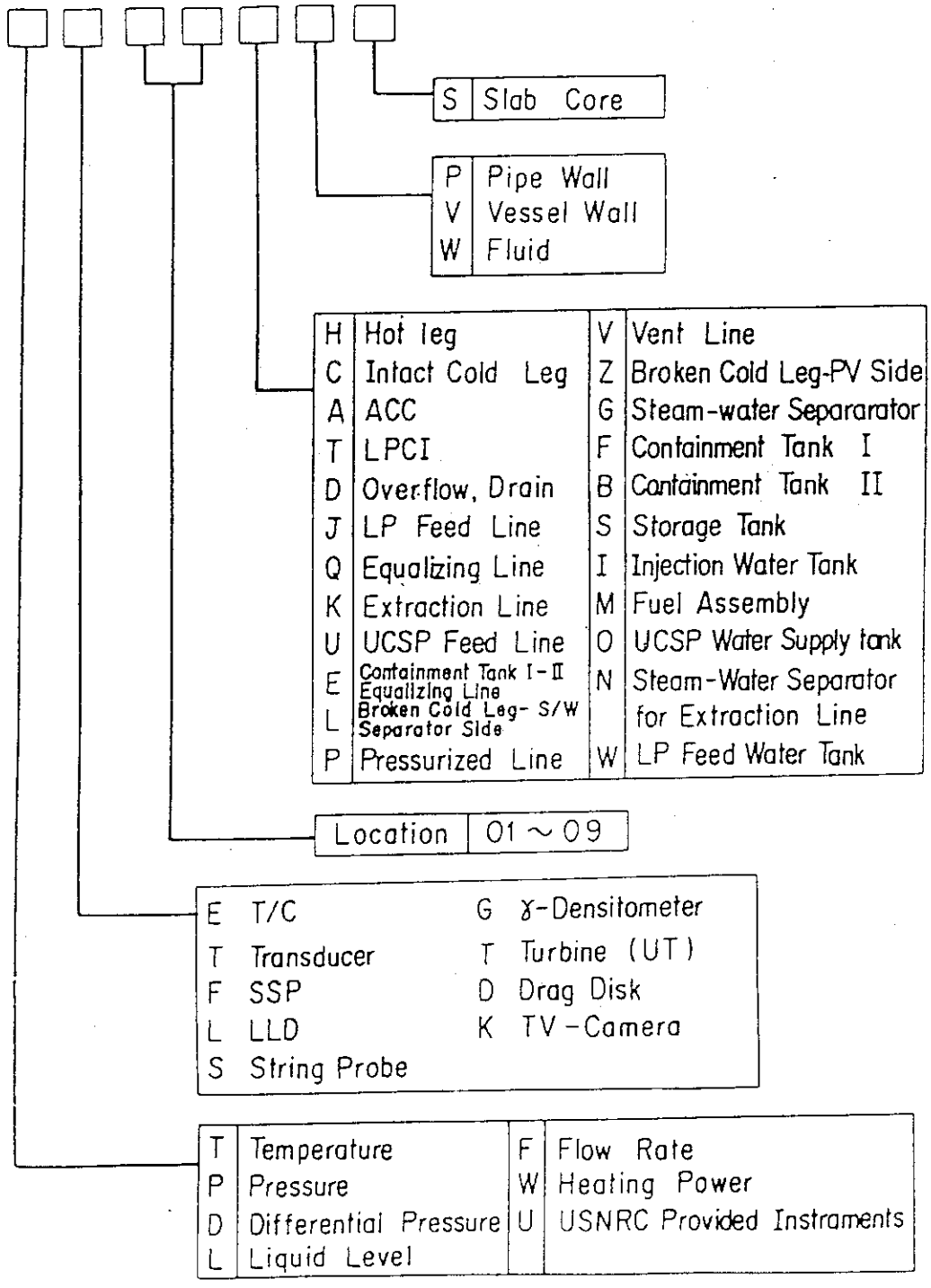

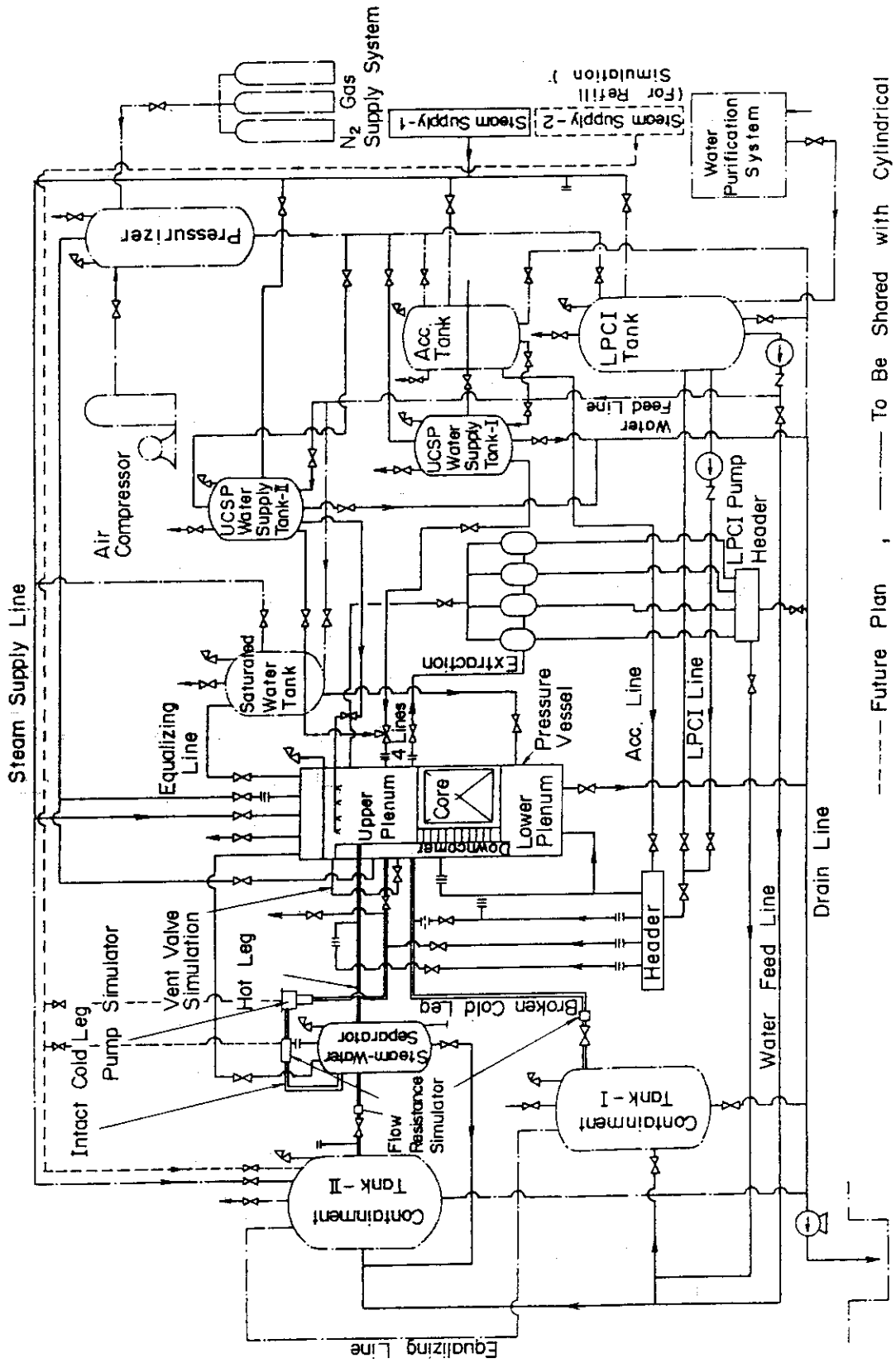

Fig. A-1 Schematic Diagram of Slab Core Test Facility

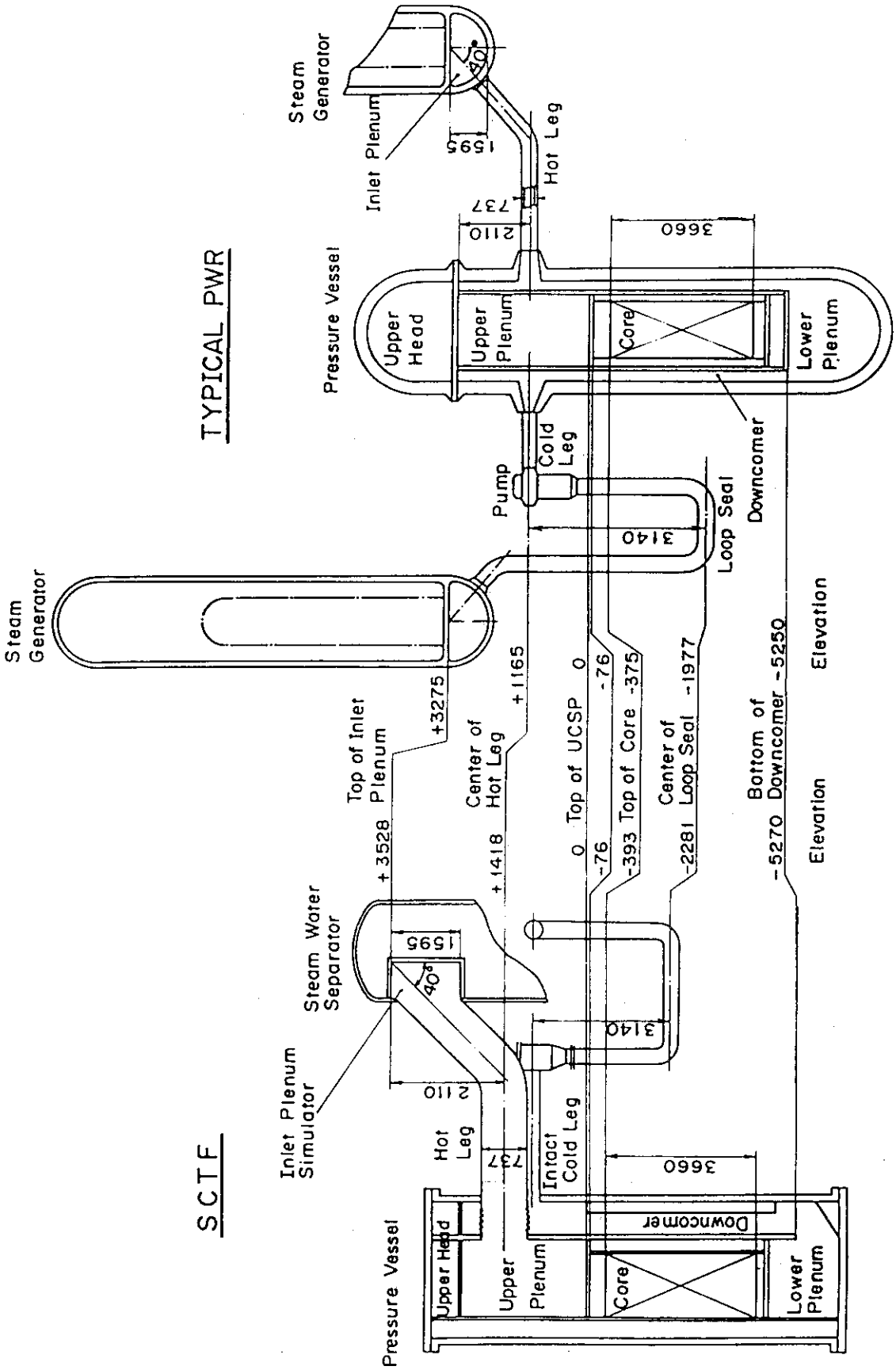

Fig. A-2 Comparison of Dimensions between SCTF and a Reference PWR

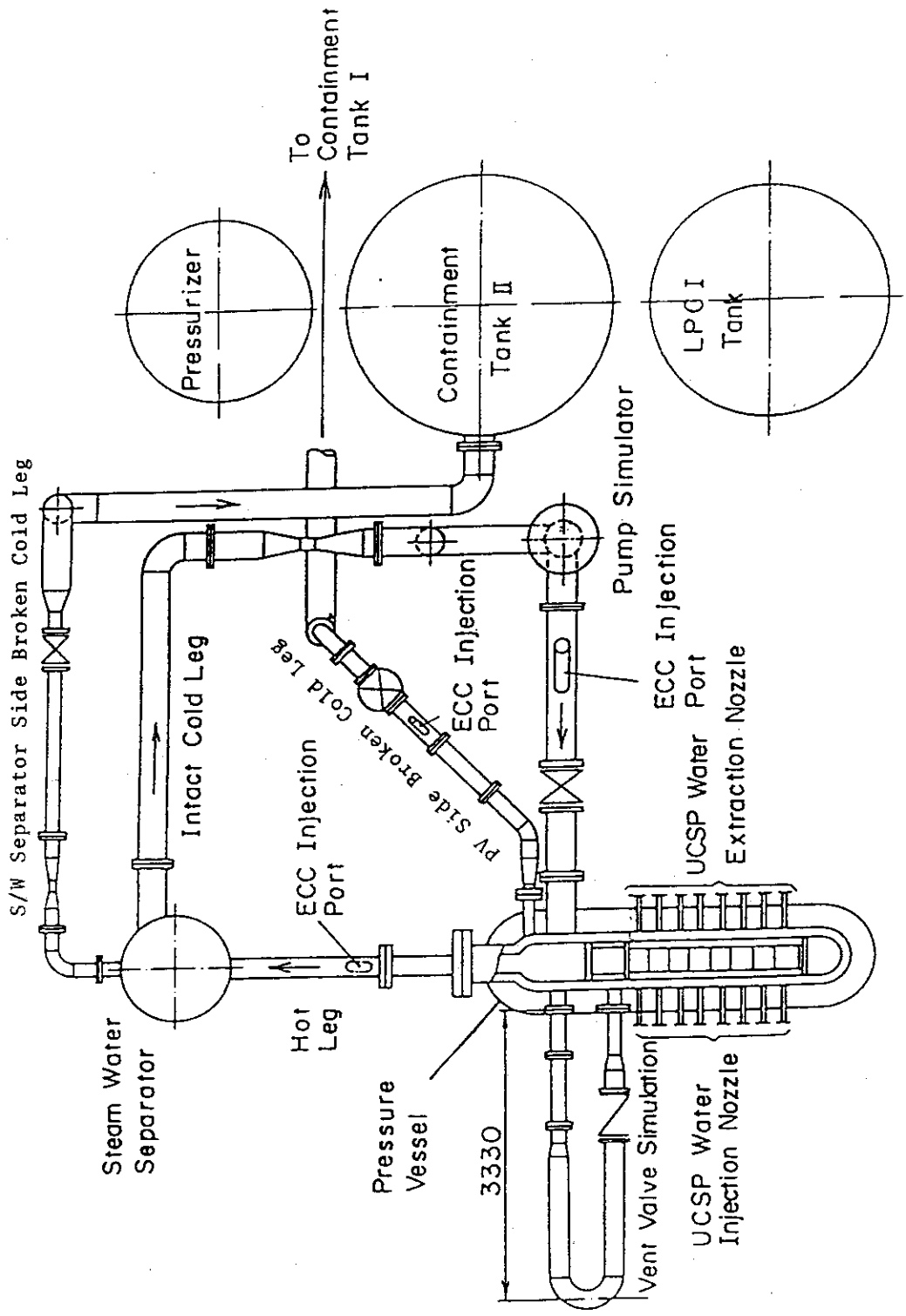

Fig. A-3 Overview of the Arrangements of the SCTF

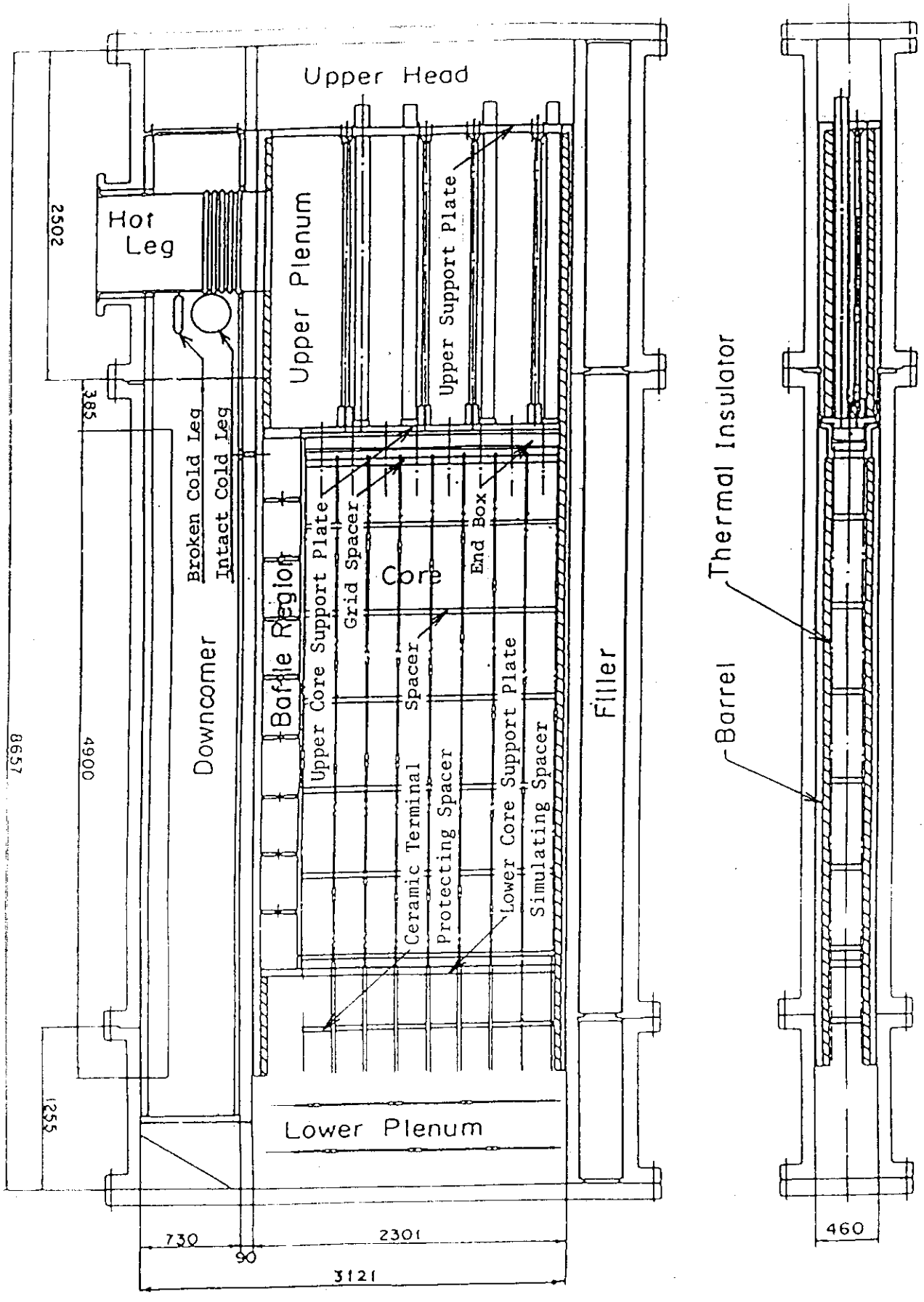

Fig. A-4 Vertical Cross Section of the Pressure Vessel

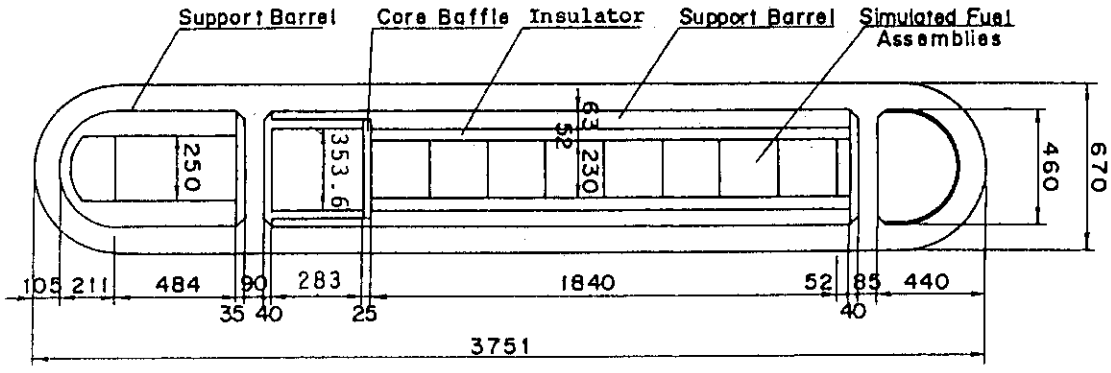

Fig.B-5 Horizontal Cross Section of the Pressure Vessel (1)

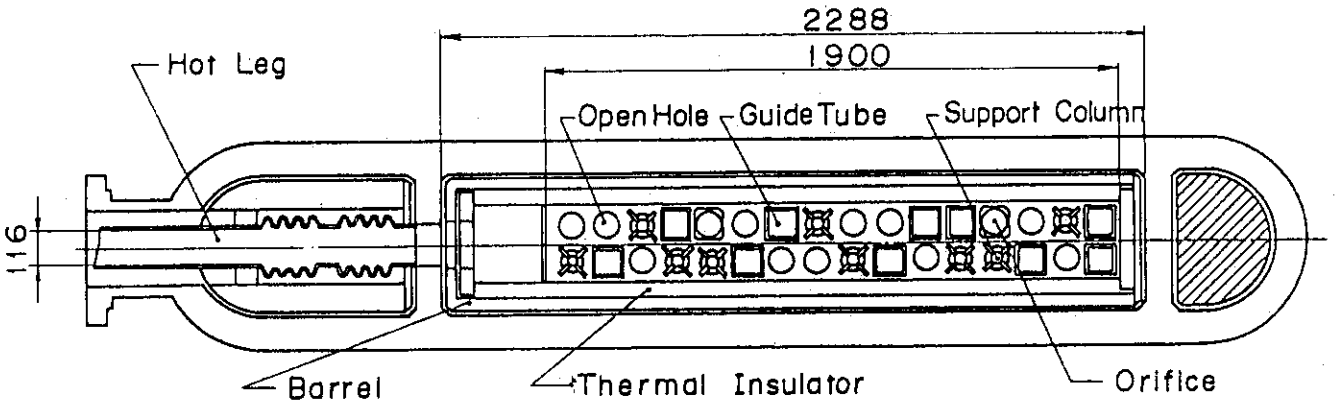

Upper Plenum Cross Section

Fig. A-5 Horizontal Cross Section of the Pressure Vessel (2)

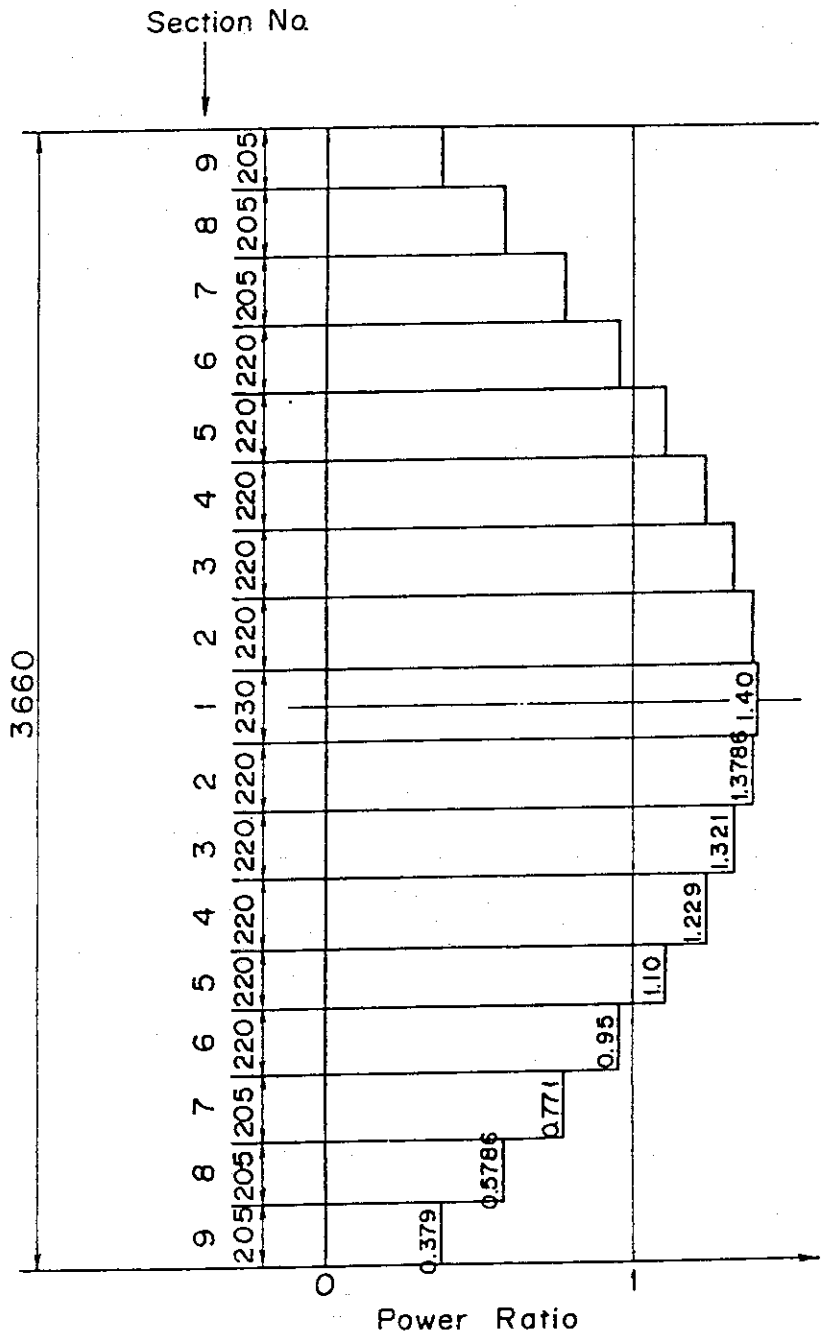

Fig. A-6 Axial Power Distribution of Heater Rod

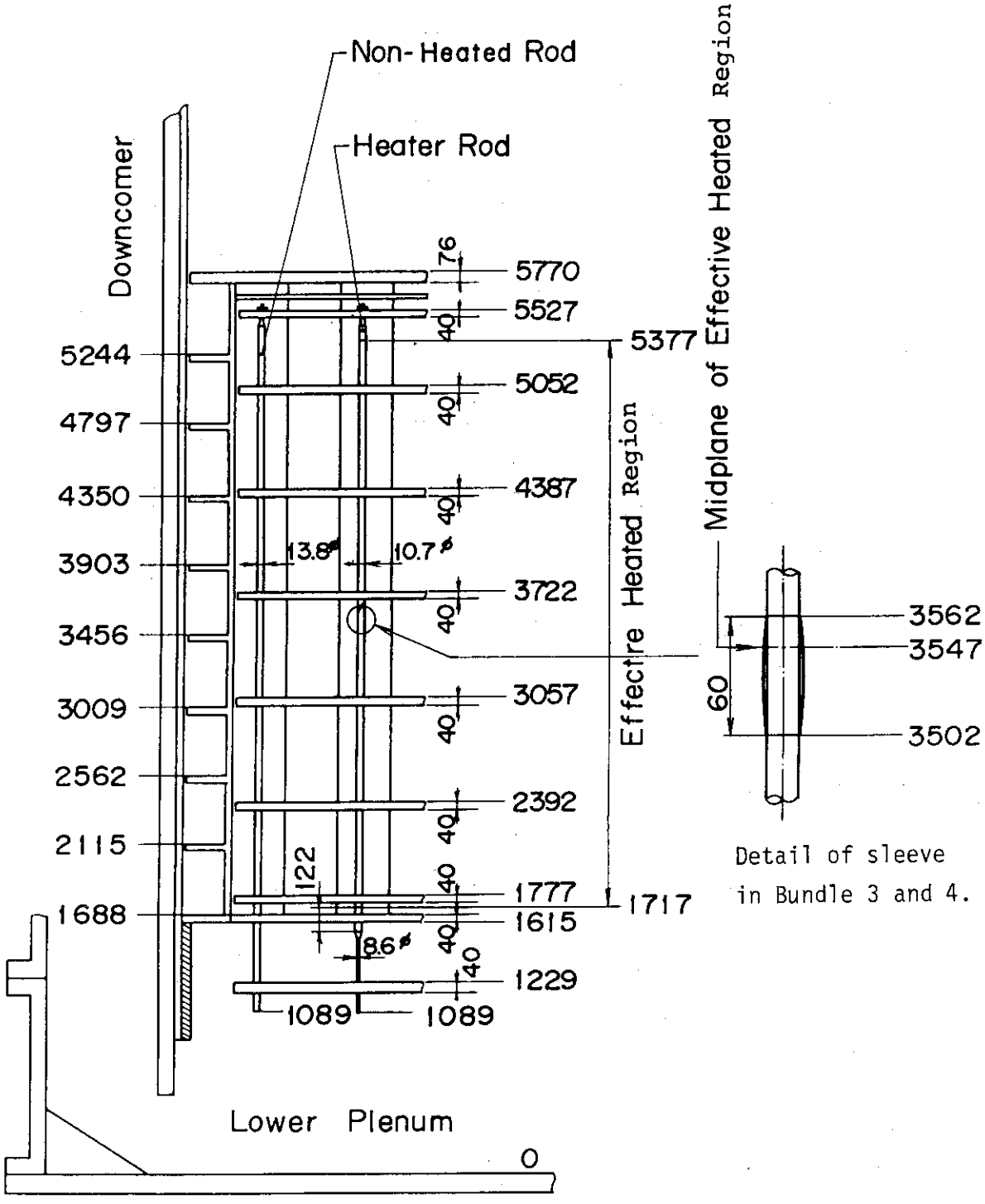

Fig. A-7 Relative Elevation and Dimension of the Core in SCTF

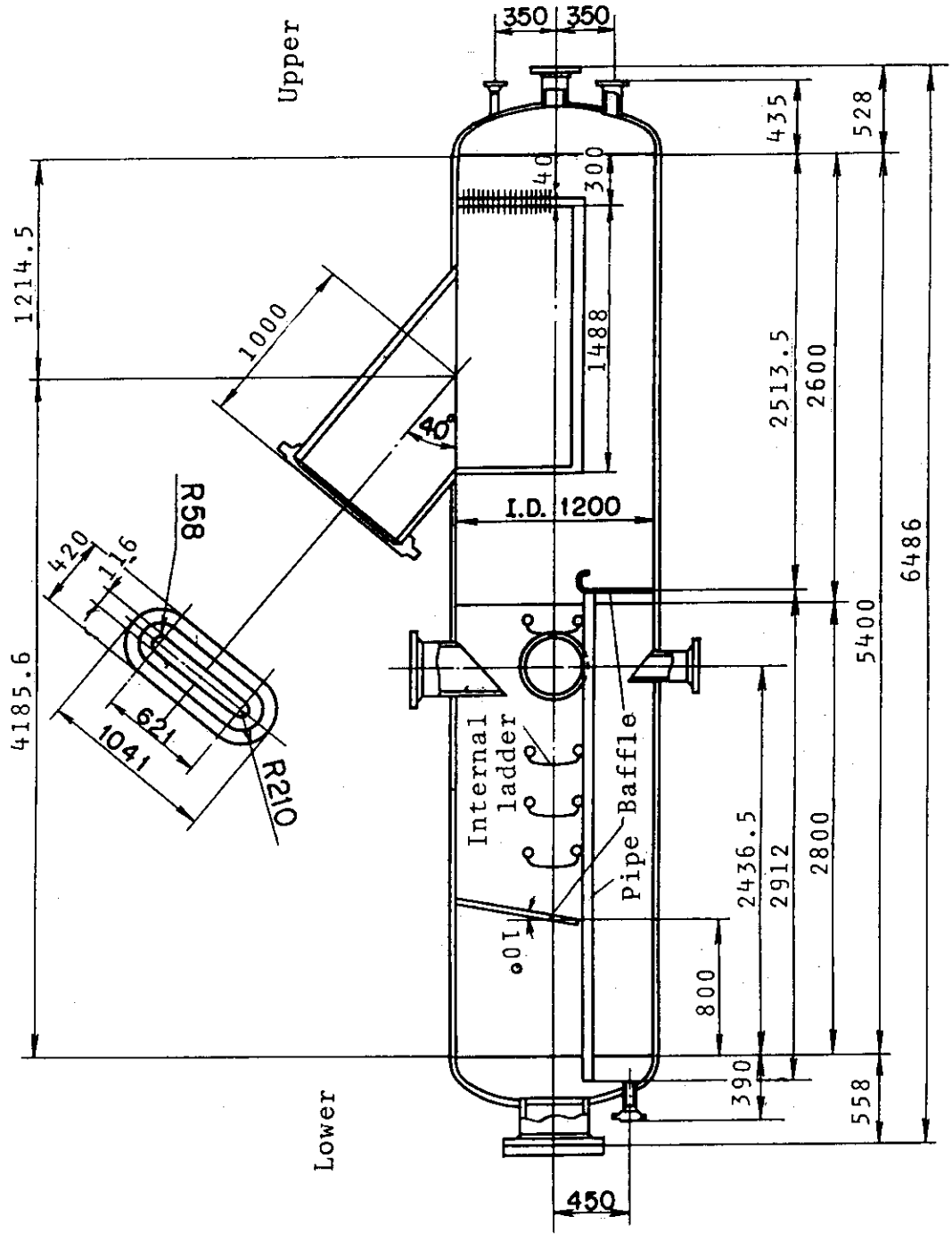

Fig. A-8 Steam Water Separator

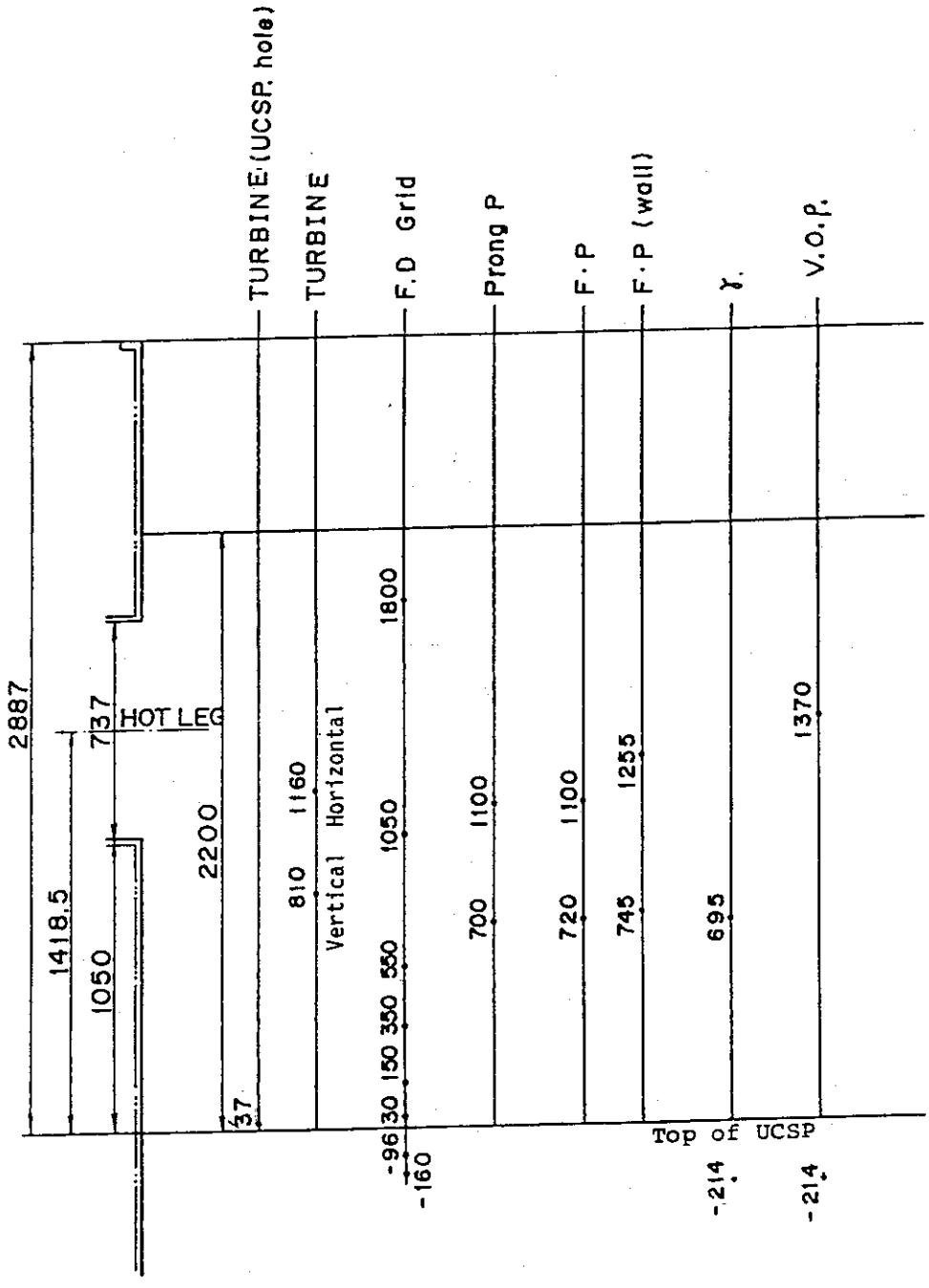

Fig. A-9 Relative Elevation of Upper Plenum Instruments

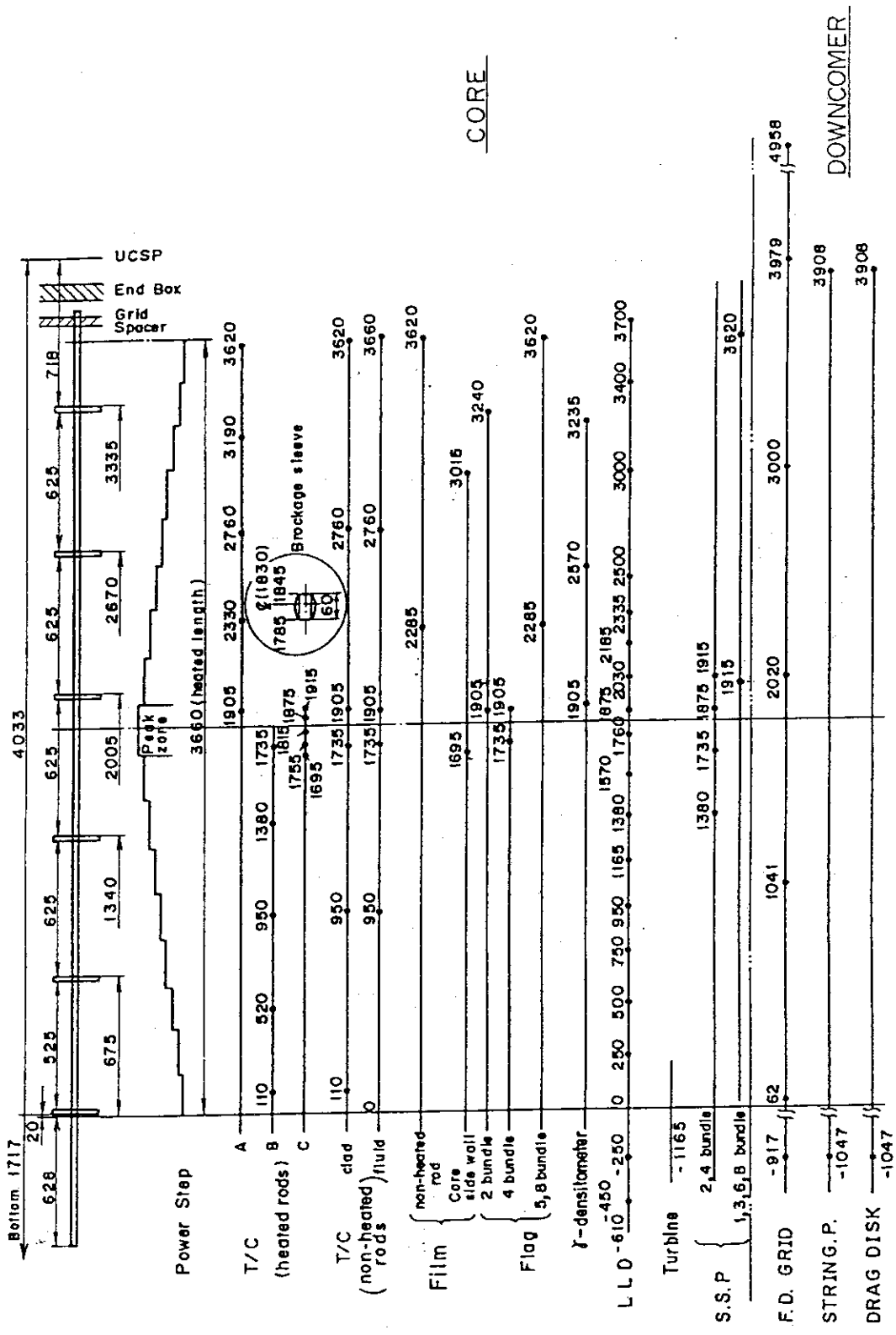

Fig. A-10 Relative Elevation of In-Core and Downcomer Instruments

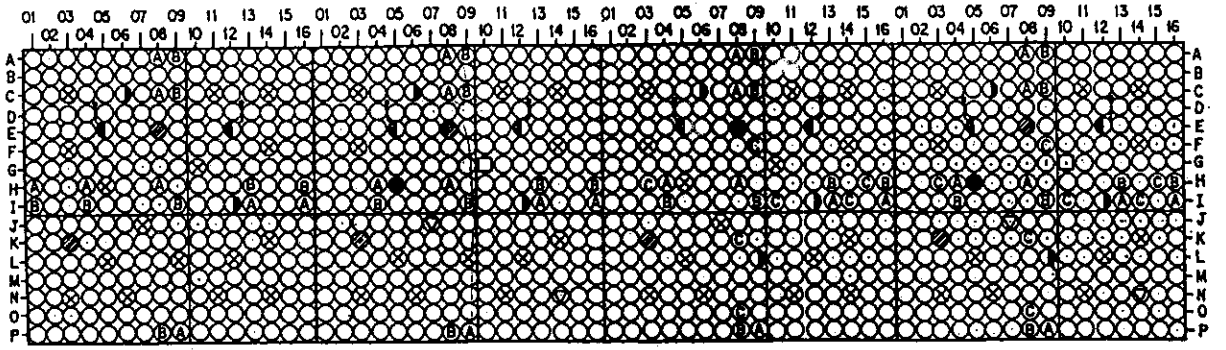

Bundle 1 Bundle 2 Bundle 3 Bundle 4

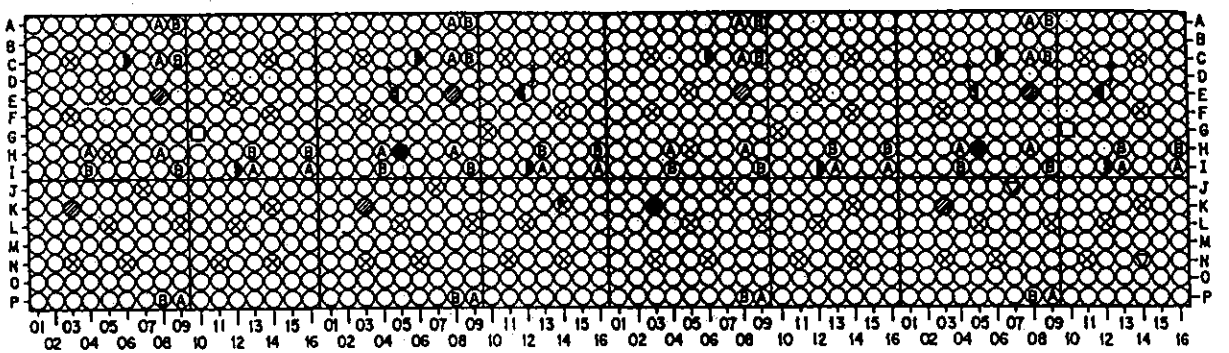

Bundle 5 Bundle 6 Bundle 7 Bundle 8

Bundle No.		1	2	3	4	5	6	7	8	Total	Symbol
Heater Rods with T/C for Surface Temp. Measurements		16	14	21	21	14	14	14	14	128	Ⓐ Ⓑ Ⓒ
Heater Rods without T/C for Surface Temp. Measurements		218	220	213	213	220	220	220	220	1744	○
Non Heated-Rods with Instruments	Surface Temp.	2	2	3	3	2	2	2	2	18	◑
	Fluid Temp.	2	2	2	2	2	2	2	2	16	⊘
	Steam Temp.	2	2	2	2	—	2	—	2	12	◐
	Film Probe	—	2	—	2	—	—	—	2	6	⊘
	Flag Probe	—	1	—	1	1	—	—	1	4	○
	LLD	—	1	—	1	—	1	—	1	4	●
Tie Rod		16	12	15	11	17	15	18	12	116	⊗
Total		256	256	256	256	256	256	256	256	2048	

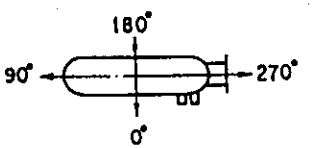

Fig. A-11 Horizontal Arrangement of Instrumented Rods

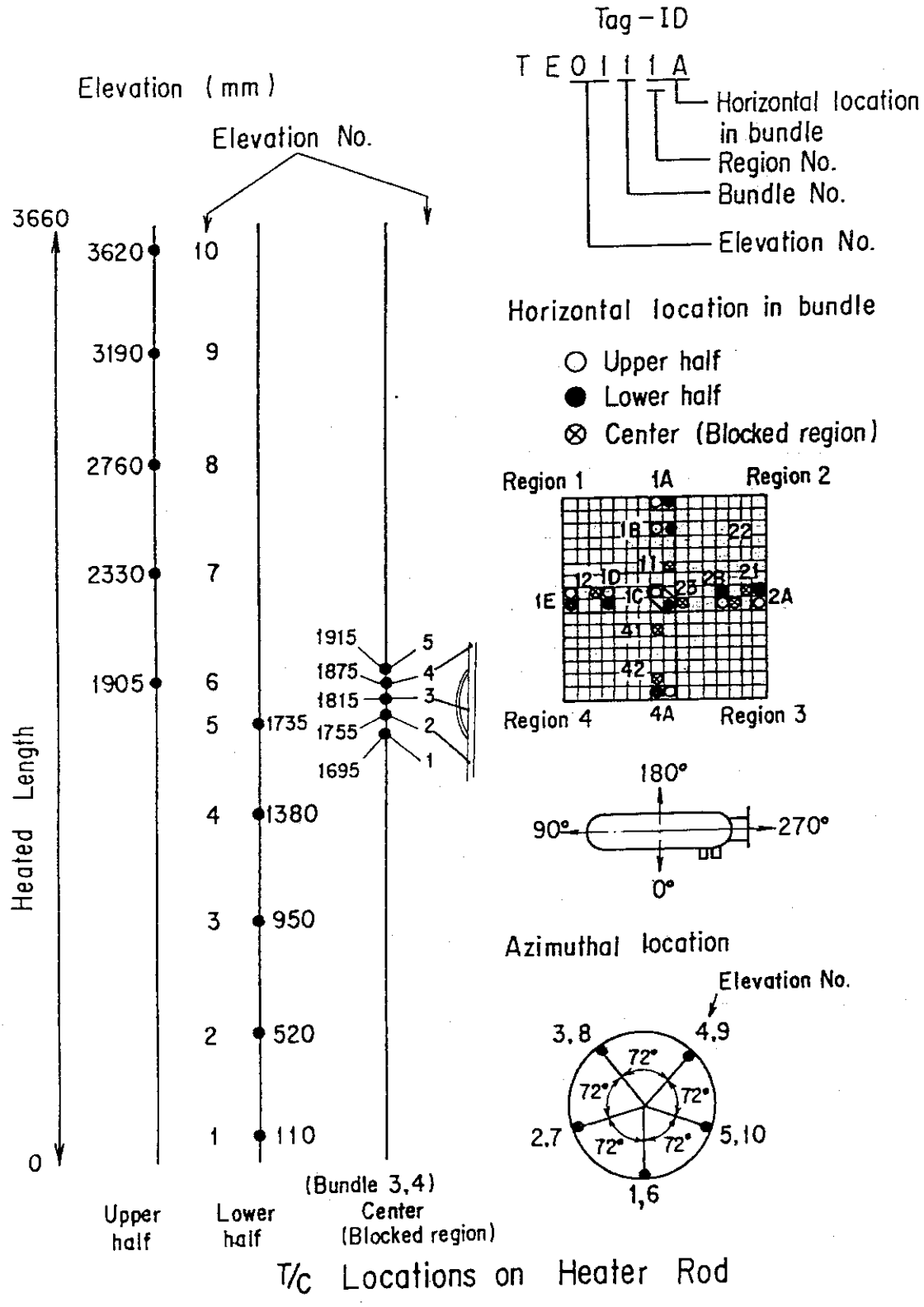

Fig. A-12 Thermocouple Locations of Heater Rod Surface Temperature Measurements

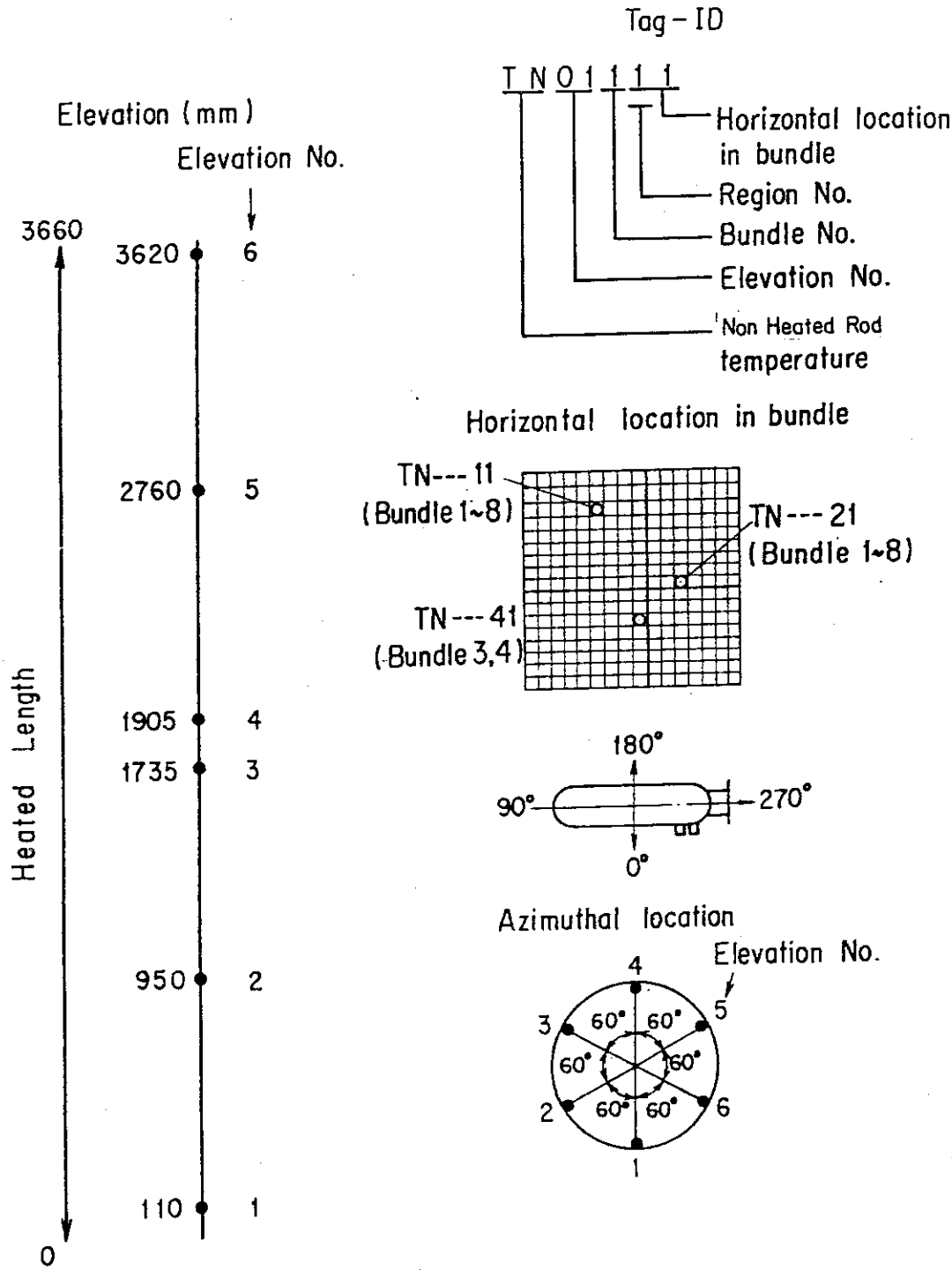

Fig. A-13 Thermocouple Locations of Non-Heated Rod Surface Temperature Measurements

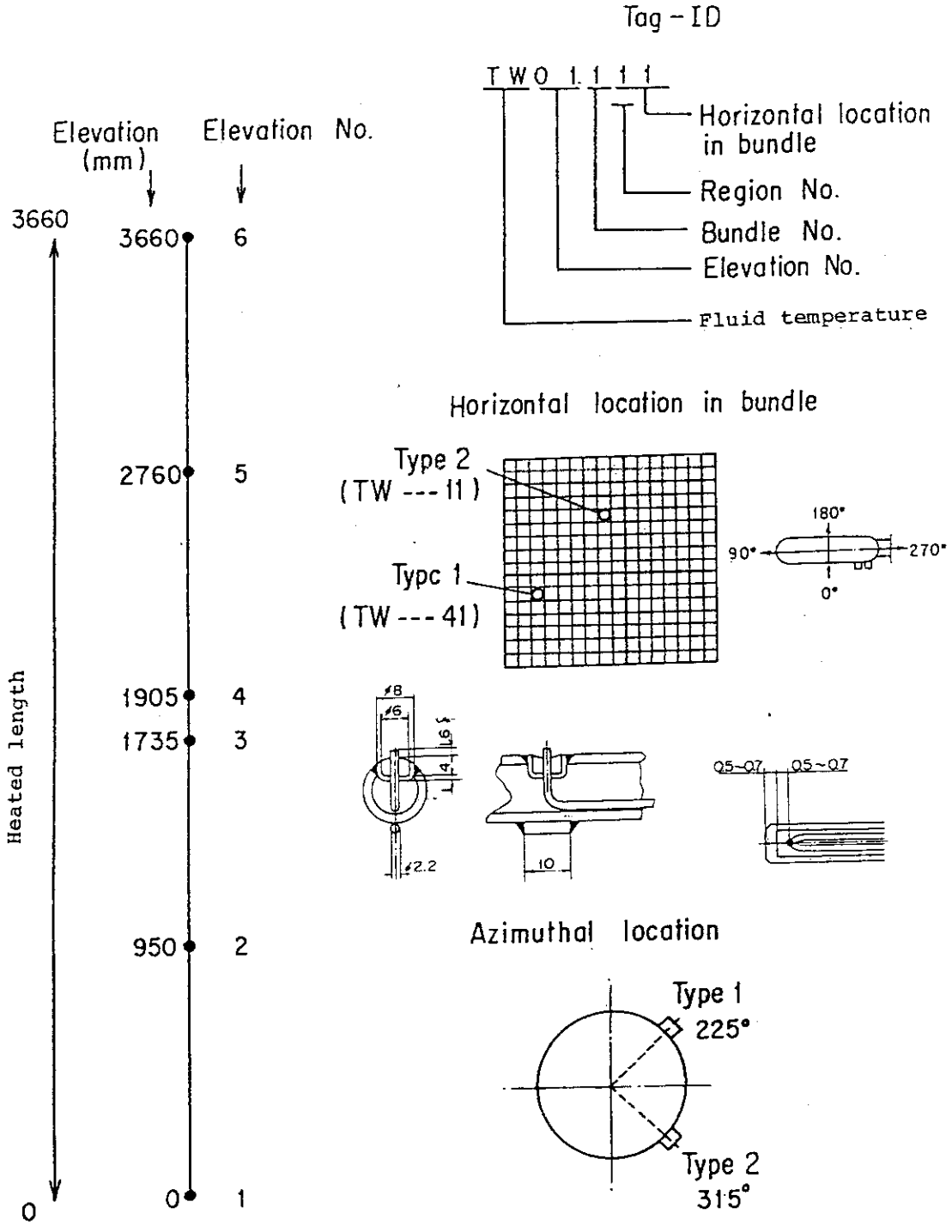

Fig. A-14 Thermocouple Locations of Fluid Temperature Measurements in Core

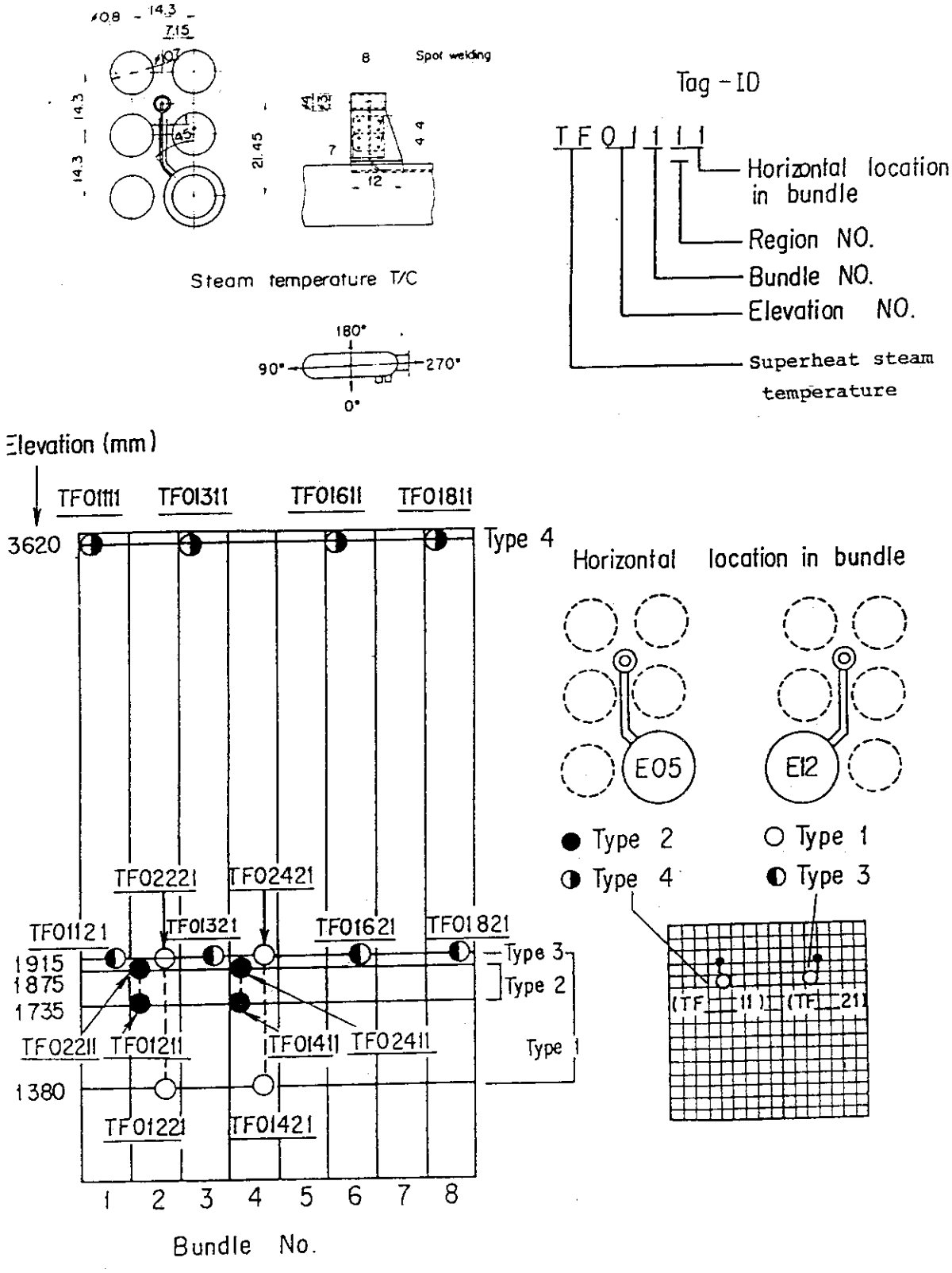

Fig. A-15 Thermocouple Locations of Steam Temperature Measurements in Core

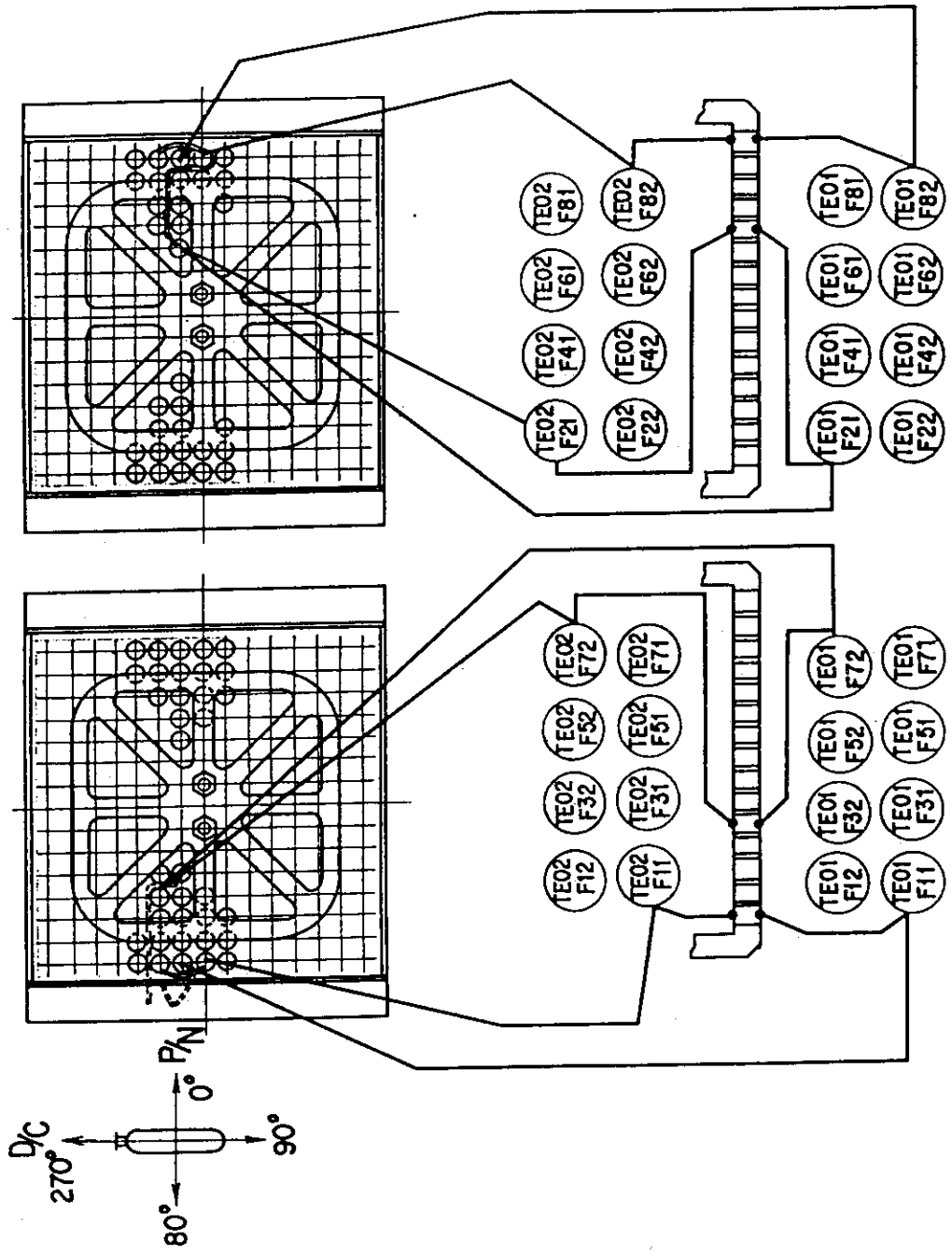

Fig. A-16 Thermocouple Locations of Fluid Temperature Measurements just above and below End Box Tie Plate

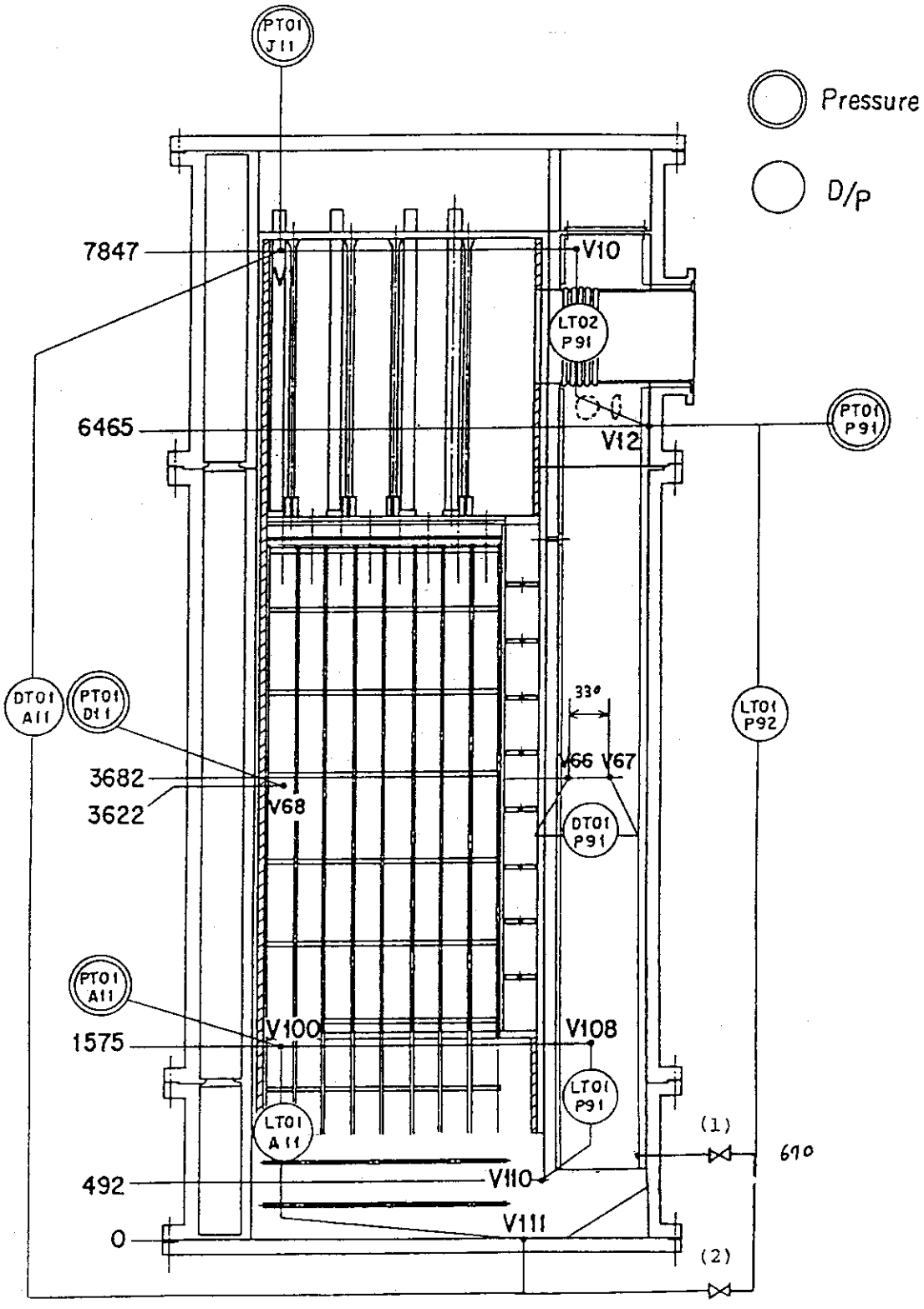

(1) used for lower plenum injection tests (the bottom of downcomer is blocked)

(2) used for the other tests

Fig. A-17 Location of Pressure Measurements in Pressure Vessel, Differential Pressure Measurements between Upper and Lower Plenums and Liquid Level Measurements in Downcomer and Lower Plenum

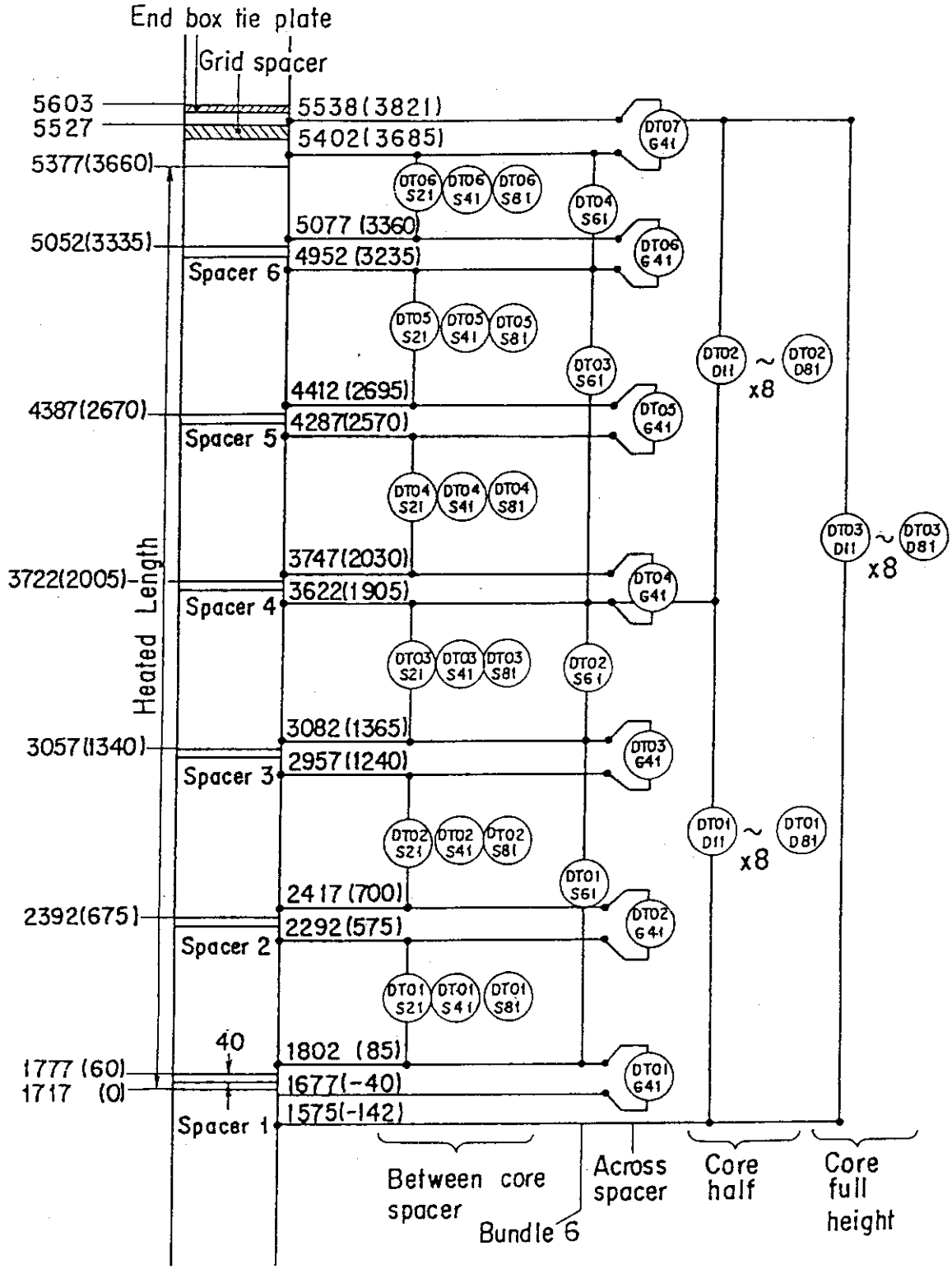

Fig. A-18 Locations of Vertical Differential Pressure Measurements in Core

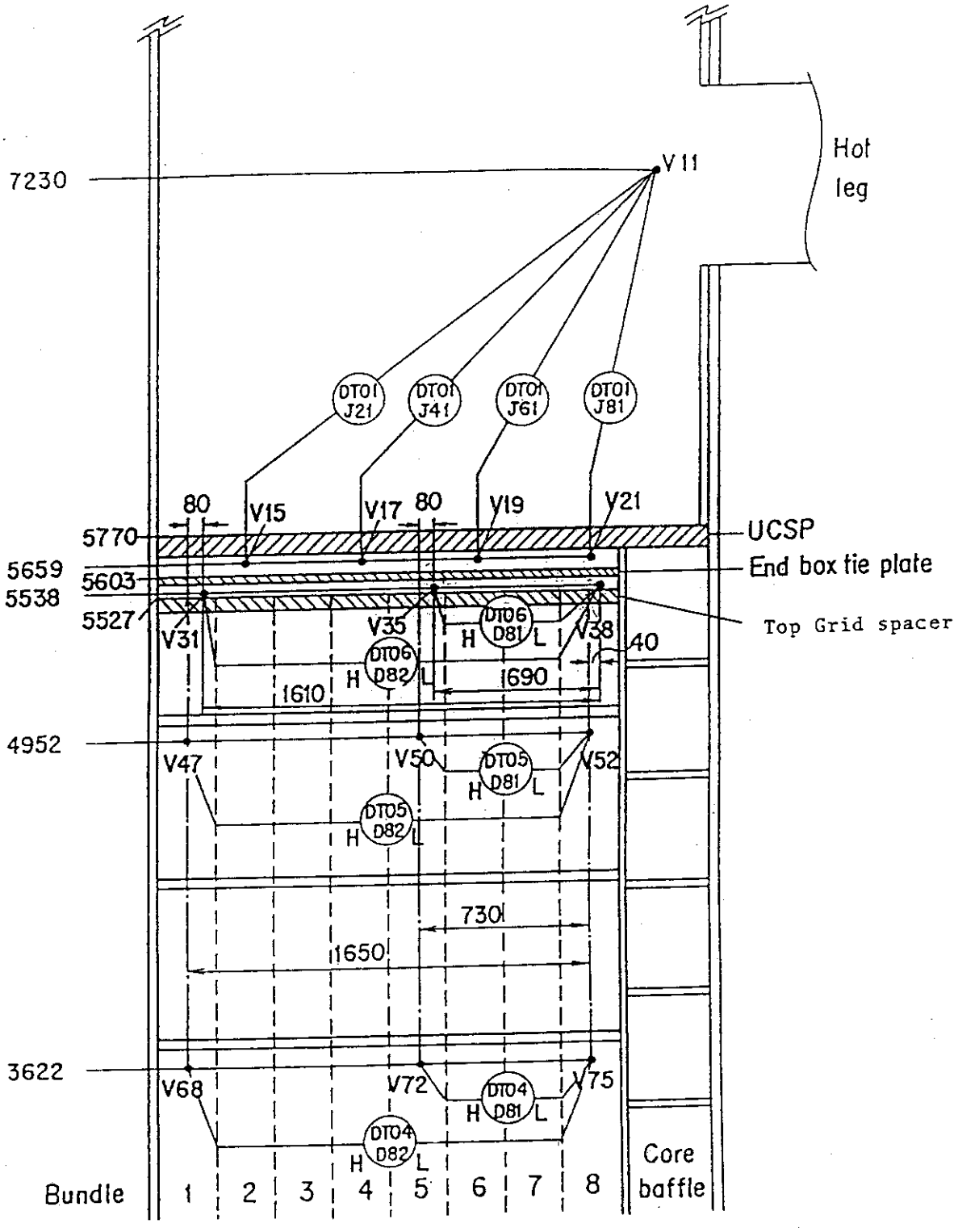

Fig. A-19 Locations of Horizontal Differential Pressure Measurements in Core and Differential Pressure Measurements between End Box and Inlet of Hot Leg

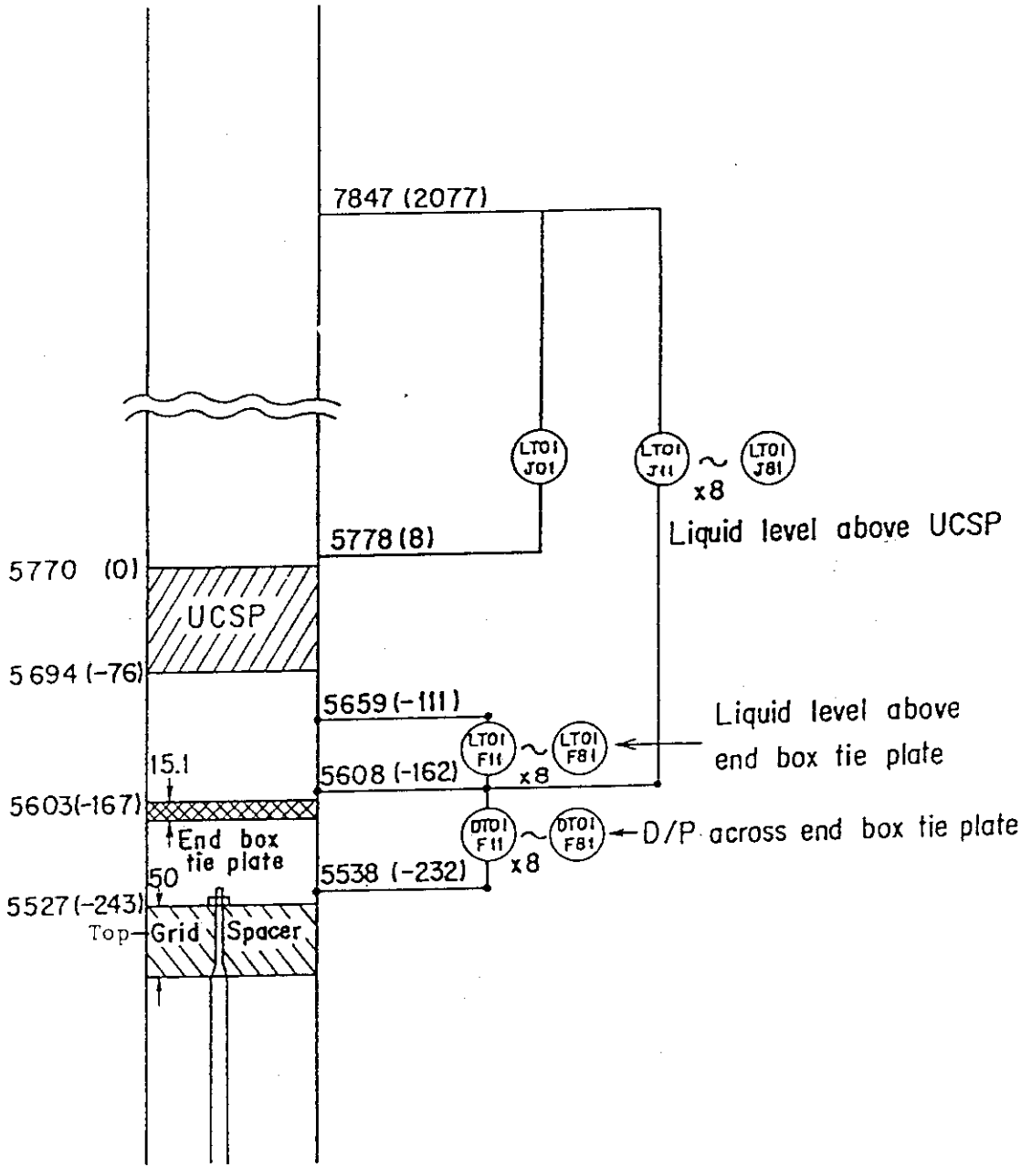

Fig. A-20 Locations of Differential Pressure Measurements across End Box Tie Plate and Liquid Level Measurements above UCSP and End Box Tie Plate

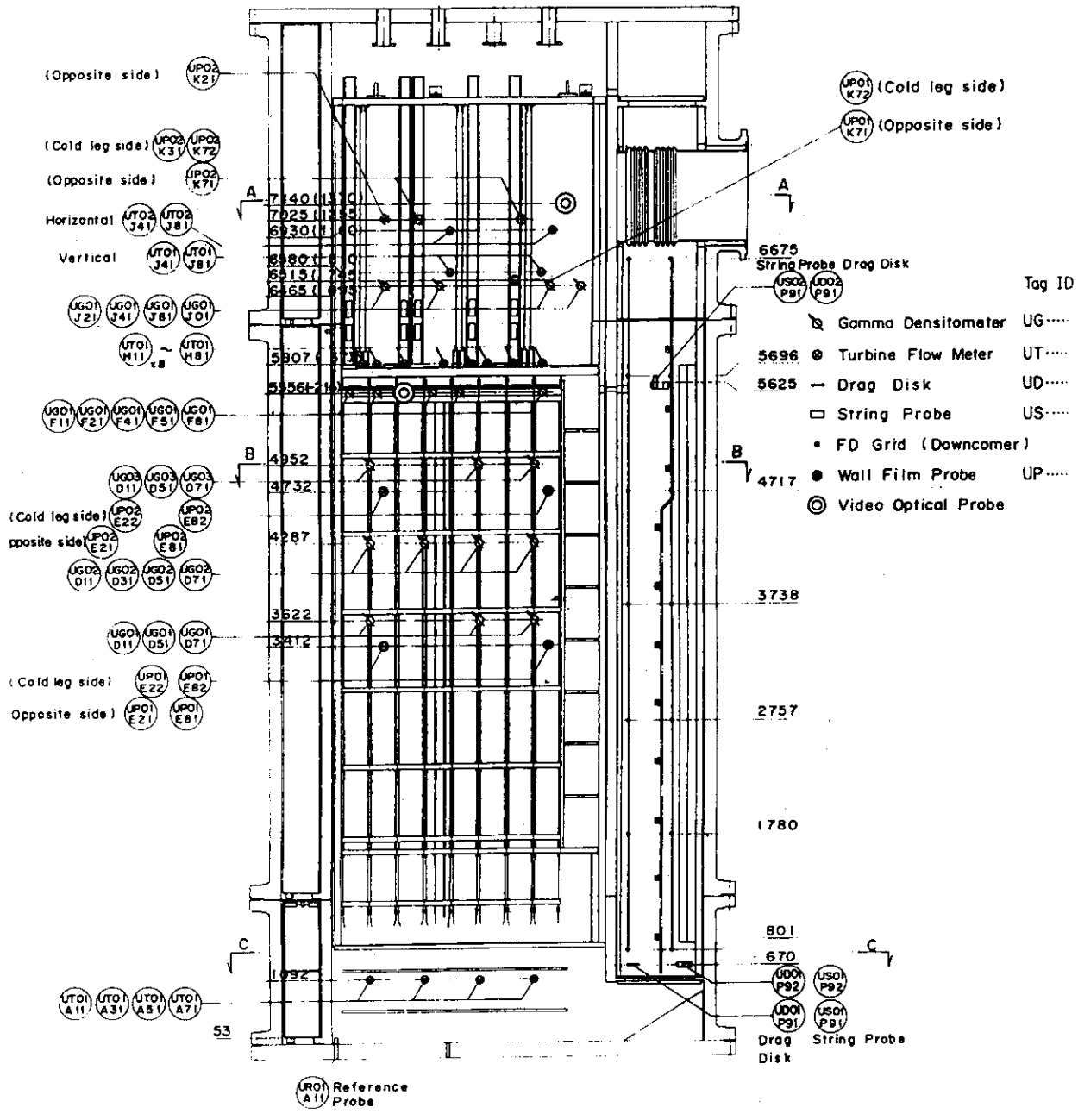

Fig. A-21 Vertical Locations of USNRC-Provided Instrumentation in Pressure Vessel

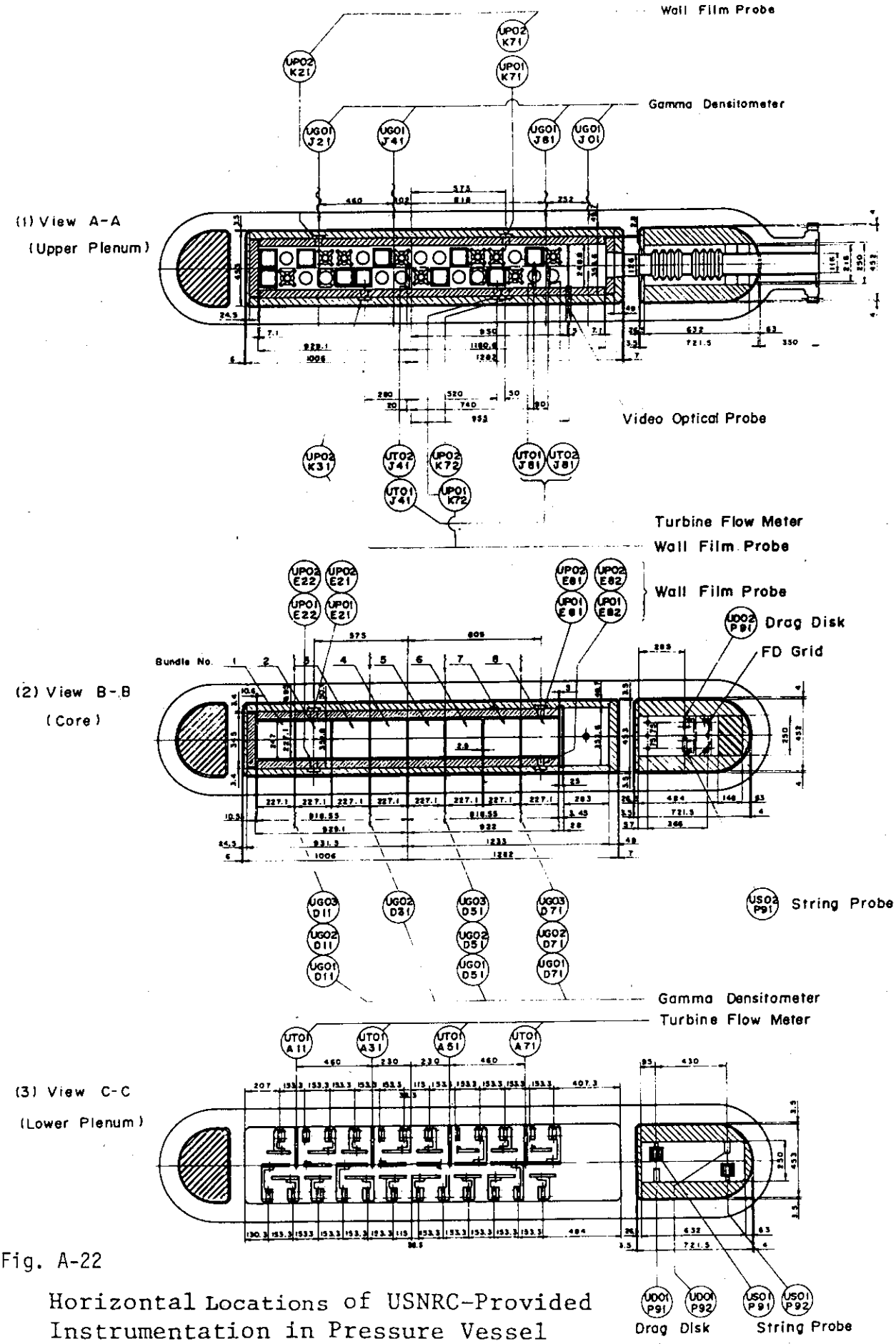

Fig. A-22

Horizontal Locations of USNRC-Provided Instrumentation in Pressure Vessel

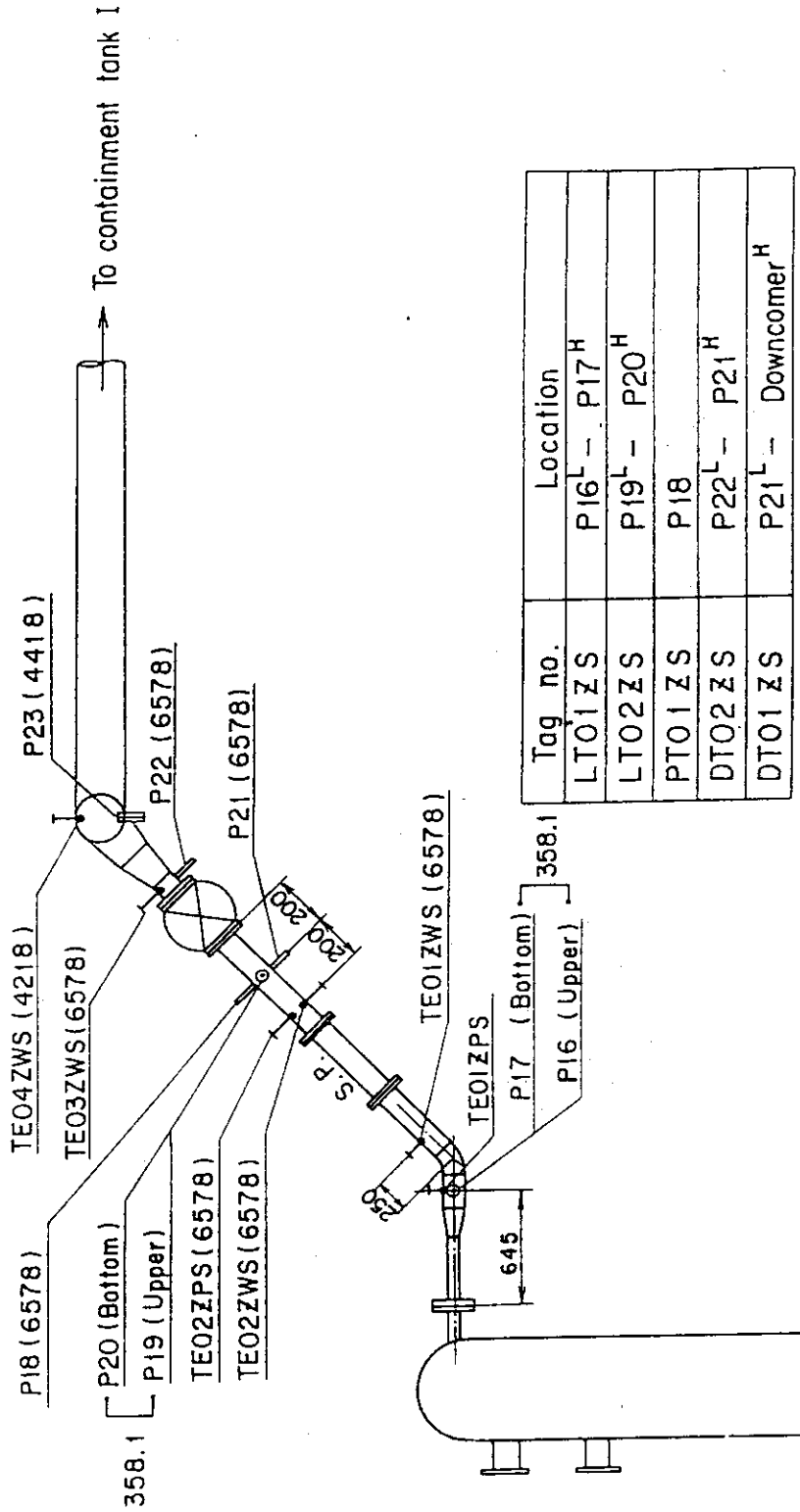

Fig. A-23 Locations of Broken Cold Leg Instrumentation (Pressure Vessel Side)

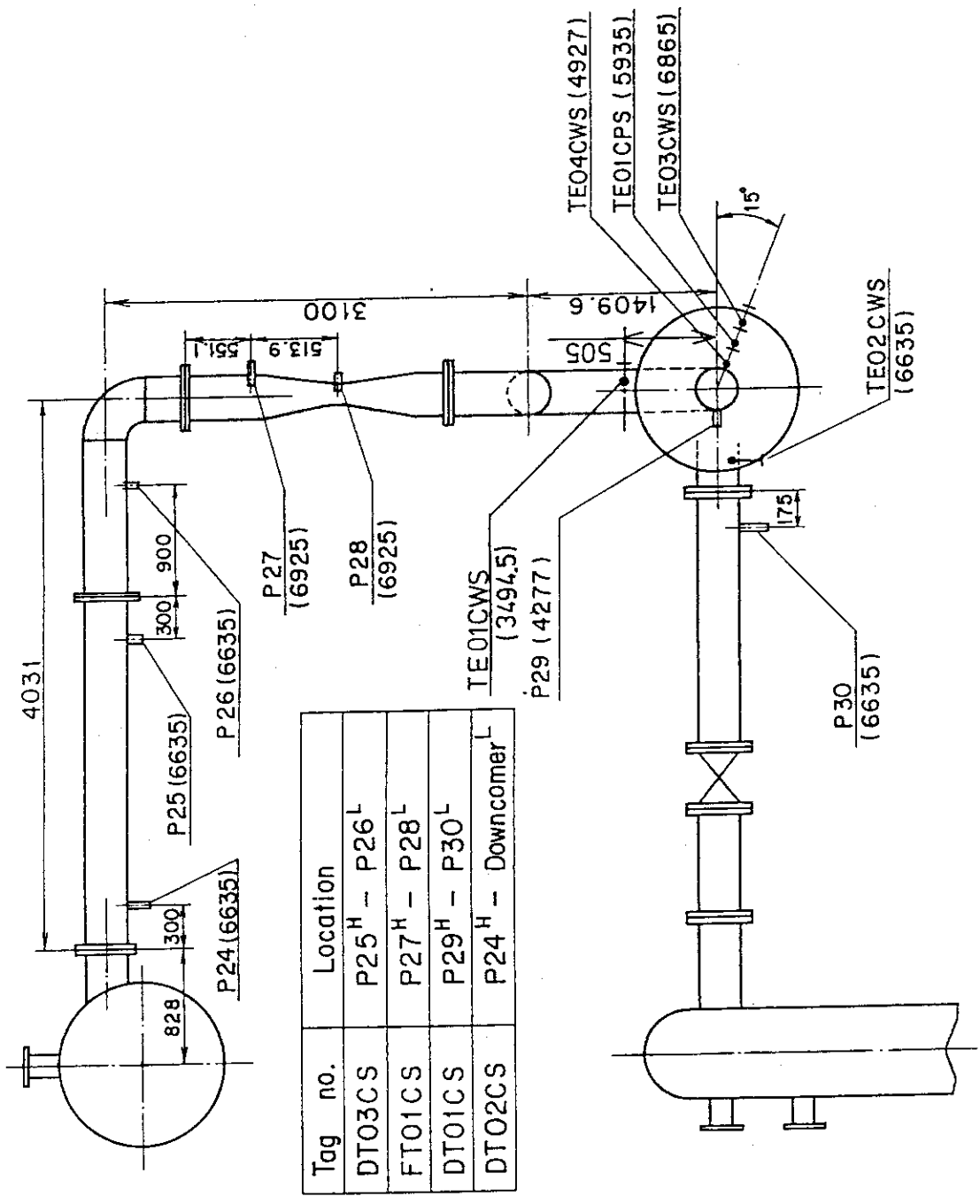

Tag no.	Location
DT03CS	$P25^{H}$ – $P26^{L}$
FT01CS	$P27^{H}$ – $P28^{L}$
DT01CS	$P29^{H}$ – $P30^{L}$
DT02CS	$P24^{H}$ – Downcomer^{L}

Fig. A-24 Locations of Intact Cold Leg Instrumentation

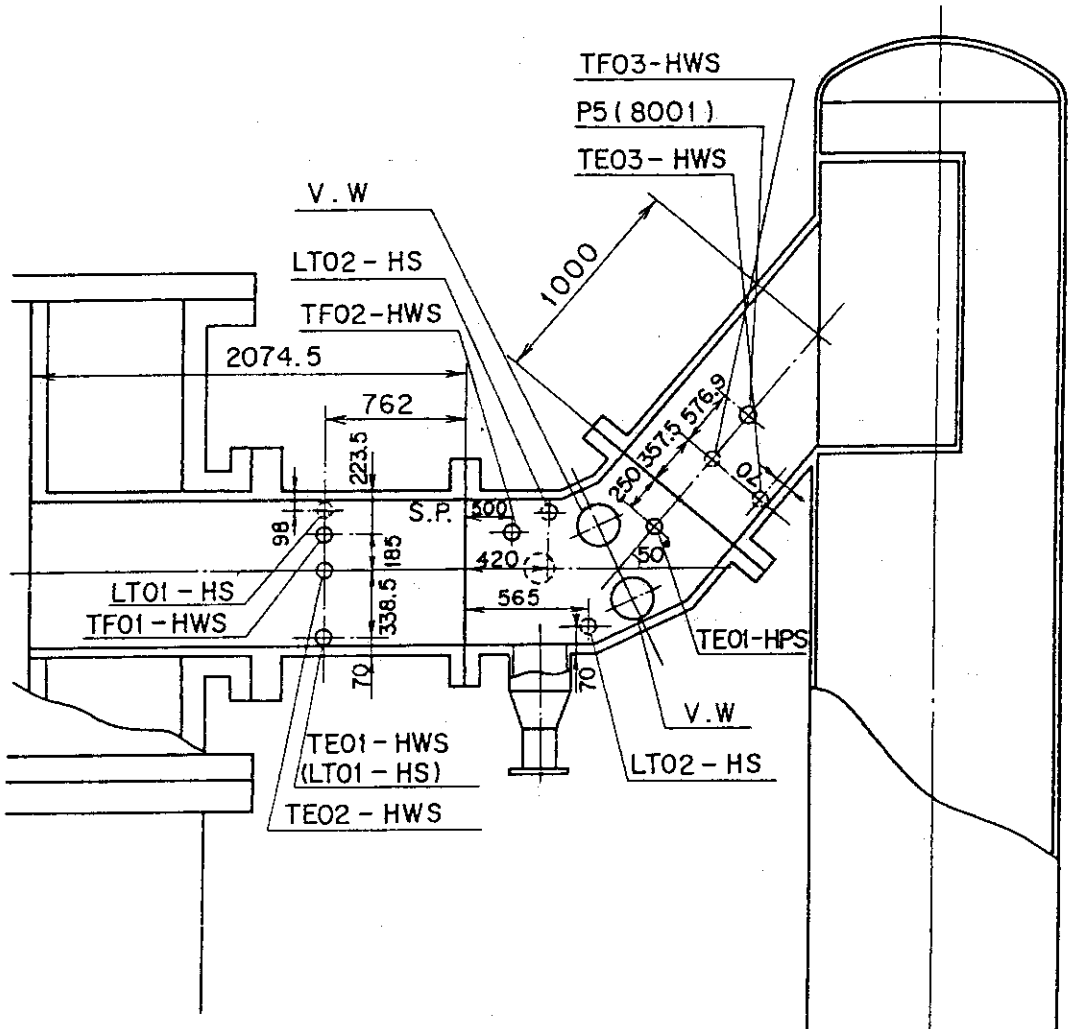

Tag no.	Location
DT01HS	P5[L]- Inlet of hot leg[H]
DT01GS	P5[L]- Broken cold leg (S-W separator side)[H]
DT02GS	P5[H]- S-W separator tank[L]

Fig. A-25 Locations of Hot Leg Instrumentation

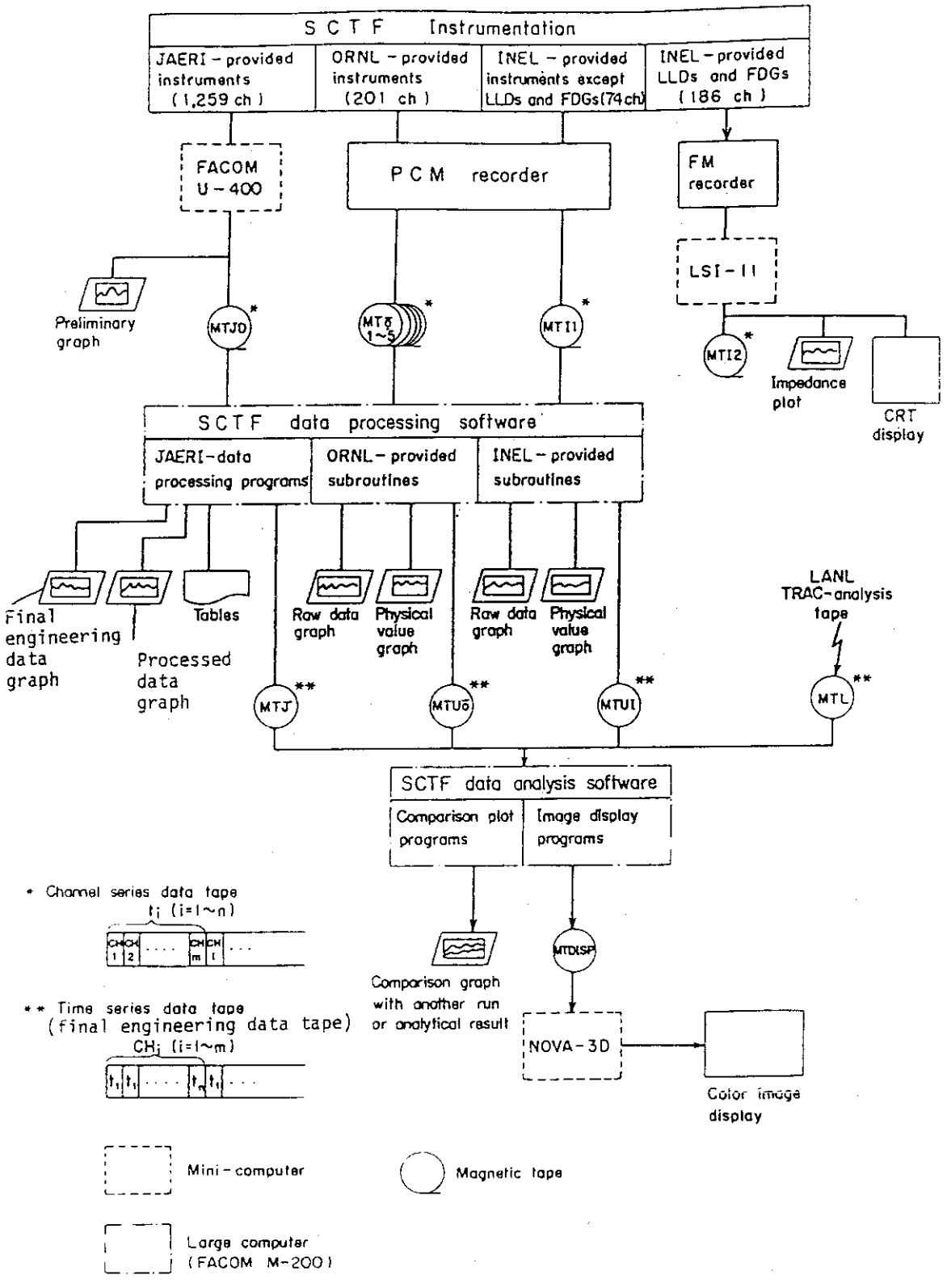

Fig. A-26 Flow Chart of Data Reduction

Appendix 2 Data Presentation

S1-12 (Run 518)

S1-13 (Run 519)

S1-22 (Run 532)

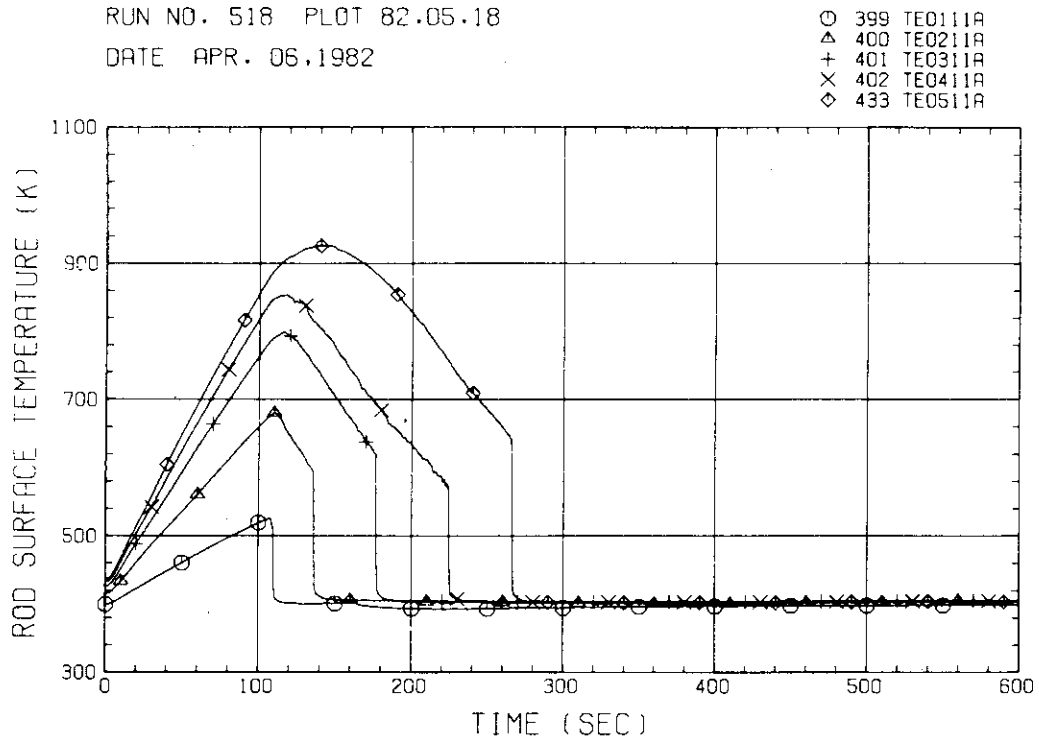

Fig. B-1 HEATER ROD TEMPERATURE (BUNDLE 1-1A, LOWER HALF)

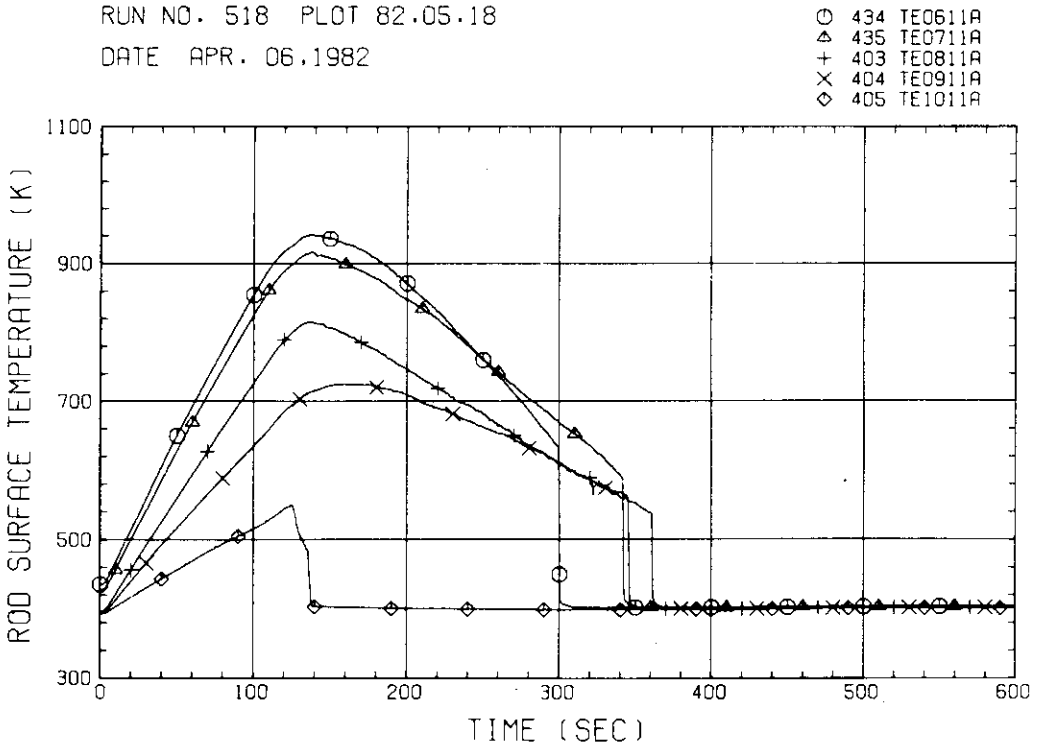

Fig. B-2 HEATER ROD TEMPERATURE (BUNDLE 1-1A, UPPER HALF)

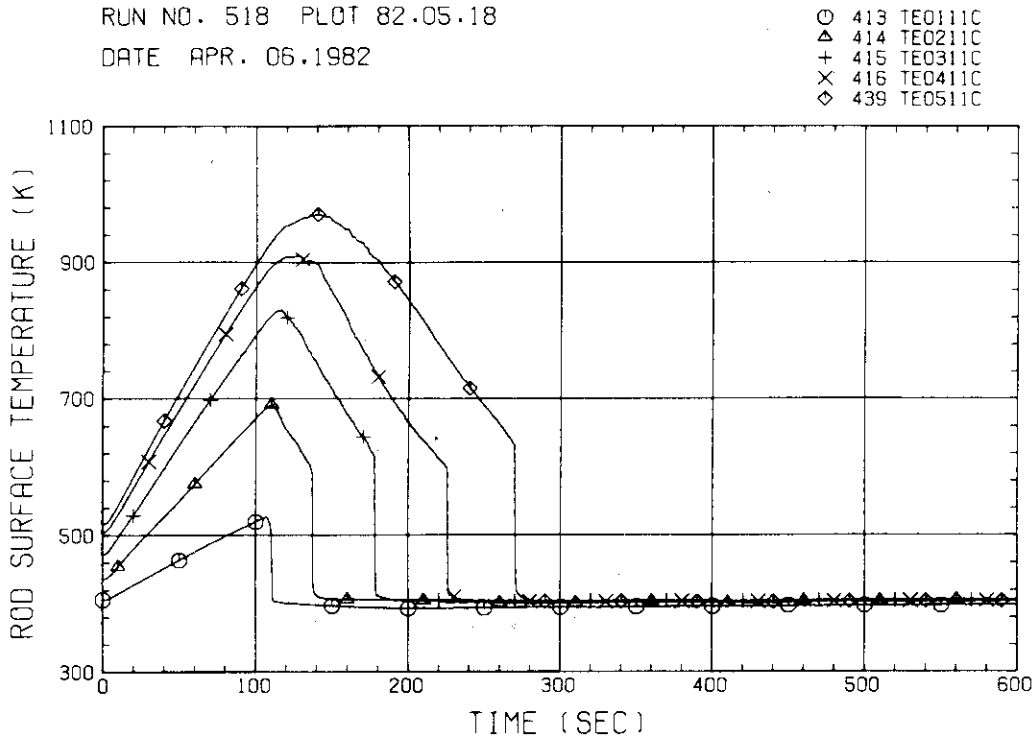

Fig. B-3 HEATER ROD TEMPERATURE (BUNDLE 1-1C, LOWER HALF)

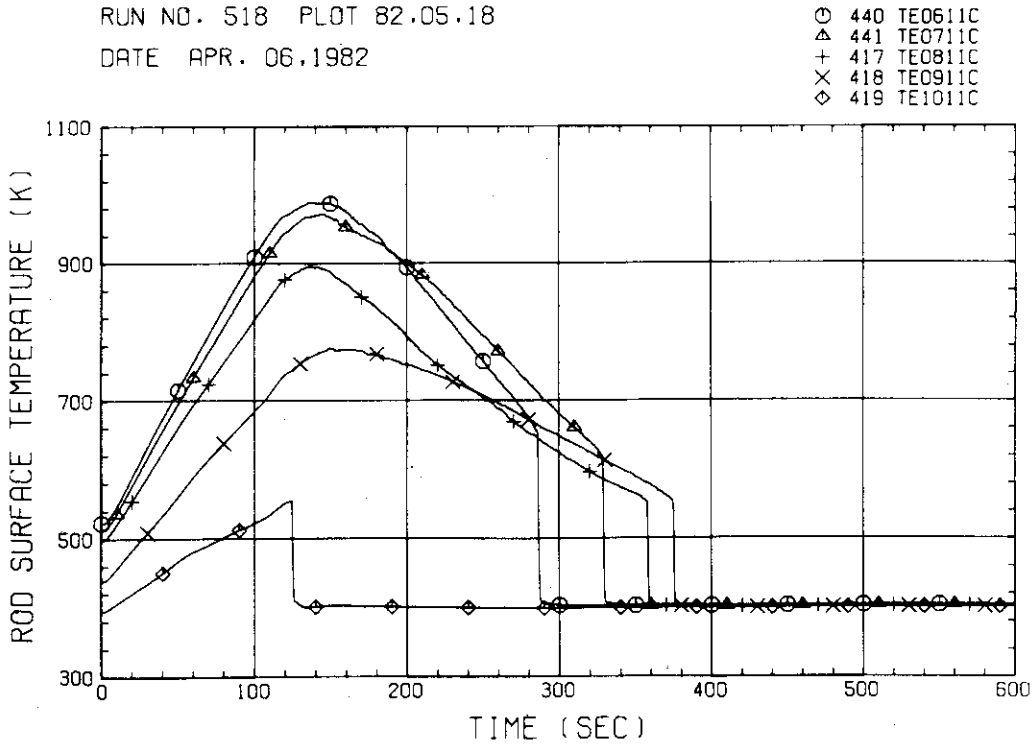

Fig. B-4 HEATER ROD TEMPERATURE (BUNDLE 1-1C, UPPER HALF)

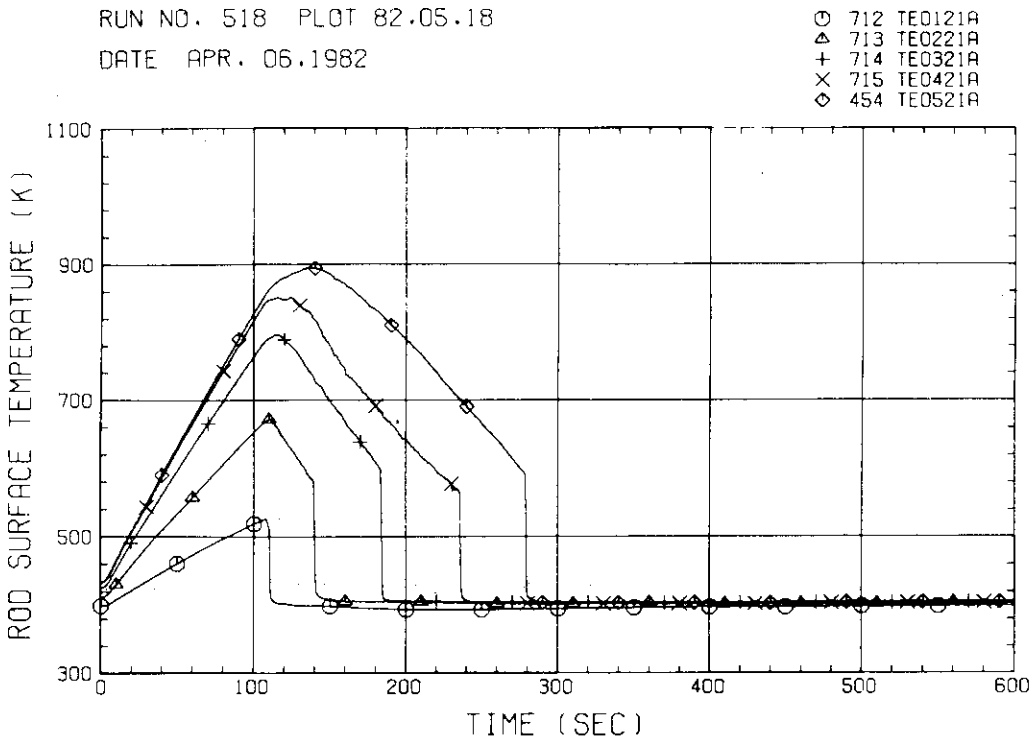

Fig. B-5 HEATER ROD TEMPERATURE (BUNDLE 2-1A, LOWER HALF)

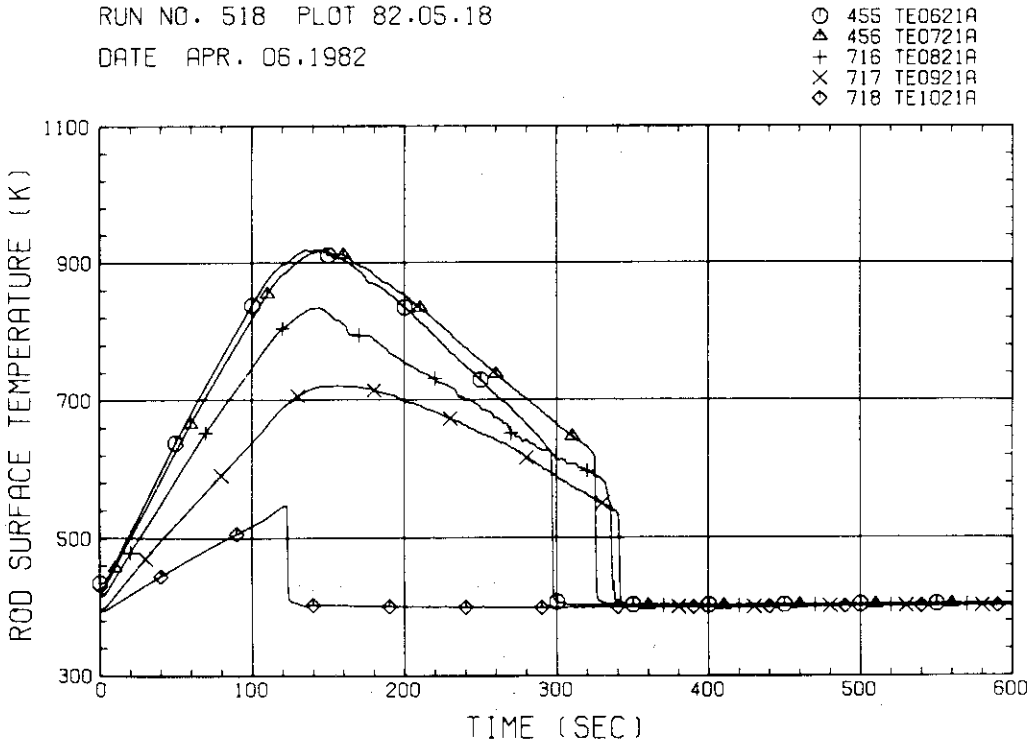

Fig. B-6 HEATER ROD TEMPERATURE (BUNDLE 2-1A, UPPER HALF)

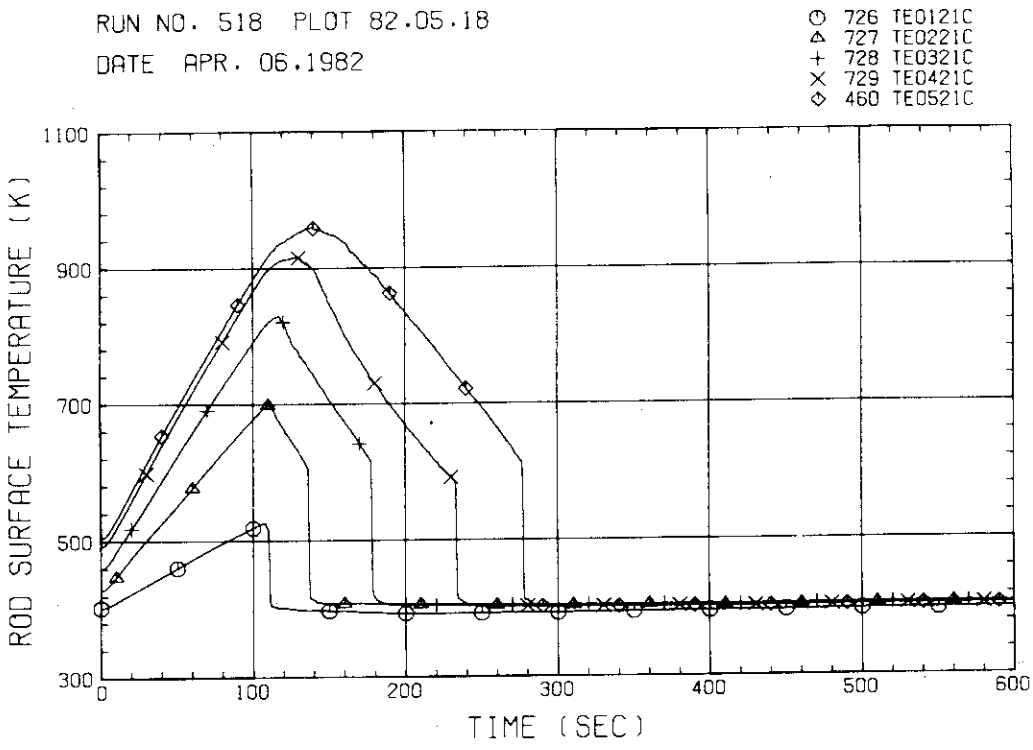

Fig. B-7 HEATER ROD TEMPERATURE (BUNDLE 2-1C, LOWER HALF)

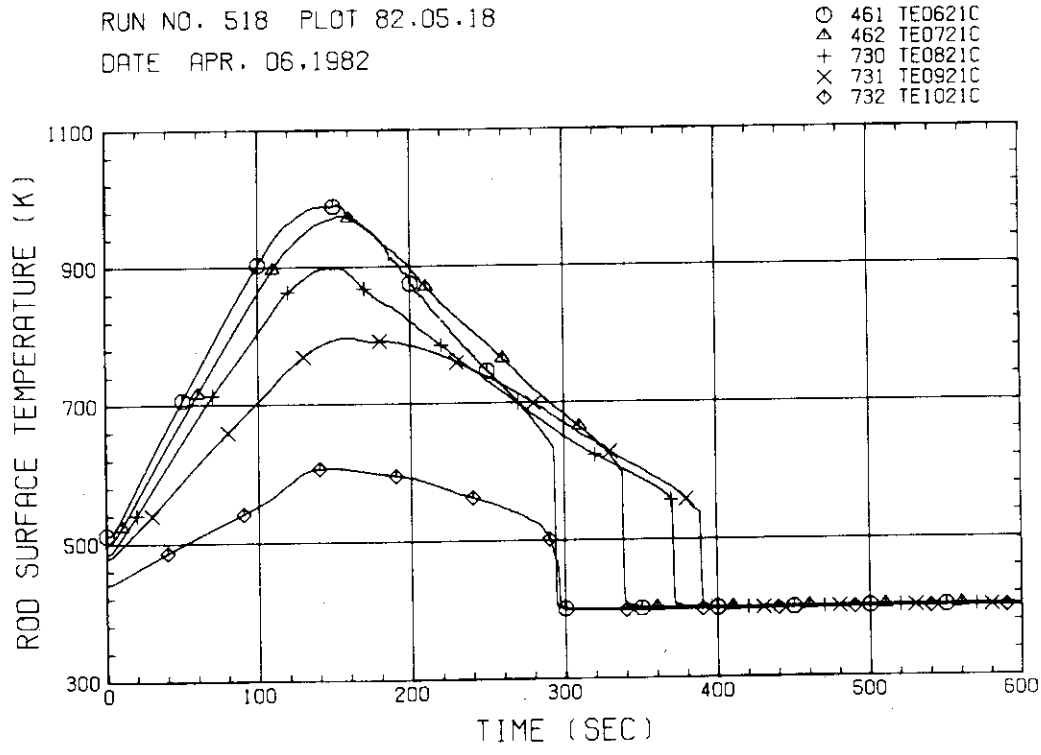

Fig. B-8 HEATER ROD TEMPERATURE (BUNDLE 2-1C, UPPER HALF)

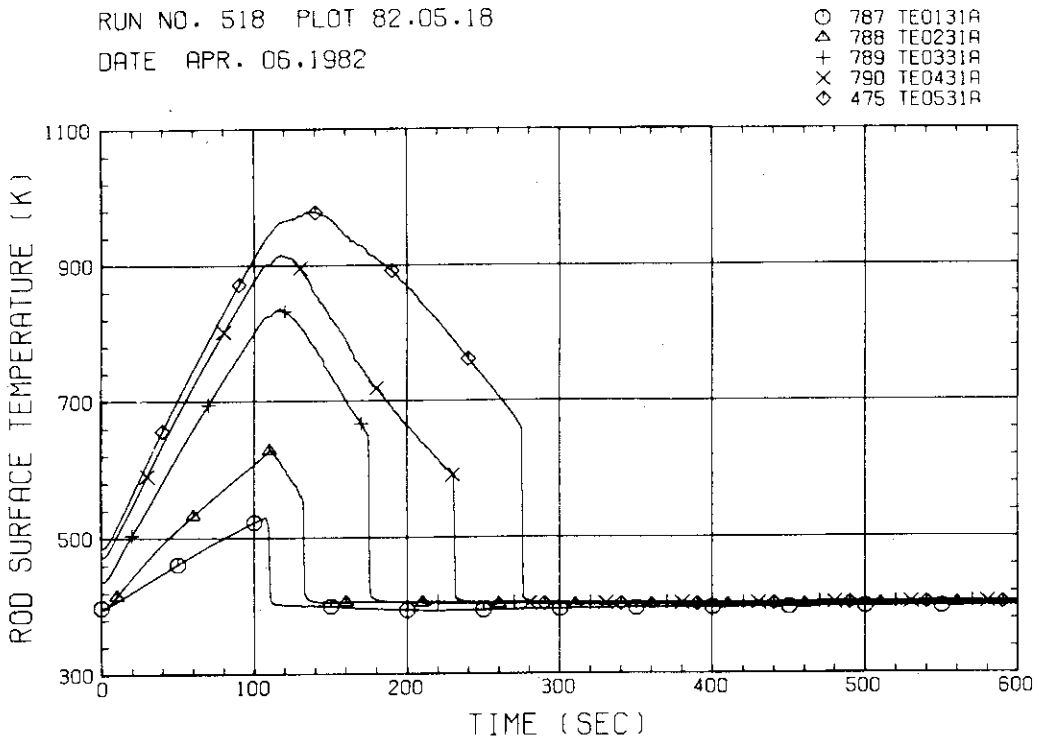

Fig. B-9 HEATER ROD TEMPERATURE (BUNDLE 3-1A, LOWER HALF)

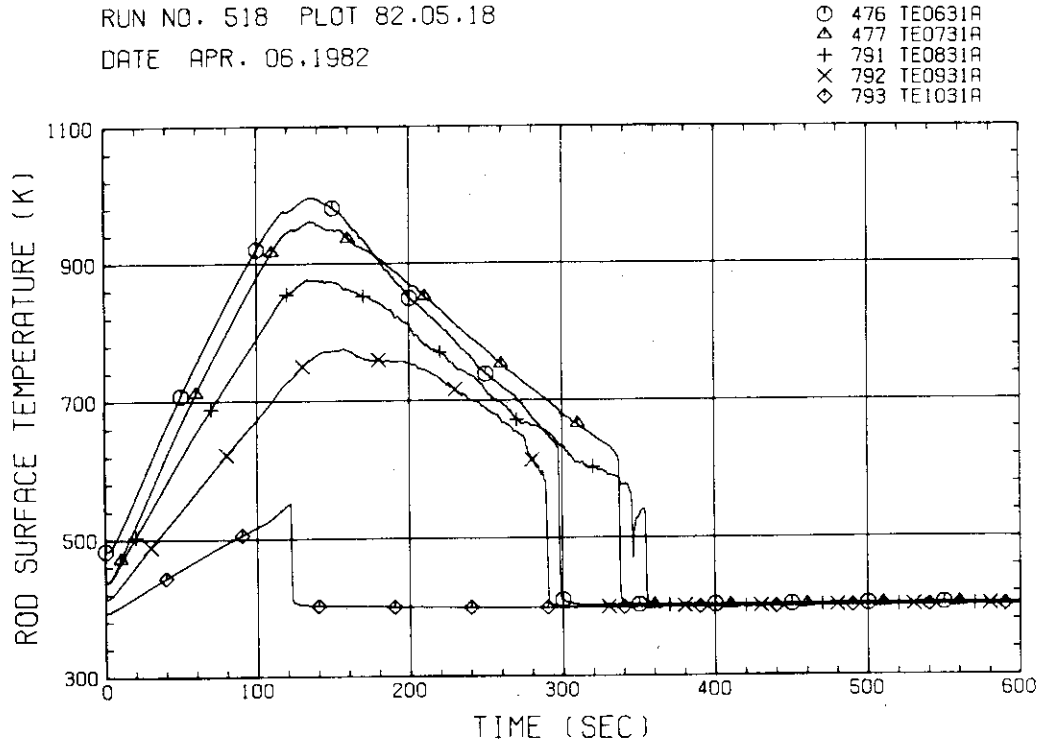

Fig. B-10 HEATER ROD TEMPERATURE (BUNDLE 3-1A, UPPER HALF)

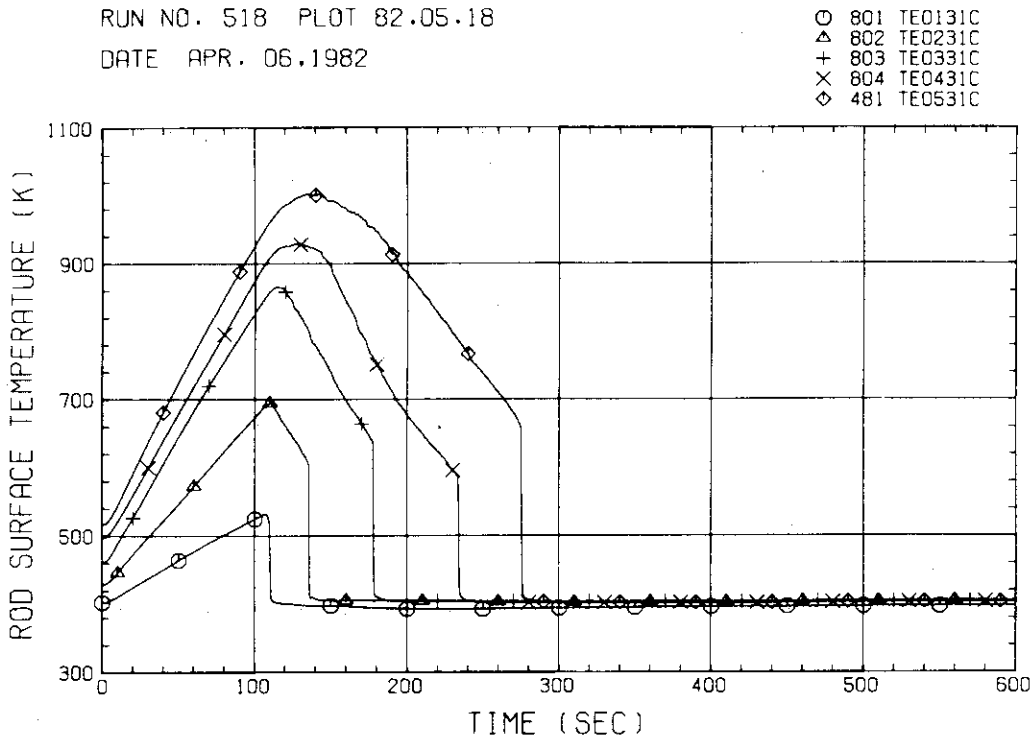

Fig. B-11 HEATER ROD TEMPERATURE (BUNDLE 3-1C, LOWER HALF)

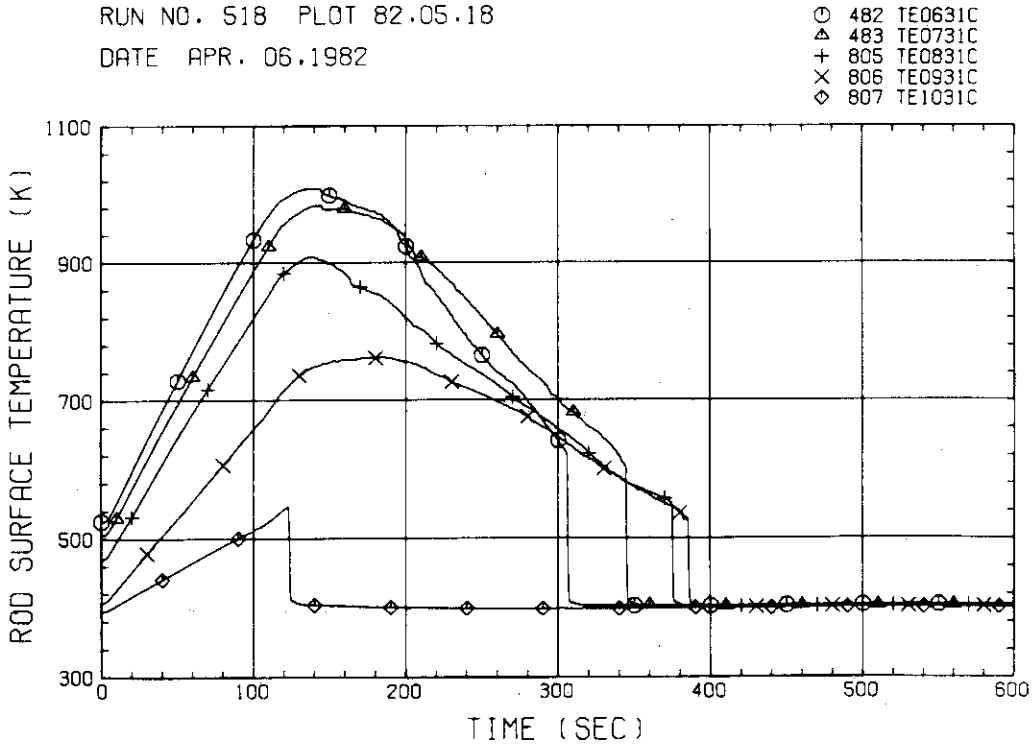

Fig. B-12 HEATER ROD TEMPERATURE (BUNDLE 3-1C, UPPER HALF)

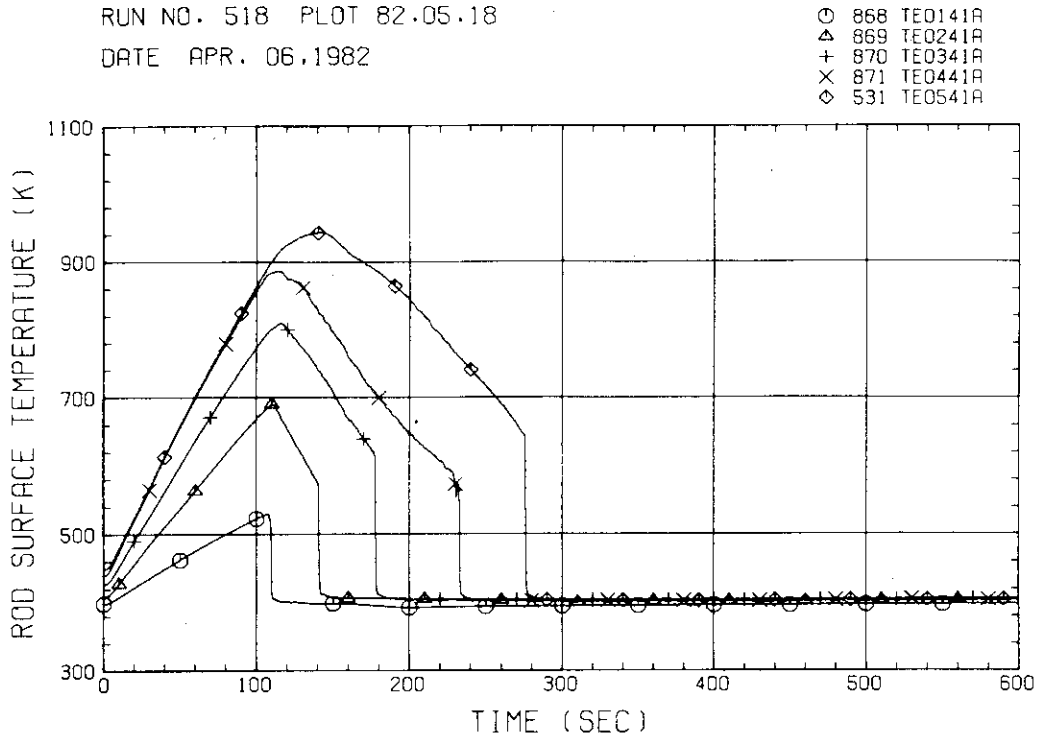

Fig. B-13 HEATER ROD TEMPERATURE (BUNDLE 4-1A, LOWER HALF)

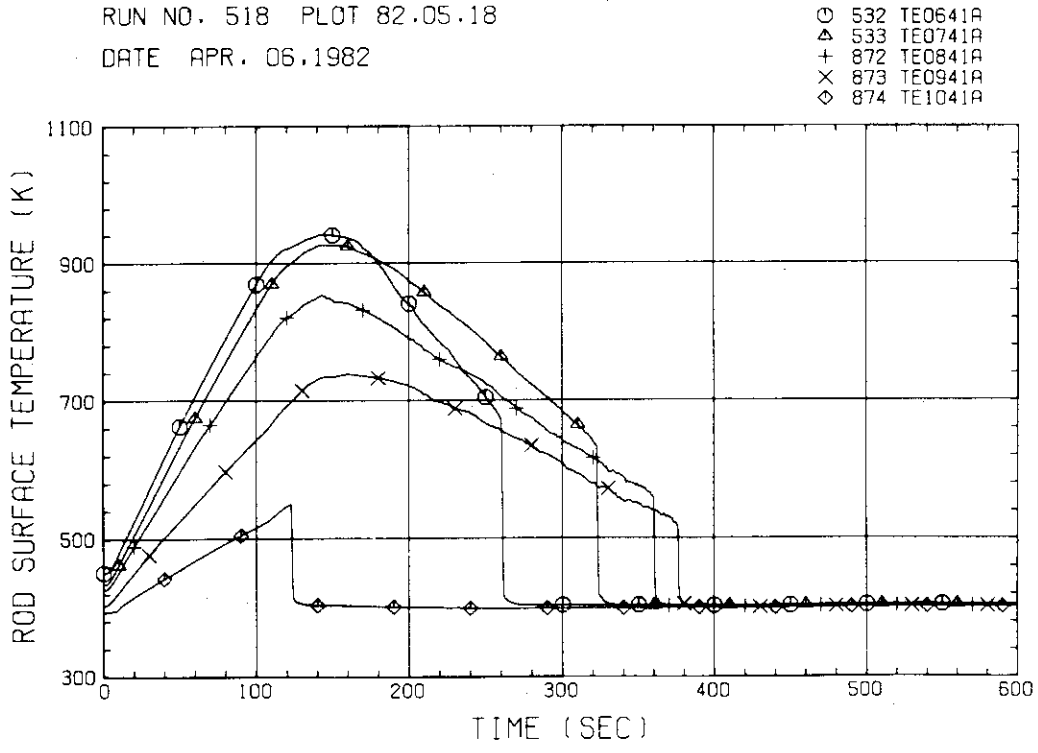

Fig. B-14 HEATER ROD TEMPERATURE (BUNDLE 4-1A, UPPER HALF)

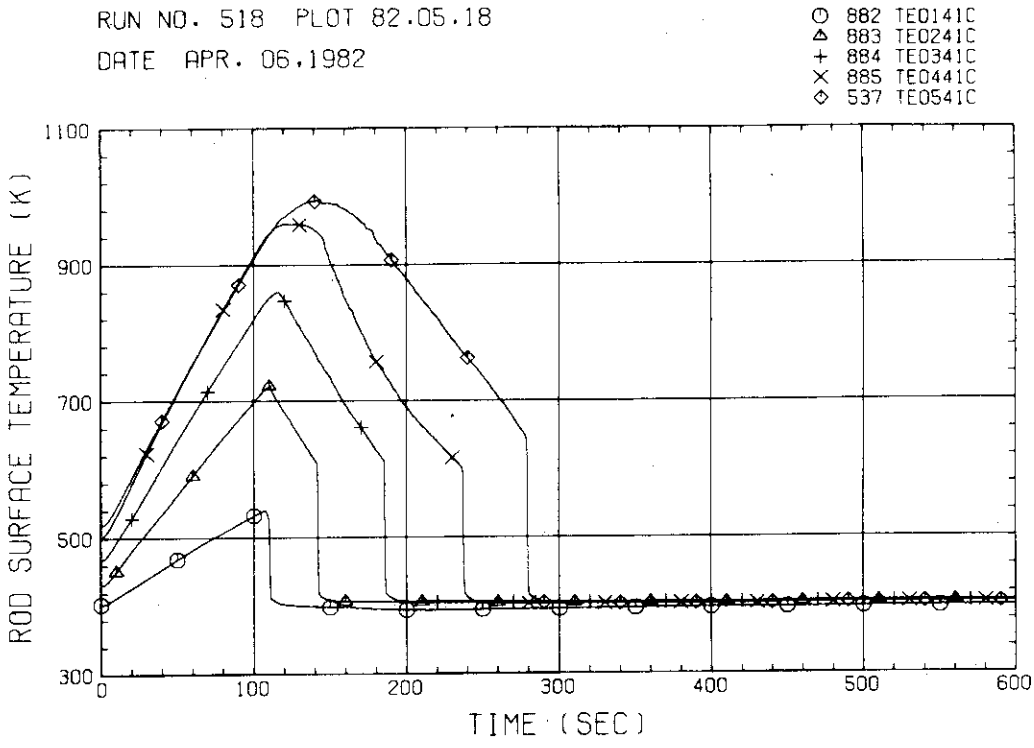

Fig. B-15 HEATER ROD TEMPERATURE (BUNDLE 4-1C, LOWER HALF)

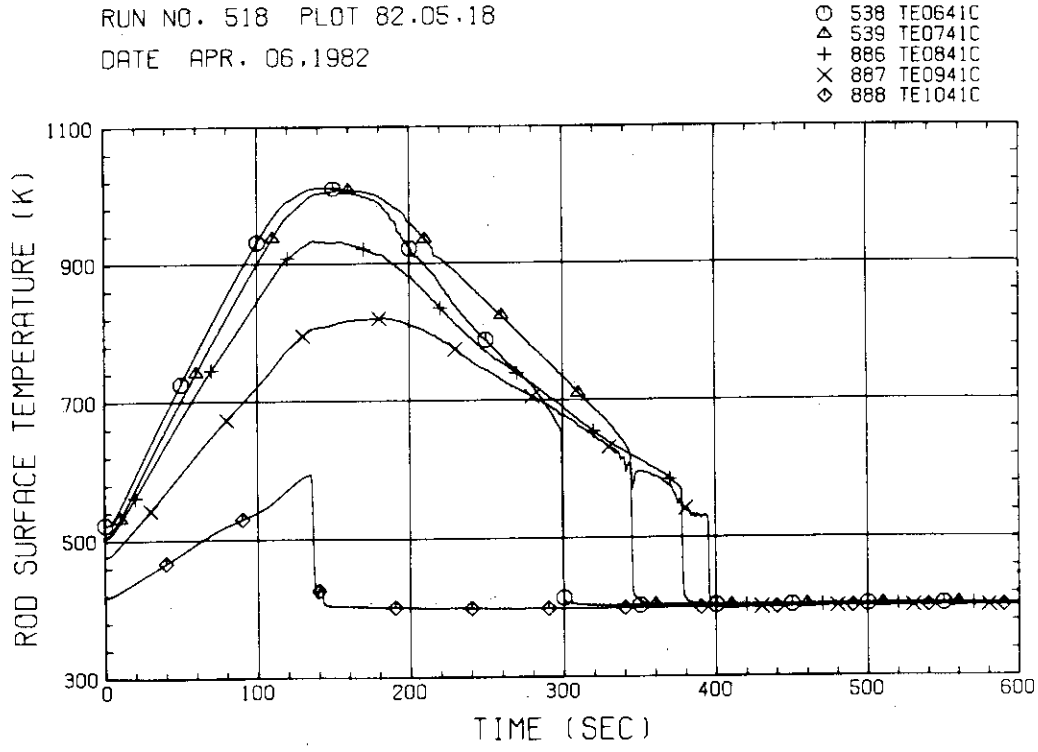

Fig. B-16 HEATER ROD TEMPERATURE (BUNDLE 4-1C, UPPER HALF)

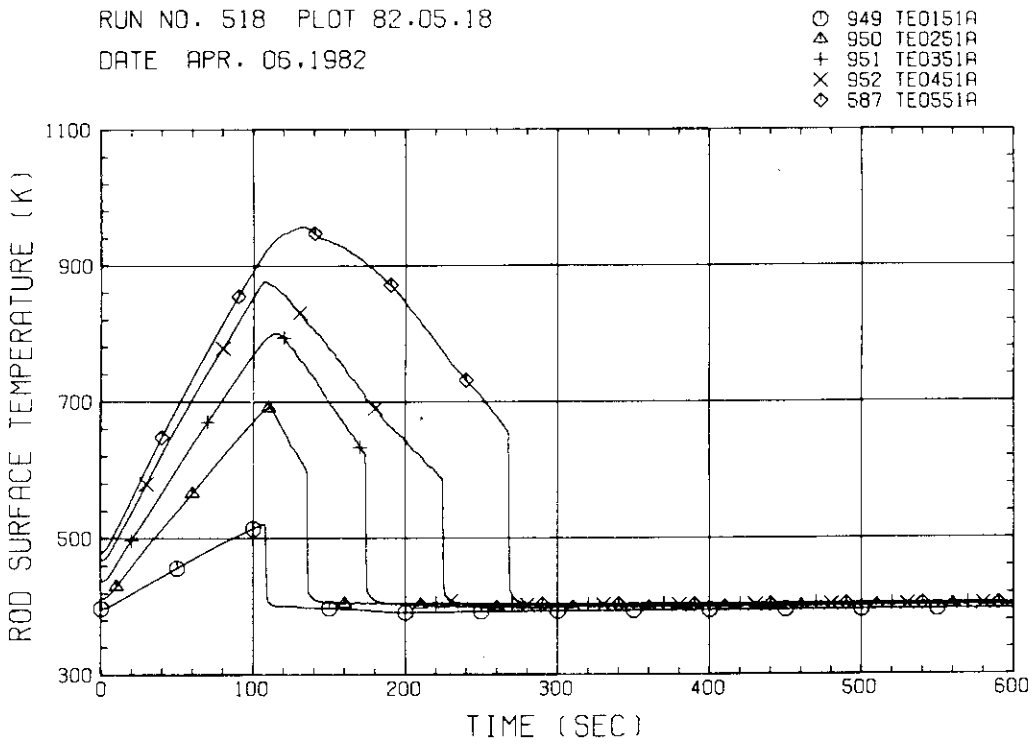

Fig. B-17 HEATER ROD TEMPERATURE (BUNDLE 5-1A, LOWER HALF)

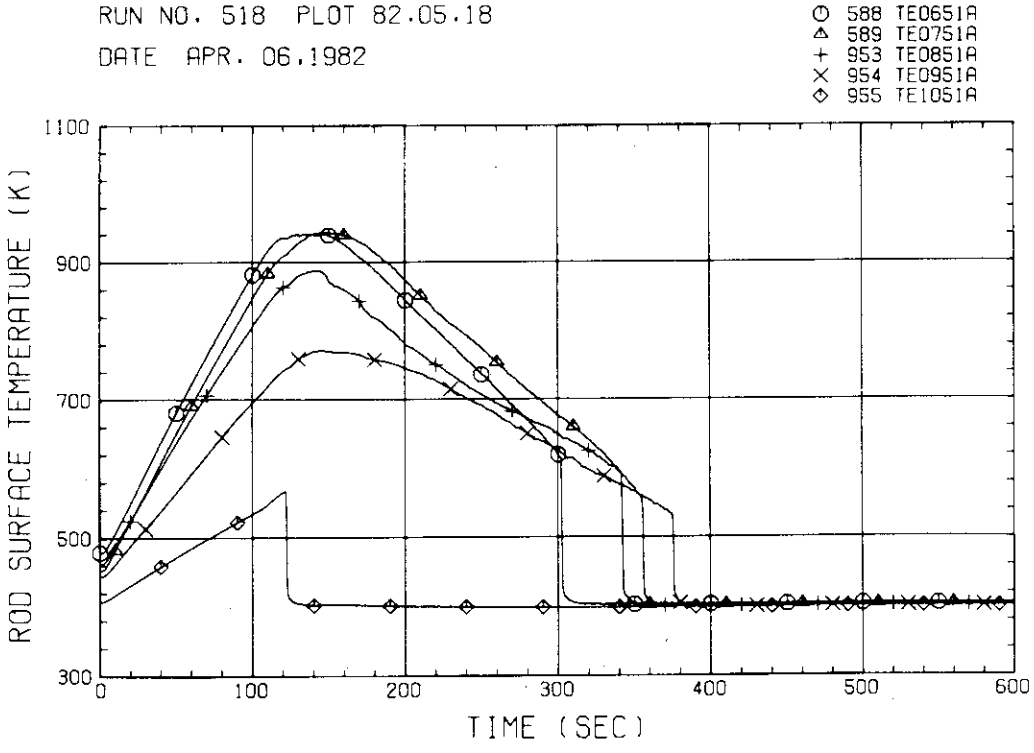

Fig. B-18 HEATER ROD TEMPERATURE (BUNDLE 5-1A, UPPER HALF)

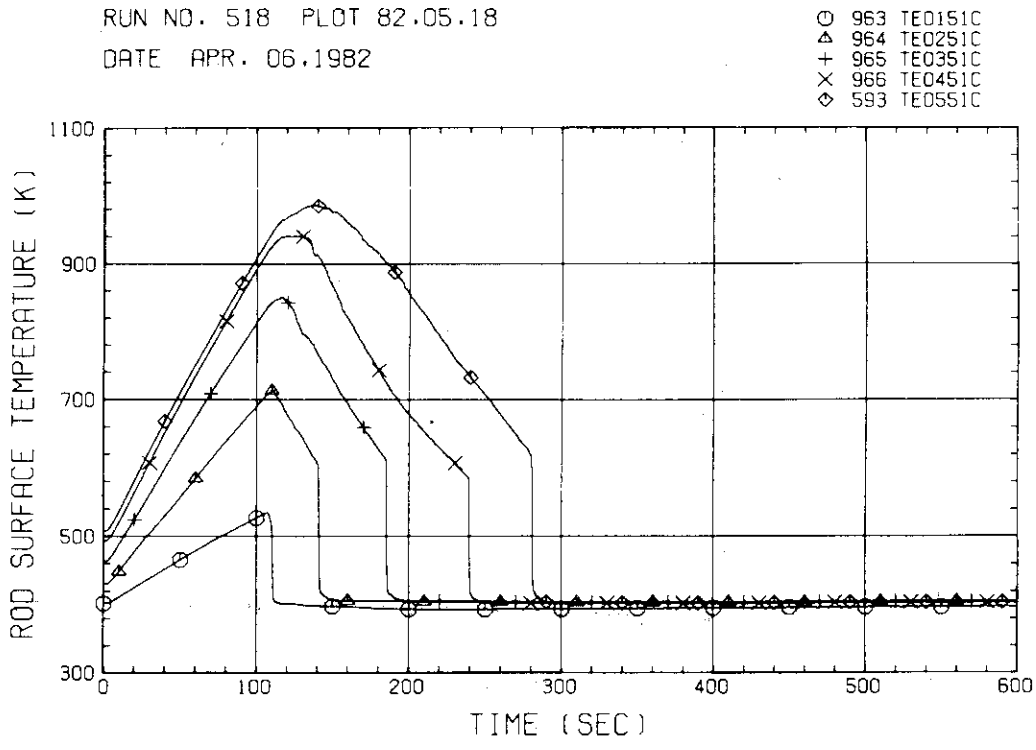

Fig. B-19 HEATER ROD TEMPERATURE (BUNDLE 5-1C, LOWER HALF)

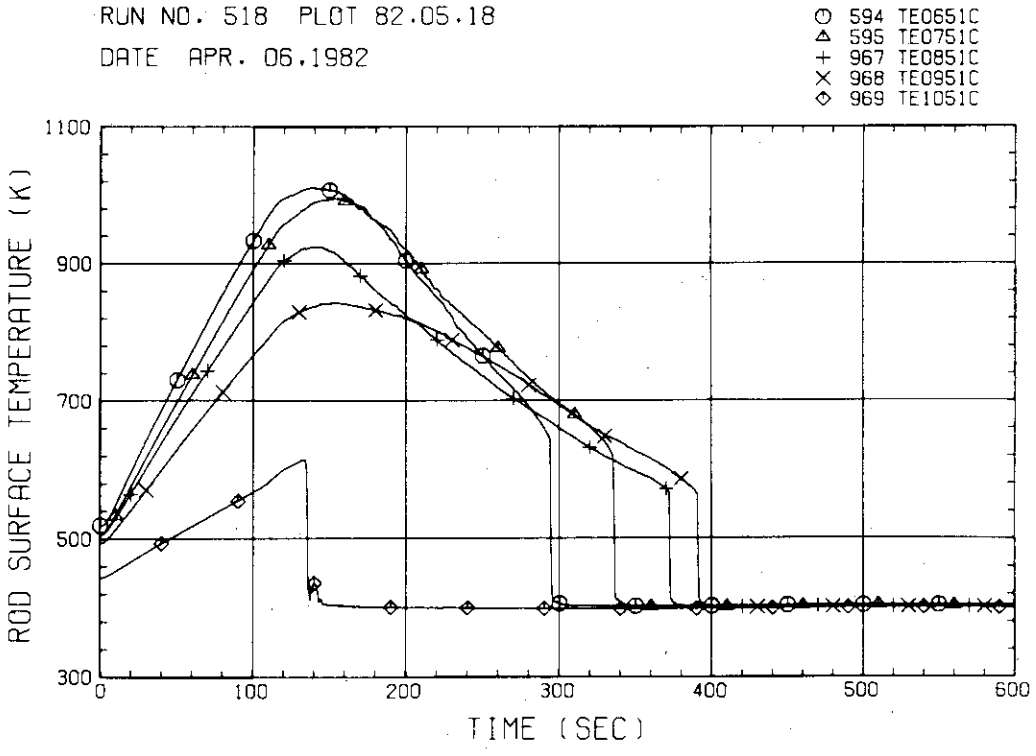

Fig. B-20 HEATER ROD TEMPERATURE (BUNDLE 5-1C, UPPER HALF)

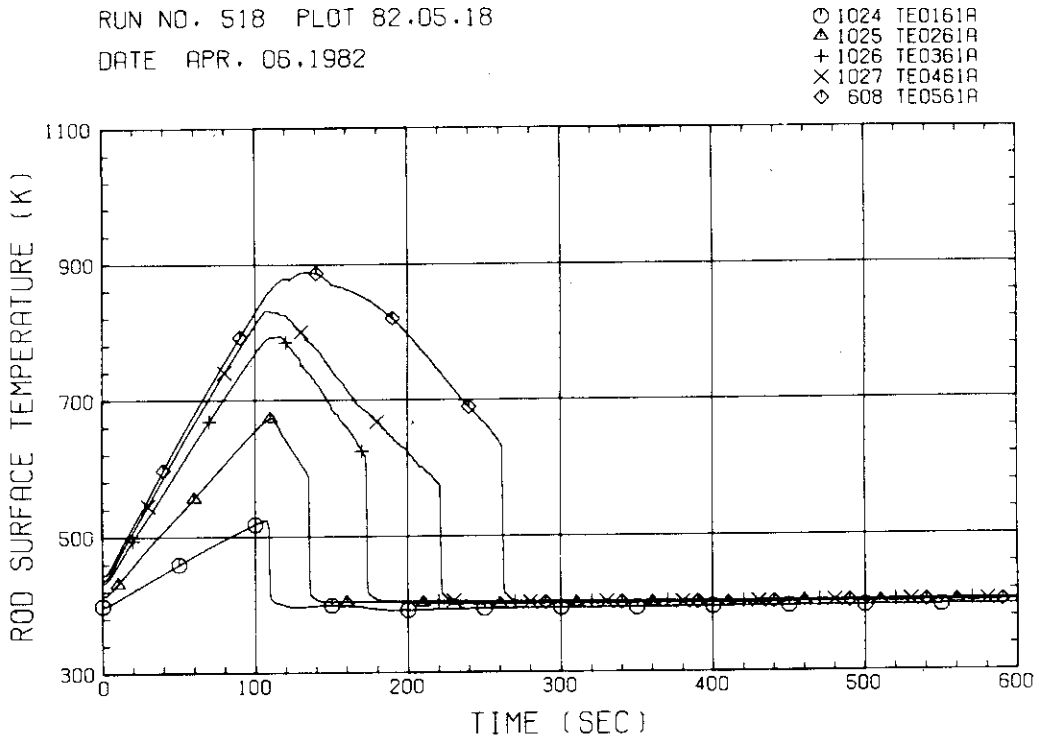

Fig. B-21 HEATER ROD TEMPERATURE (BUNDLE 6-1A, LOWER HALF)

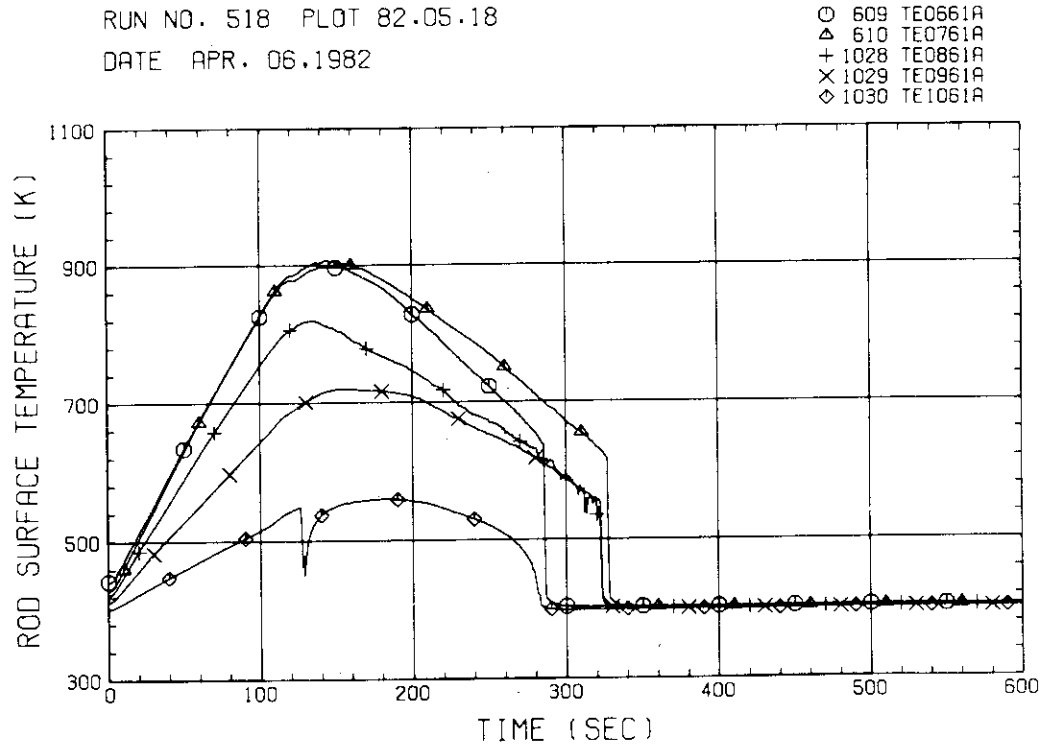

Fig. B-22 HEATER ROD TEMPERATURE (BUNDLE 6-1A, UPPER HALF)

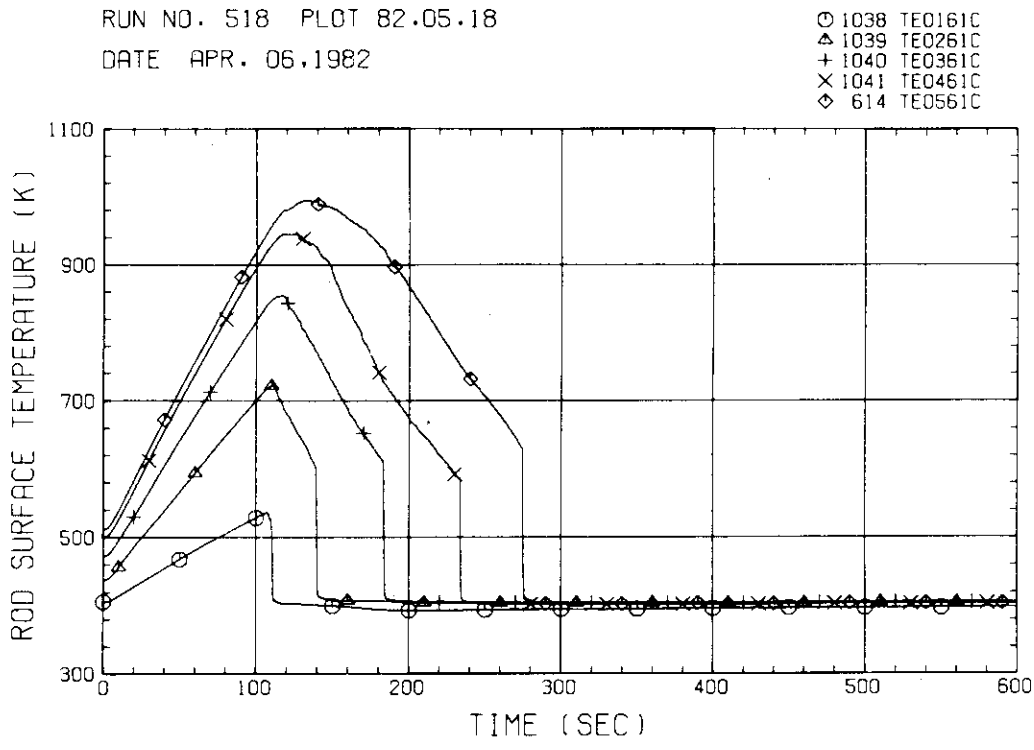

Fig. B-23 HEATER ROD TEMPERATURE (BUNDLE 6-1C, LOWER HALF)

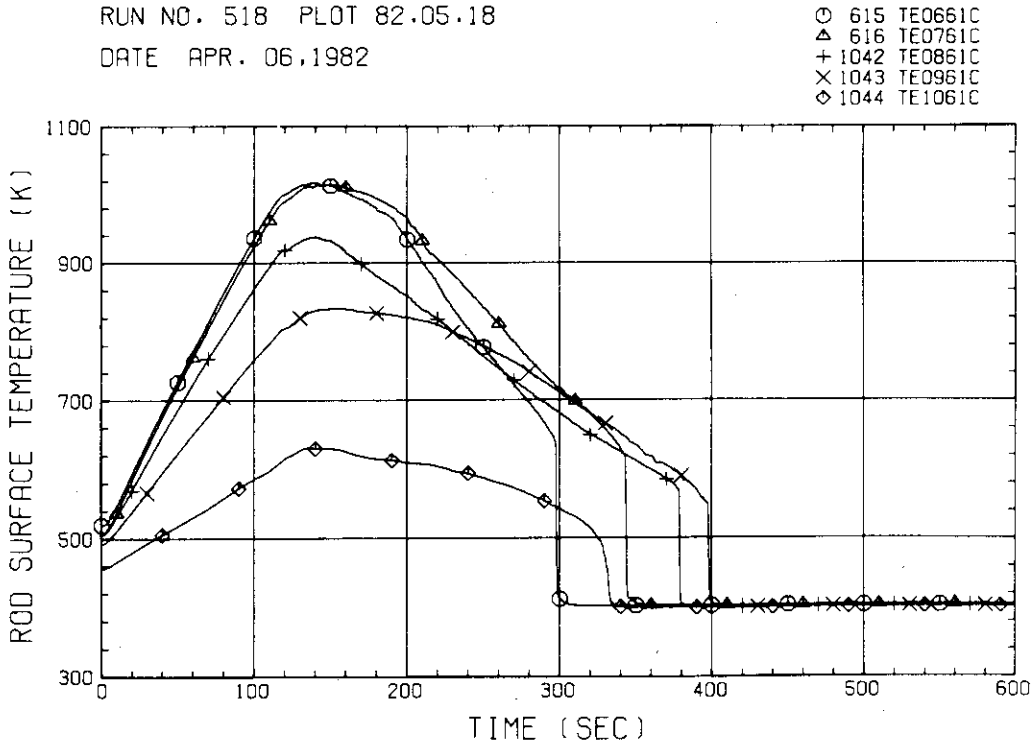

Fig. B-24 HEATER ROD TEMPERATURE (BUNDLE 6-1C, UPPER HALF)

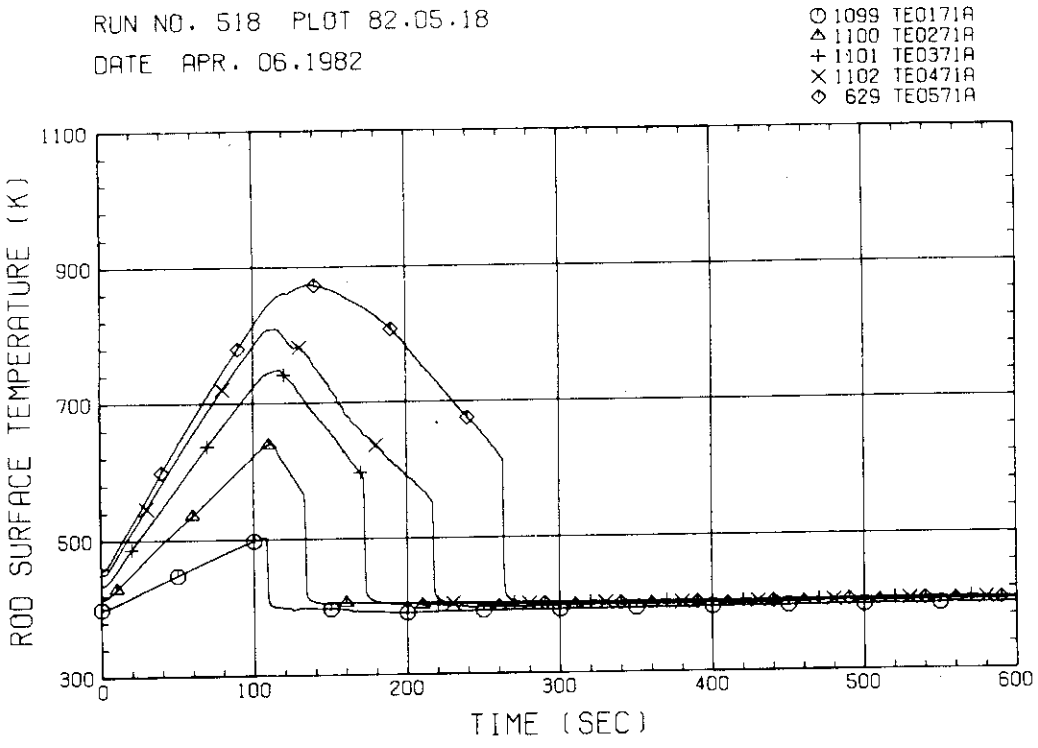

Fig. B-25 HEATER ROD TEMPERATURE (BUNDLE 7-1A, LOWER HALF)

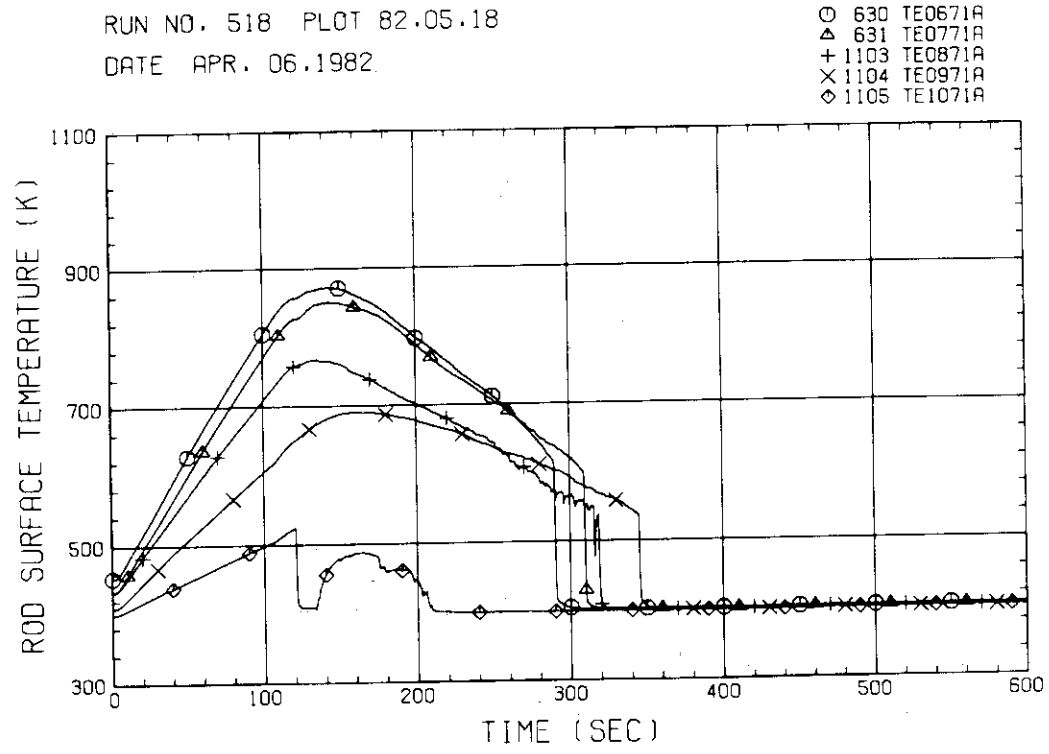

Fig. B-26 HEATER ROD TEMPERATURE (BUNDLE 7-1A, UPPER HALF)

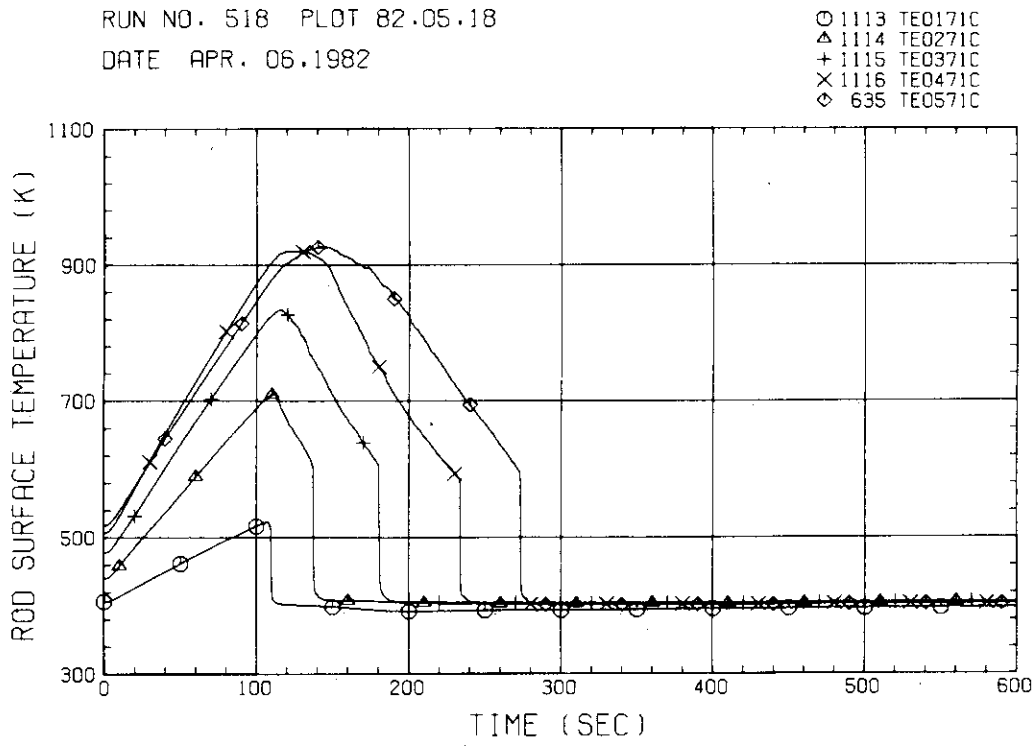

Fig. B-27 HEATER ROD TEMPERATURE (BUNDLE 7-1C, LOWER HALF)

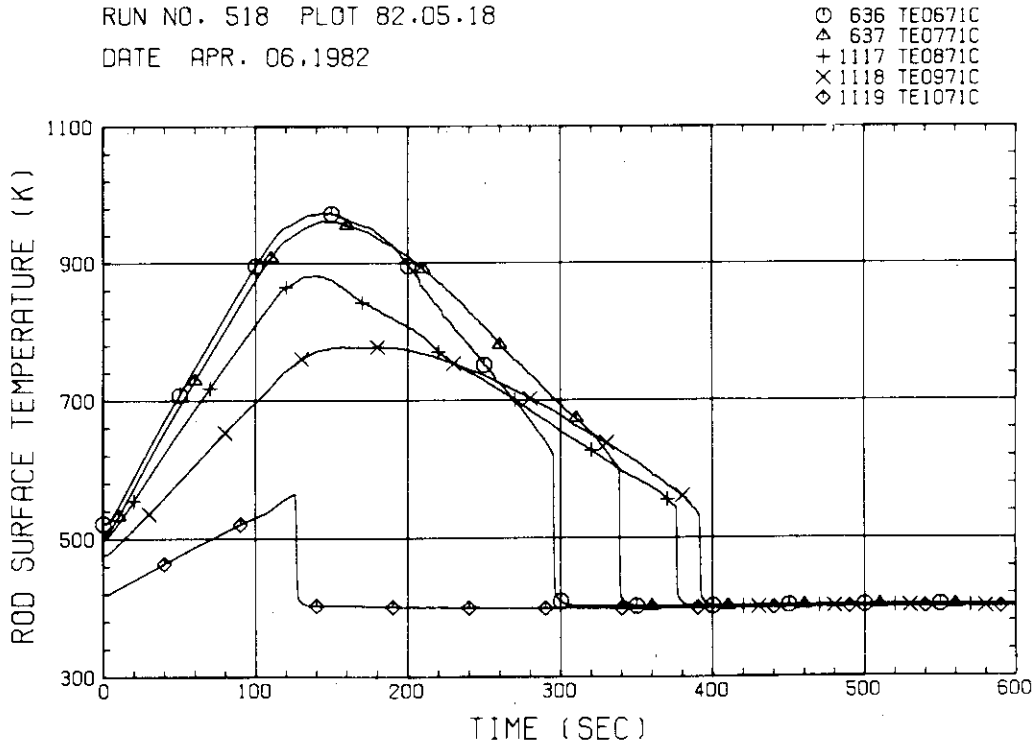

Fig. B-28 HEATER ROD TEMPERATURE (BUNDLE 7-1C, UPPER HALF)

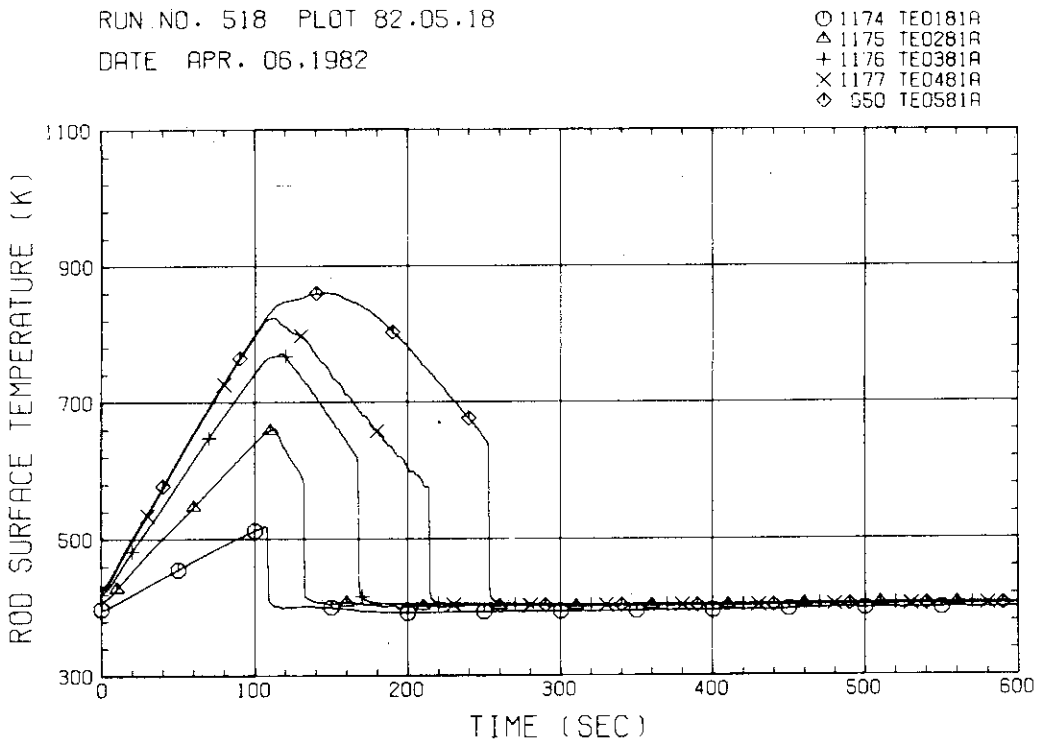

Fig. B-29 HEATER ROD TEMPERATURE (BUNDLE 8-1A, LOWER HALF)

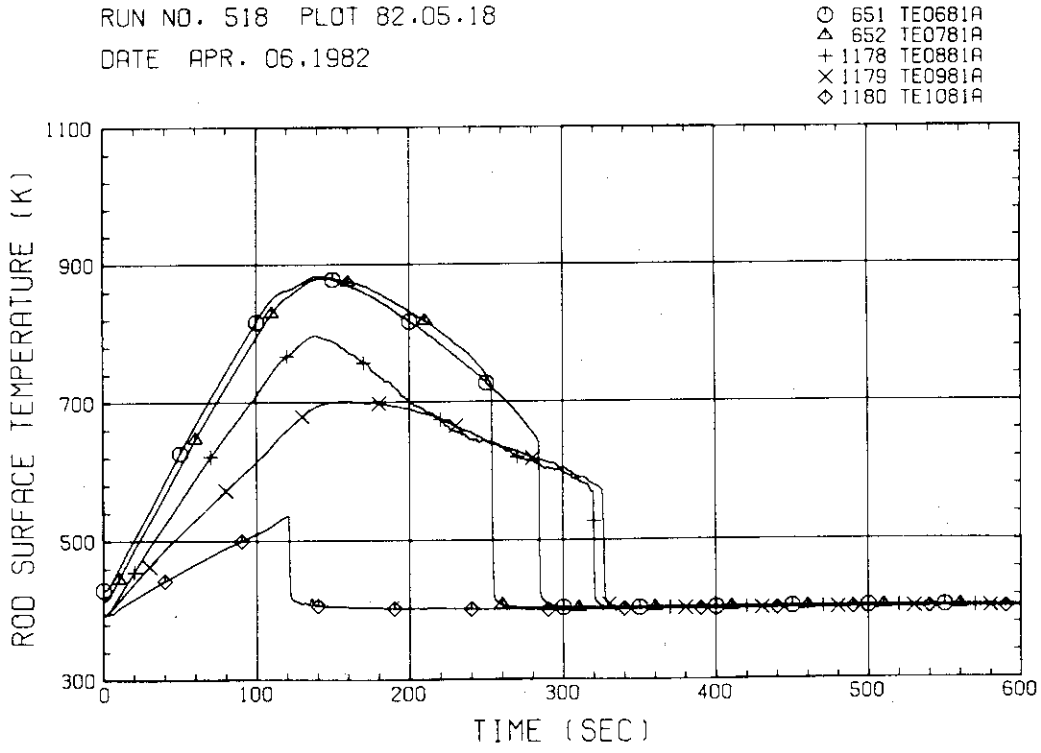

Fig. B-30 HEATER ROD TEMPERATURE (BUNDLE 8-1A, UPPER HALF)

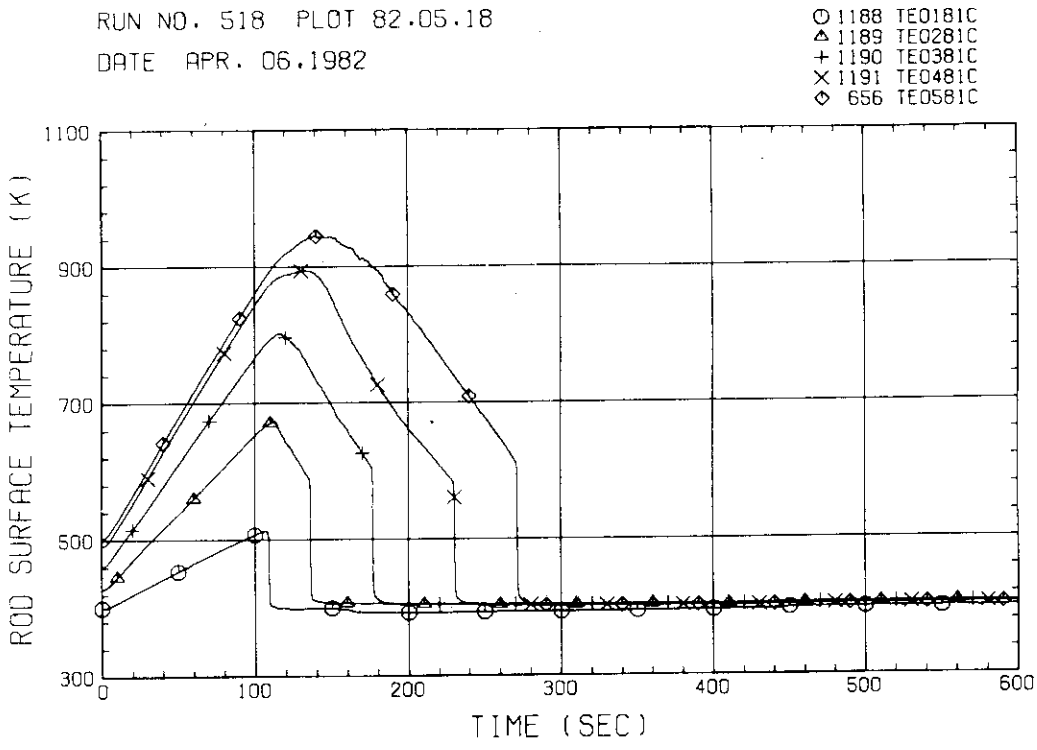

Fig. B-31 HEATER ROD TEMPERATURE (BUNDLE 8-1C, LOWER HALF)

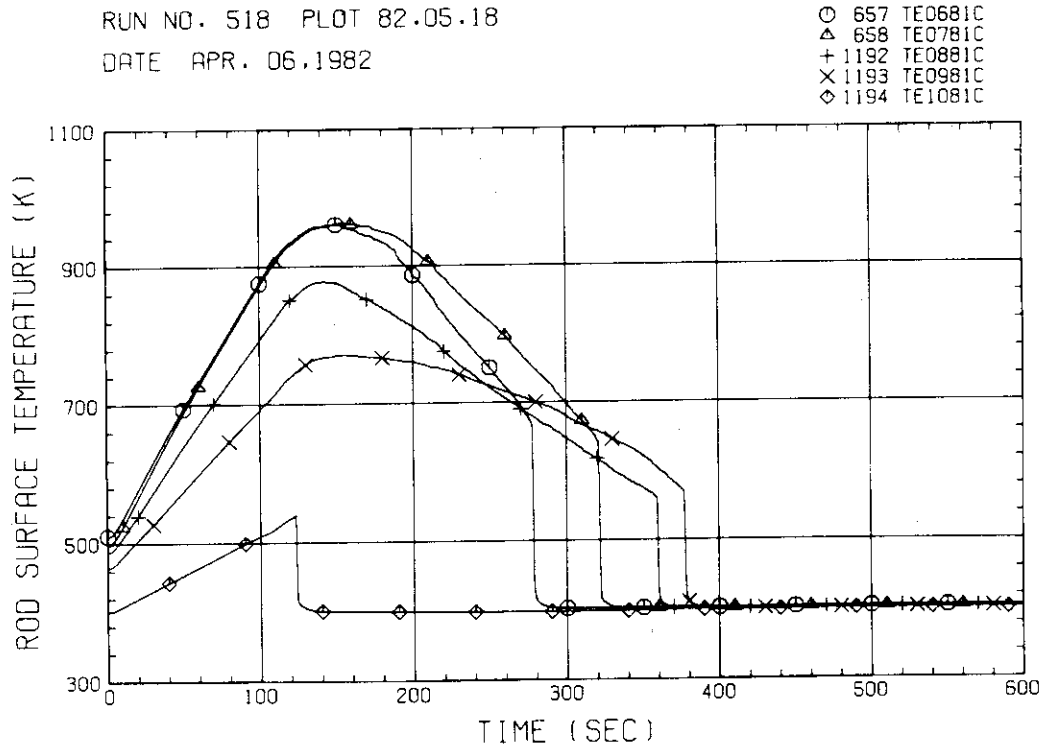

Fig. B-32 HEATER ROD TEMPERATURE (BUNDLE 8-1C, UPPER HALF)

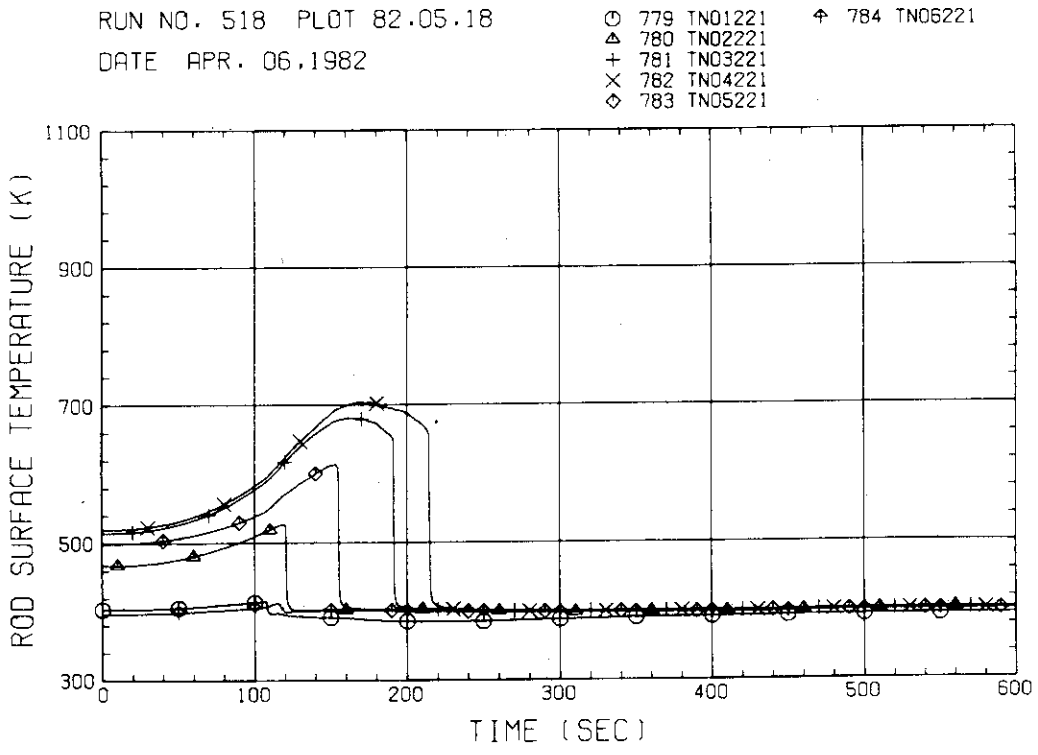

Fig. B-33 NON-HEATED ROD TEMPERATURE (BUNDLE 2-2)

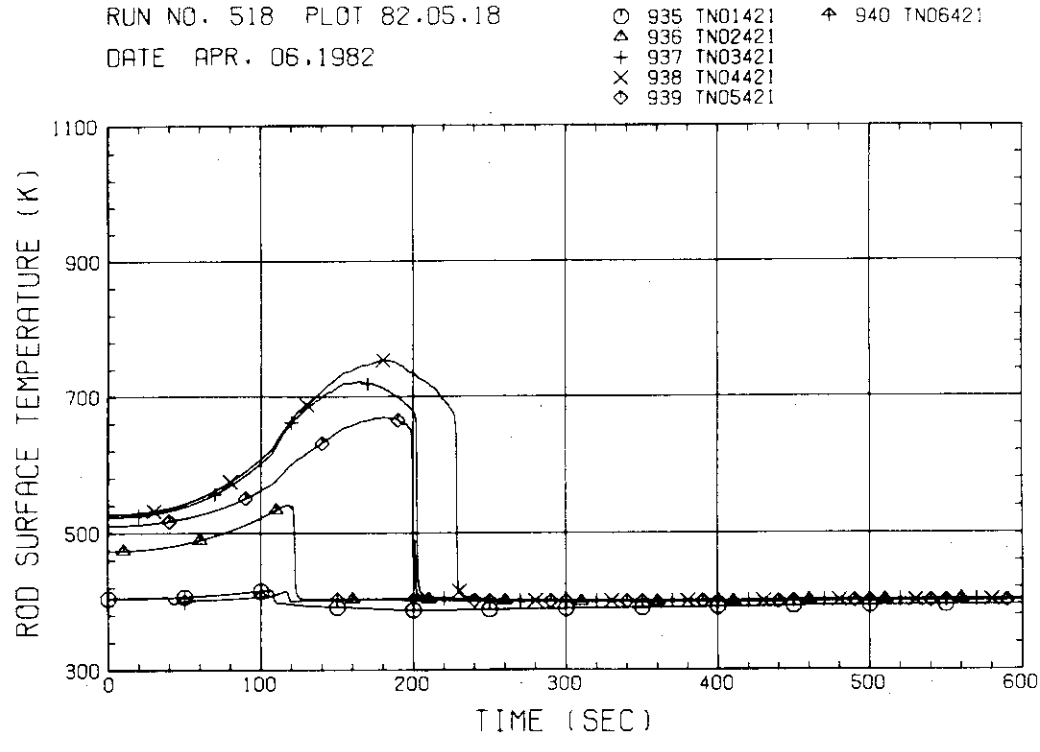

Fig. B-34 NON-HEATED ROD TEMPERATURE (BUNDLE 4-2)

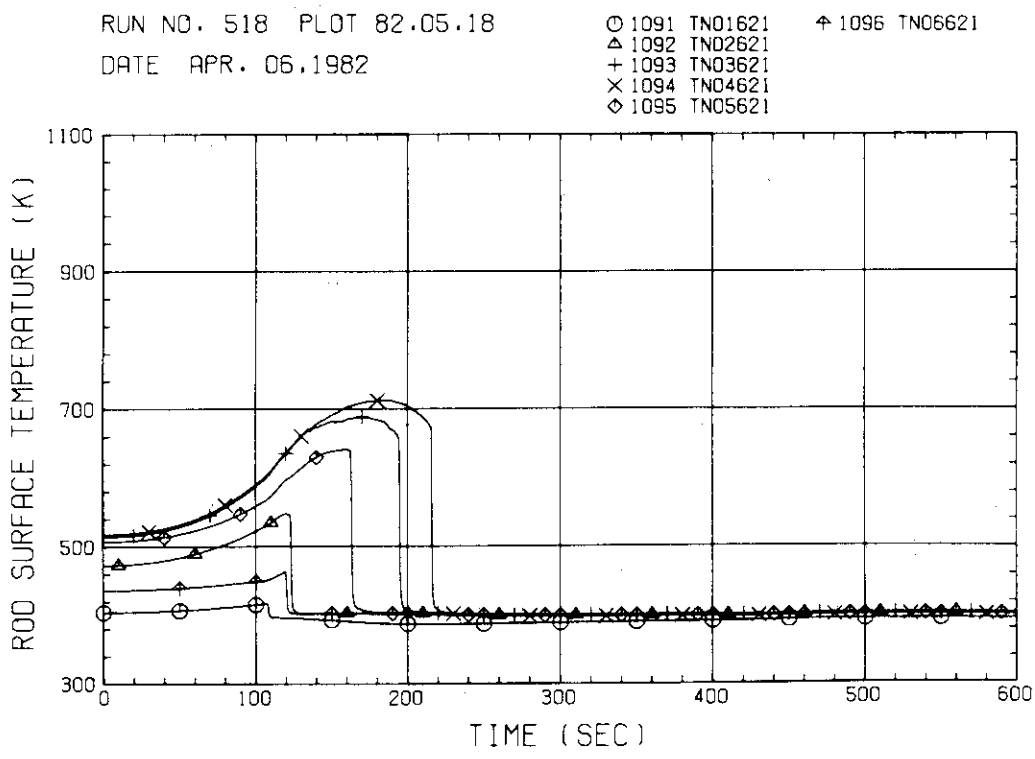

Fig. B-35 NON-HEATED ROD TEMPERATURE (BUNDLE 6-2)

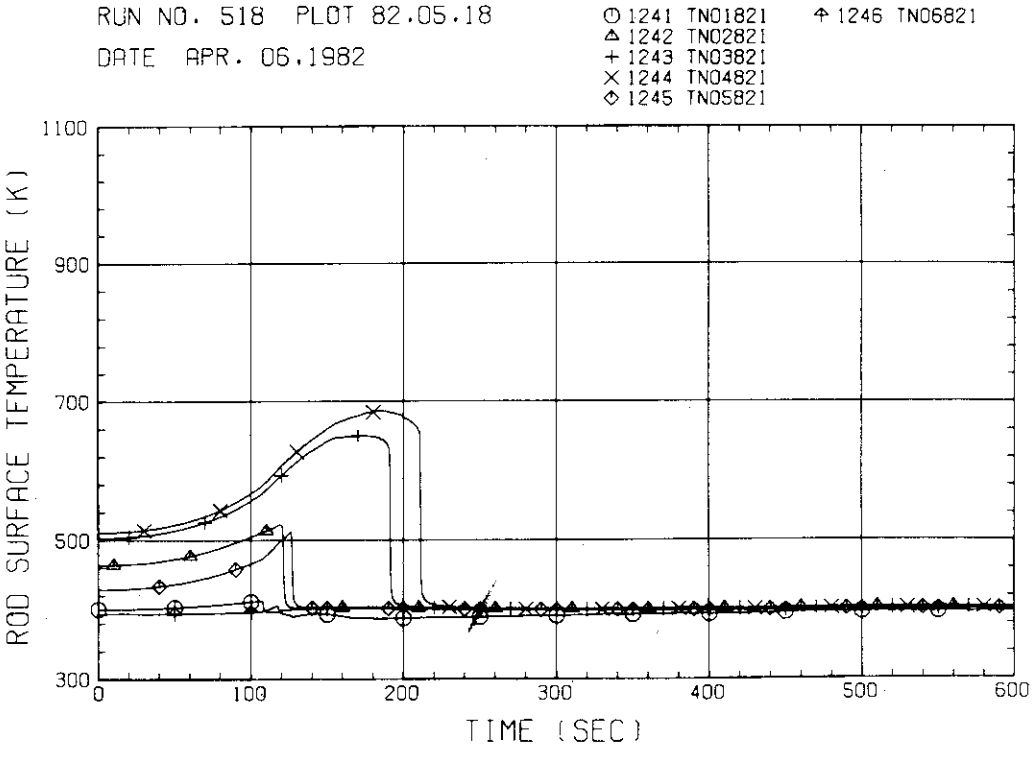

Fig. B-36 NON-HEATED ROD TEMPERATURE (BUNDLE 8-2)

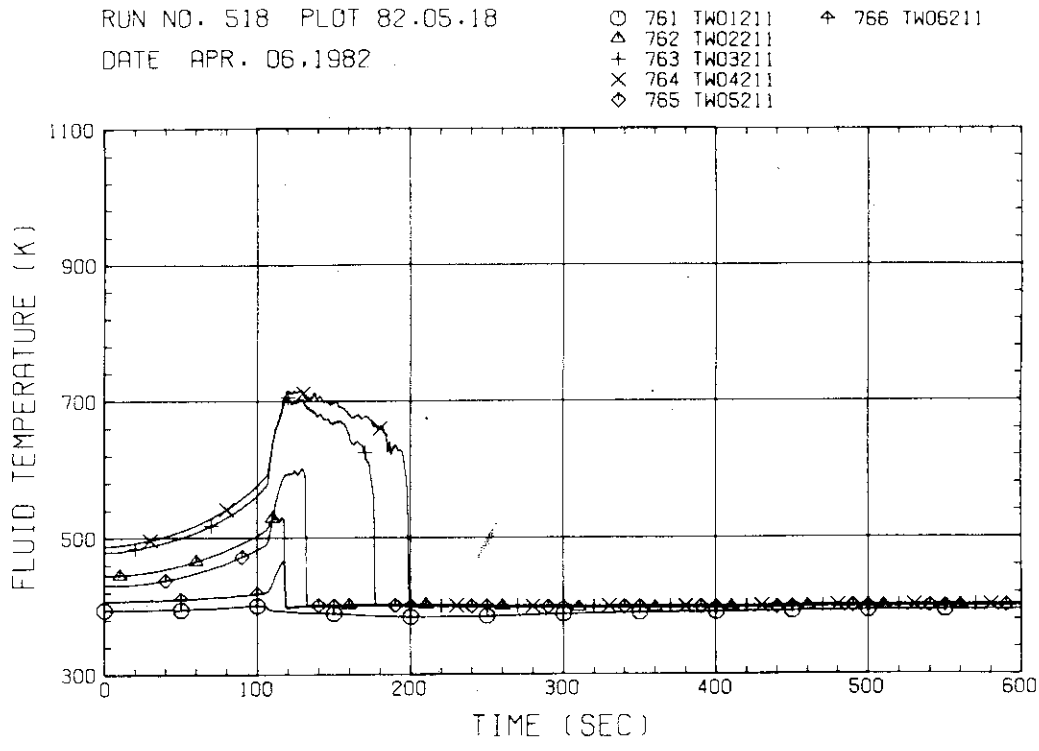

Fig. B-37 FLUID TEMPERATURE IN CORE (BUNDLE 2-1)

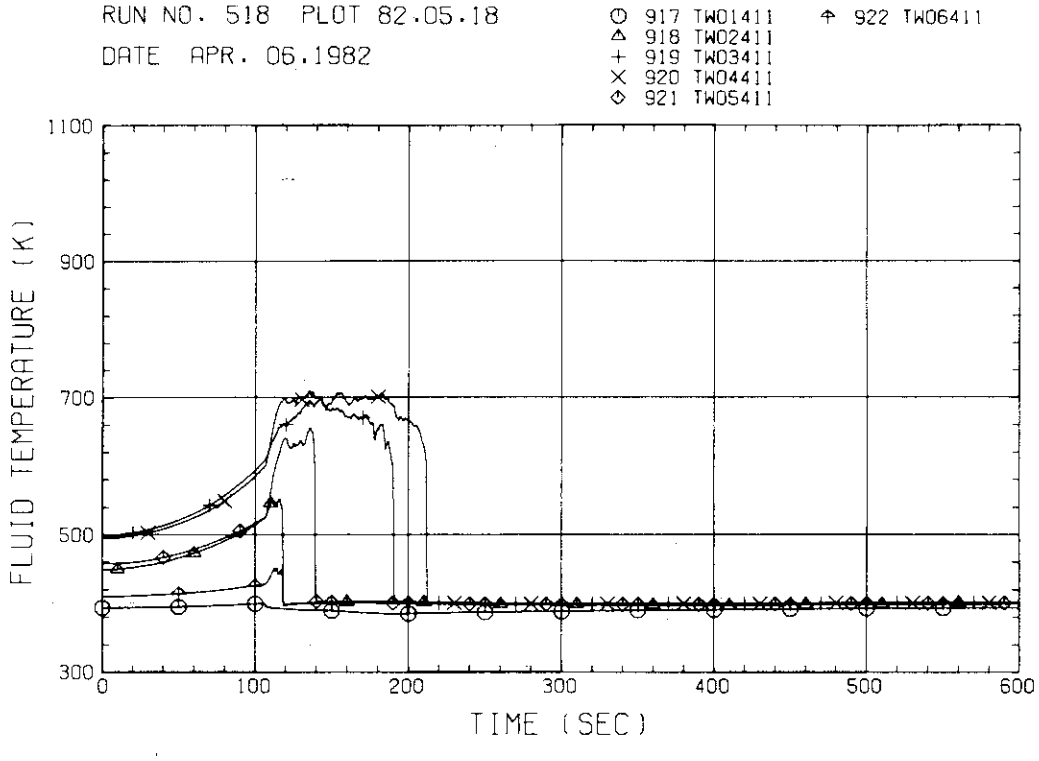

Fig. B-38 FLUID TEMPERATURE IN CORE (BUNDLE 4-1)

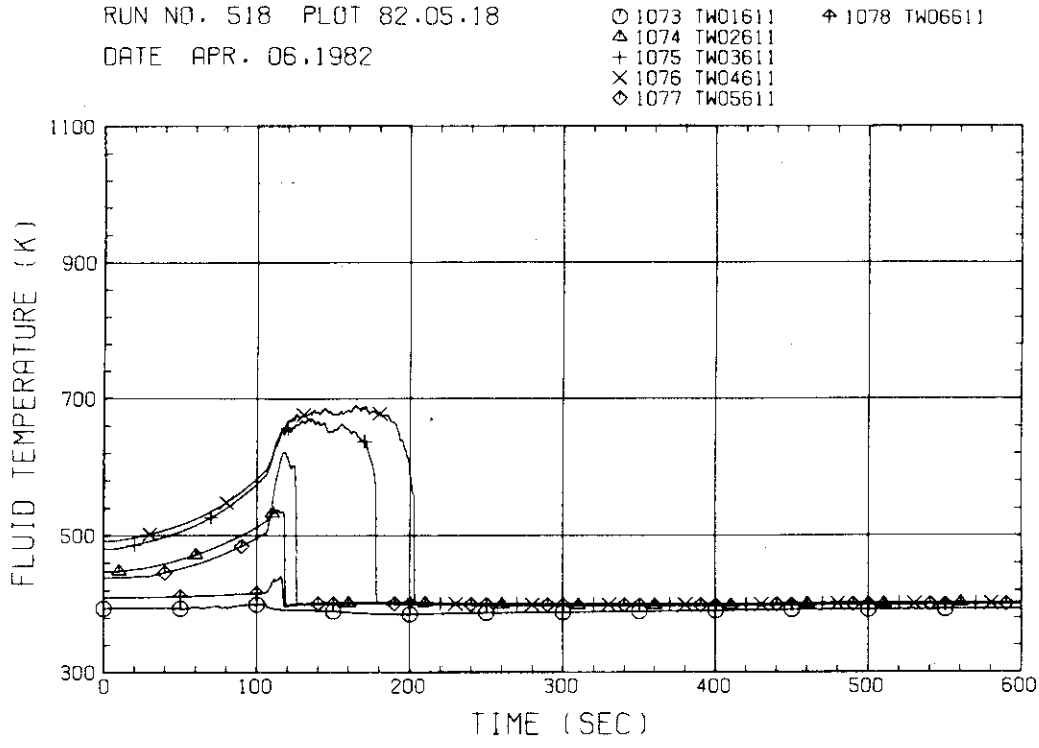

Fig. B-39 FLUID TEMPERATURE IN CORE (BUNDLE 6-1)

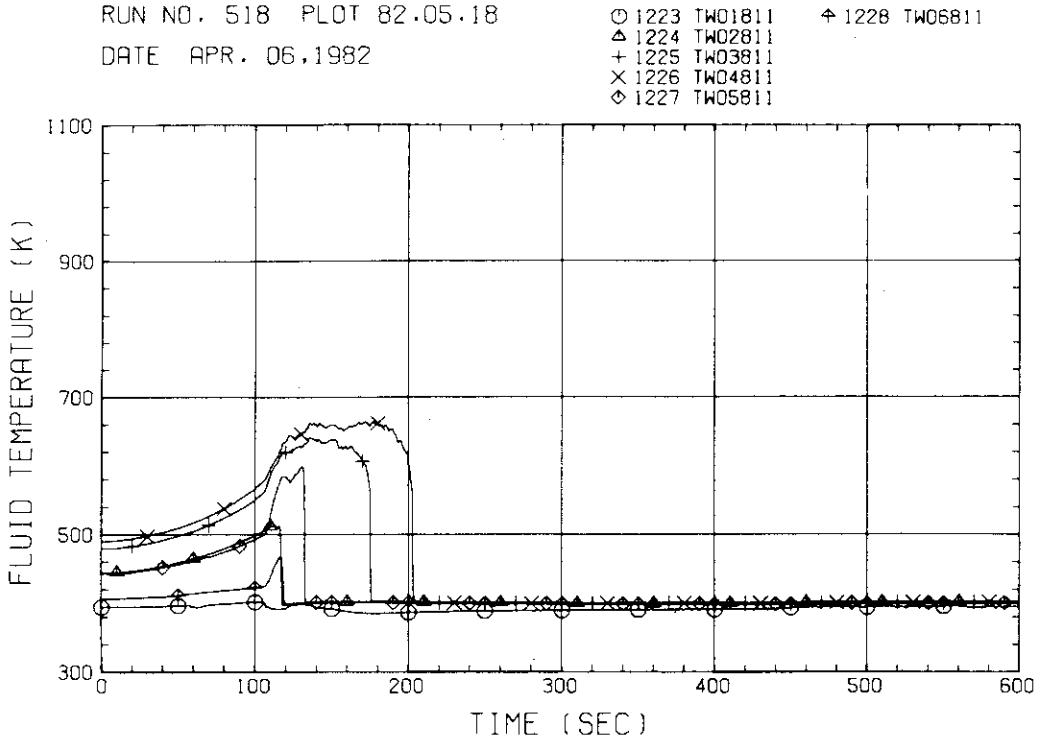

Fig. B-40 FLUID TEMPERATURE IN CORE (BUNDLE 8-1)

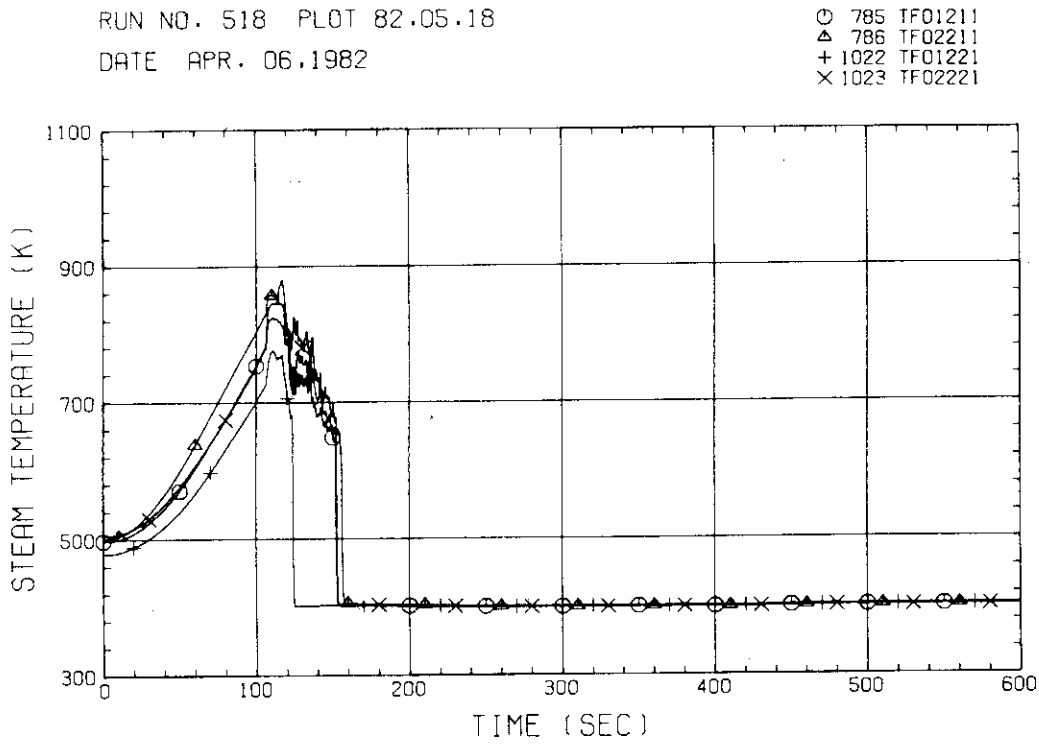

Fig. B-41 STEAM TEMPERATURE IN CORE, BUNDLE 2
(01211-1.735M, 02211-1.875M, 01221-1.38M, 02221-1.915M)

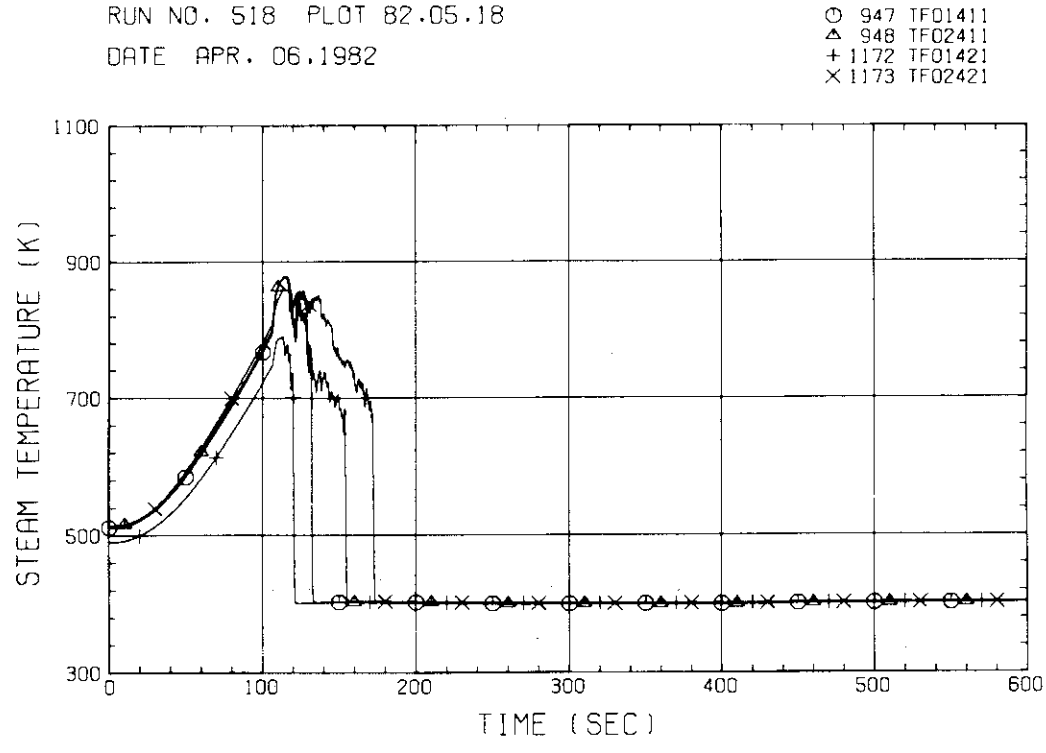

Fig. B-42 STEAM TEMPERATURE IN CORE, BUNDLE 4
(01411-1.735M, 02411-1.875M, 01421-1.38M, 02421-1.915M)

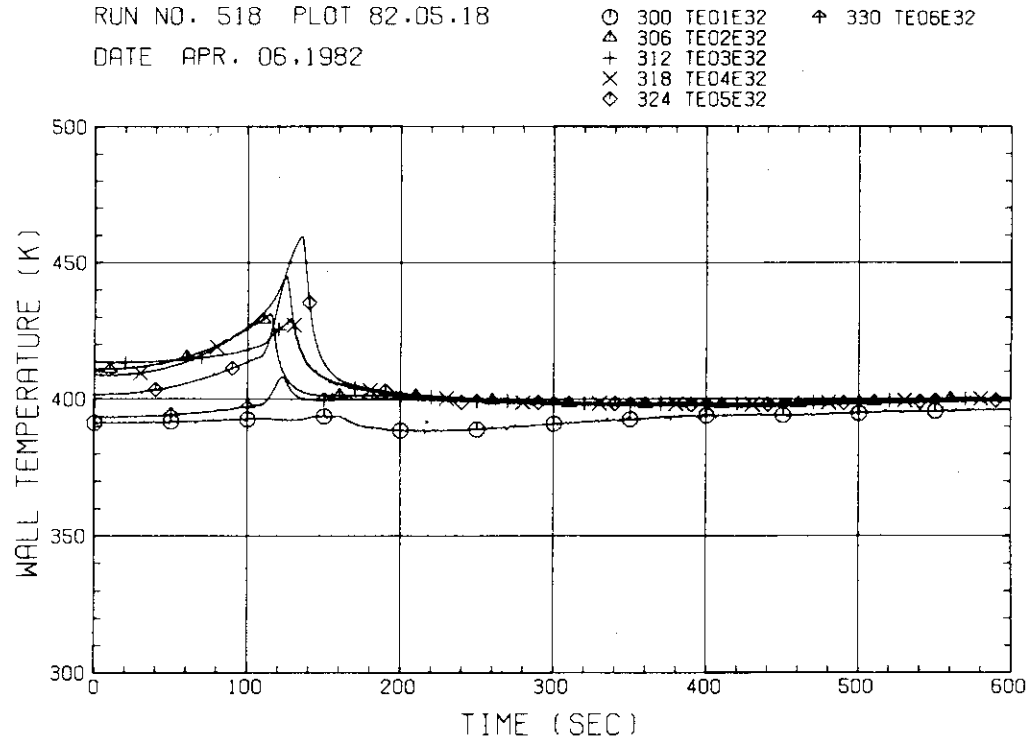

Fig. B-43 SURFACE TEMPERATURE OF CORE SIDE WALL (BUNDLE 3, OPPOSITE SIDE OF COLD LEG, INNER SURFACE)

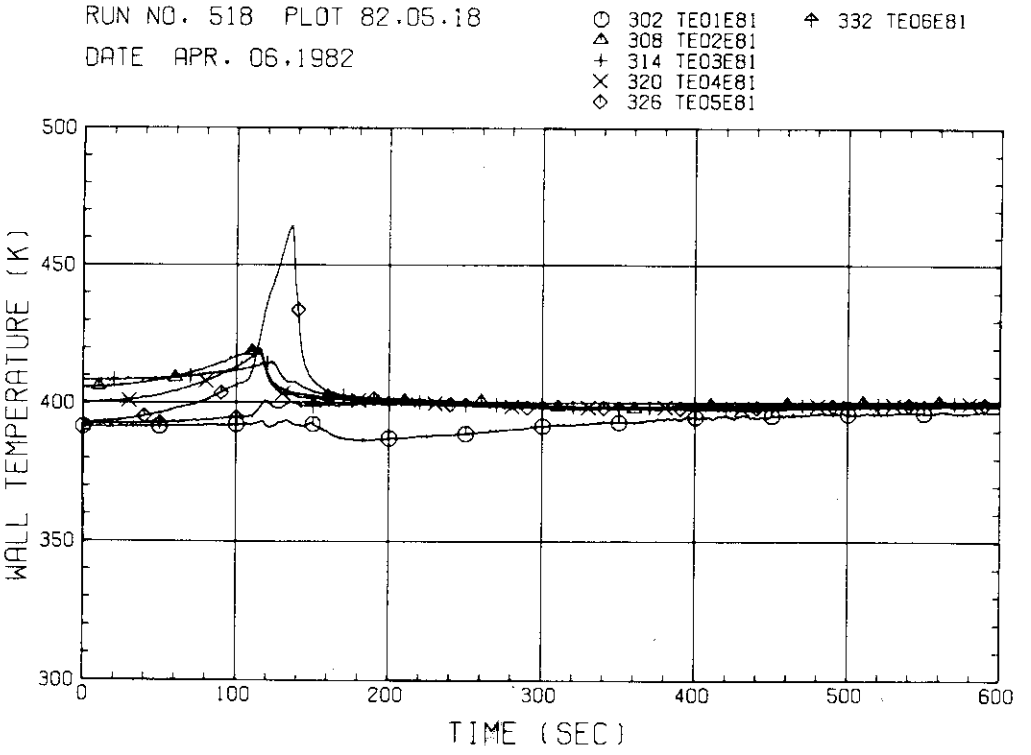

Fig. B-44 SURFACE TEMPERATURE OF CORE SIDE WALL (BUNDLE 8, OPPOSITE SIDE OF COLD LEG, INNER SURFACE)

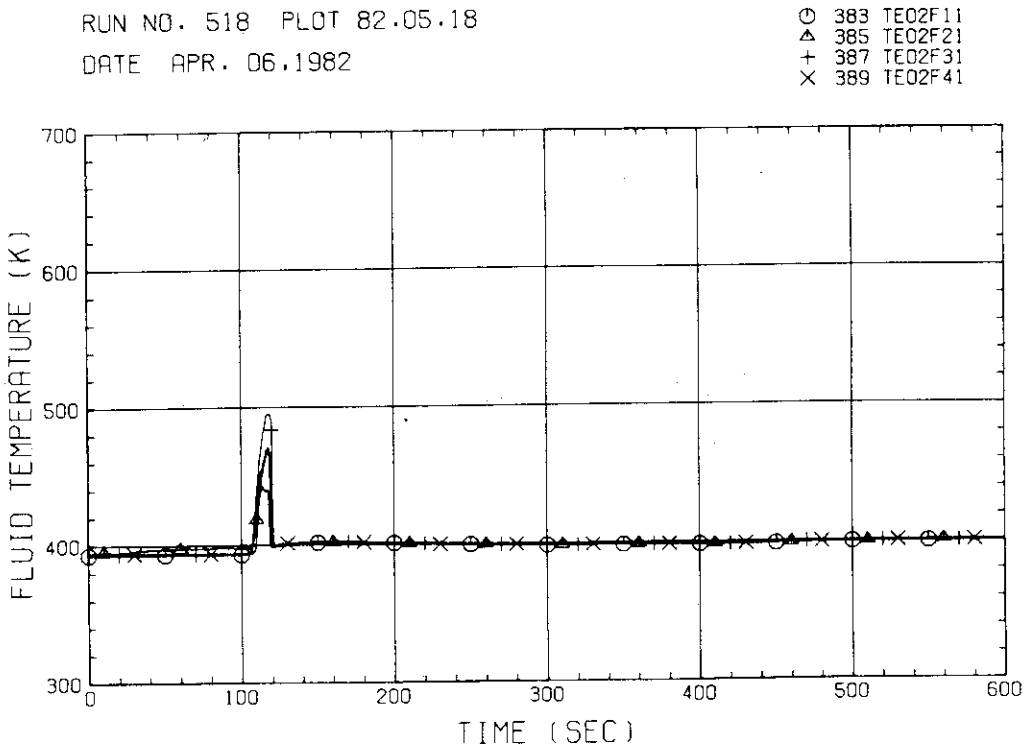

Fig. B-45 FLUID TEMPERATURE JUST ABOVE END BOX TIE PLATE (BUNDLE 1,2,3,4, OPPOSITE SIDE OF COLD LEG)

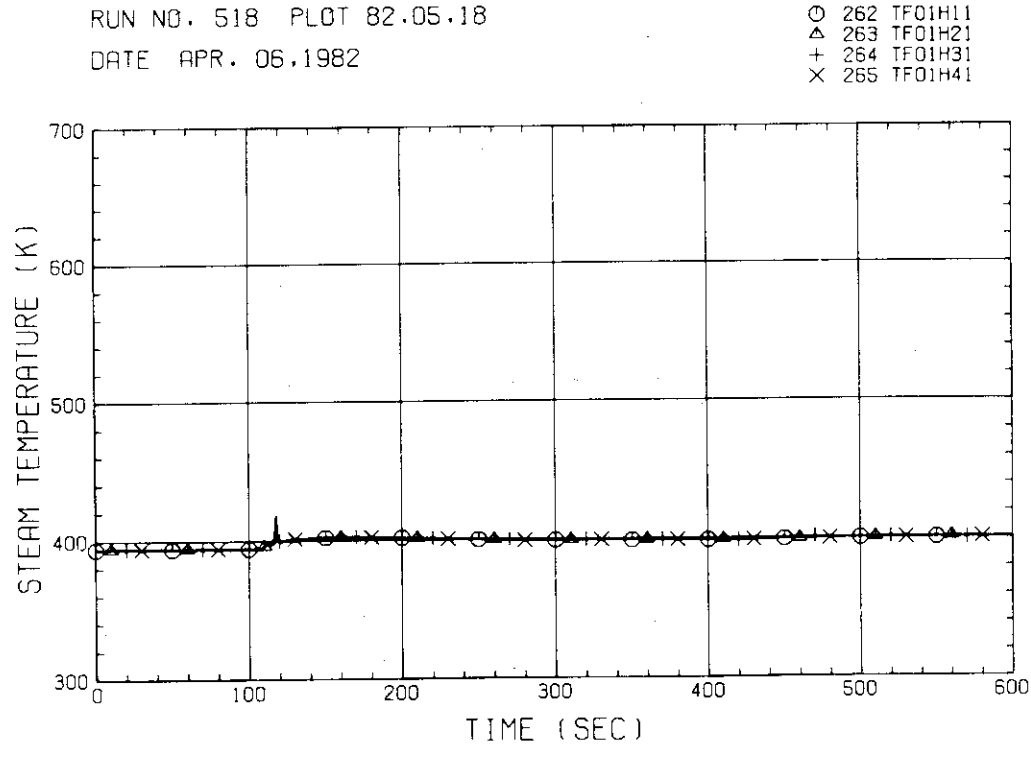

Fig. B-46 STEAM TEMPERATURE ABOVE UCSP HOLE (BUNDLE 1,2,3,4)

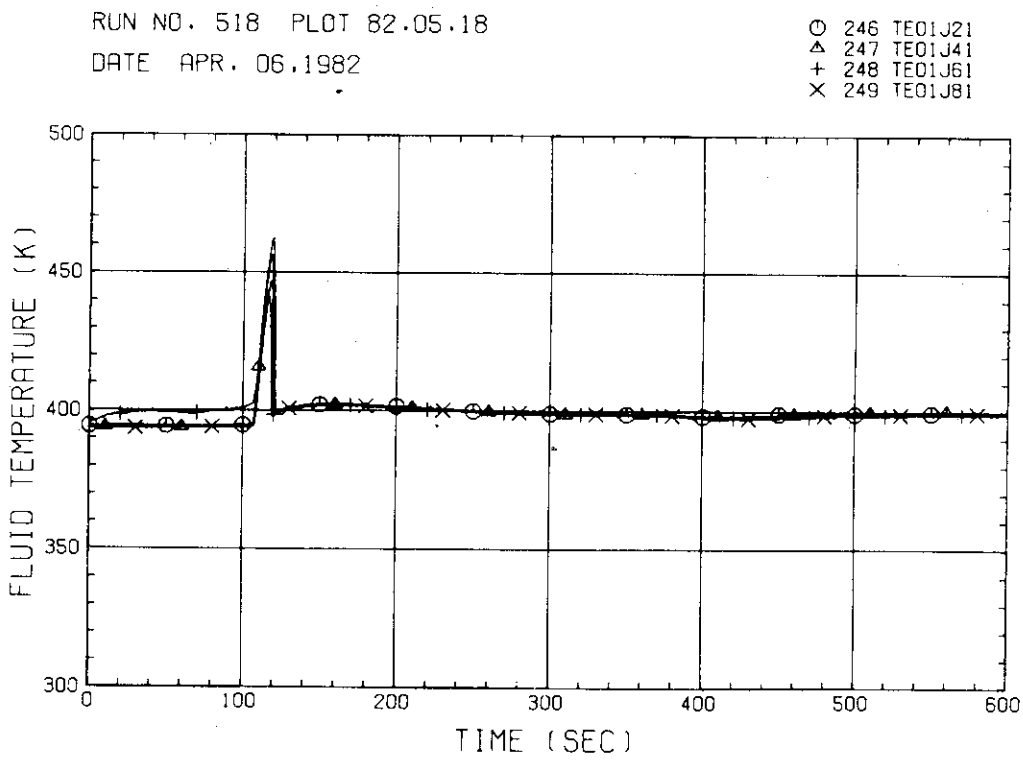

Fig. B-47 FLUID TEMPERATURE ABOVE UCSP
(BUNDLE 2,4,6,8, 250MM ABOVE UCSP)

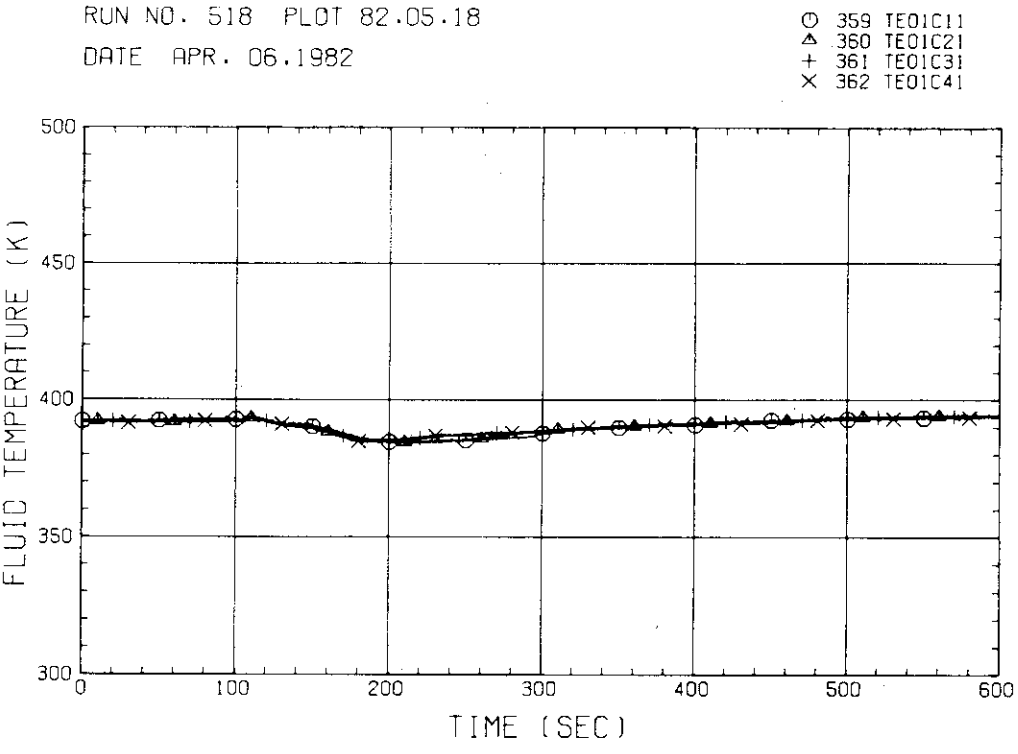

Fig. B-48 FLUID TEMPERATURE AT CORE INLET
(BUNDLE 1,2,3,4, 100MM BELOW HEATED PART)

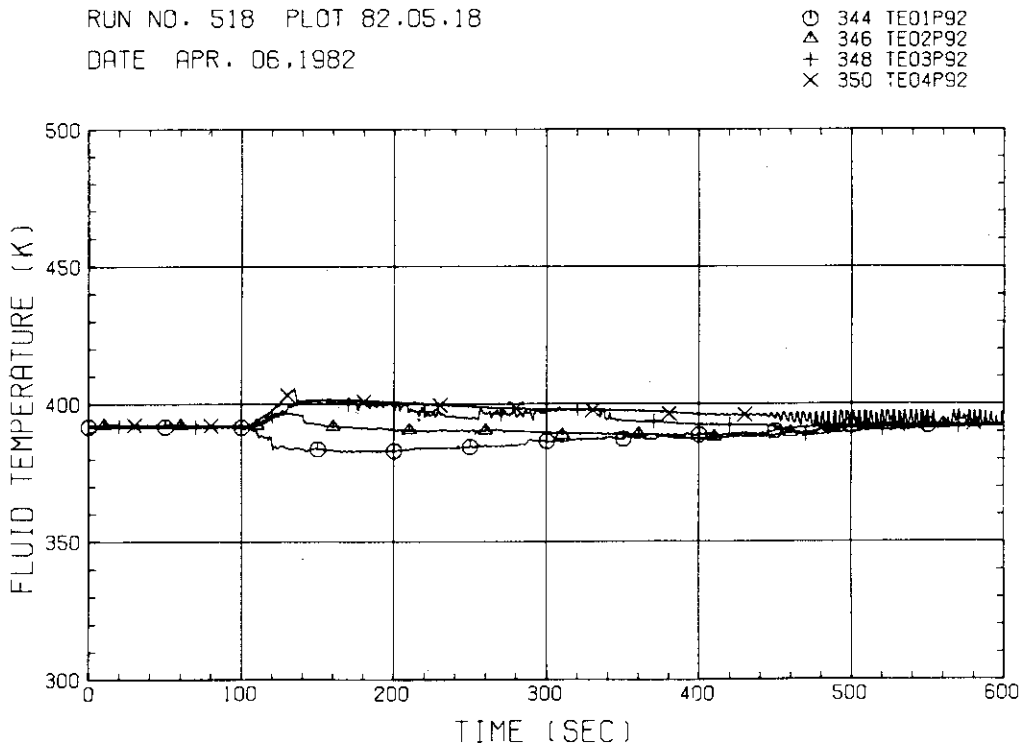

Fig. B-49 FLUID TEMPERATURE IN DOWNCOMER (BELOW BROKEN COLD LEG - PV SIDE)

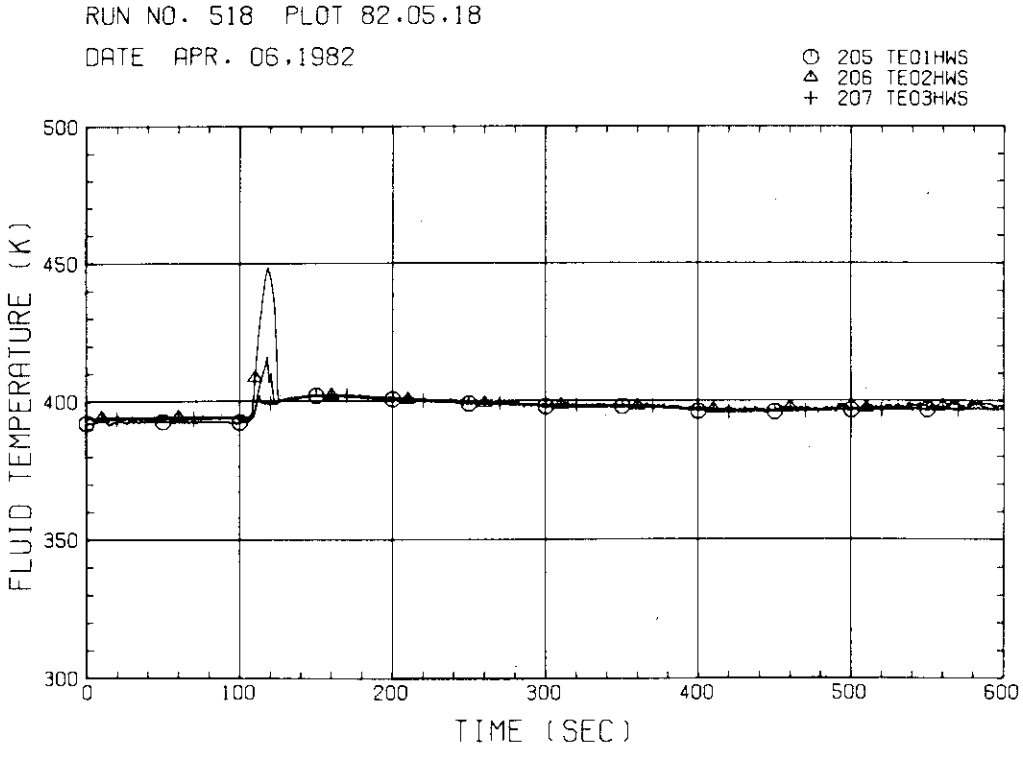

Fig. B-50 FLUID TEMPERATURE IN HOT LEG (01,02,03 - FROM PV TO STEAM/WATER SEPARATOR)

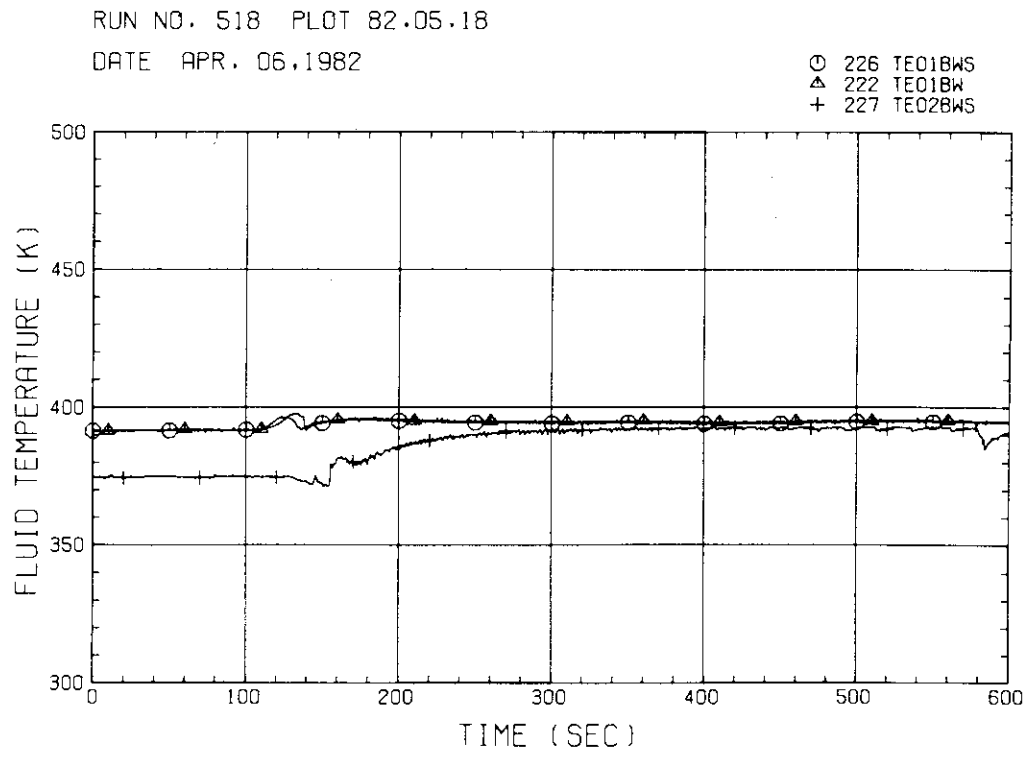

Fig. B-51 FLUID TEMPERATURE IN CONTAINMENT TANK-II
(01BWS - TOP, 01BW - MIDDLE, 02BWS - BOTTOM)

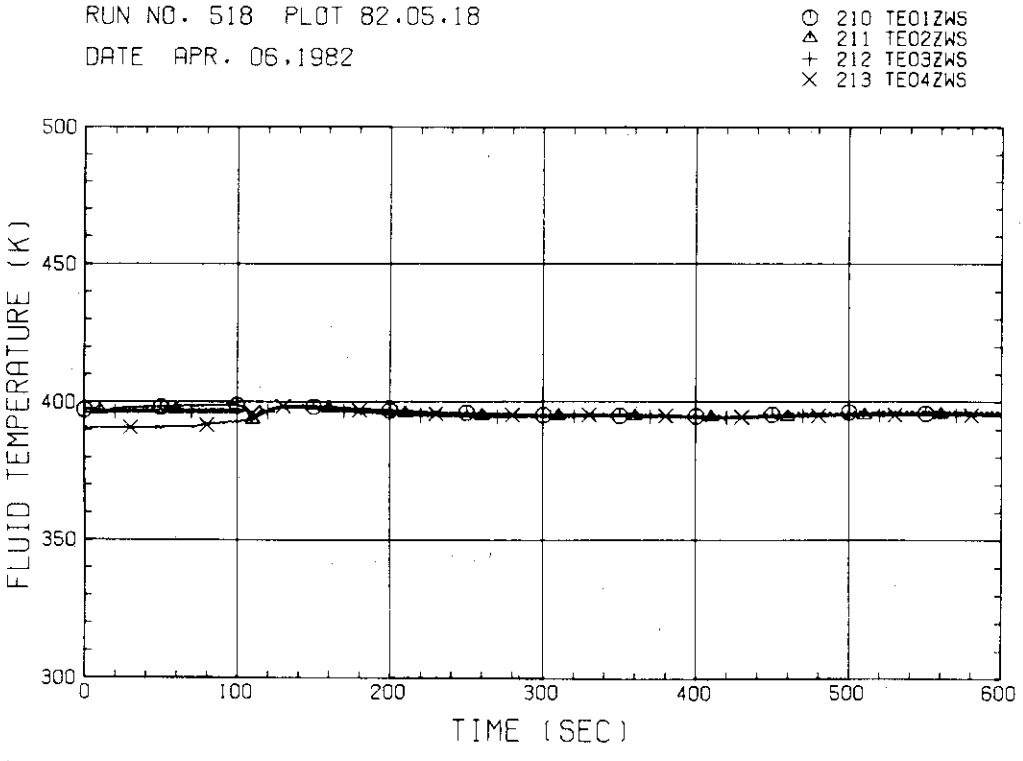

Fig. B-52 FLUID TEMPERATURE IN BROKEN COLD LEG - PV SIDE
(01,02,03,04 - FROM PV TO CONTAINMENT TANK-I)

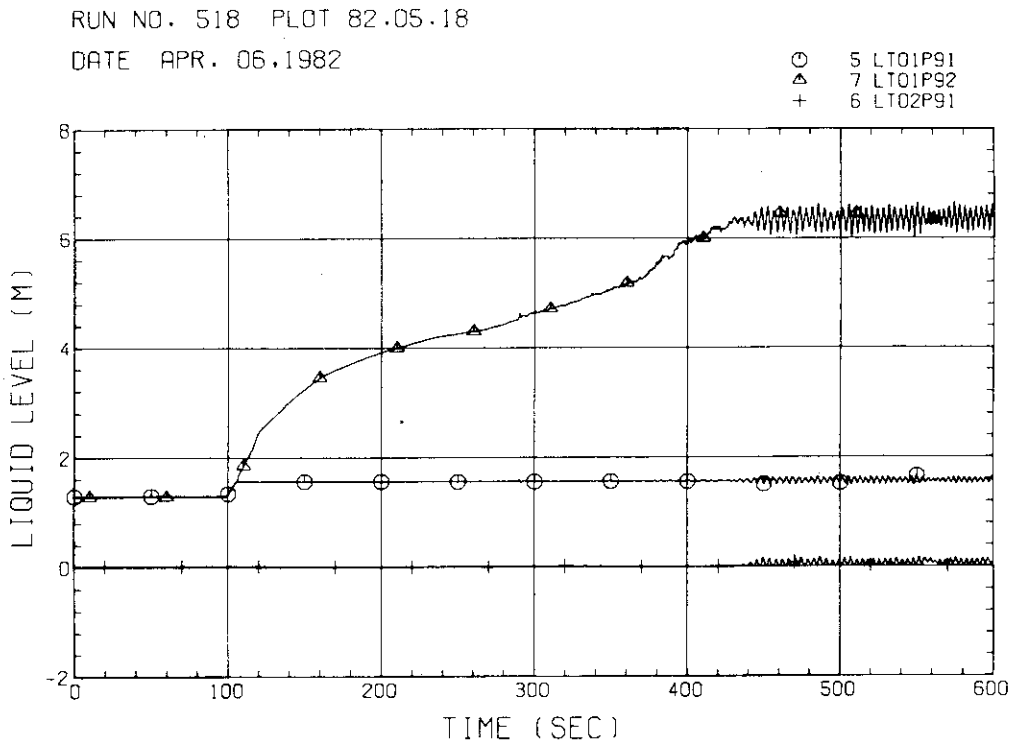

Fig. B-53 LIQUID LEVEL IN DOWNCOMER (01P91-BELOW CORE INLET, 01P92-BOTTOM TO COLD LEG, 02P91-COLD LEG TO TOP OF PV)

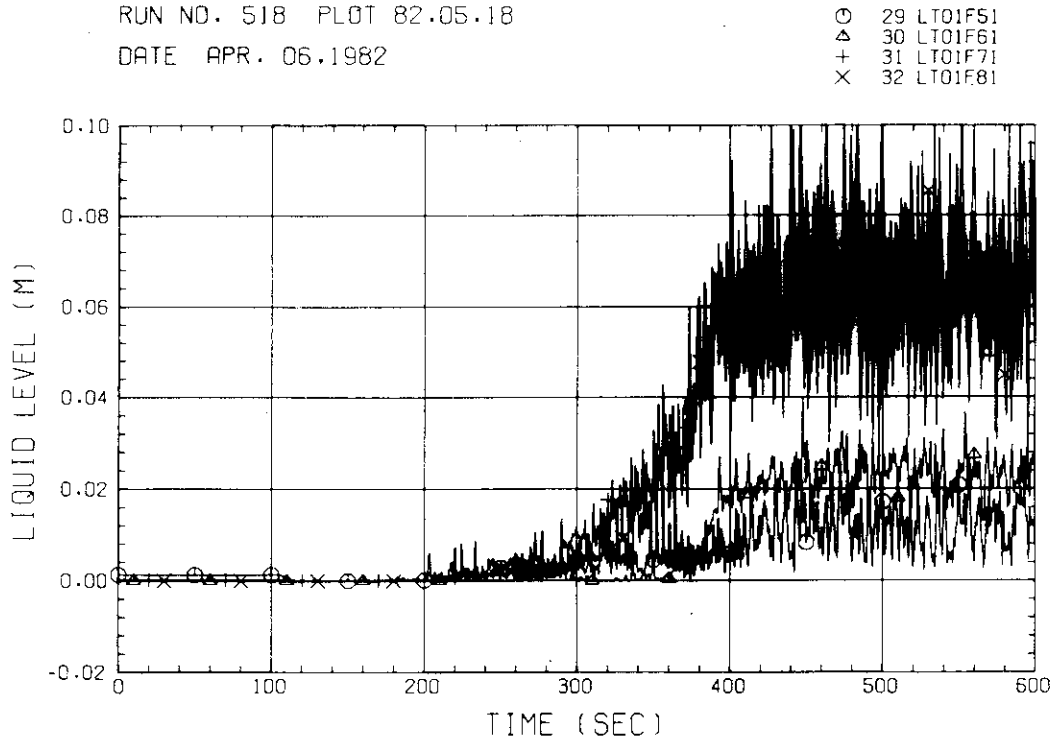

Fig. B-54 LIQUID LEVEL ABOVE END BOX TIE PLATE (BUNDLE 5,6,7,8)

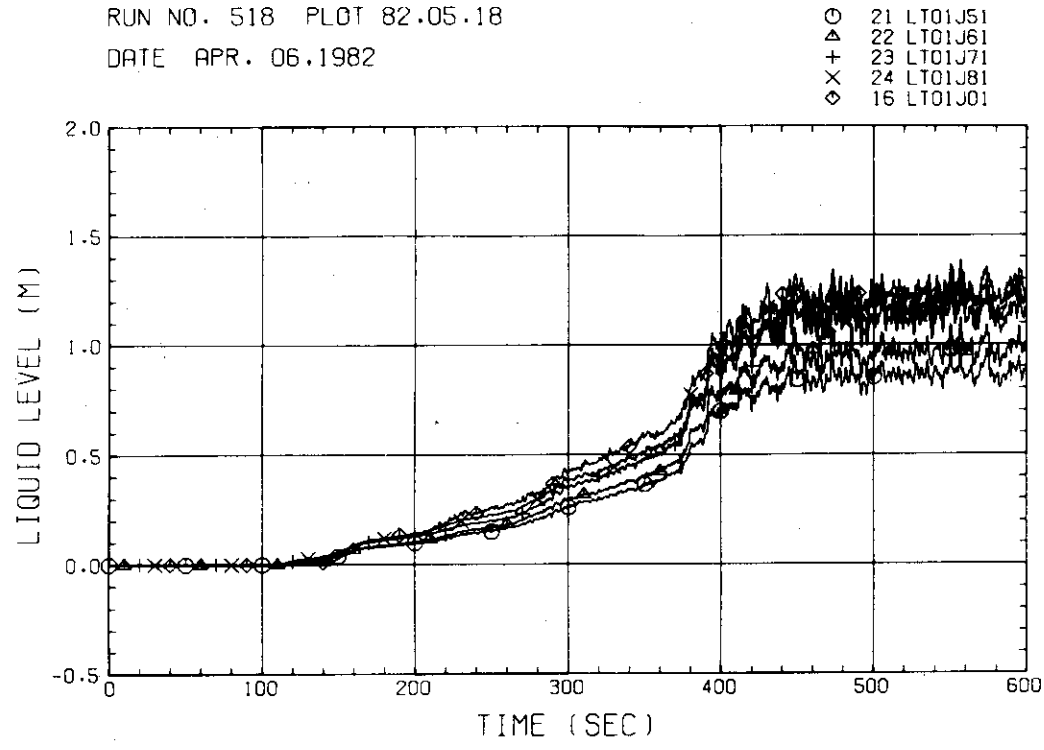

Fig. B-55 LIQUID LEVEL ABOVE UCSP
(BUNDLE 5.6.7.8 AND CORE BAFFLE)

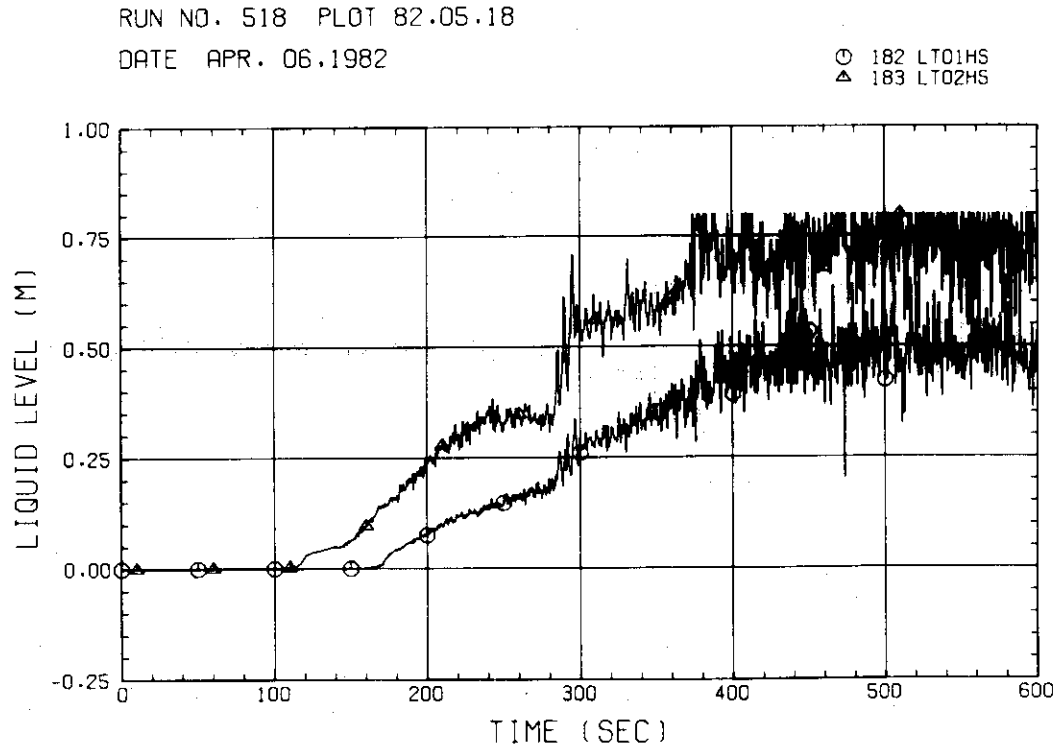

Fig. B-56 LIQUID LEVEL IN HOT LEG
(01HS - PV SIDE, 02HS - STEAM/WATER SEPARATOR SIDE)

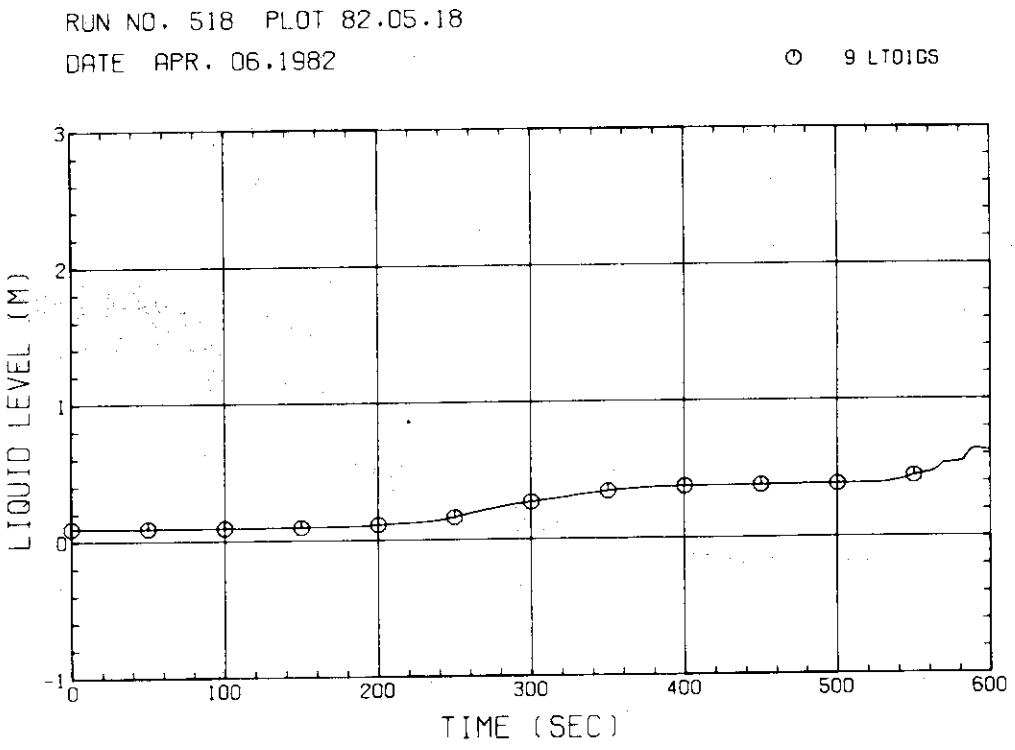

Fig. B-57 LIQUID LEVEL IN STEAM/WATER SEPARATOR

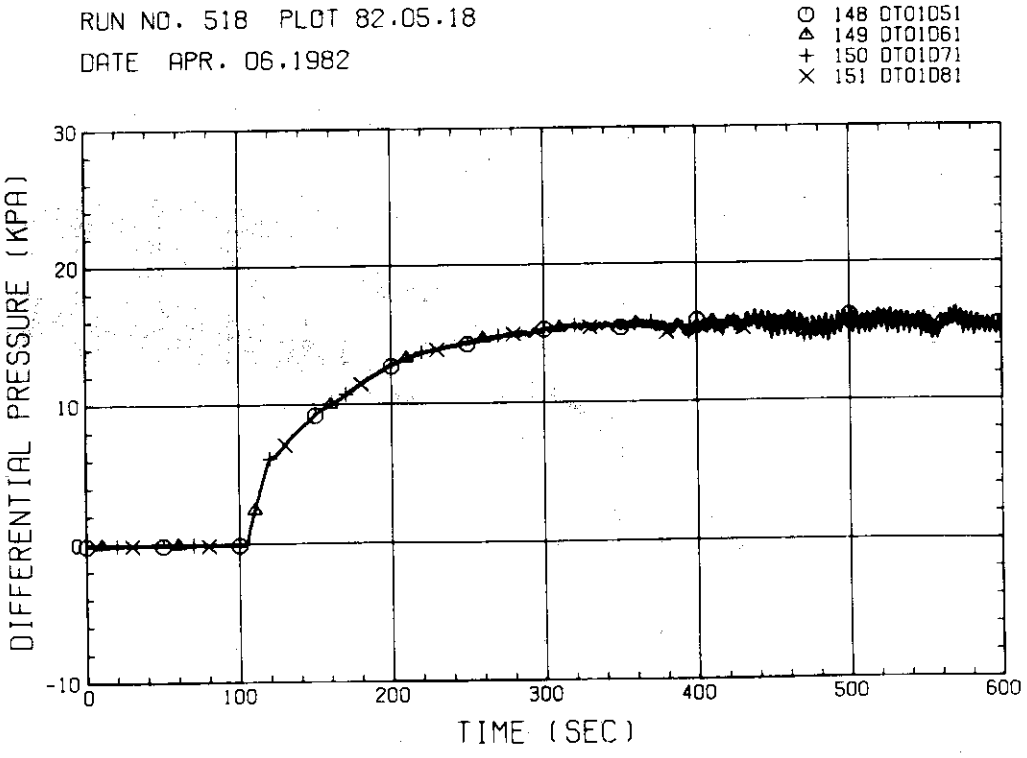

Fig. B-58 DIFFERENTIAL PRESSURE OF CORE LOWER HALF (BUNDLE 5,6,7,8)

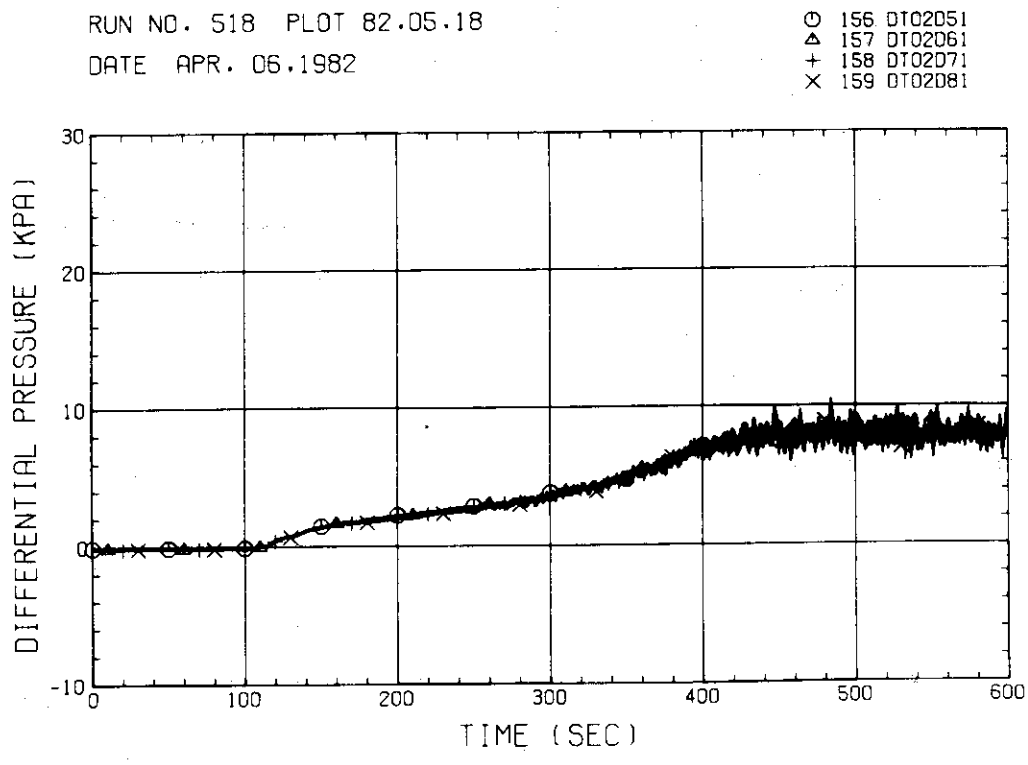

Fig. B-59 DIFFERENTIAL PRESSURE OF CORE UPPER HALF (BUNDLE 5,6,7,8)

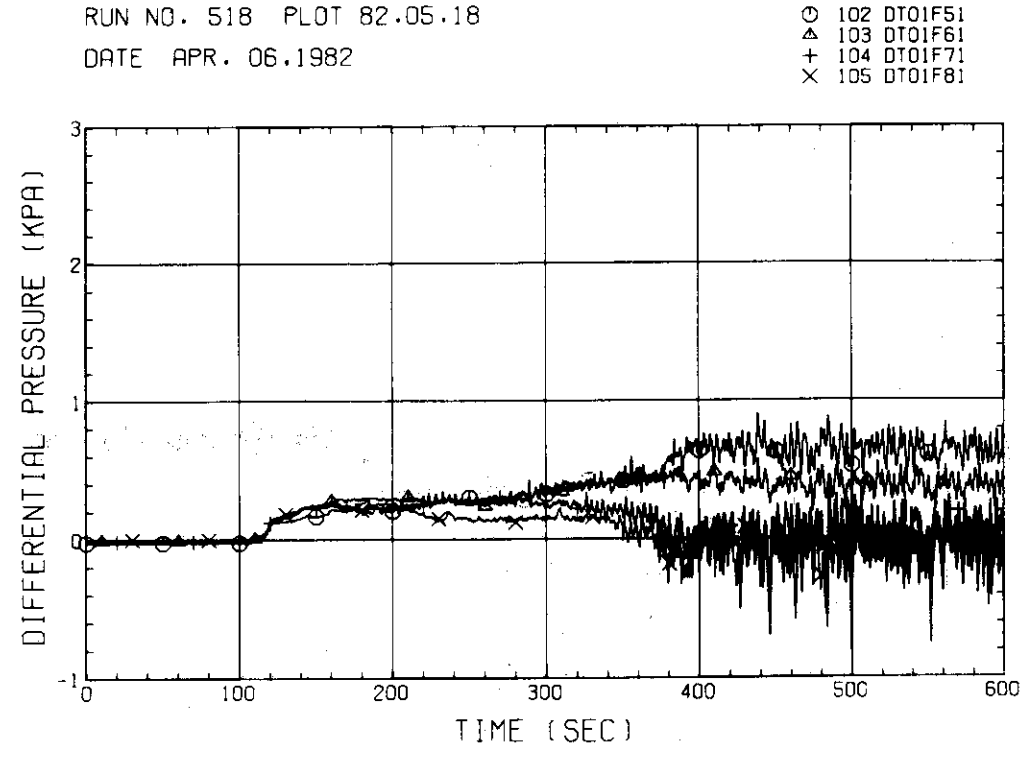

Fig. B-60 DIFFERENTIAL PRESSURE ACROSS END BOX TIE PLATE (BUNDLE 5,6,7,8)

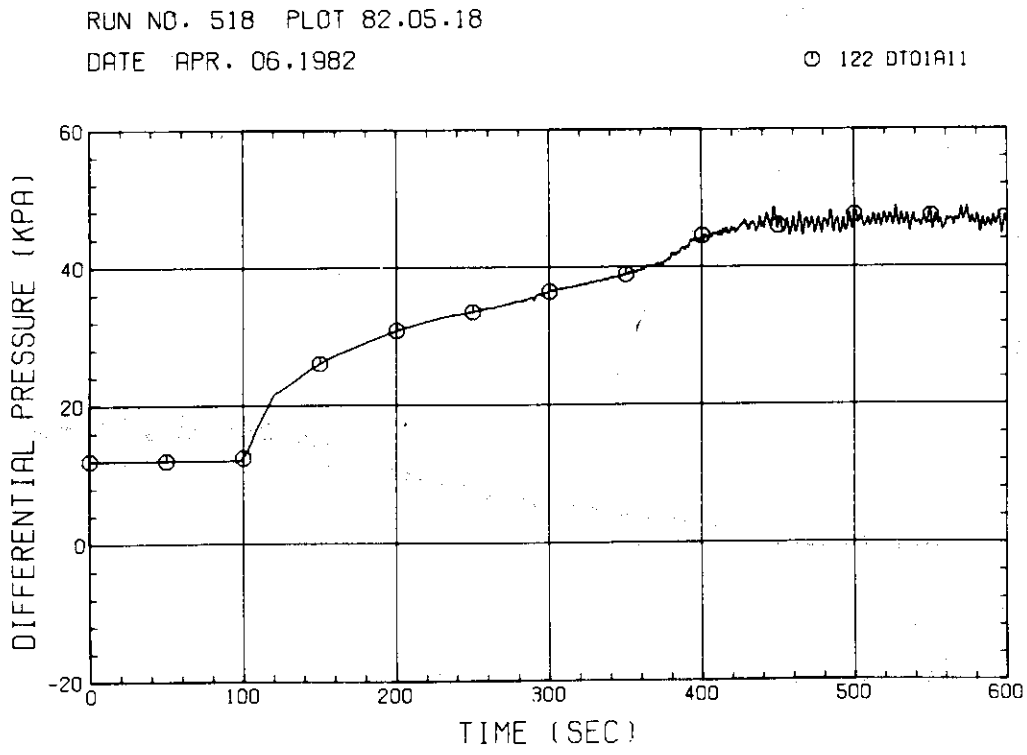

Fig. B-61 DIFFERENTIAL PRESSURE, BOTTOM OF LOWER PLENUM - TOP OF UPPER PLENUM

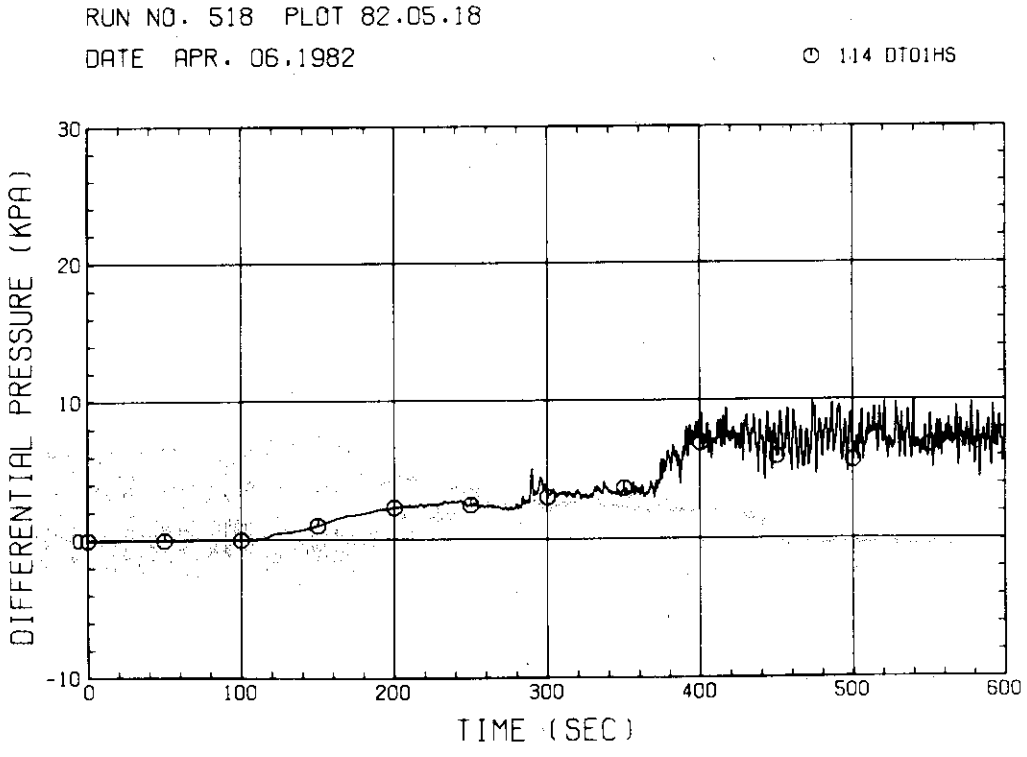

Fig. B-62 DIFFERENTIAL PRESSURE OF HOT LEG, HOT LEG INLET - STEAM/WATER SEPARATOR INLET

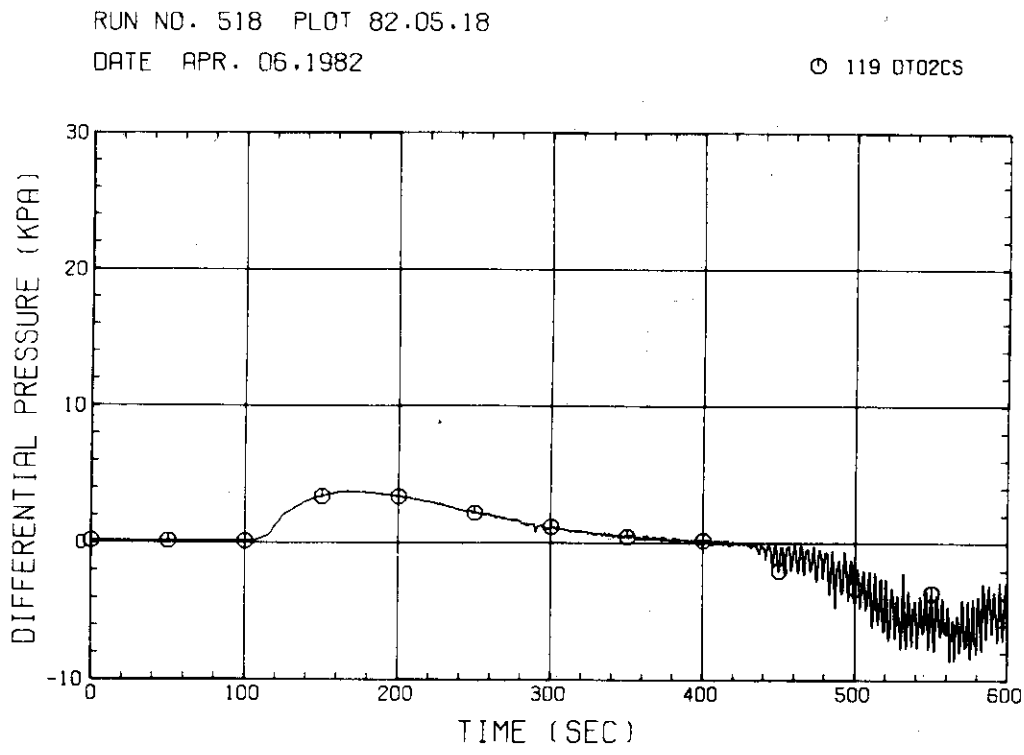

Fig. B-63 DIFFERENTIAL PRESSURE OF INTACT COLD LEG

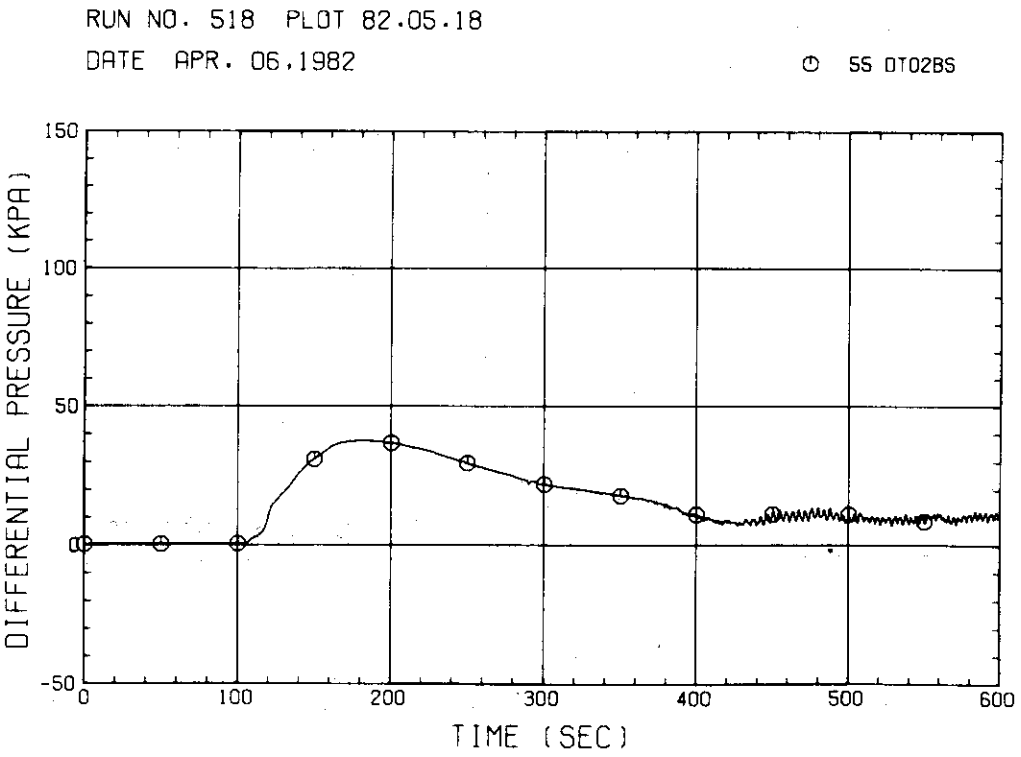

Fig. B-64 DIFFERENTIAL PRESSURE. STEAM/WATER SEPARATOR - CONTAINMENT TANK-II

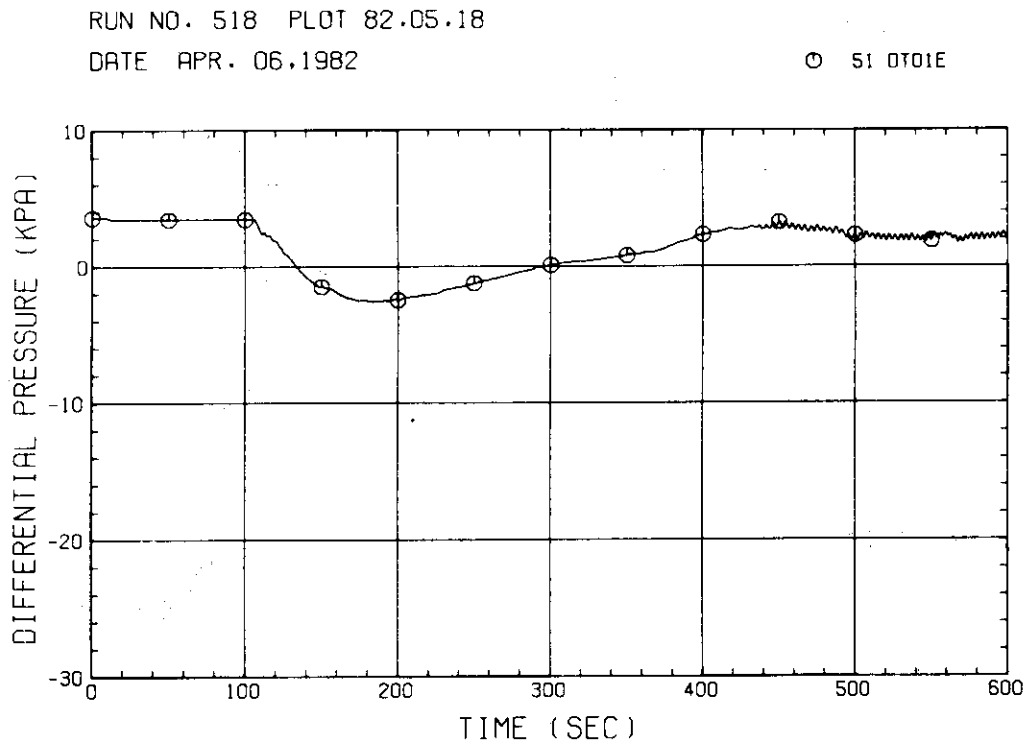

Fig. B-65 DIFFERENTIAL PRESSURE, CONTAINMENT TANK-II - CONTAINMENT TANK-I

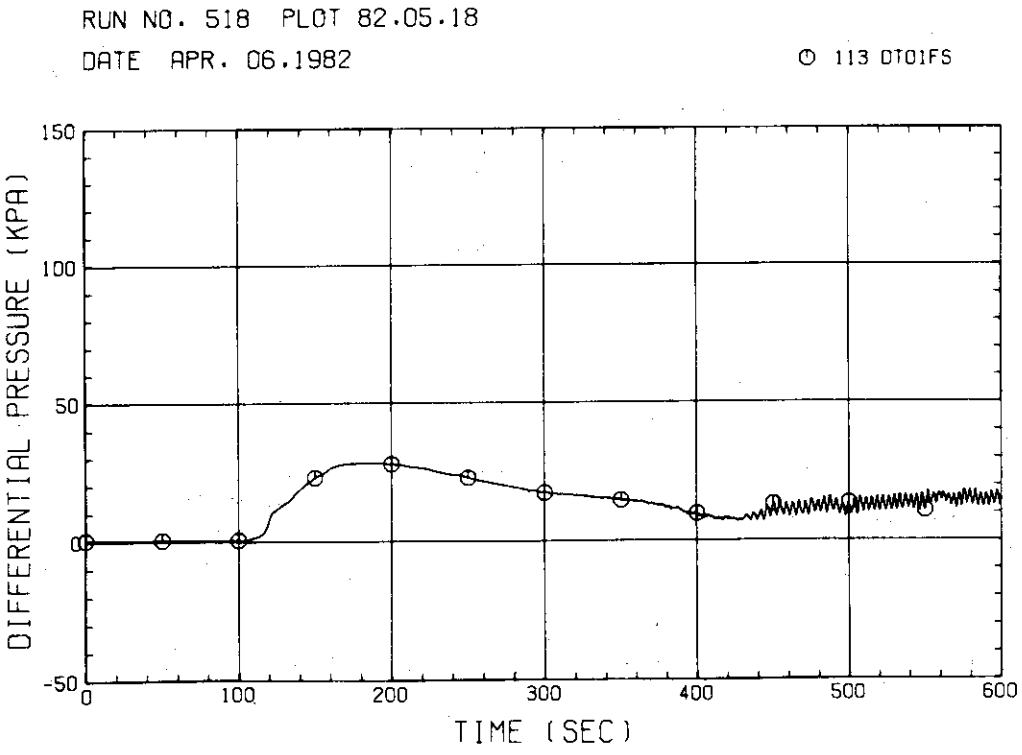

Fig. B-66 DIFFERENTIAL PRESSURE OF BROKEN COLD LEG - PV SIDE, DOWNCOMER - CONTAINMENT TANK-I

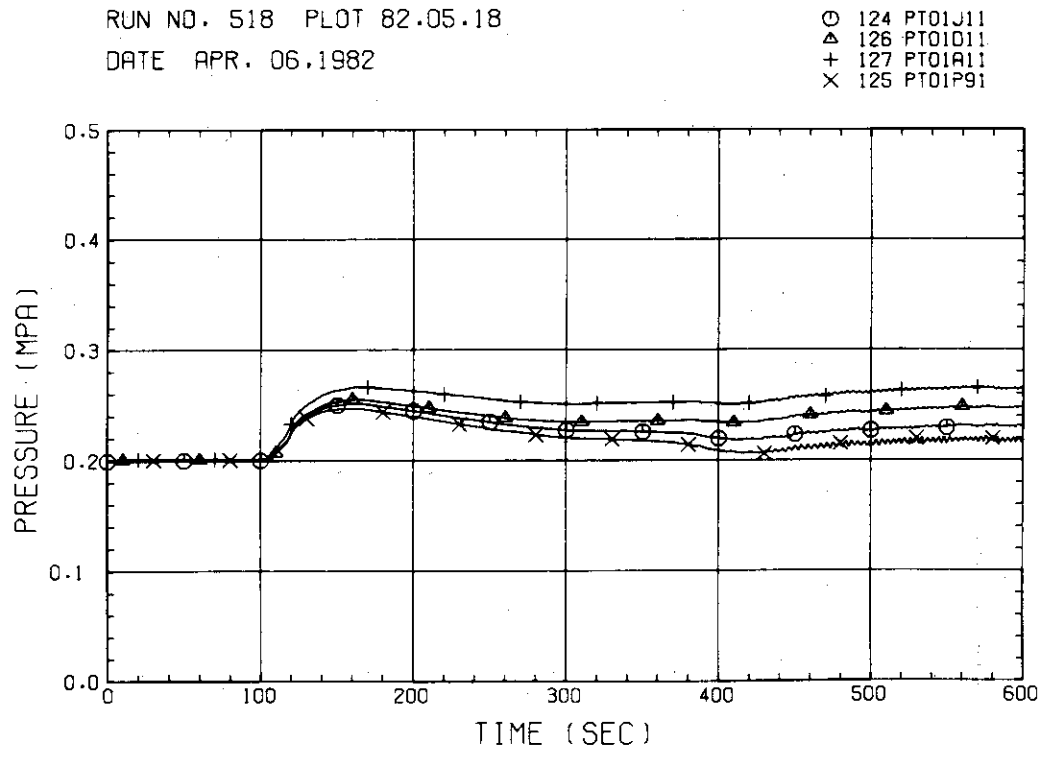

Fig. B-67 PRESSURE IN PV (J - TOP OF PV, D - CORE CENTER, A - CORE INLET, P - BELOW COLD LEG NOZZLE IN DOWNCOMER)

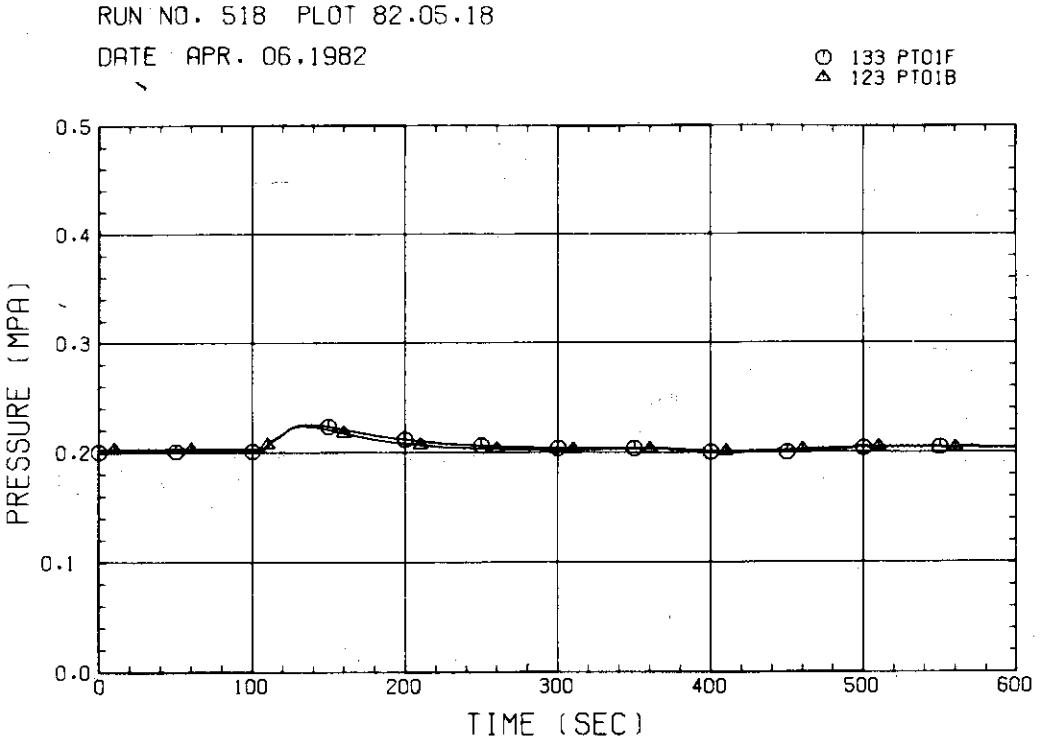

Fig. B-68 PRESSURE AT TOP OF CONTAINMENT TANK-I AND CONTAINMENT TANK-II (F-CONTAINMENT TANK-I, B-CONTAINMENT TANK-II)

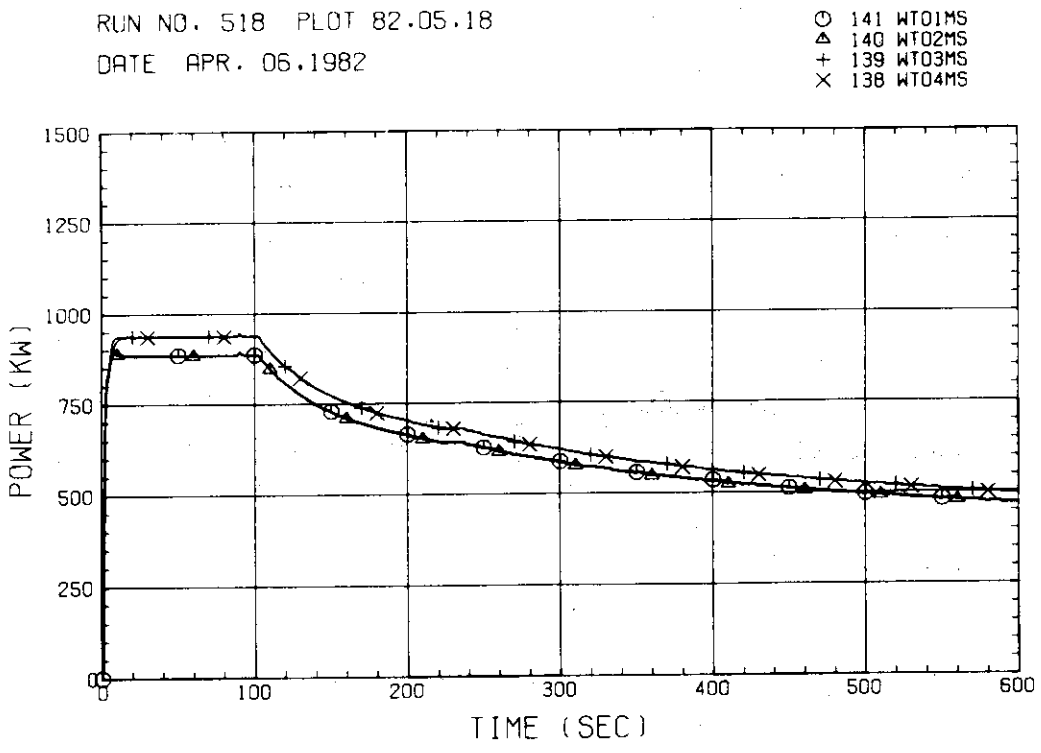

Fig. B-69 BUNDLE POWER (BUNDLE 1.2.3.4)

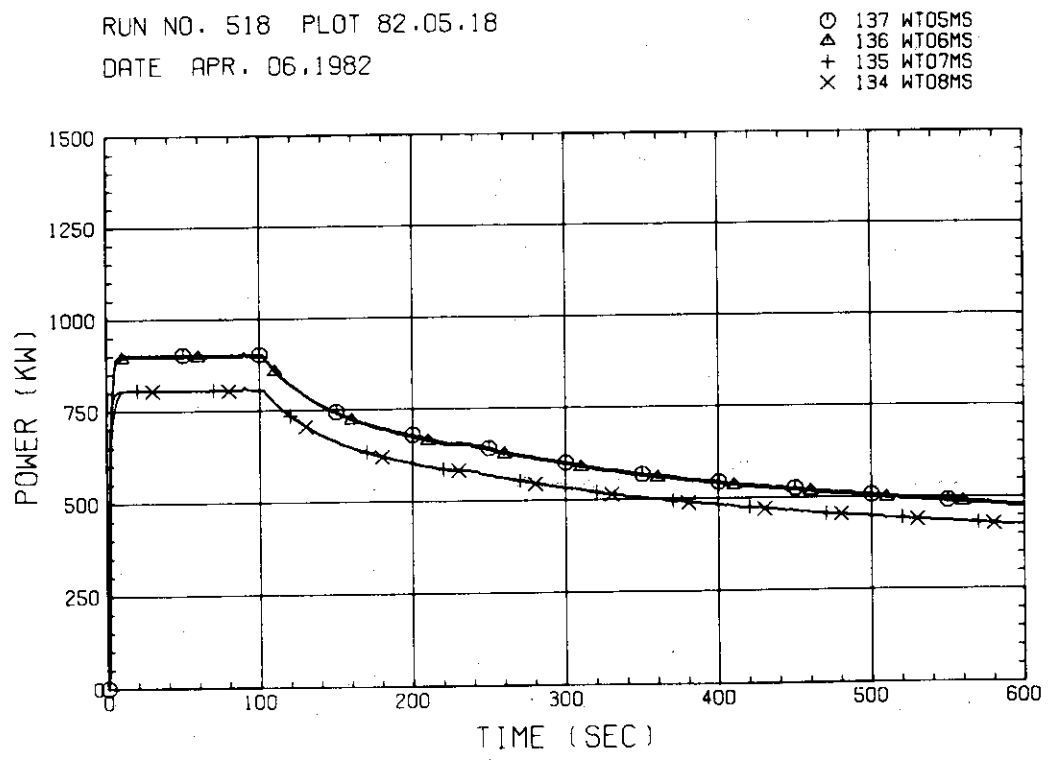

Fig. B-70 BUNDLE POWER (BUNDLE 5.6.7.8)

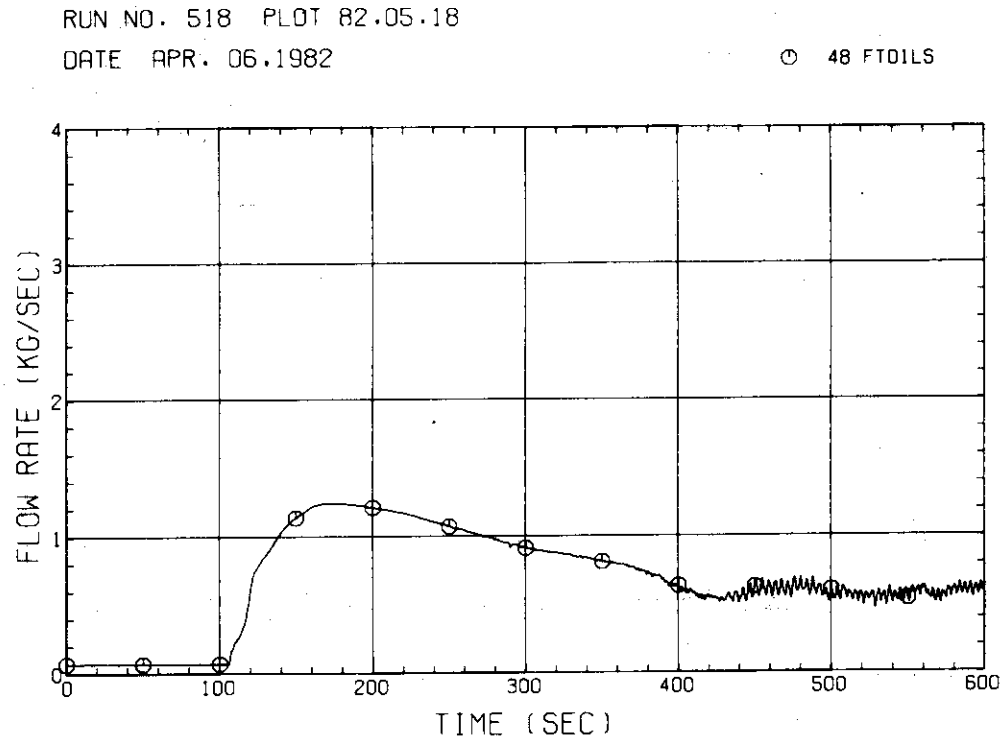

Fig. B-71 MASS FLOW RATE OF BROKEN COLD LEG - STEAM/WATER SEPARATOR SIDE

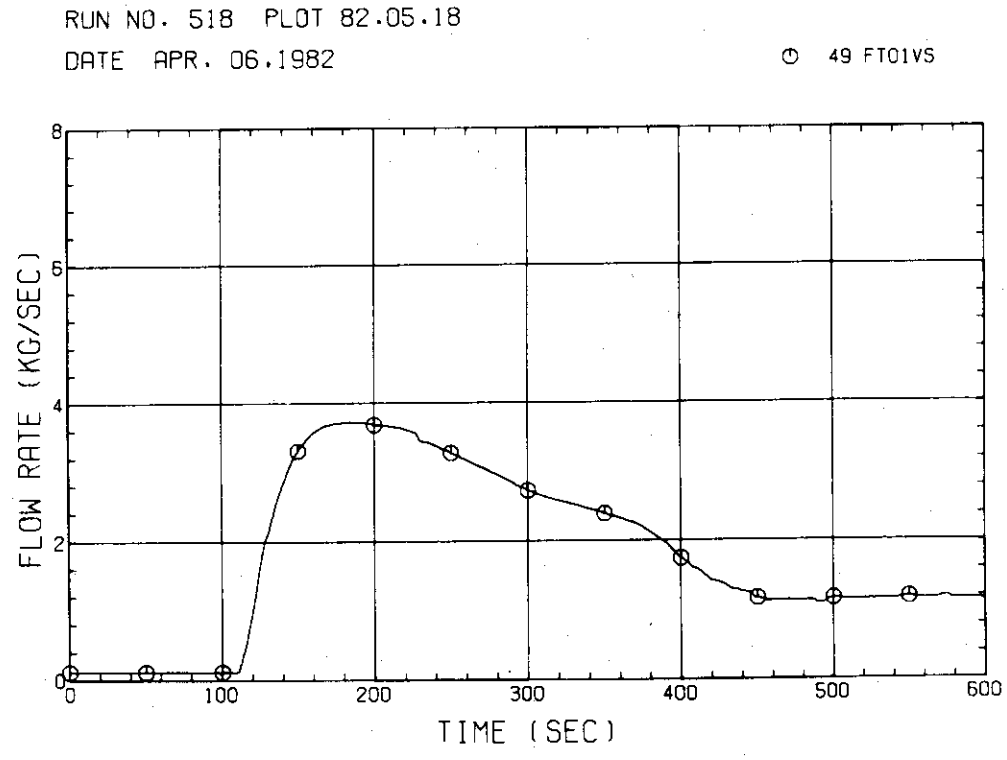

Fig. B-72 STEAM FLOW RATE OF DISCHARGE FROM CONTAINMENT TANK-II

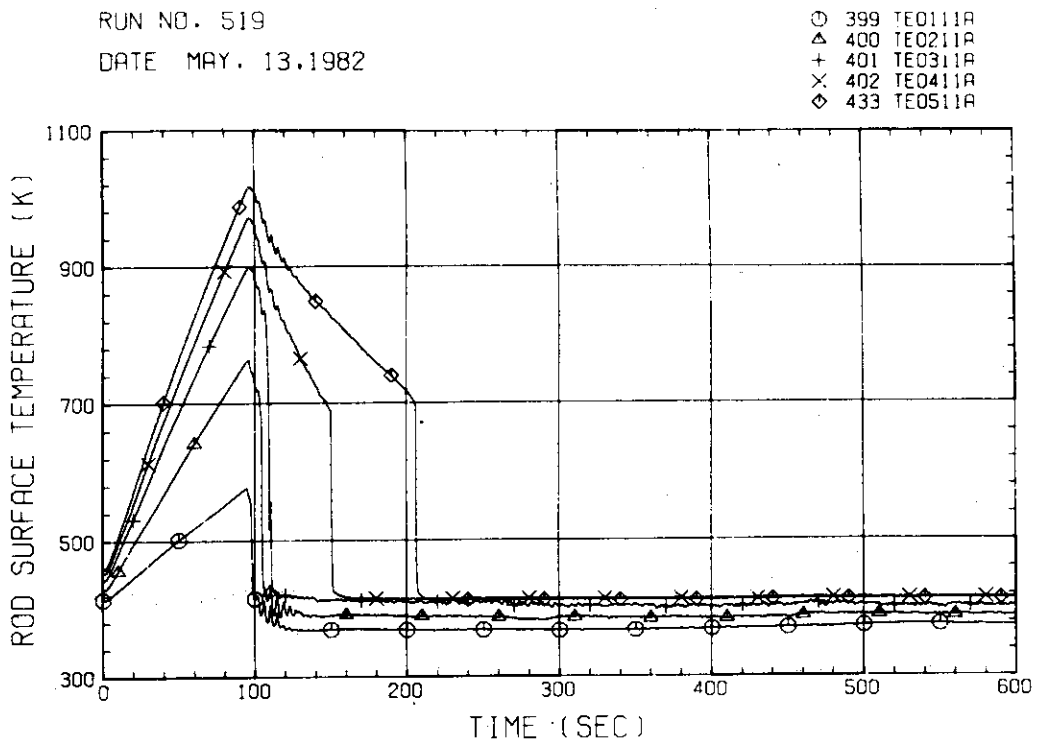

Fig. C-1 HEATER ROD TEMPERATURE (BUNDLE 1-1A, LOWER HALF)

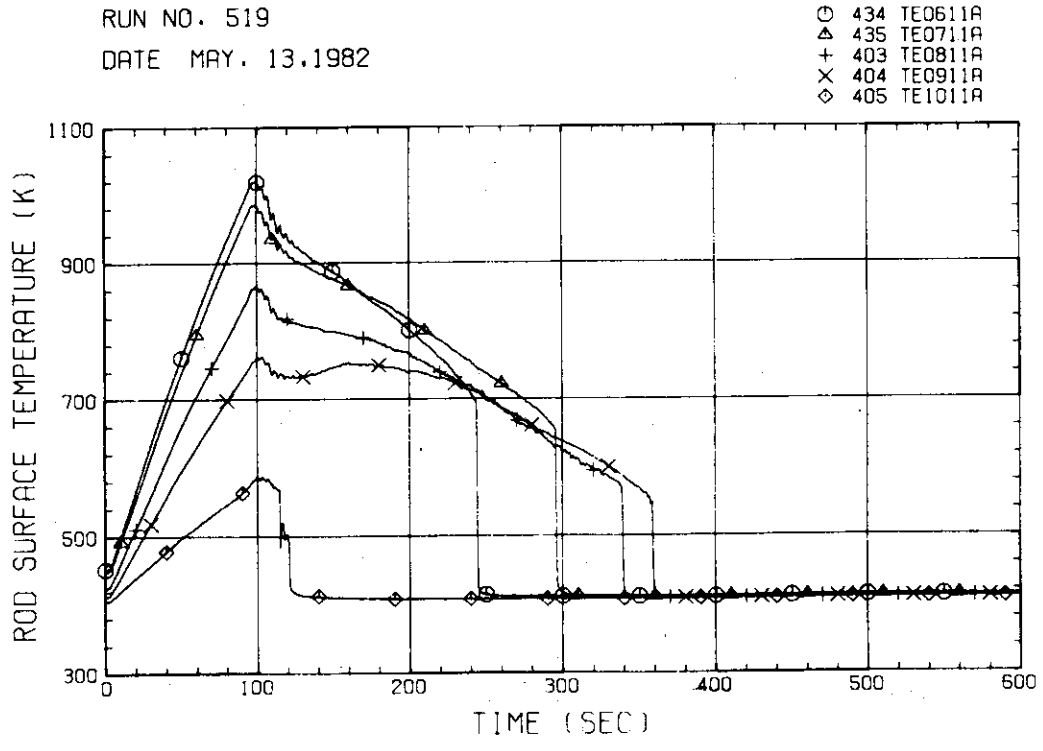

Fig. C-2 HEATER ROD TEMPERATURE (BUNDLE 1-1A, UPPER HALF)

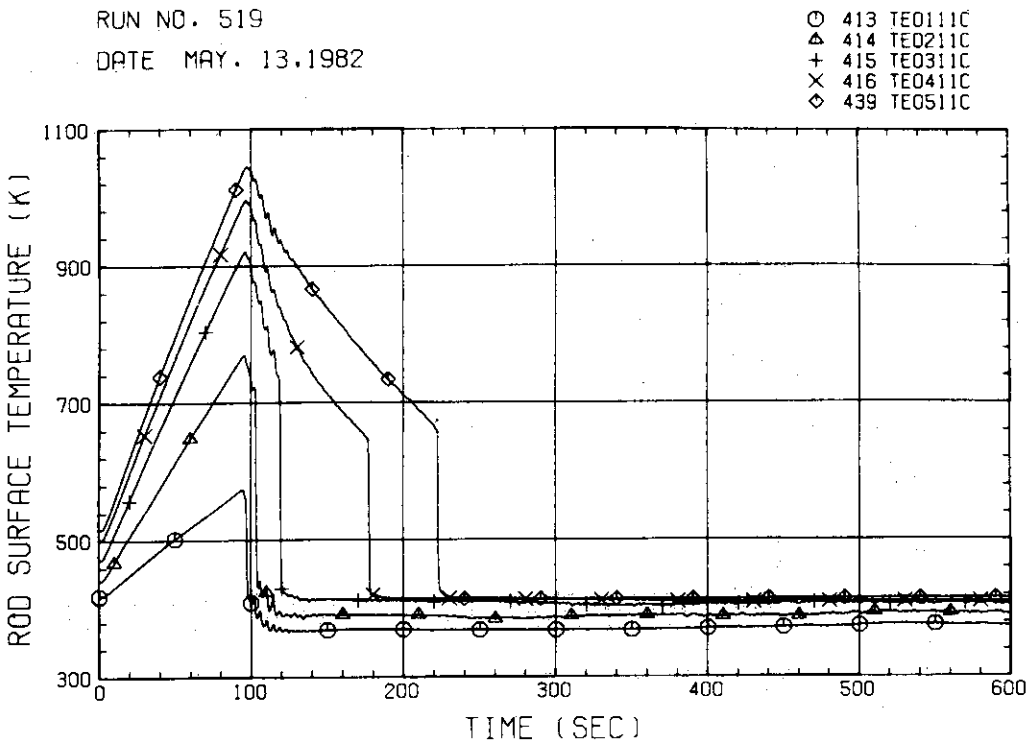

Fig. C-3 HEATER ROD TEMPERATURE (BUNDLE 1-1C, LOWER HALF)

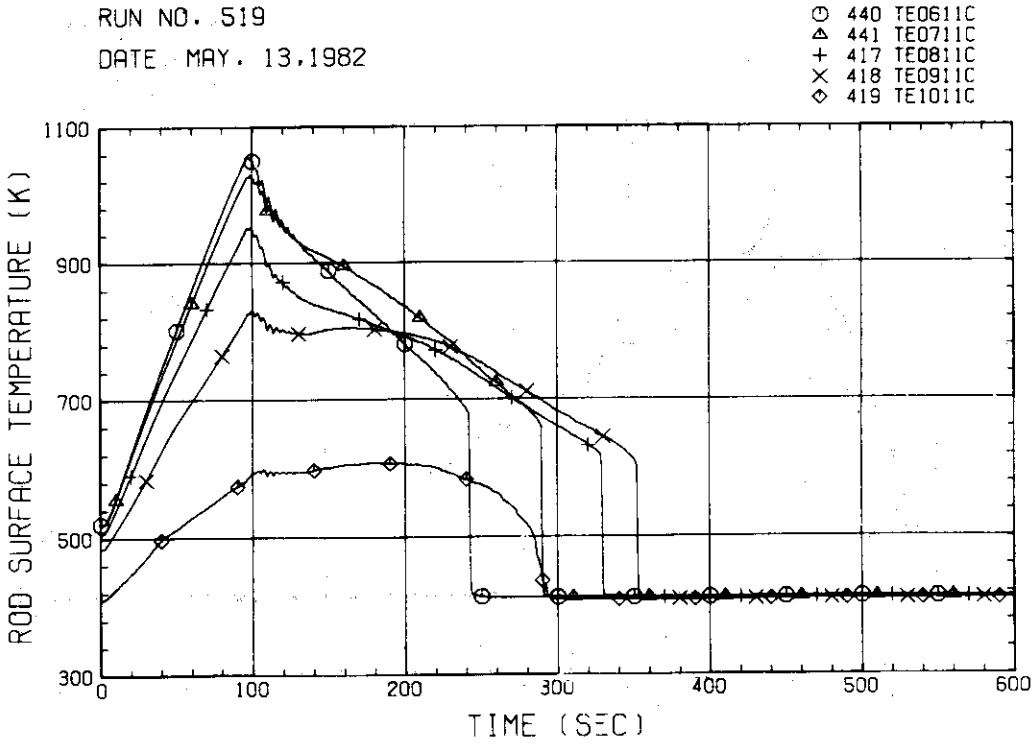

Fig. C-4 HEATER ROD TEMPERATURE (BUNDLE 1-1C, UPPER HALF)

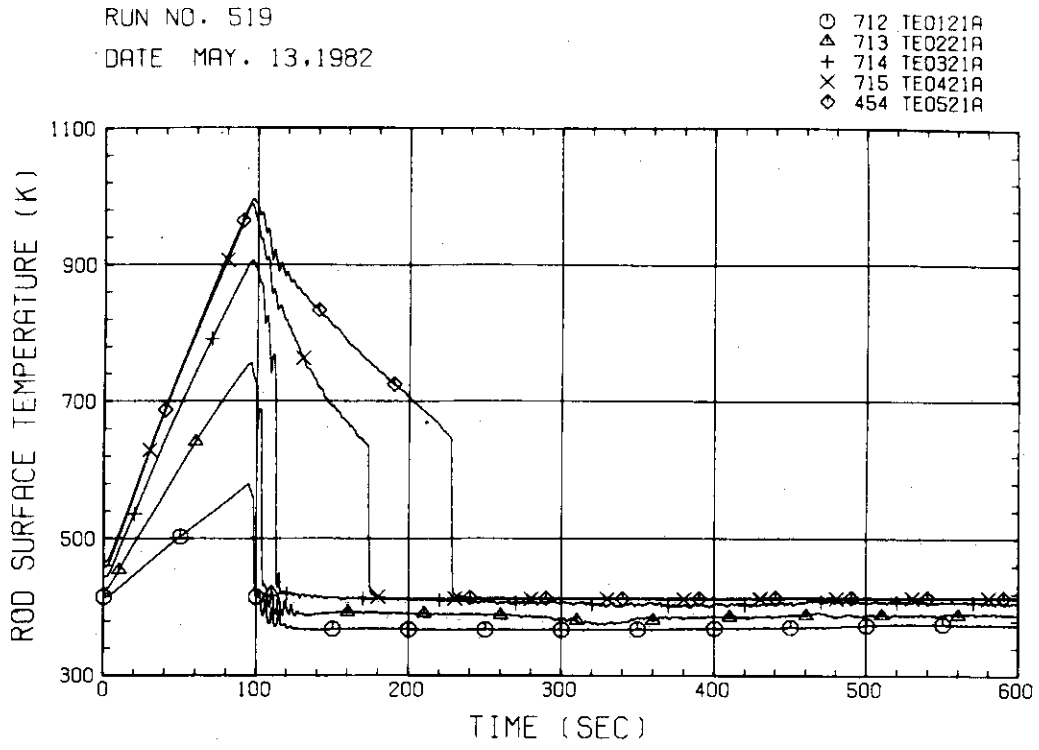

Fig. C-5 HEATER ROD TEMPERATURE (BUNDLE 2-1A, LOWER HALF)

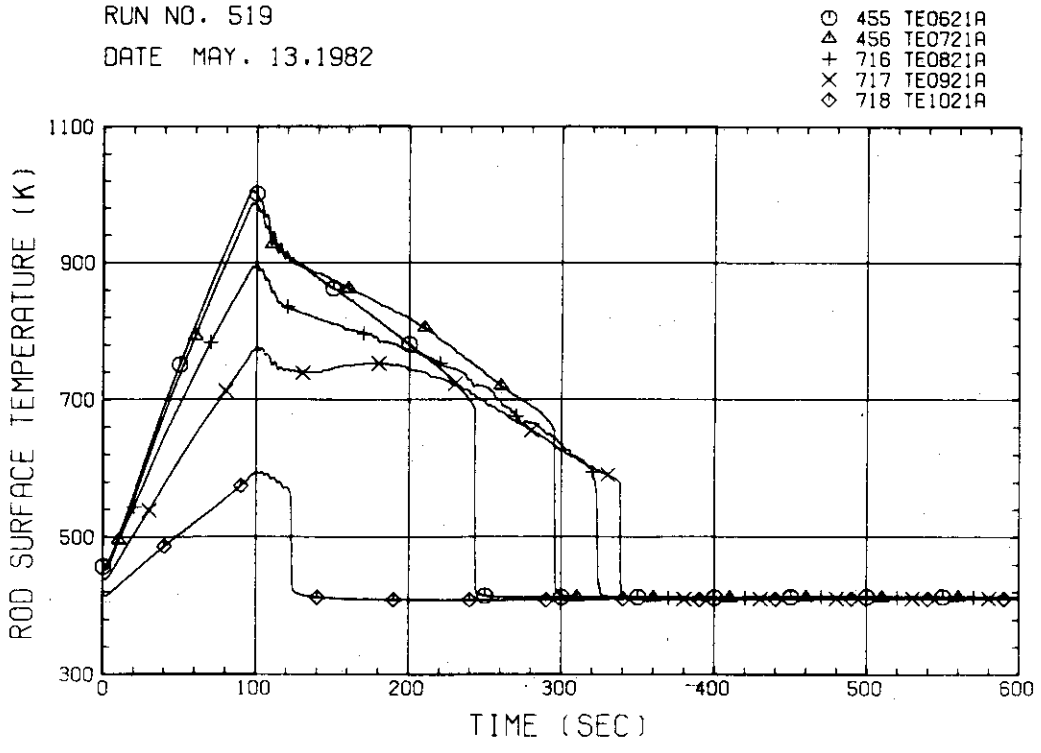

Fig. C-6 HEATER ROD TEMPERATURE (BUNDLE 2-1A, UPPER HALF)

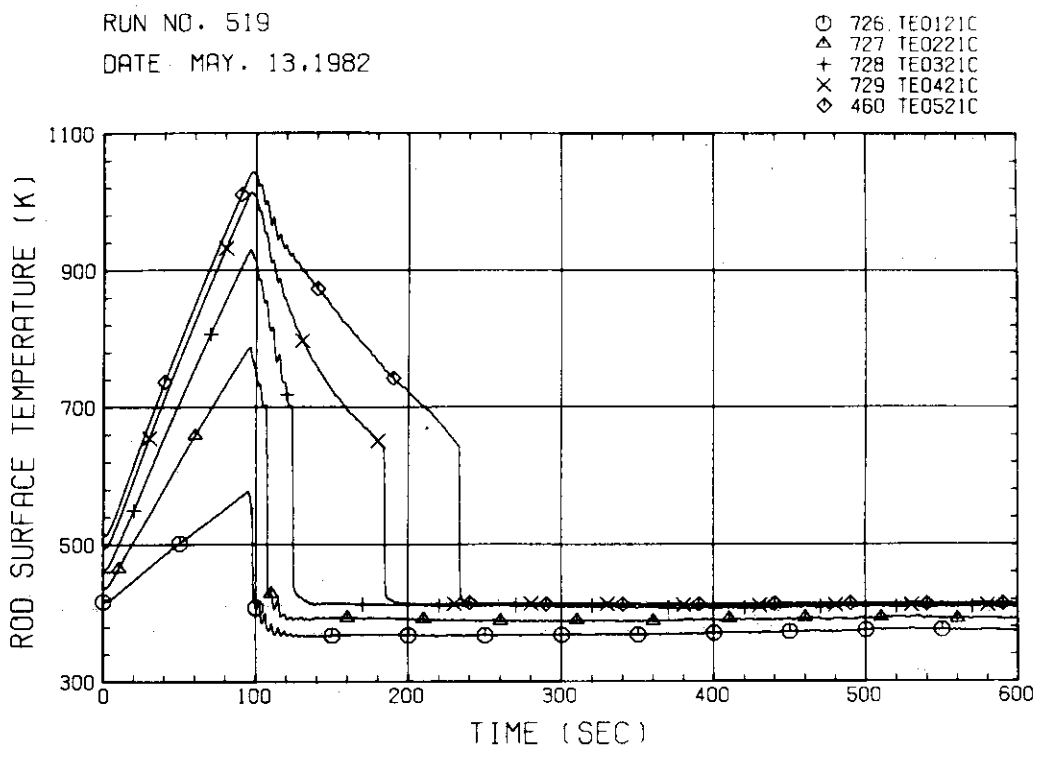

Fig. C-7 HEATER ROD TEMPERATURE (BUNDLE 2-1C, LOWER HALF)

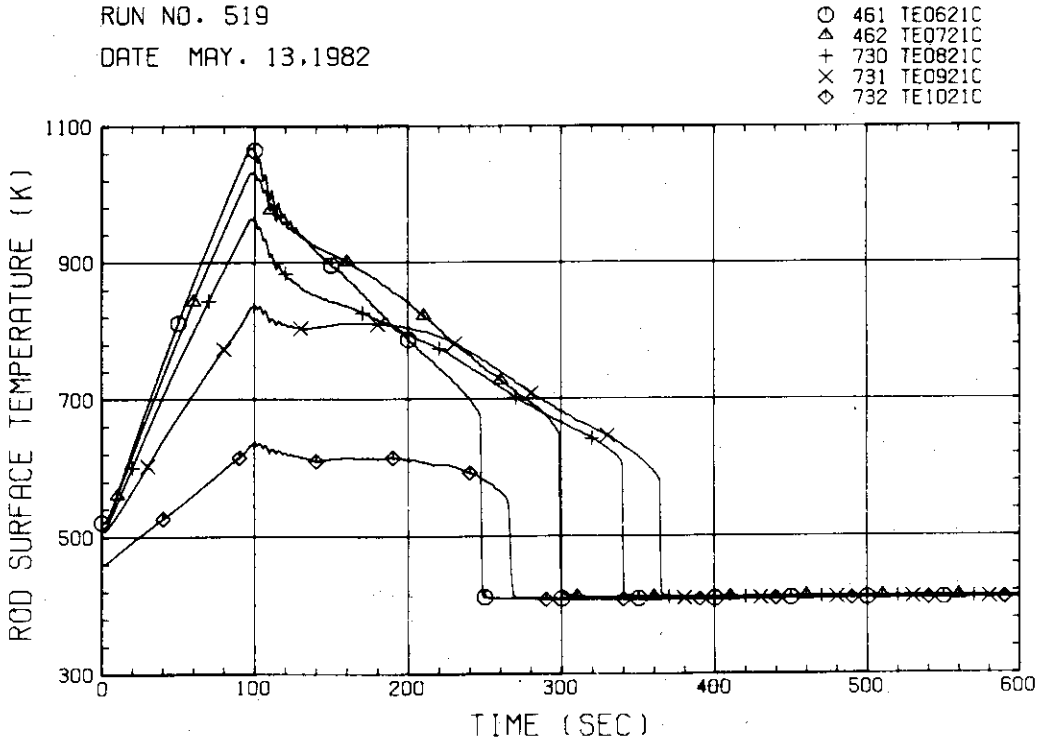

Fig. C-8 HEATER ROD TEMPERATURE (BUNDLE 2-1C, UPPER HALF)

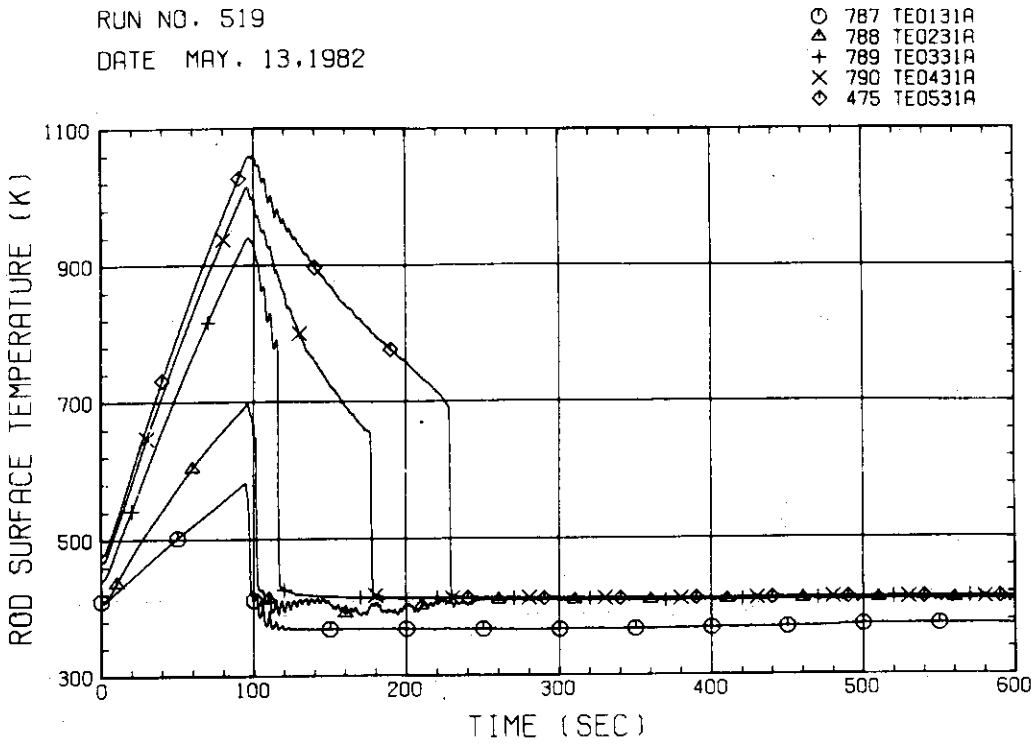

Fig. C-9 HEATER ROD TEMPERATURE (BUNDLE 3-1A, LOWER HALF)

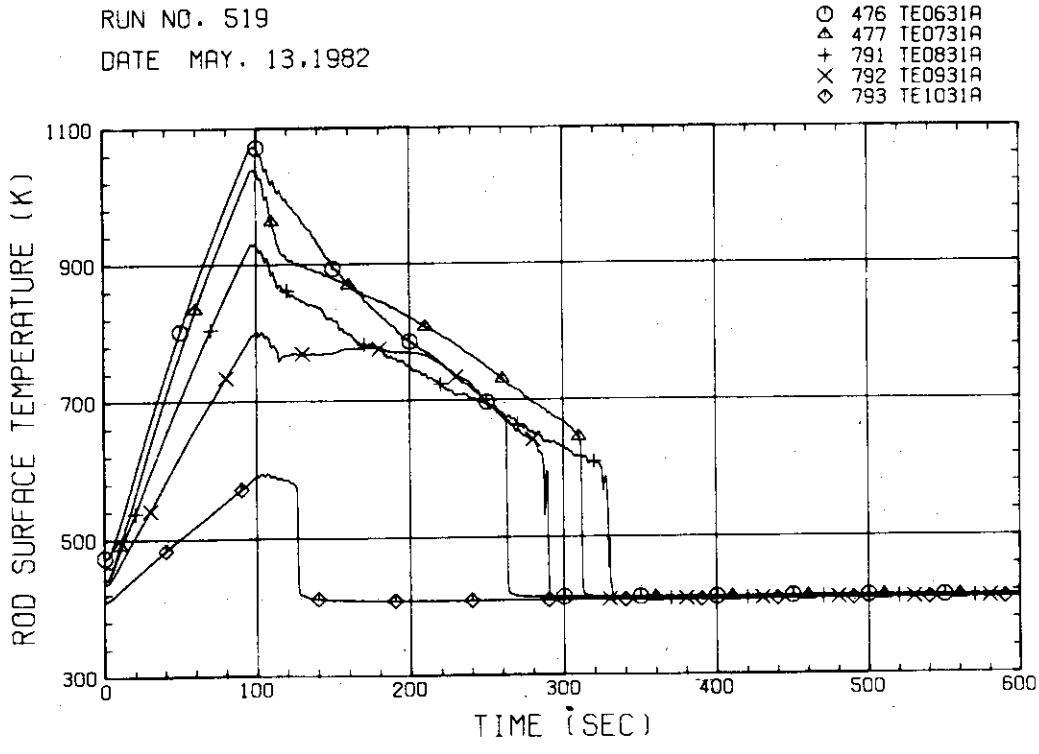

Fig. C-10 HEATER ROD TEMPERATURE (BUNDLE 3-1A, UPPER HALF)

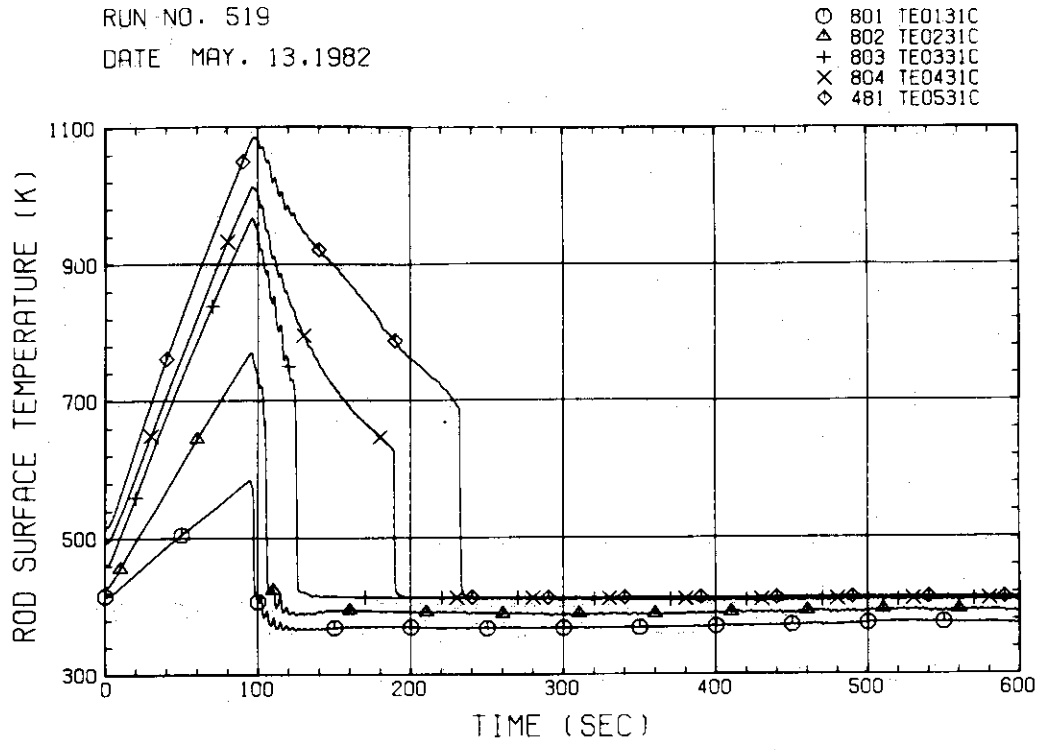

Fig. C-11 HEATER ROD TEMPERATURE (BUNDLE 3-1C, LOWER HALF)

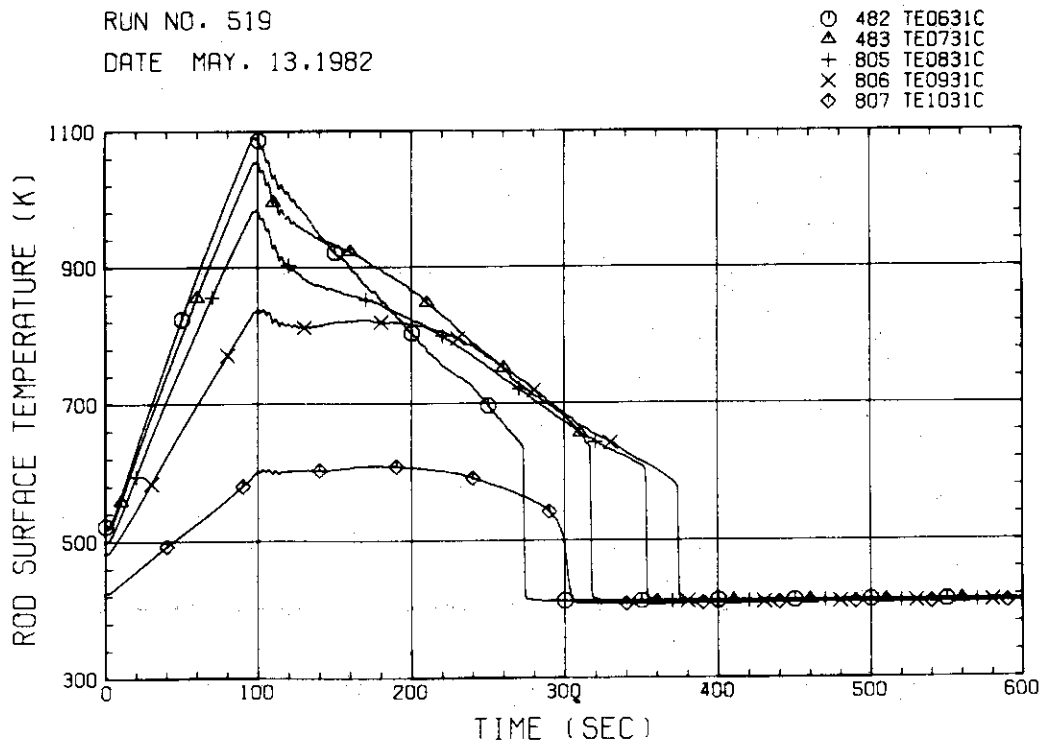

Fig. C-12 HEATER ROD TEMPERATURE (BUNDLE 3-1C, UPPER HALF)

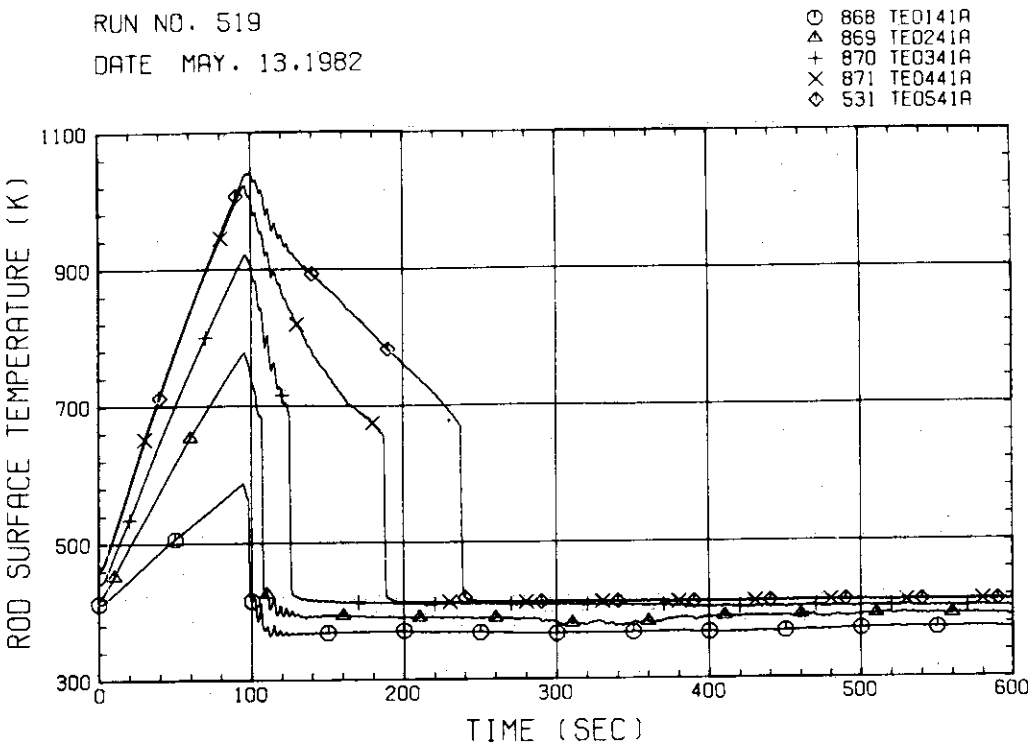

Fig. C-13 HEATER ROD TEMPERATURE (BUNDLE 4-1A, LOWER HALF)

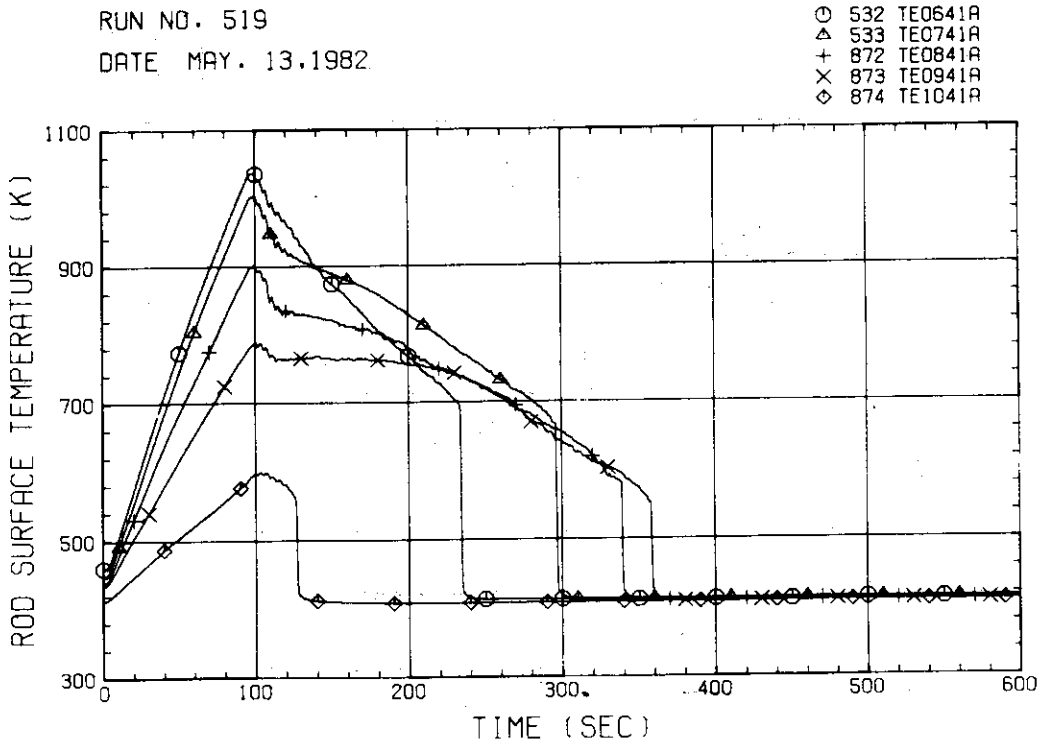

Fig. C-14 HEATER ROD TEMPERATURE (BUNDLE 4-1A, UPPER HALF)

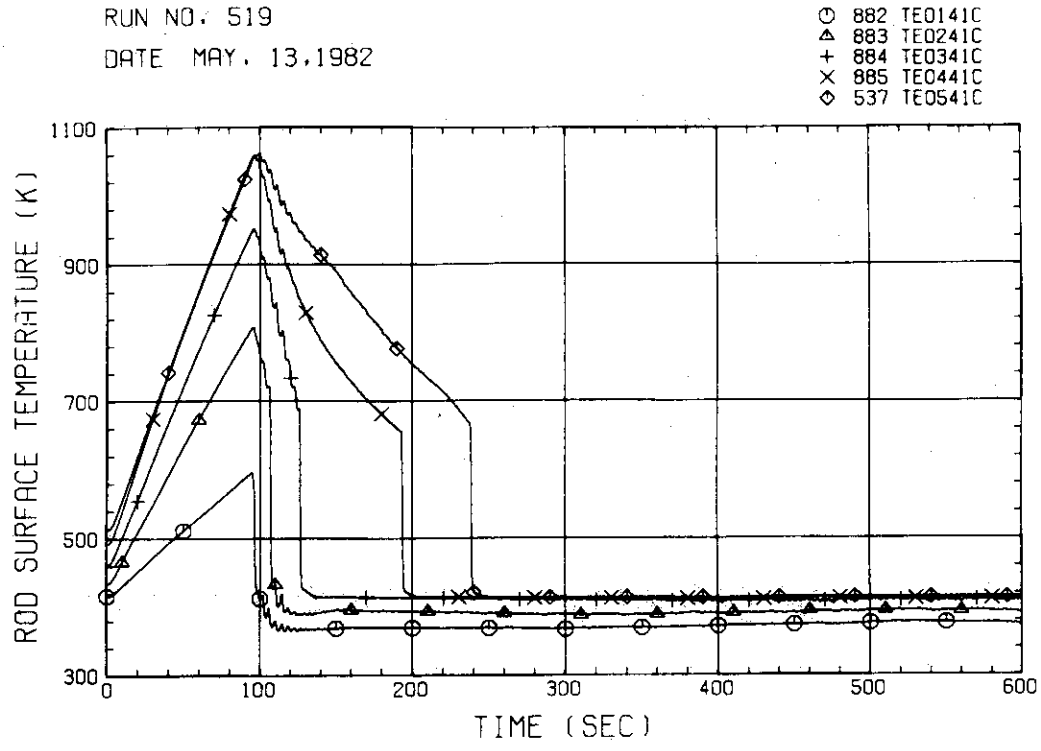

Fig. C-15 HEATER ROD TEMPERATURE (BUNDLE 4-1C, LOWER HALF)

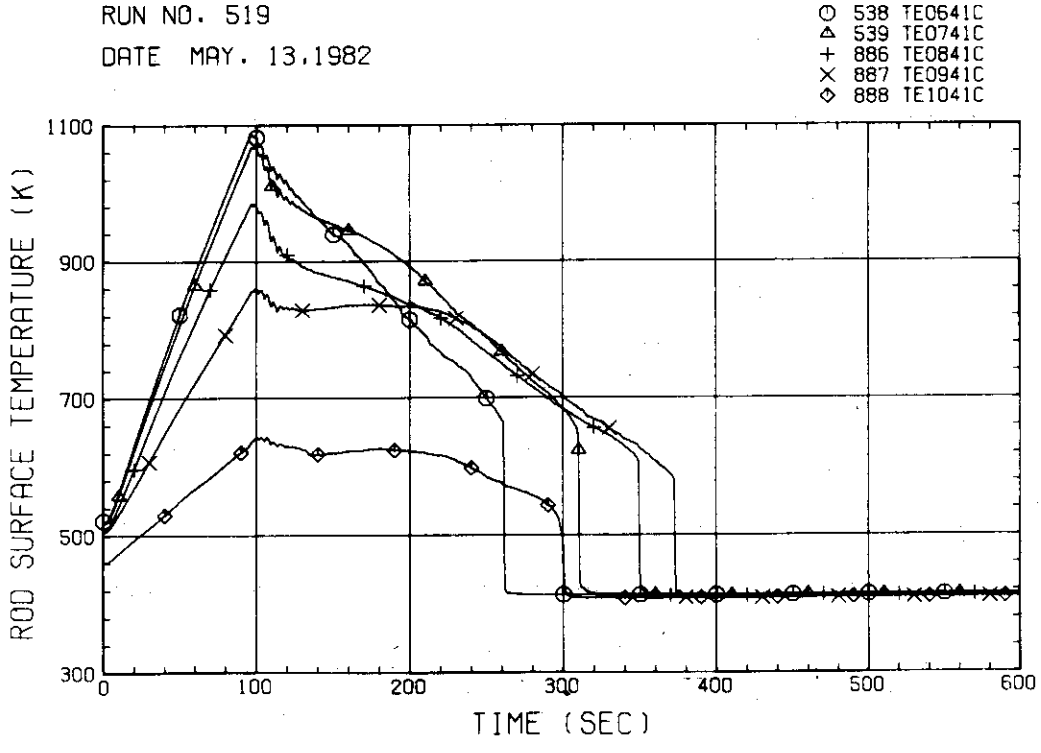

Fig. C-16 HEATER ROD TEMPERATURE (BUNDLE 4-1C, UPPER HALF)

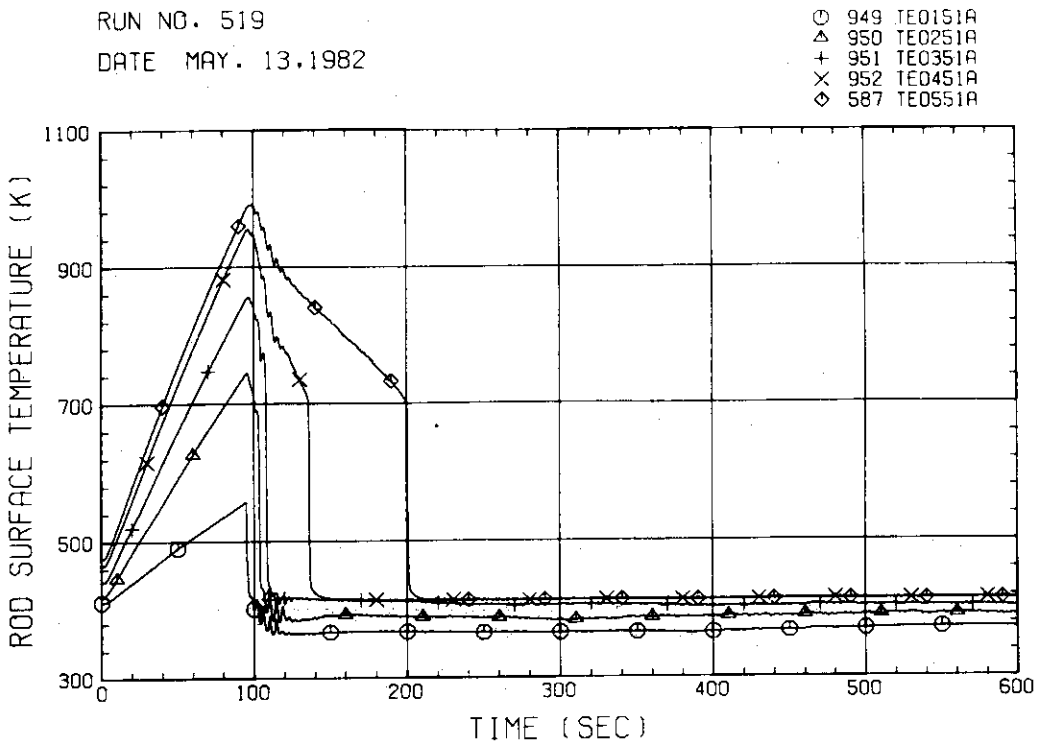

Fig. C-17 HEATER ROD TEMPERATURE (BUNDLE 5-1A, LOWER HALF)

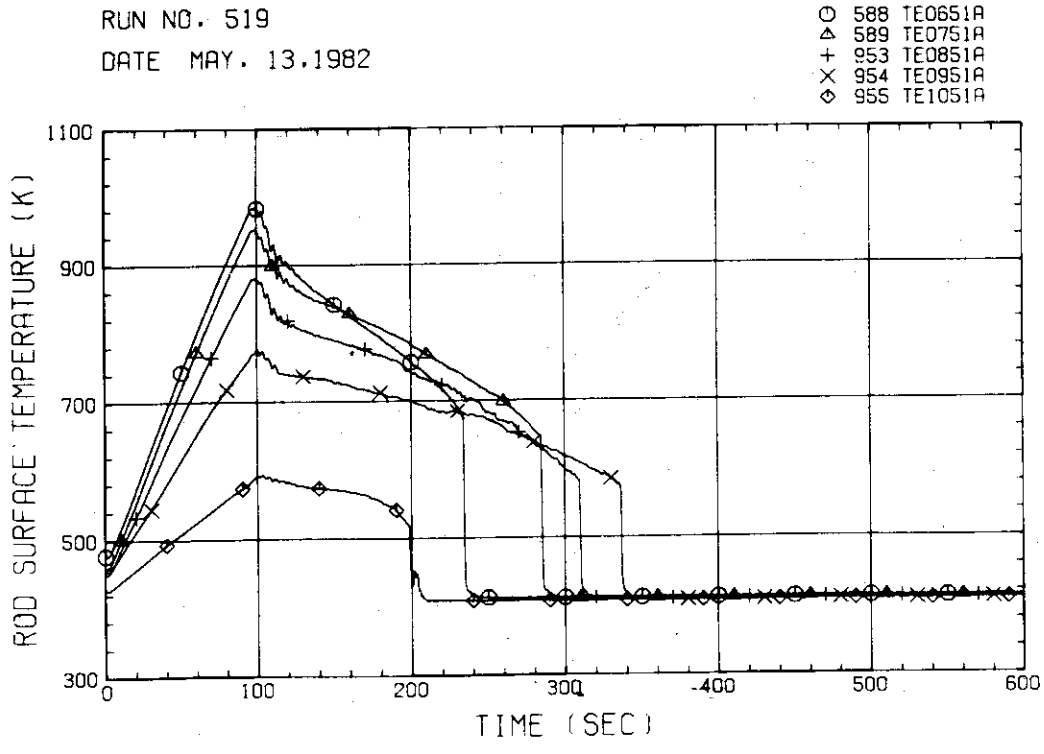

Fig. C-18 HEATER ROD TEMPERATURE (BUNDLE 5-1A, UPPER HALF)

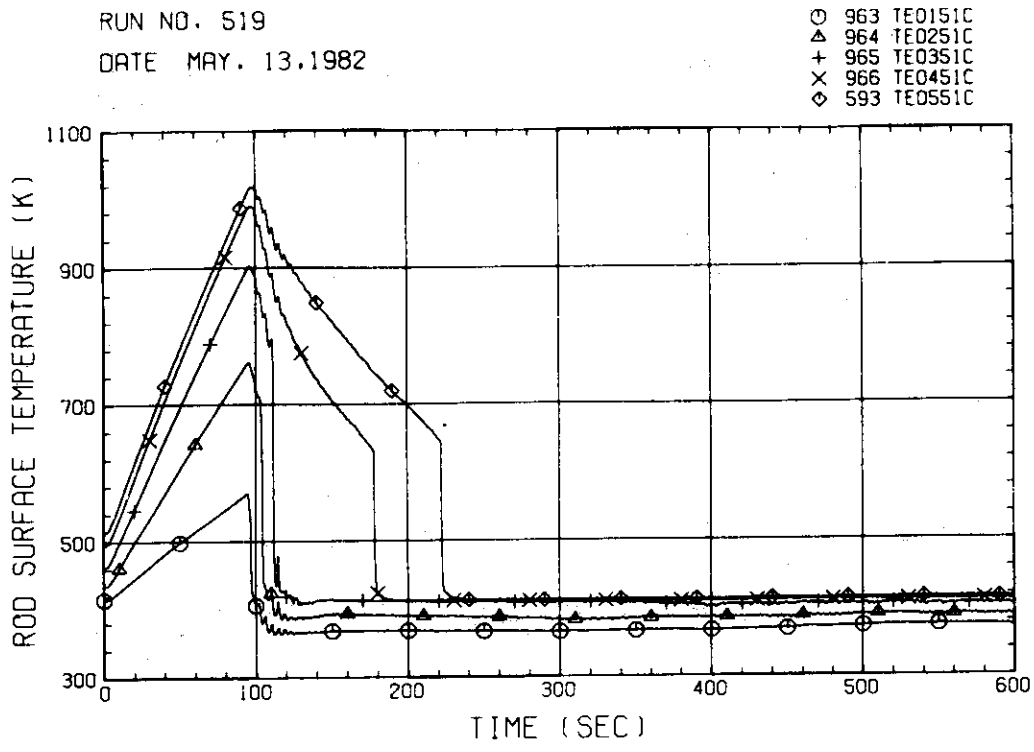

Fig. C-19 HEATER ROD TEMPERATURE (BUNDLE 5-1C, LOWER HALF)

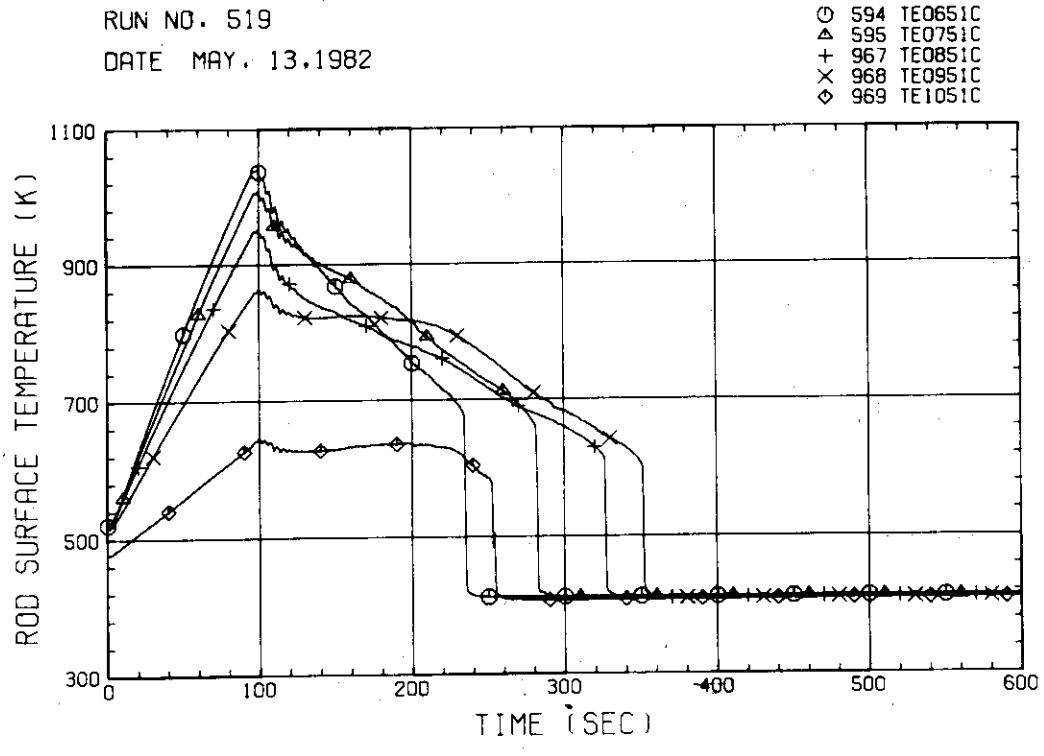

Fig. C-20 HEATER ROD TEMPERATURE (BUNDLE 5-1C, UPPER HALF)

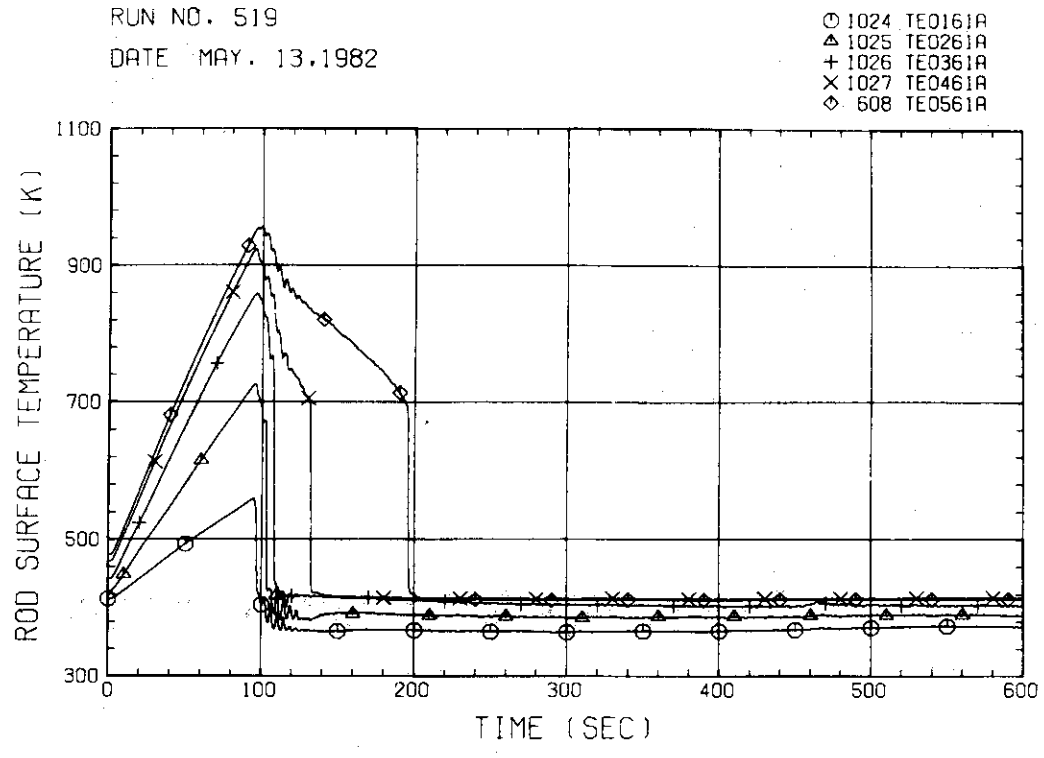

Fig. C-21 HEATER ROD TEMPERATURE (BUNDLE 6-1A, LOWER HALF)

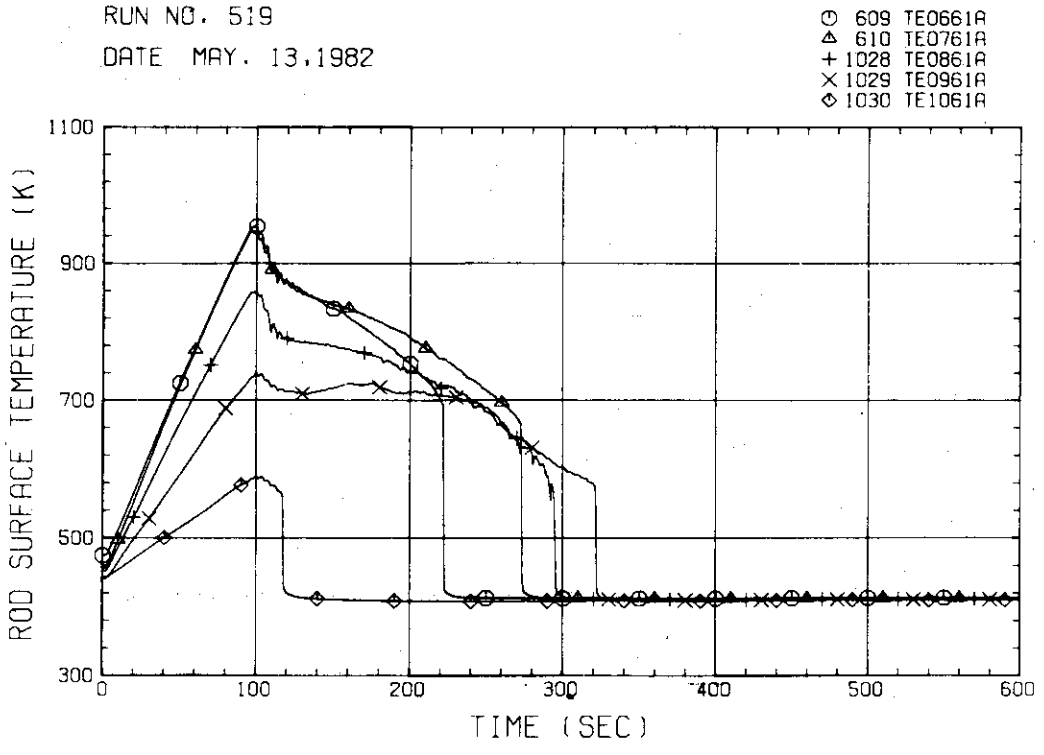

Fig. C-22 HEATER ROD TEMPERATURE (BUNDLE 6-1A, UPPER HALF)

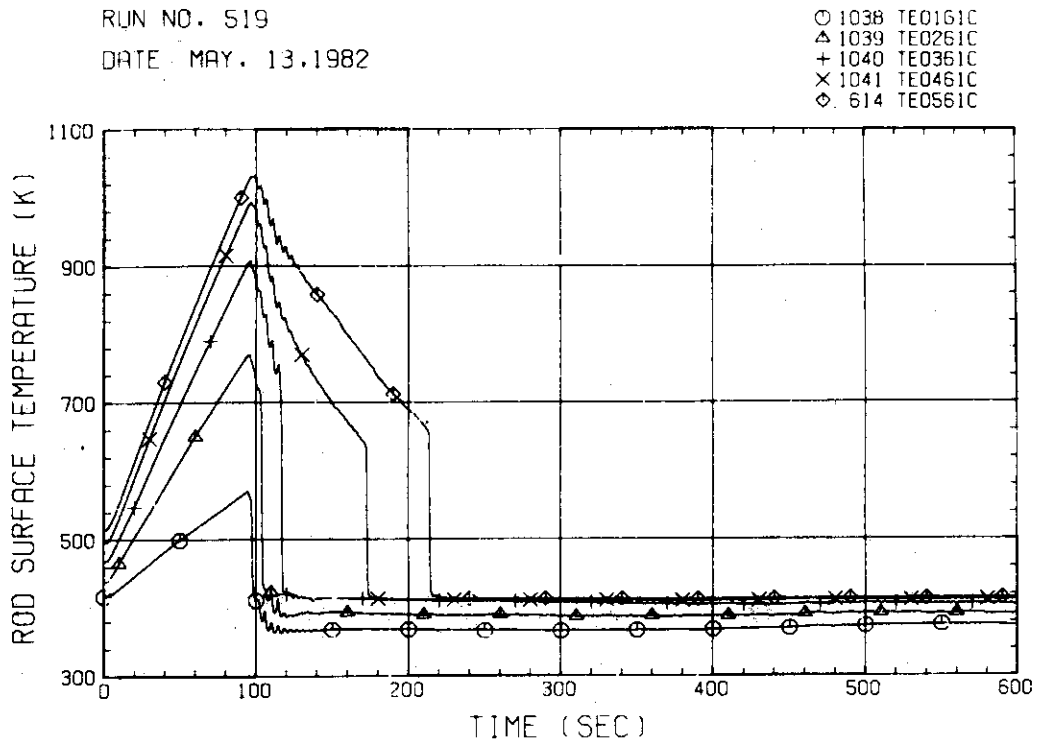

Fig. C-23 HEATER ROD TEMPERATURE (BUNDLE 6-1C, LOWER HALF)

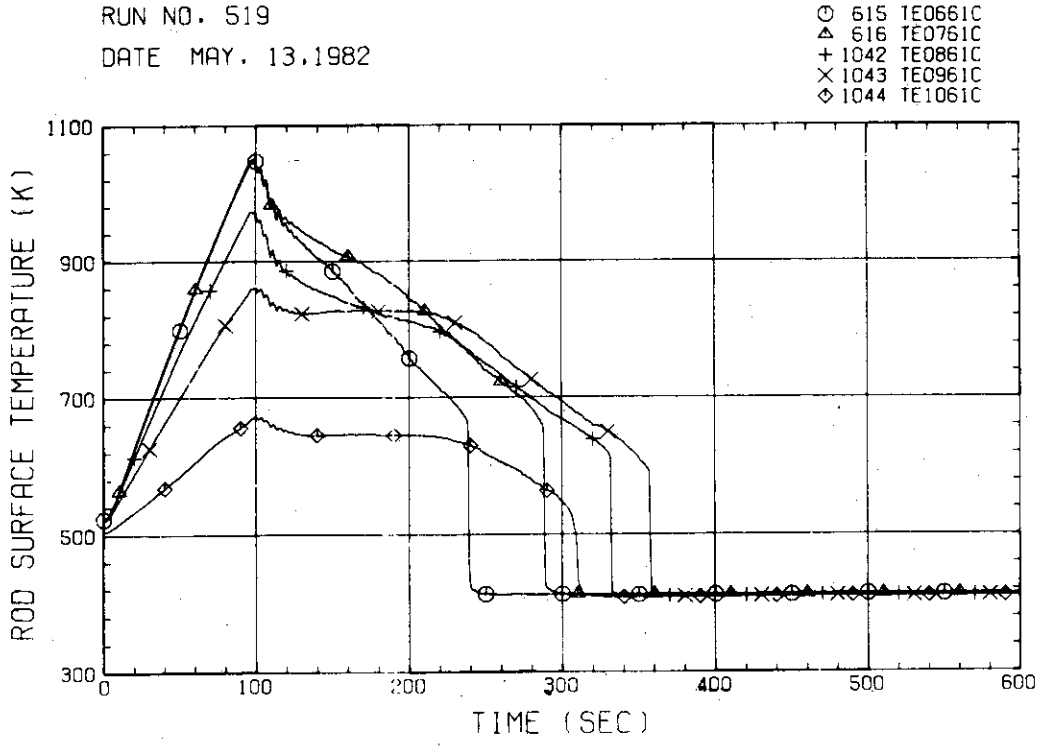

Fig. C-24 HEATER ROD TEMPERATURE (BUNDLE 6-1C, UPPER HALF)

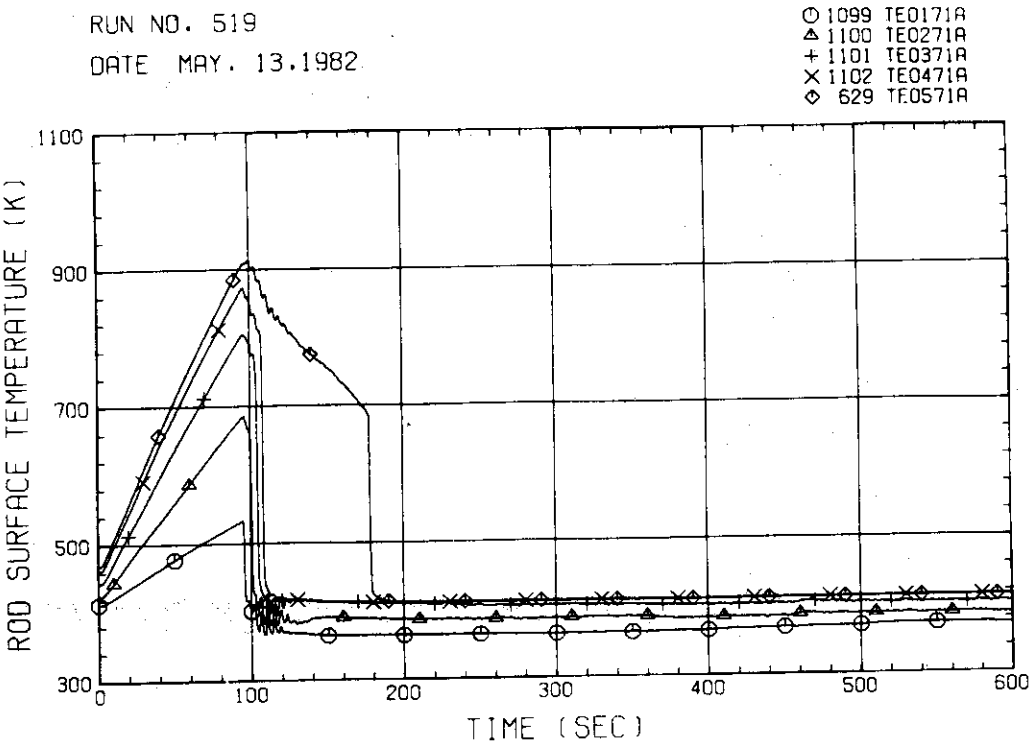

Fig. C-25 HEATER ROD TEMPERATURE (BUNDLE 7-1A. LOWER HALF)

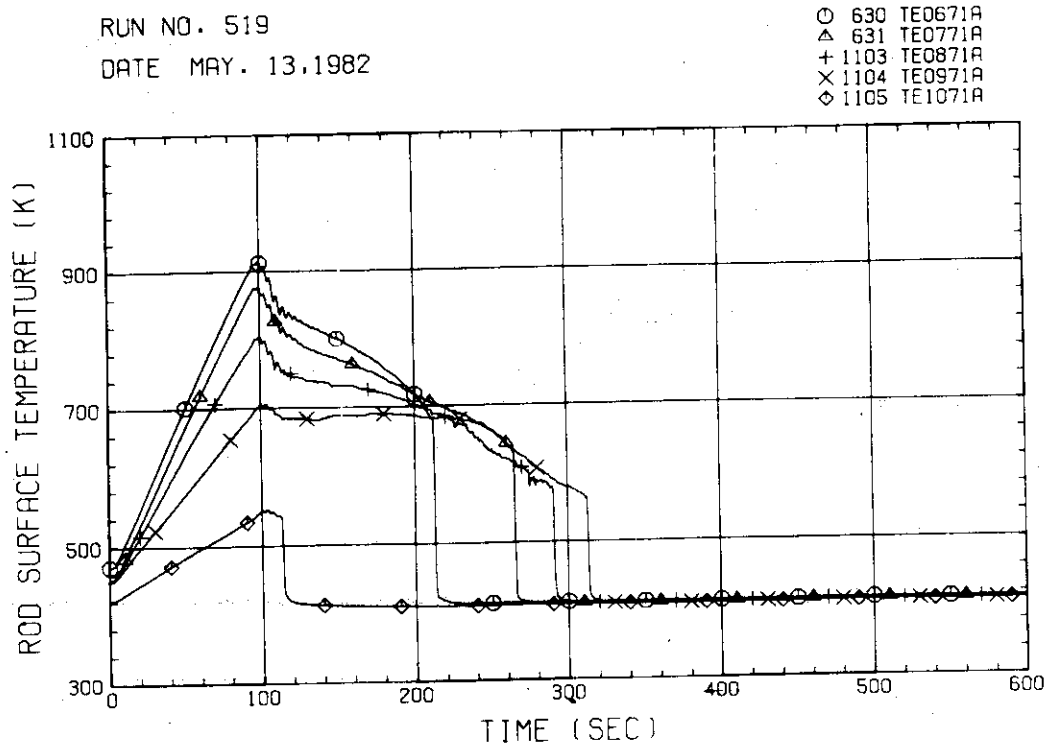

Fig. C-26 HEATER ROD TEMPERATURE (BUNDLE 7-1A. UPPER HALF)

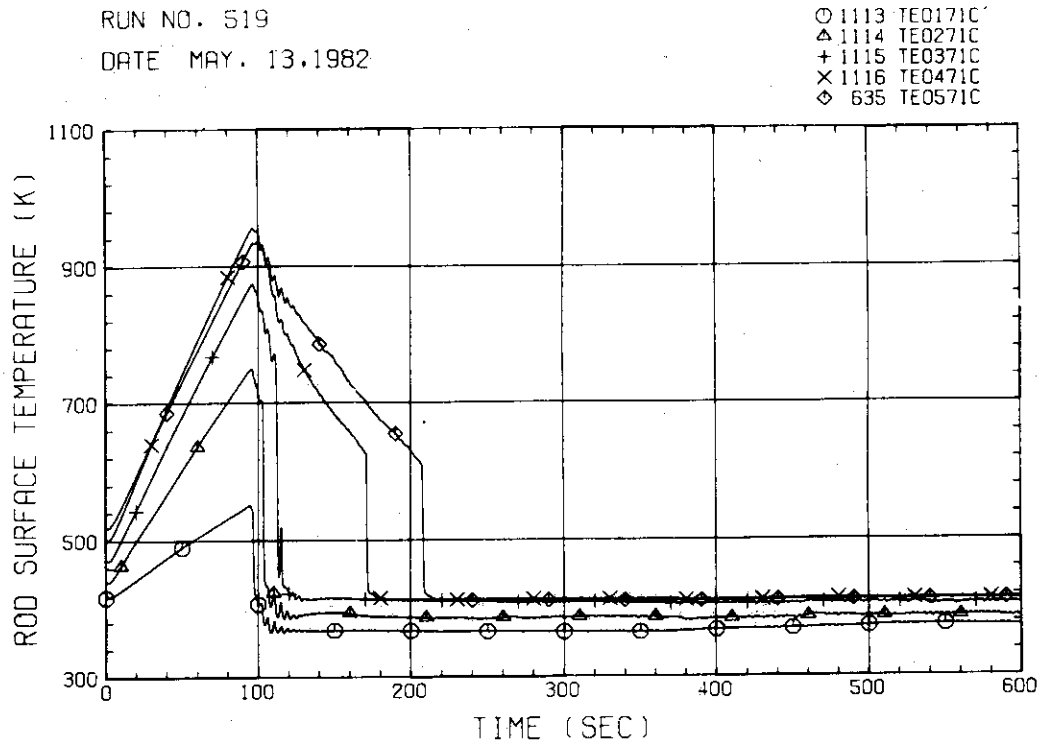

Fig. C-27 HEATER ROD TEMPERATURE (BUNDLE 7-1C, LOWER HALF)

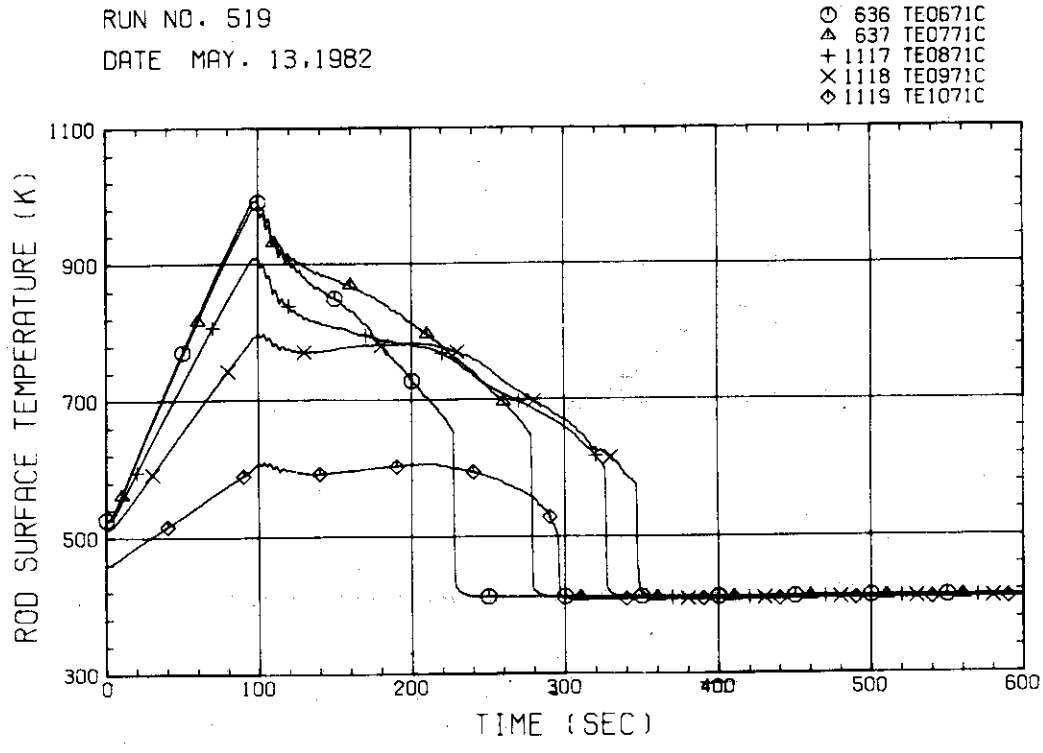

Fig. C-28 HEATER ROD TEMPERATURE (BUNDLE 7-1C, UPPER HALF)

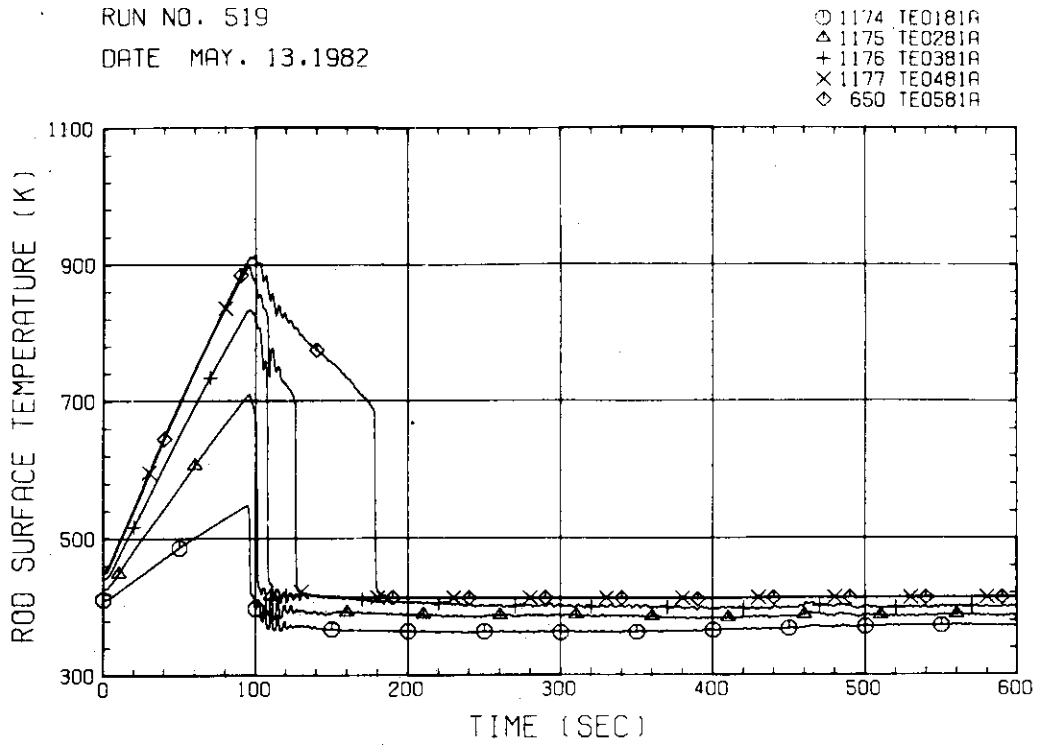

Fig. C-29 HEATER ROD TEMPERATURE (BUNDLE 8-1A, LOWER HALF)

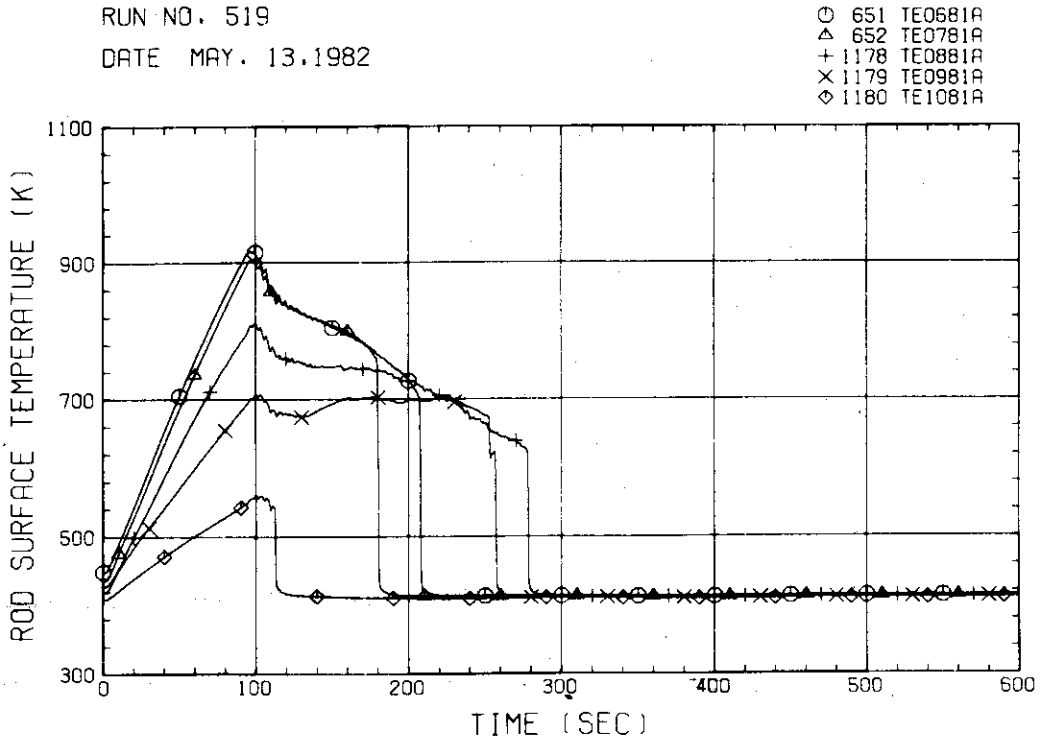

Fig. C-30 HEATER ROD TEMPERATURE (BUNDLE 8-1A, UPPER HALF)

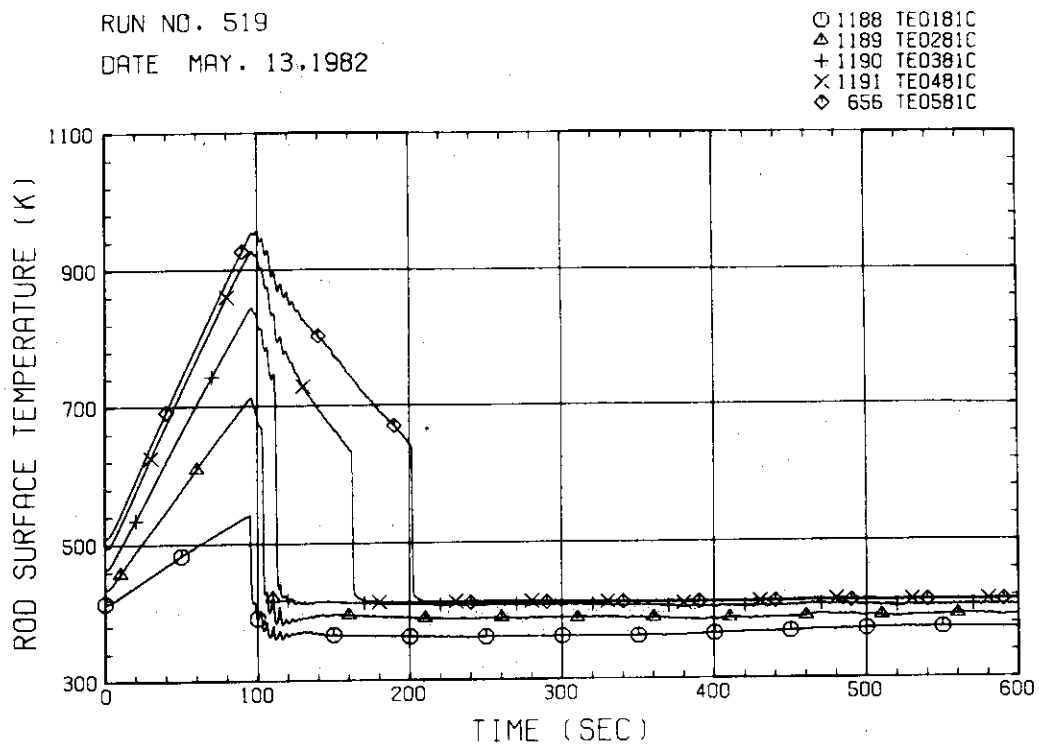

Fig. C-31 HEATER ROD TEMPERATURE (BUNDLE 8-1C, LOWER HALF)

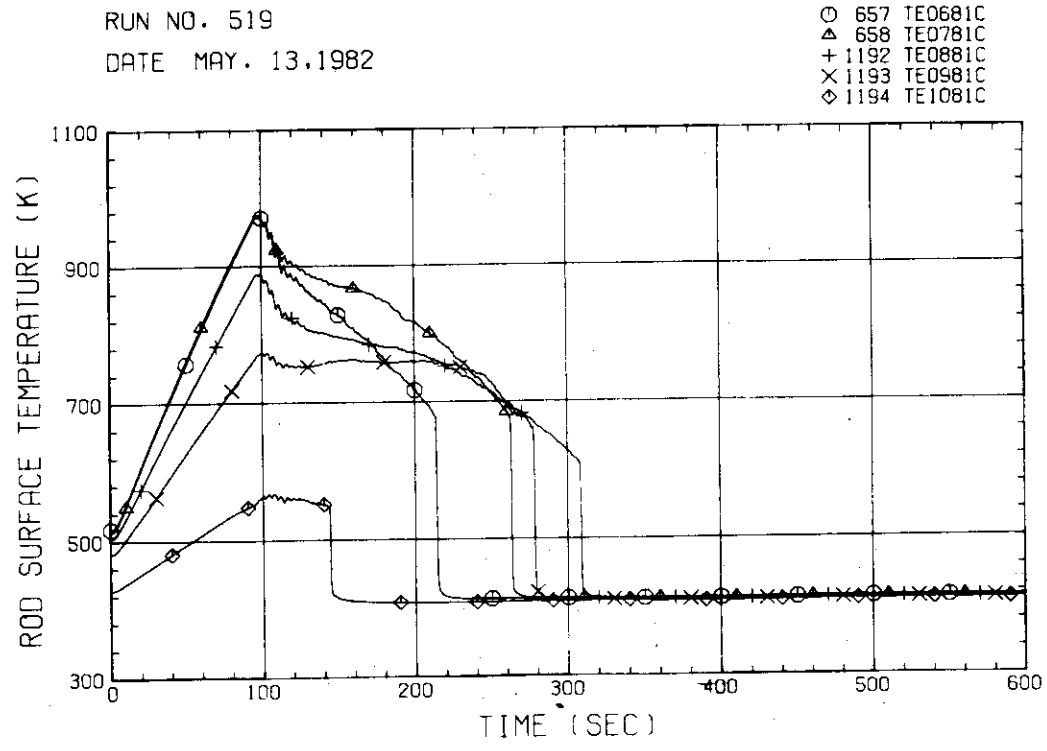

Fig. C-32 HEATER ROD TEMPERATURE (BUNDLE 8-1C, UPPER HALF)

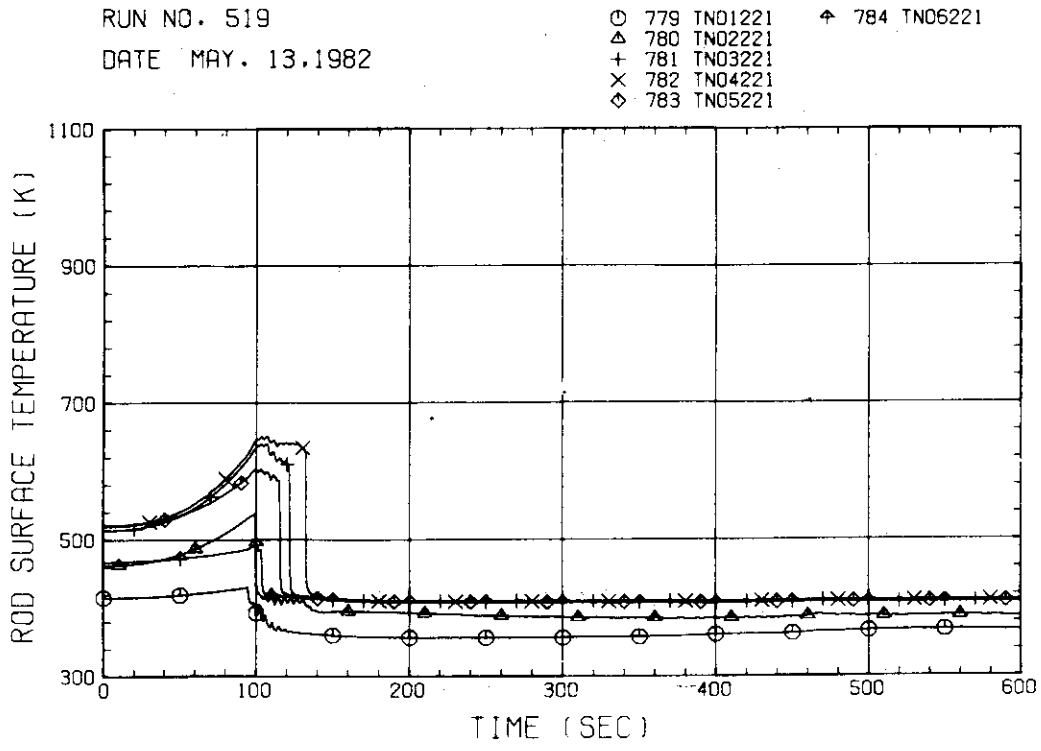

Fig. C-33 NON-HEATED ROD TEMPERATURE (BUNDLE 2-2)

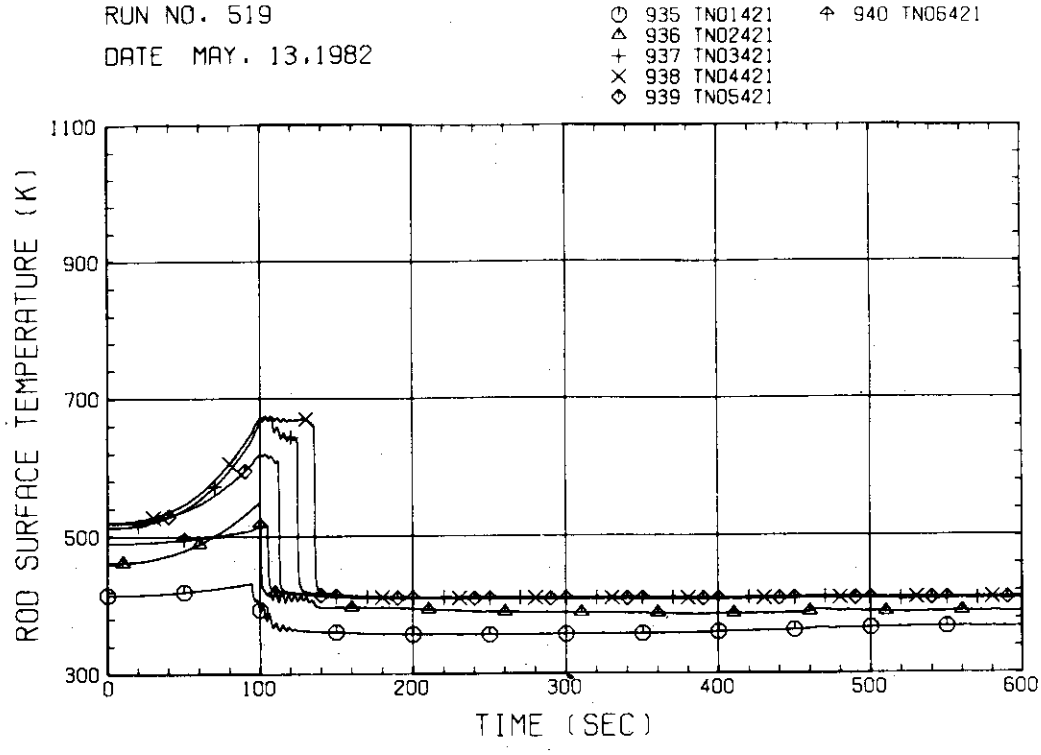

Fig. C-34 NON-HEATED ROD TEMPERATURE (BUNDLE 4-2)

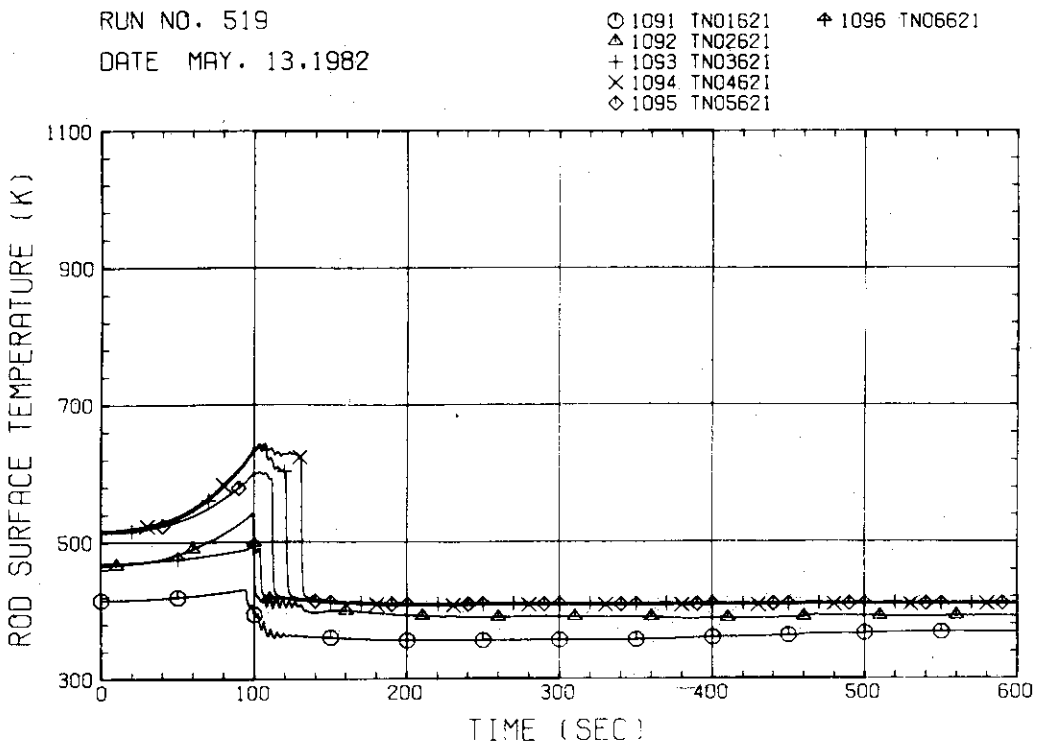

Fig. C-35 NON-HEATED ROD TEMPERATURE (BUNDLE 6-2)

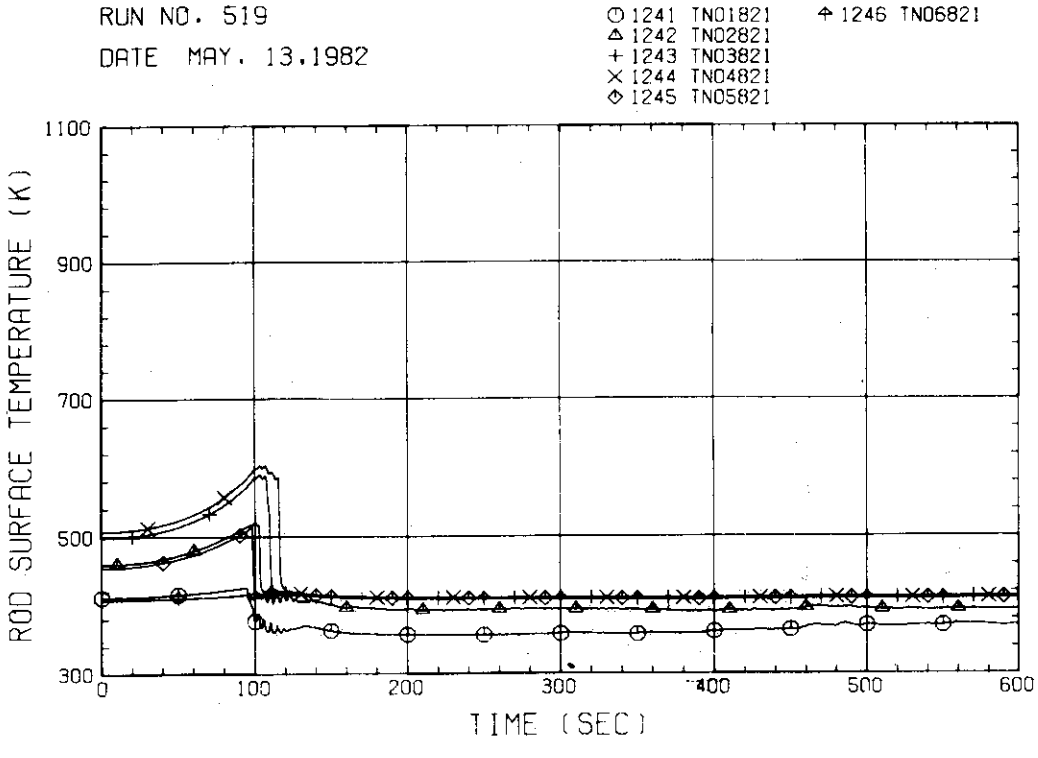

Fig. C-36 NON-HEATED ROD TEMPERATURE (BUNDLE 8-2)

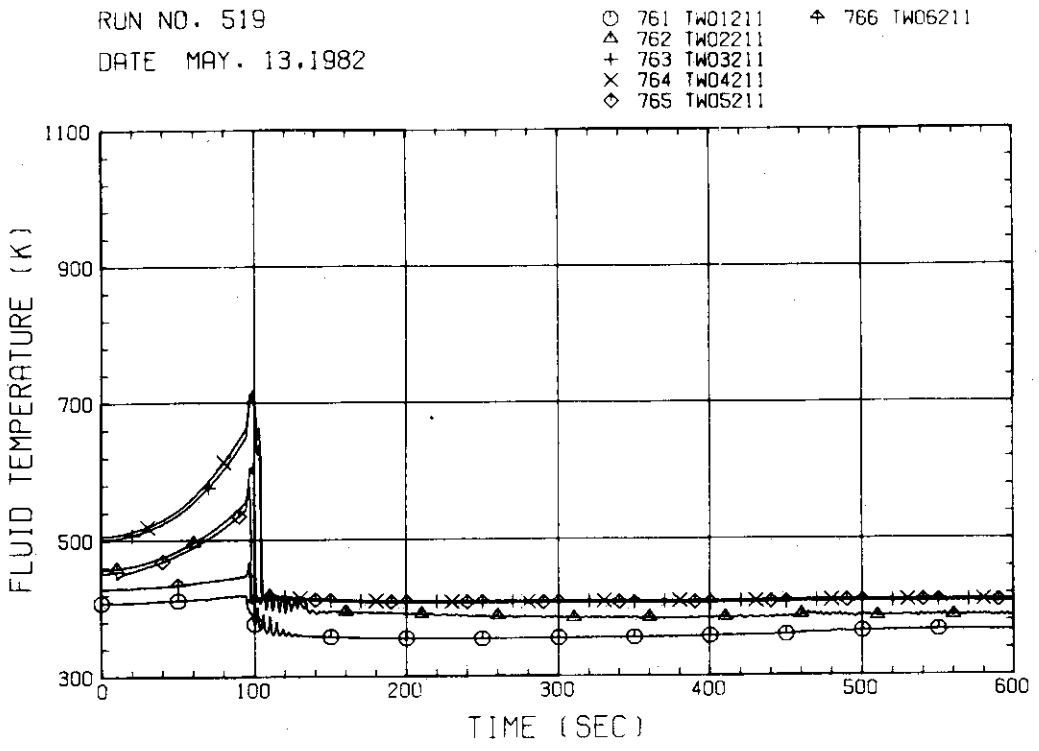

Fig. C-37 FLUID TEMPERATURE IN CORE (BUNDLE 2-1)

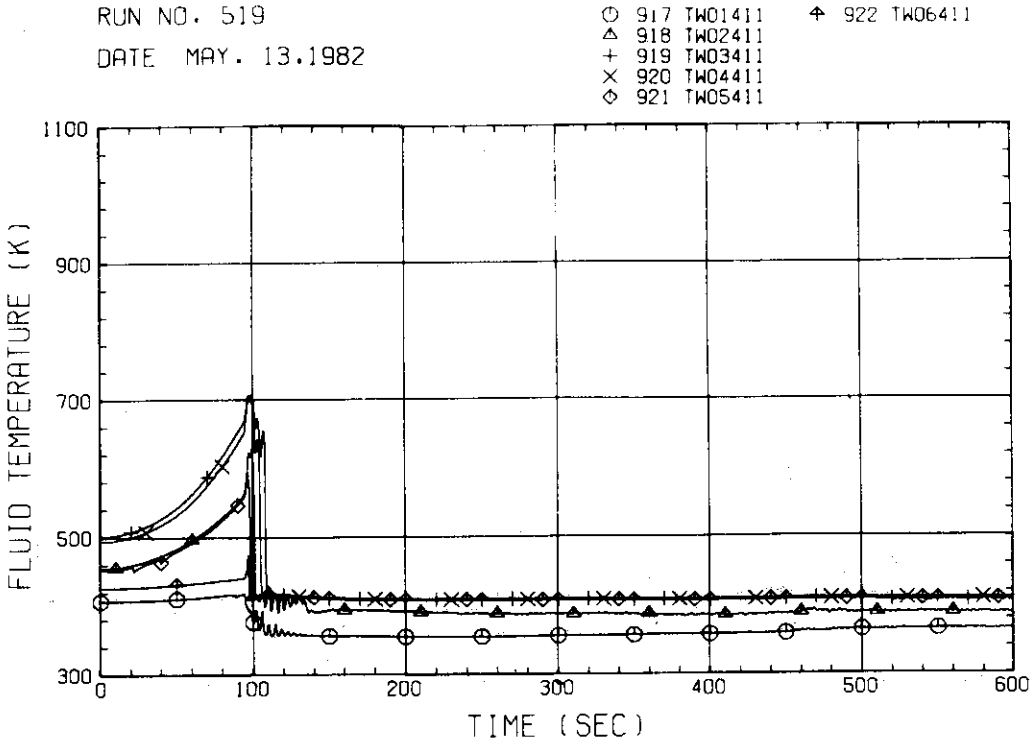

Fig. C-38 FLUID TEMPERATURE IN CORE (BUNDLE 4-1)

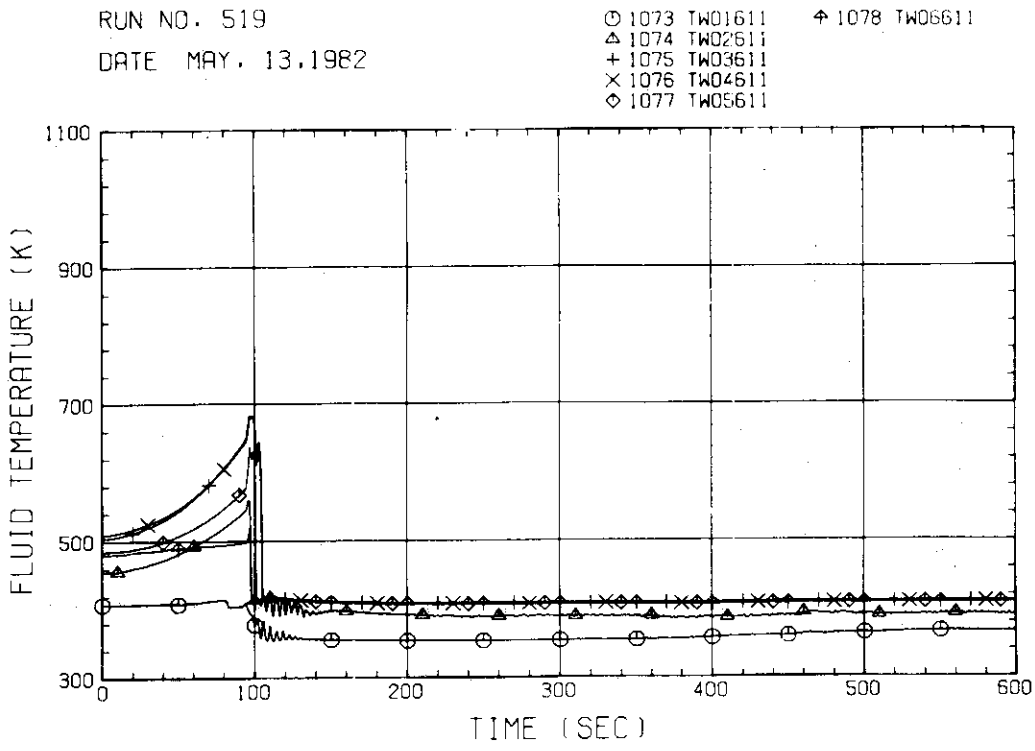

Fig. C-39 FLUID TEMPERATURE IN CORE (BUNDLE 6-1)

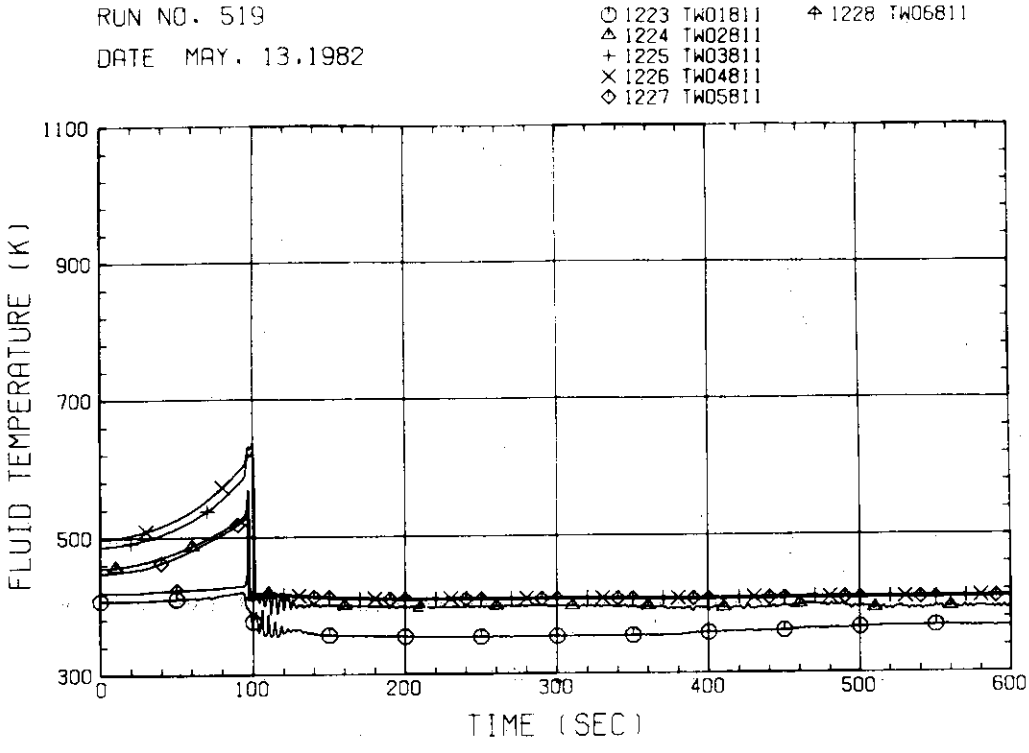

Fig. C-40 FLUID TEMPERATURE IN CORE (BUNDLE 8-1)

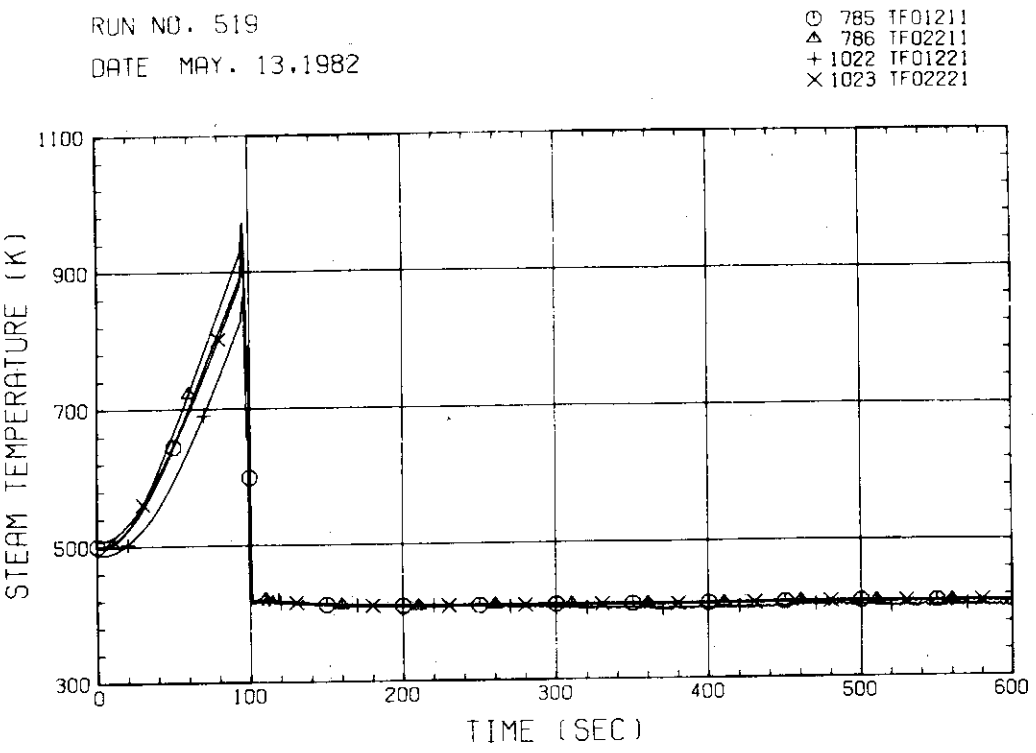

Fig. C-41 STEAM TEMPERATURE IN CORE, BUNDLE 2
(01211-1.735M, 02211-1.875M, 01221-1.38M, 02221-1.915M)

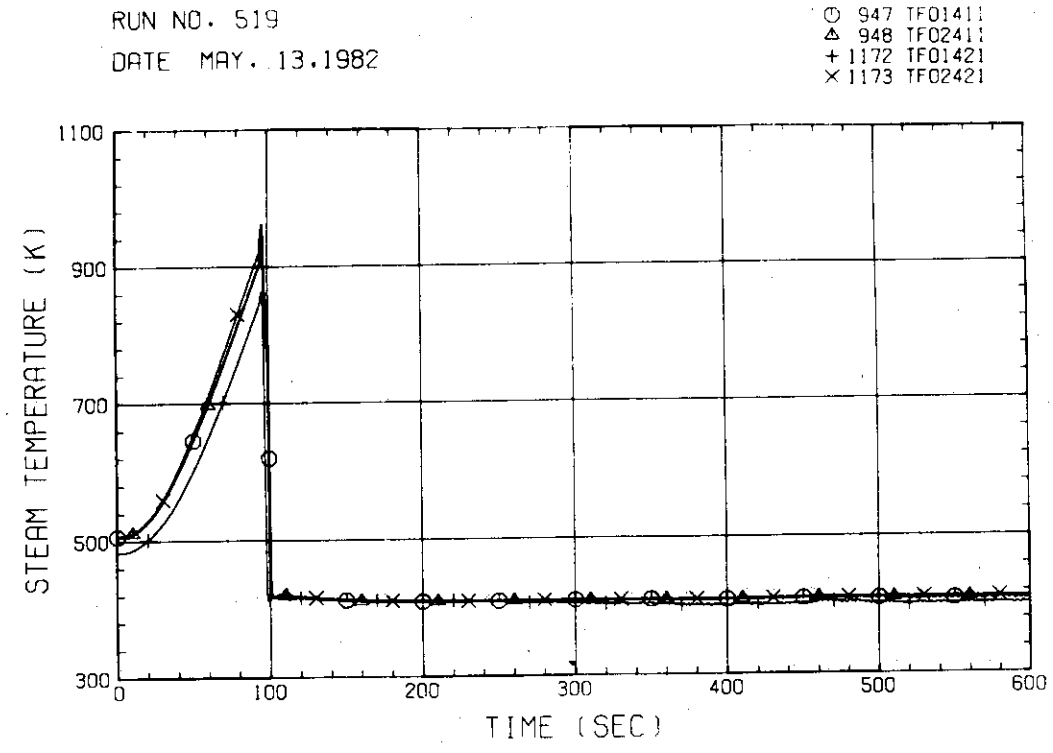

Fig. C-42 STEAM TEMPERATURE IN CORE, BUNDLE 4
(01411-1.735M, 02411-1.875M, 01421-1.38M, 02421-1.915M)

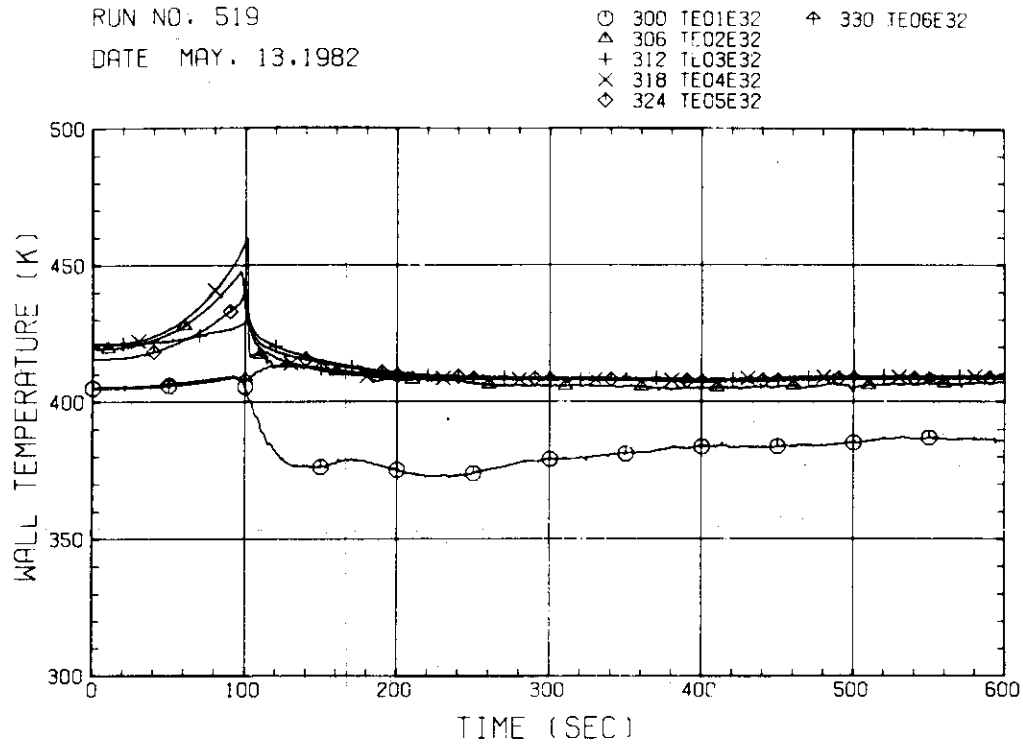

Fig. C-43 SURFACE TEMPERATURE OF CORE SIDE WALL (BUNDLE 3, OPPOSITE SIDE OF COLD LEG, INNER SURFACE)

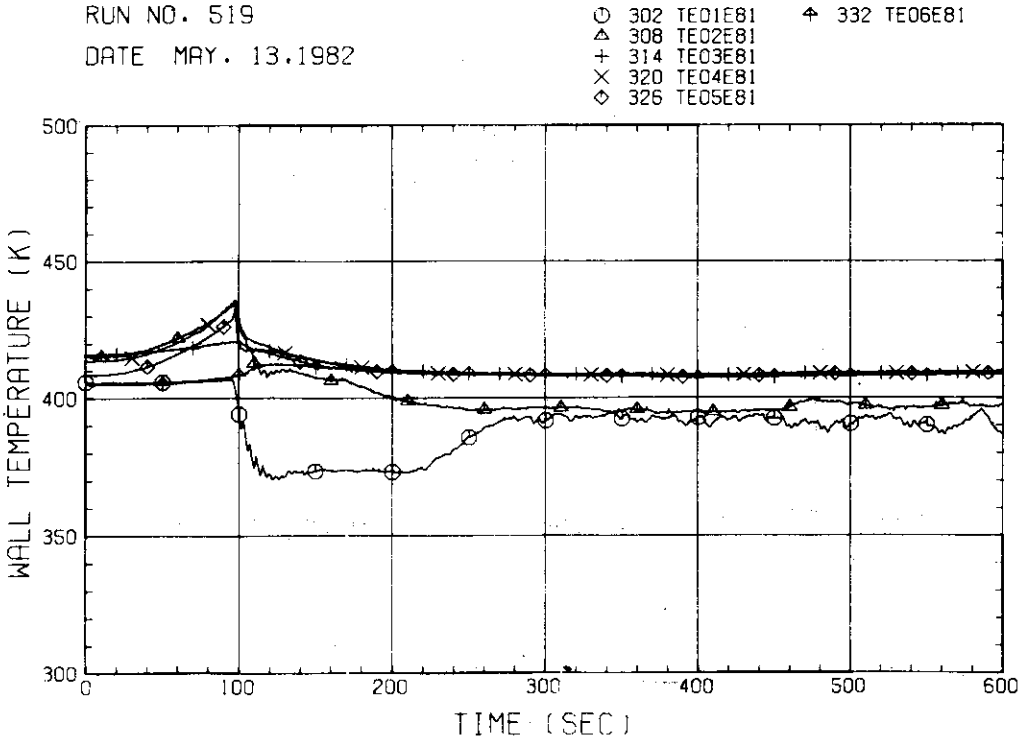

Fig. C-44 SURFACE TEMPERATURE OF CORE SIDE WALL (BUNDLE 8, OPPOSITE SIDE OF COLD LEG, INNER SURFACE)

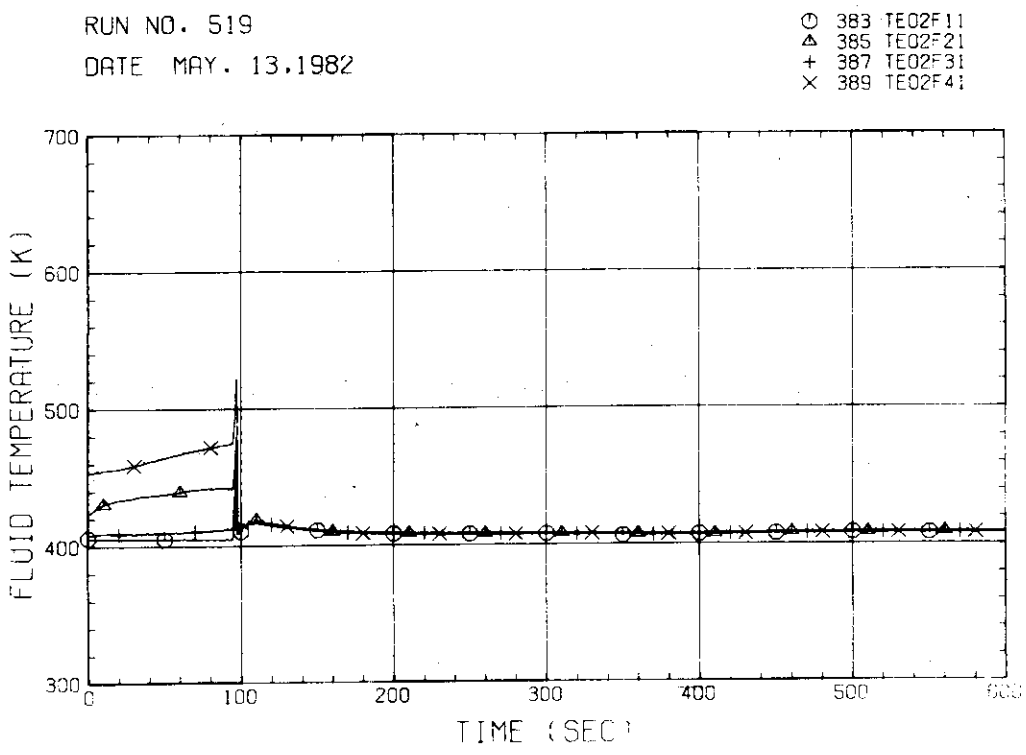

Fig. C-45 FLUID TEMPERATURE JUST ABOVE END BOX TIE PLATE (BUNDLE 1.2.3.4. OPPOSITE SIDE OF COLD LEG)

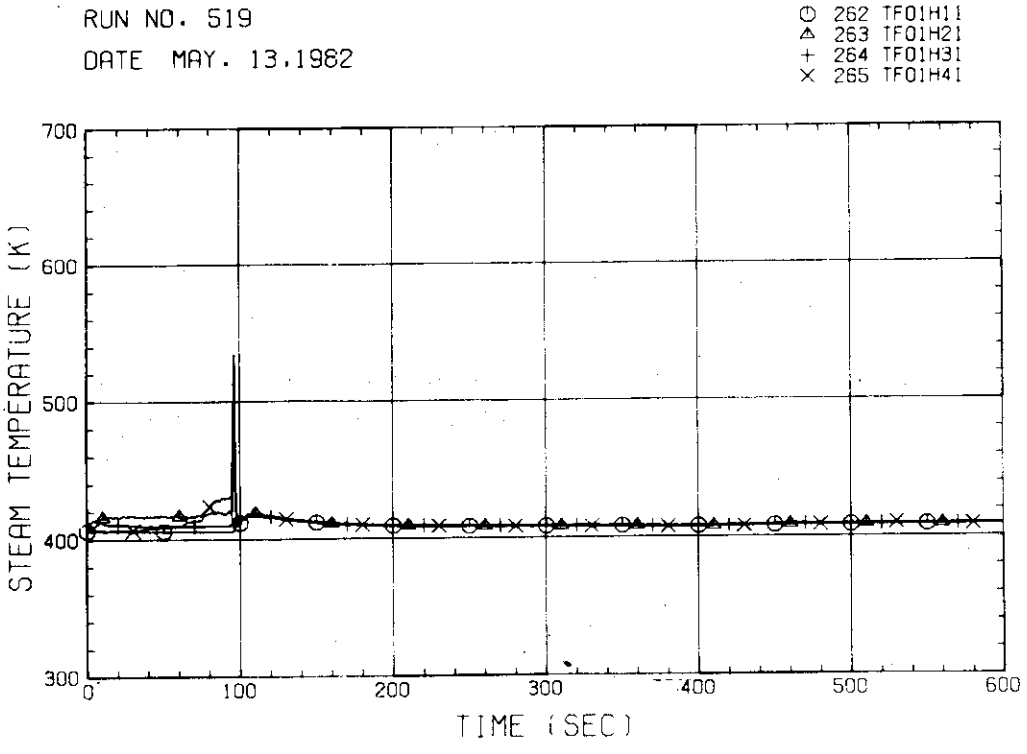

Fig. C-46 STEAM TEMPERATURE ABOVE UCSP HOLE (BUNDLE 1.2.3.4)

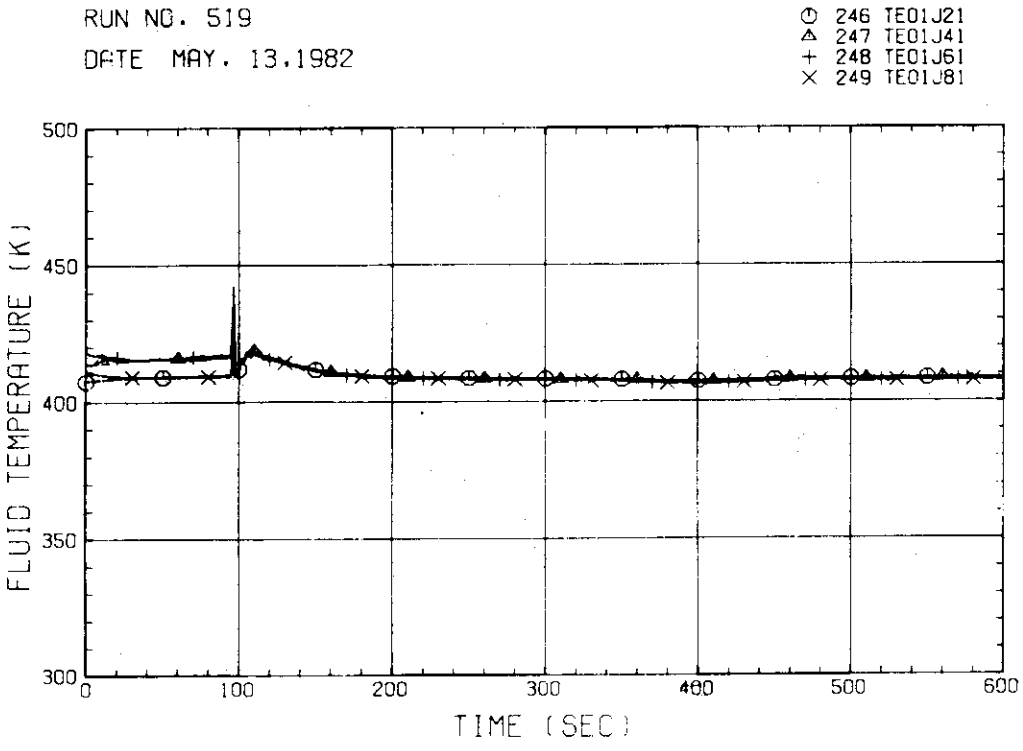

Fig. C-47 FLUID TEMPERATURE ABOVE UCSP
(BUNDLE 2.4.6.8. 250MM ABOVE UCSP)

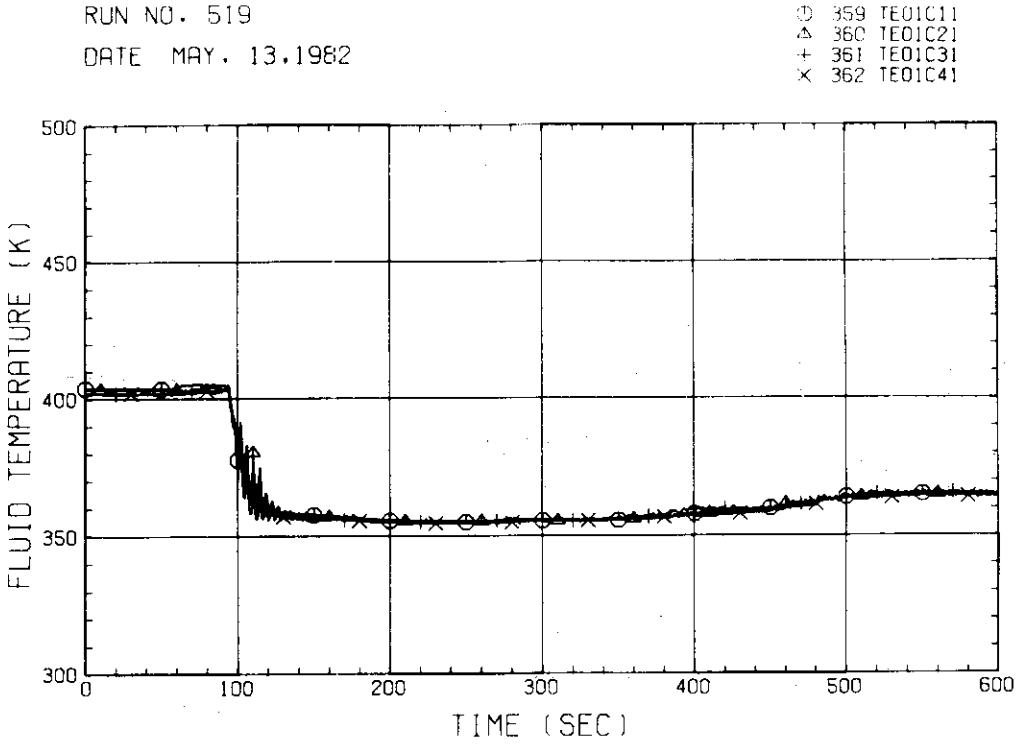

Fig. C-48 FLUID TEMPERATURE AT CORE INLET
(BUNDLE 1.2.3.4. 100MM BELOW HEATED PART)

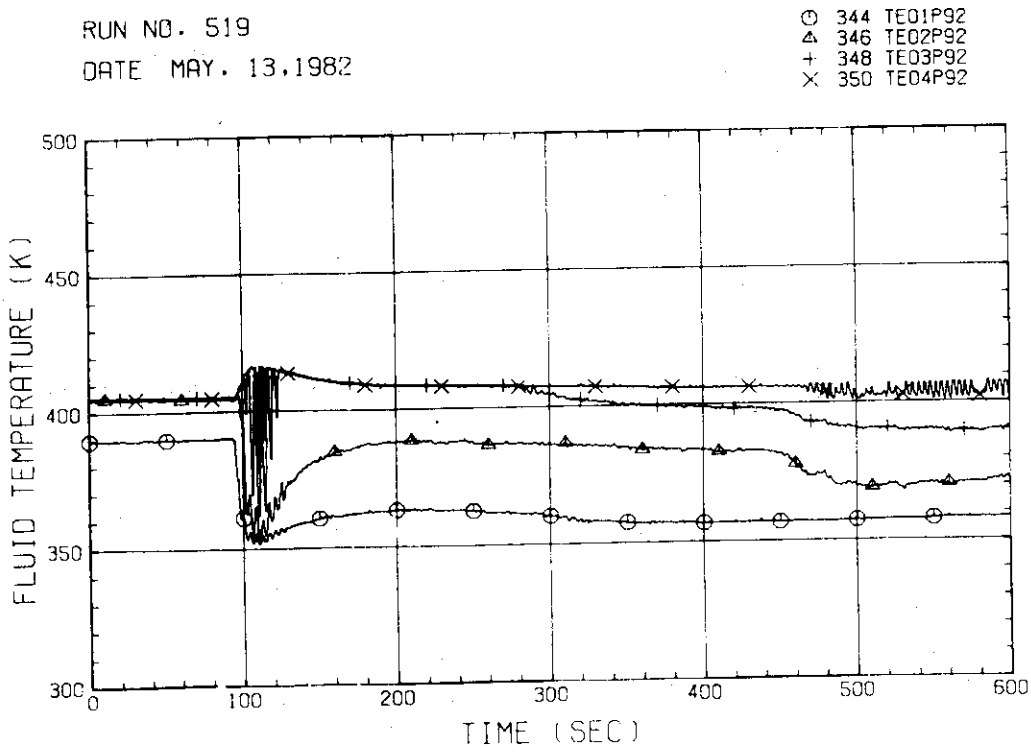

Fig. C-49 FLUID TEMPERATURE IN DOWNCOMER (BELOW BROKEN COLD LEG - PV SIDE)

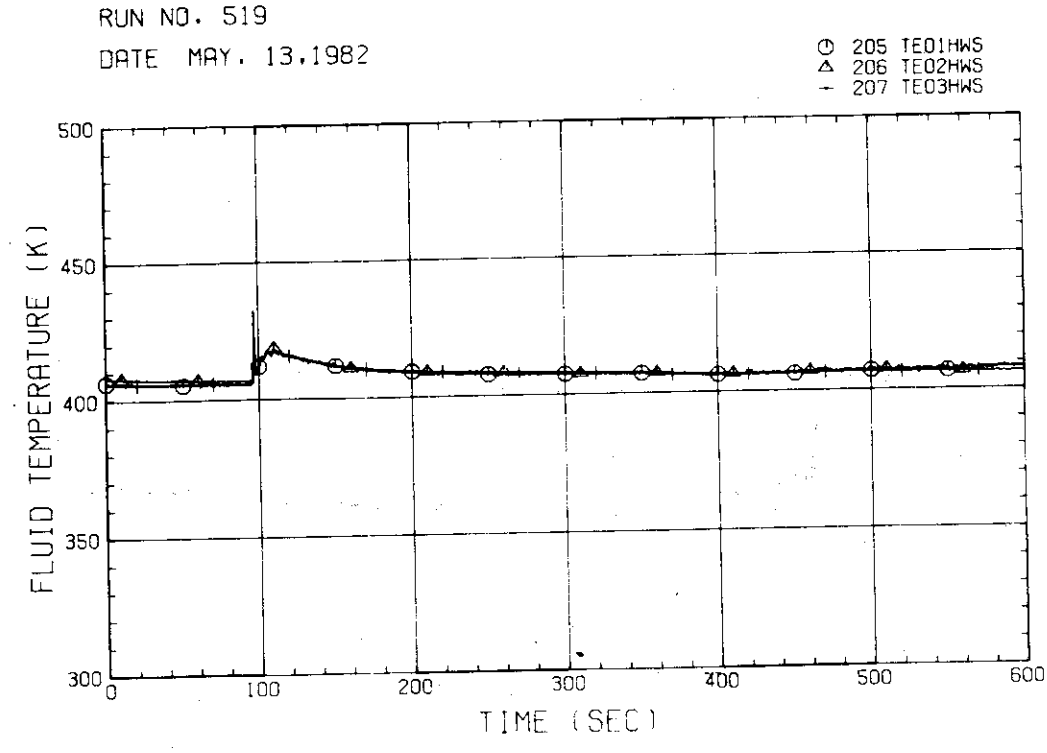

Fig. C-50 FLUID TEMPERATURE IN HOT LEG (01,02,03 - FROM PV TO STEAM/WATER SEPARATOR)

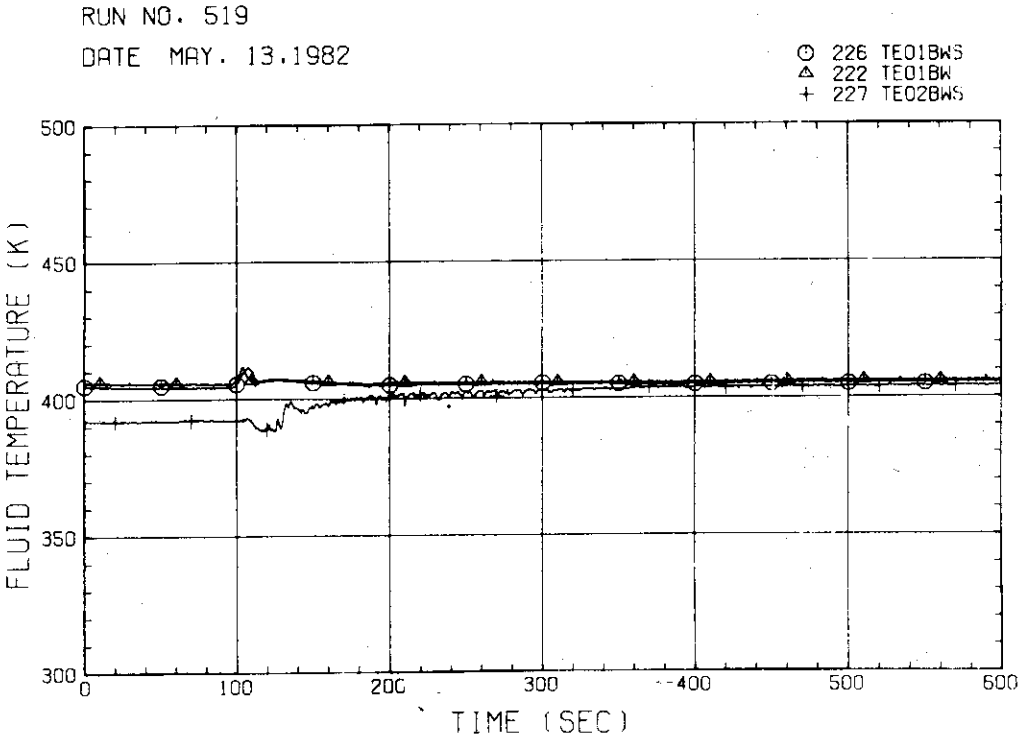

Fig. C-51 FLUID TEMPERATURE IN CONTAINMENT TANK-II
(01BWS - TOP, 01BW - MIDDLE, 02BWS - BOTTOM)

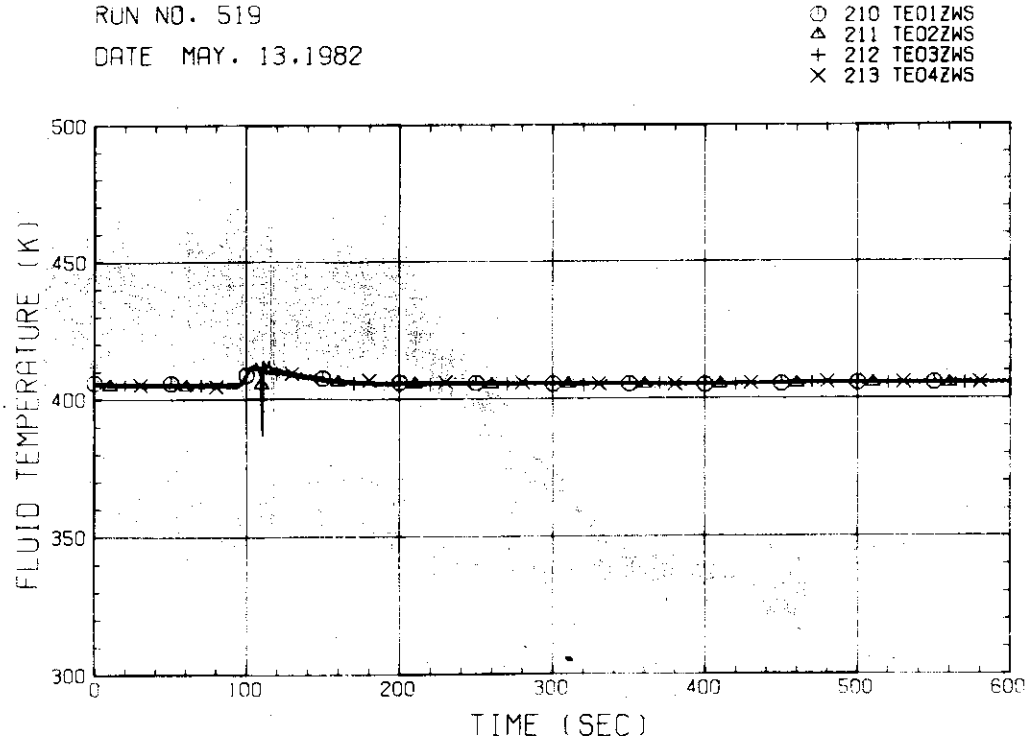

Fig. C-52 FLUID TEMPERATURE IN BROKEN COLD LEG - PV SIDE
(01.02.03.04 FROM PV TO CONTAINMENT TANK-I)

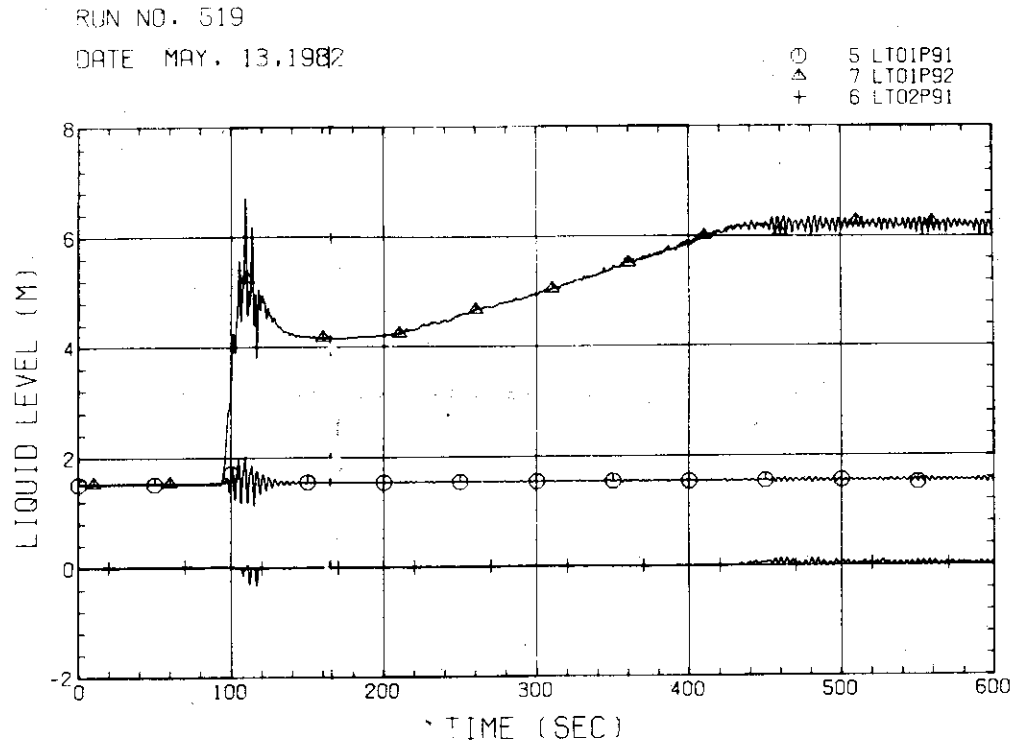

Fig. C-53 LIQUID LEVEL IN DOWNCOMER (01P91-BELOW CORE INLET, 01P92-BOTTOM TO COLD LEG, 02P91-COLD LEG TO TOP OF PV)

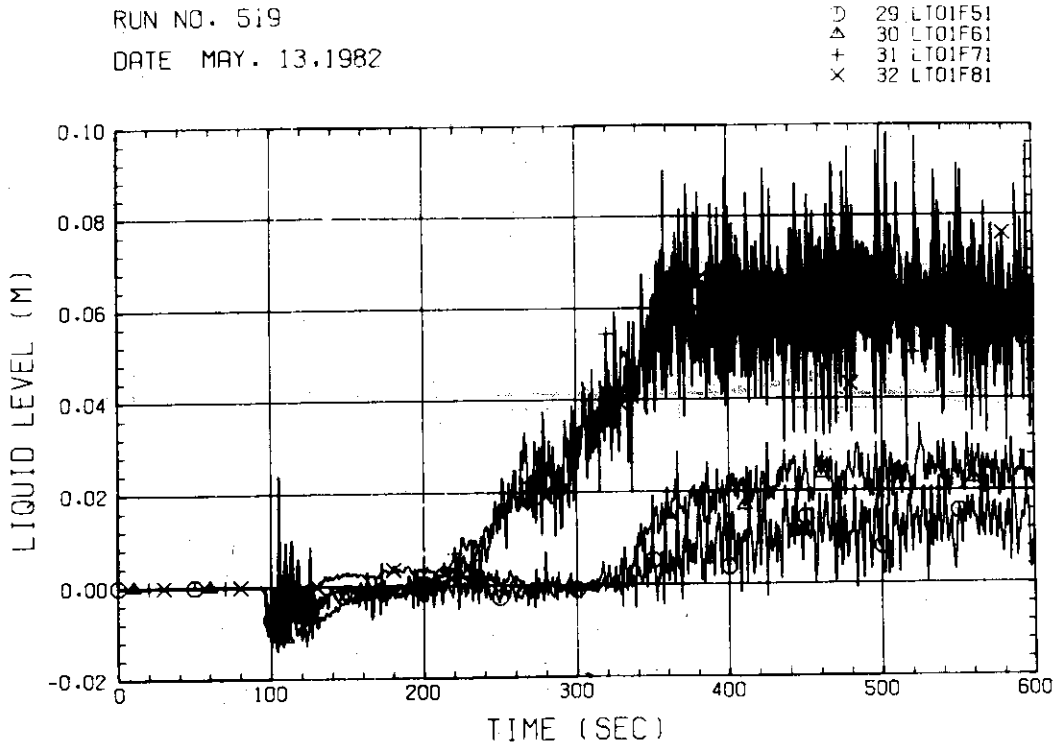

Fig. C-54 LIQUID LEVEL ABOVE END BOX TIE PLATE (BUNDLE 5,6,7,8)

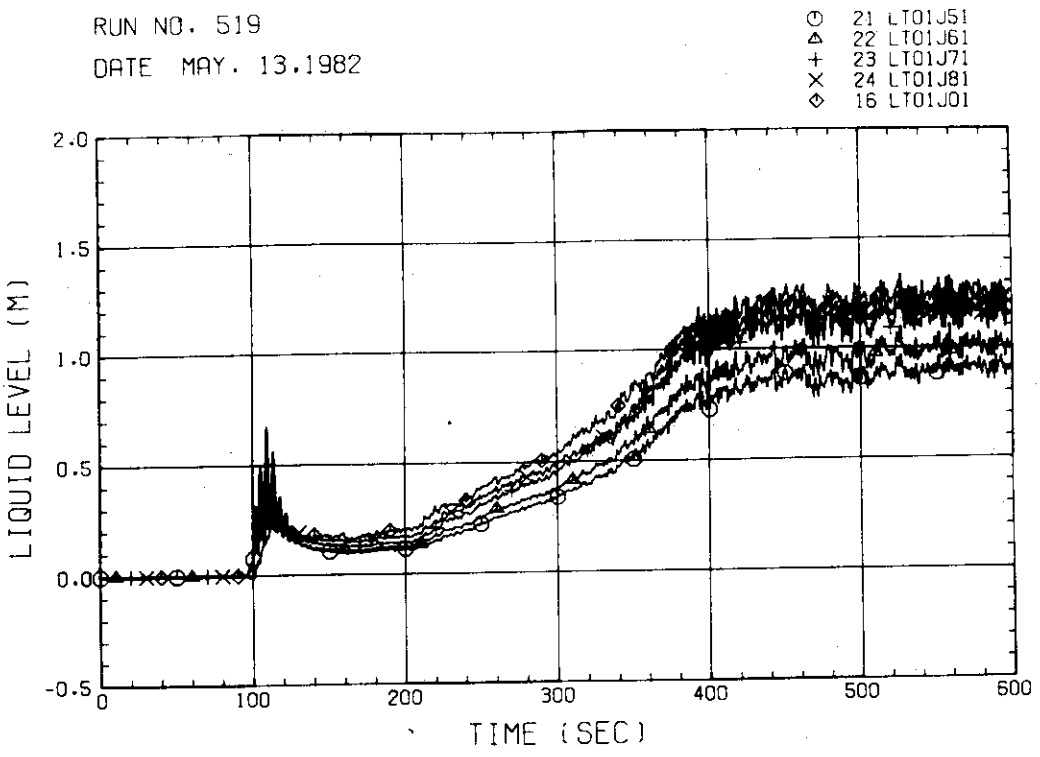

Fig. C-55 LIQUID LEVEL ABOVE UCSP
(BUNDLE 5,6,7,8 AND CORE BAFFLE)

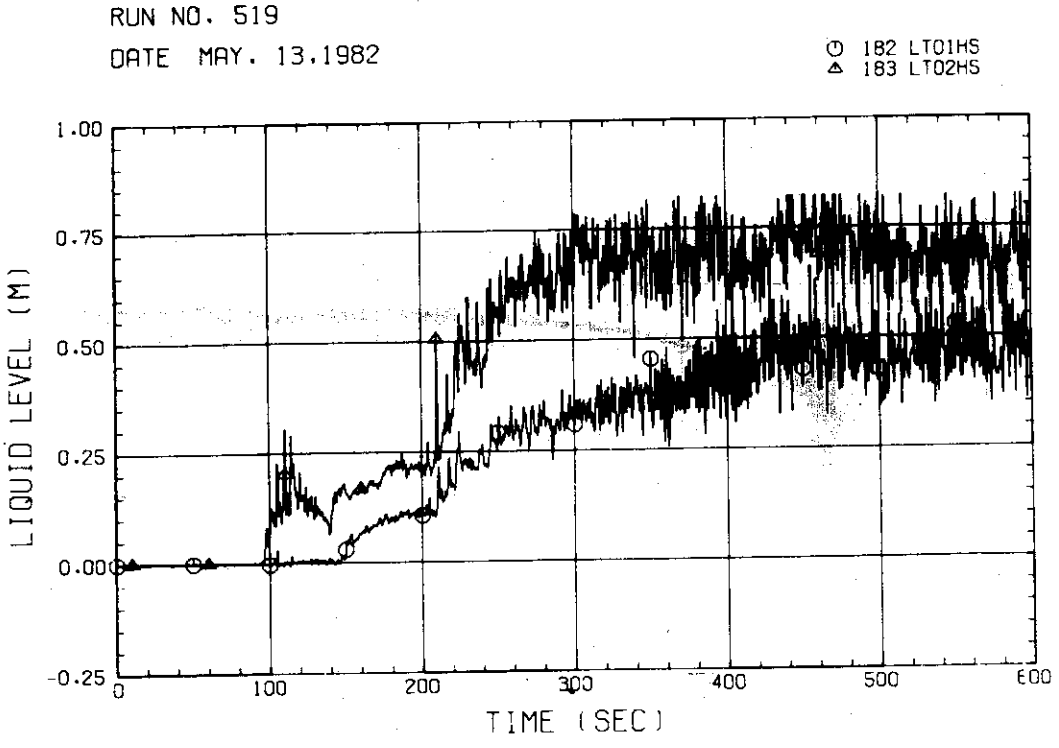

Fig. C-56 LIQUID LEVEL IN HOT LEG
(01HS - PV SIDE, 02HS - STEAM/WATER SEPARATOR SIDE)

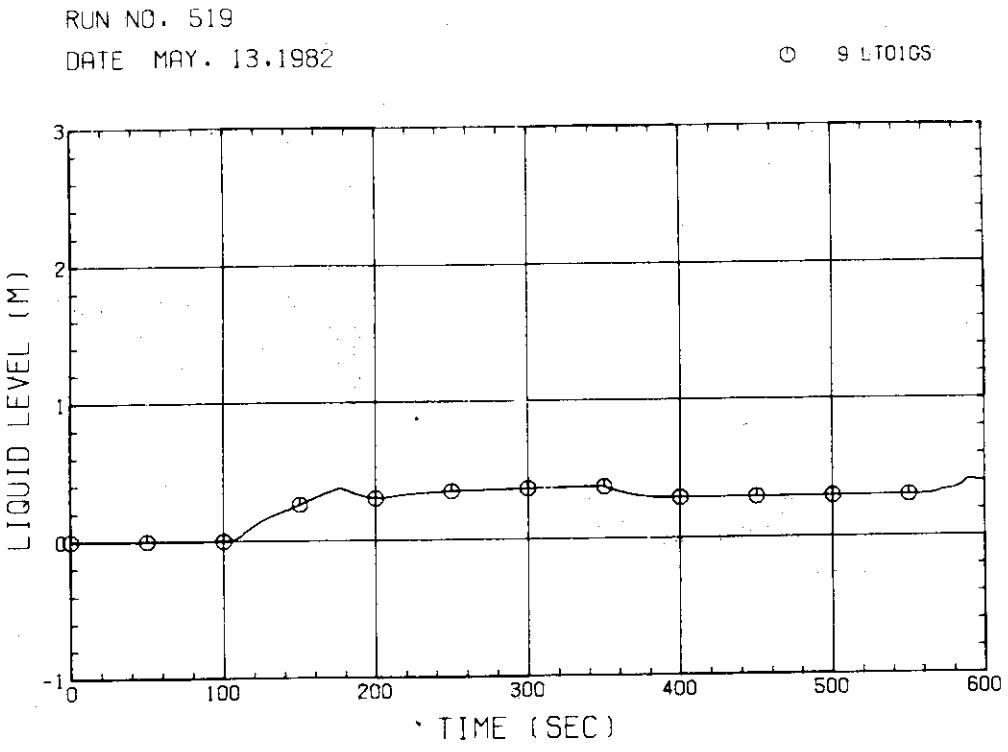

Fig. C-57 LIQUID LEVEL IN STEAM/WATER SEPARATOR

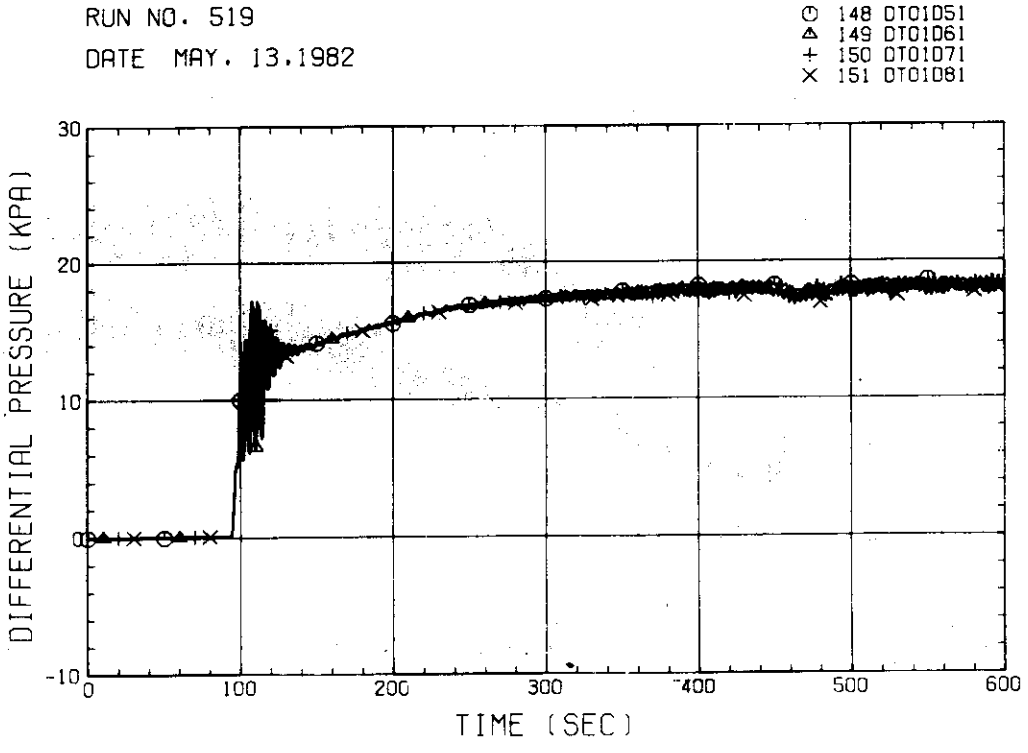

Fig. C-58 DIFFERENTIAL PRESSURE OF CORE LOWER HALF (BUNDLE 5,6,7,8)

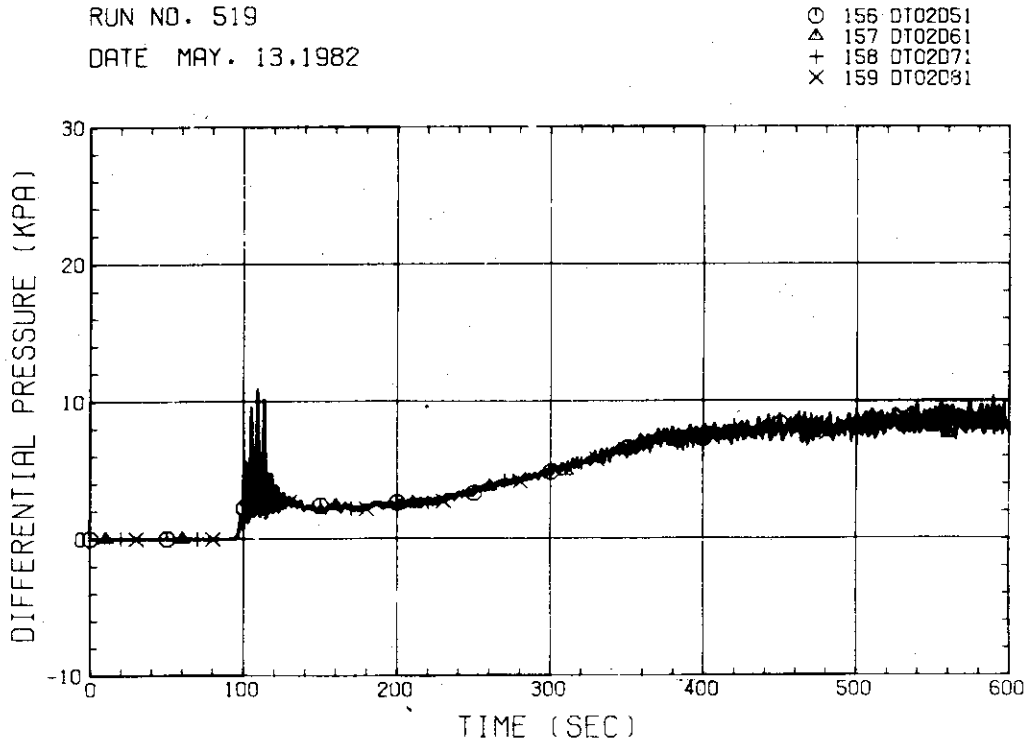

Fig. C-59 DIFFERENTIAL PRESSURE OF CORE UPPER HALF (BUNDLE 5.6.7.8)

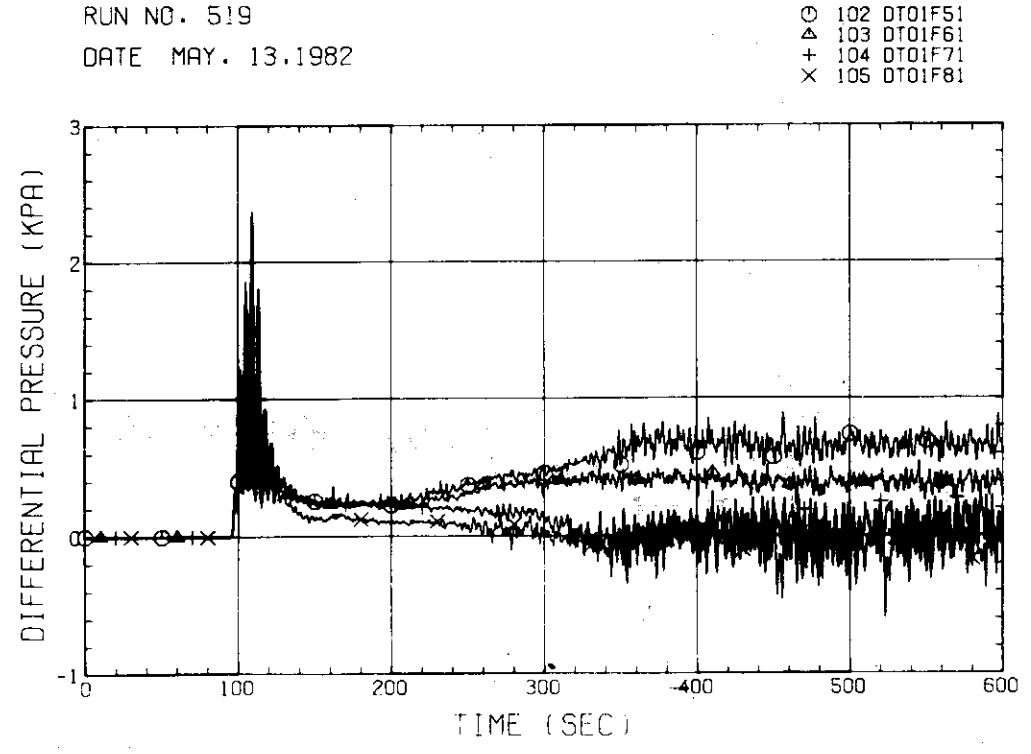

Fig. C-60 DIFFERENTIAL PRESSURE ACROSS END BOX TIE PLATE (BUNDLE 5.6.7.8)

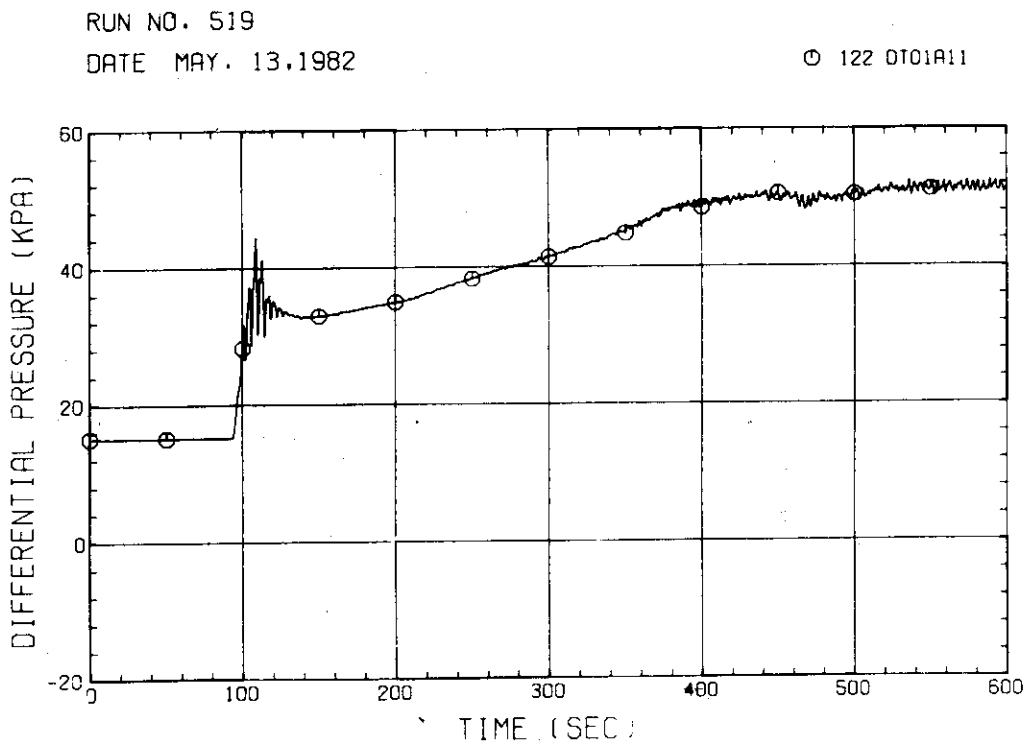

Fig. C-61 DIFFERENTIAL PRESSURE, BOTTOM OF LOWER PLENUM - TOP OF UPPER PLENUM

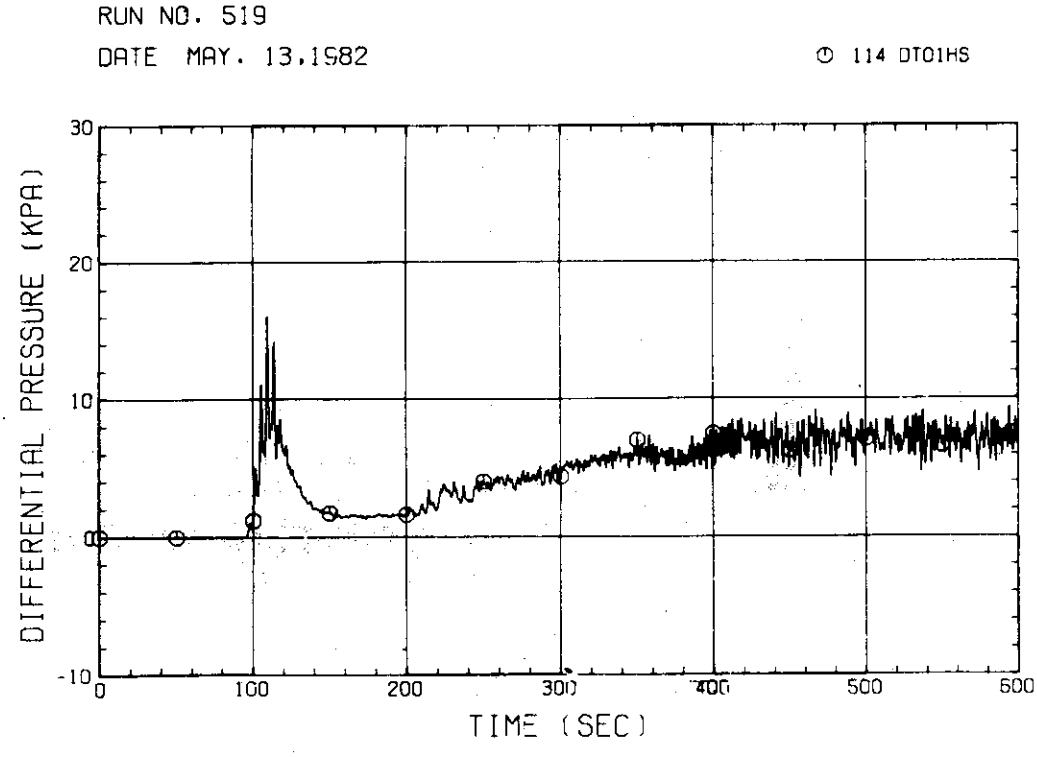

Fig. C-62 DIFFERENTIAL PRESSURE OF HOT LEG, HOT LEG INLET - STEAM/WATER SEPARATOR INLET

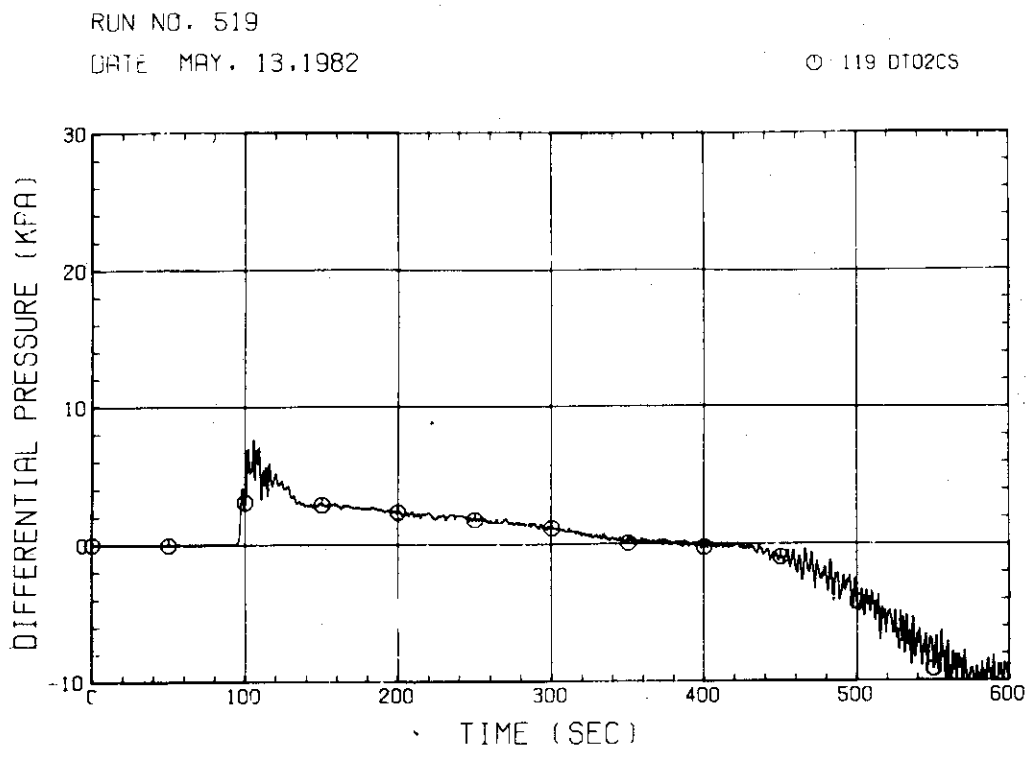

Fig. C-63 DIFFERENTIAL PRESSURE OF INTACT COLD LEG

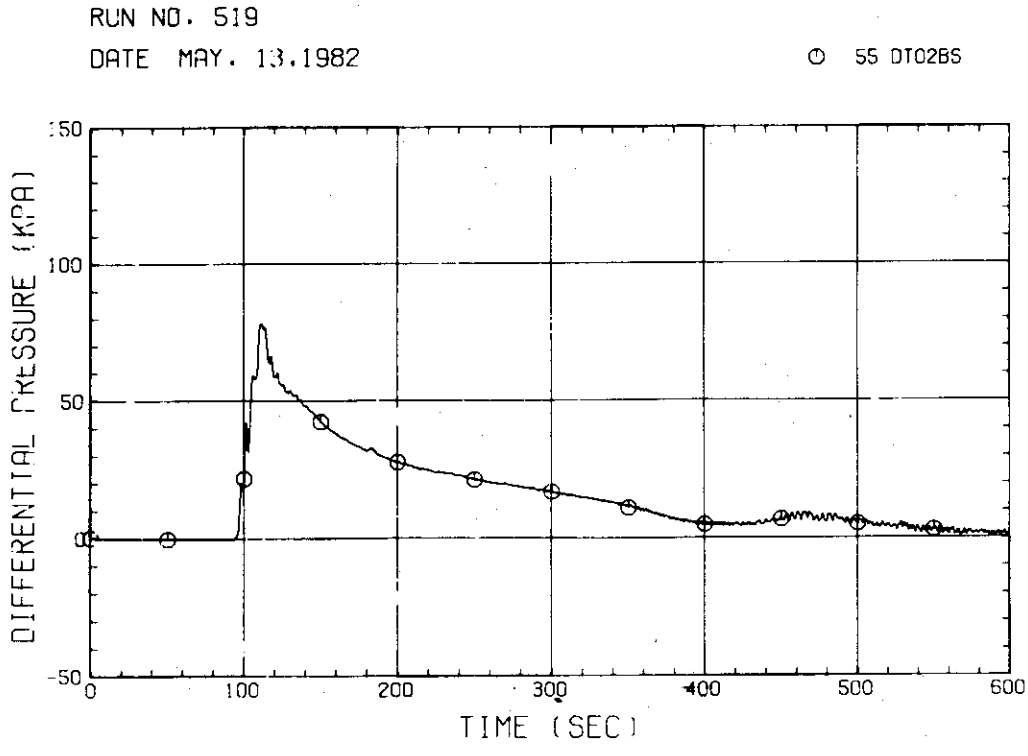

Fig. C-64 DIFFERENTIAL PRESSURE, STEAM/WATER SEPARATOR - CONTAINMENT TANK-II

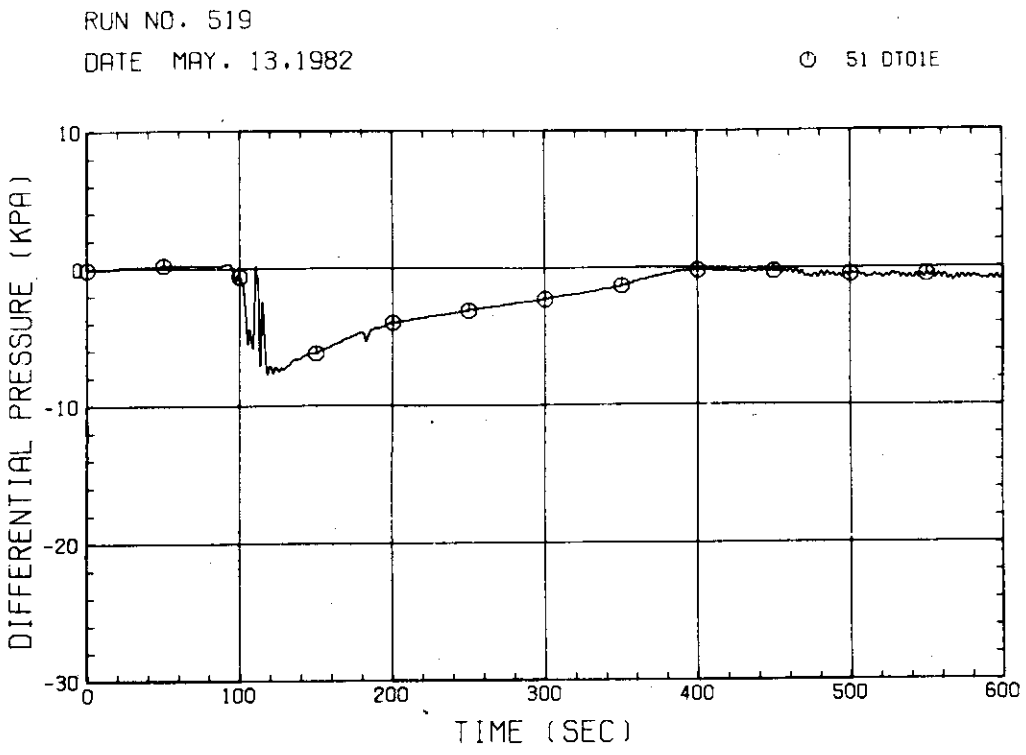

Fig. C-65 DIFFERENTIAL PRESSURE, CONTAINMENT TANK-II - CONTAINMENT TANK-I

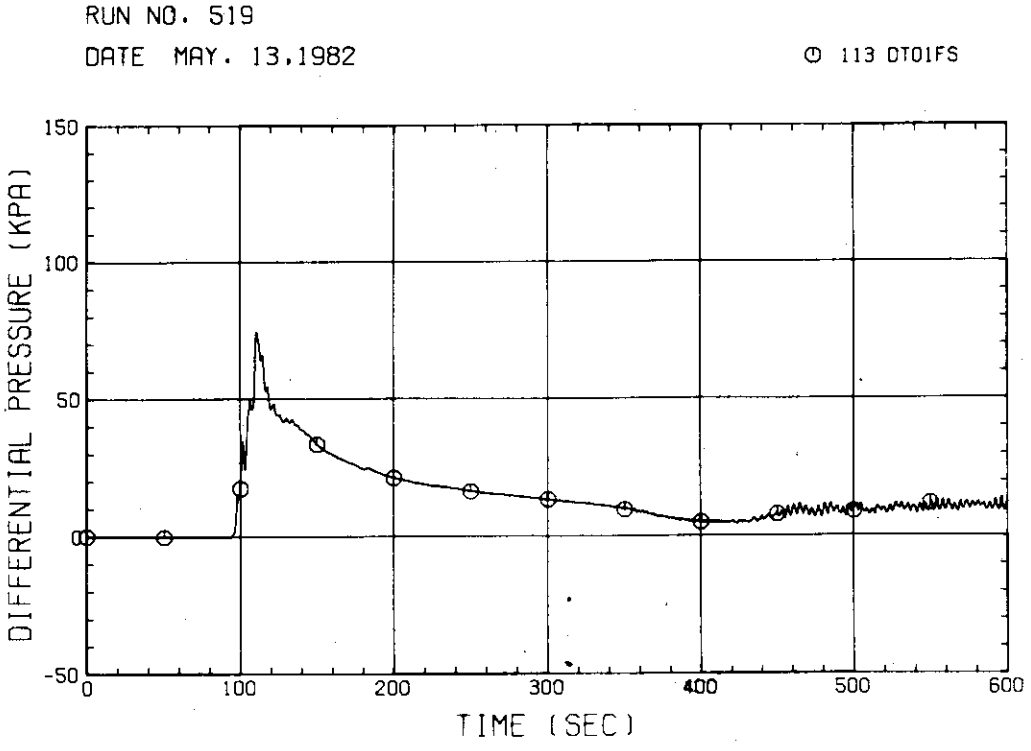

Fig. C-66 DIFFERENTIAL PRESSURE OF BROKEN COLD LEG - PV SIDE, DOWNCOMER - CONTAINMENT TANK-I

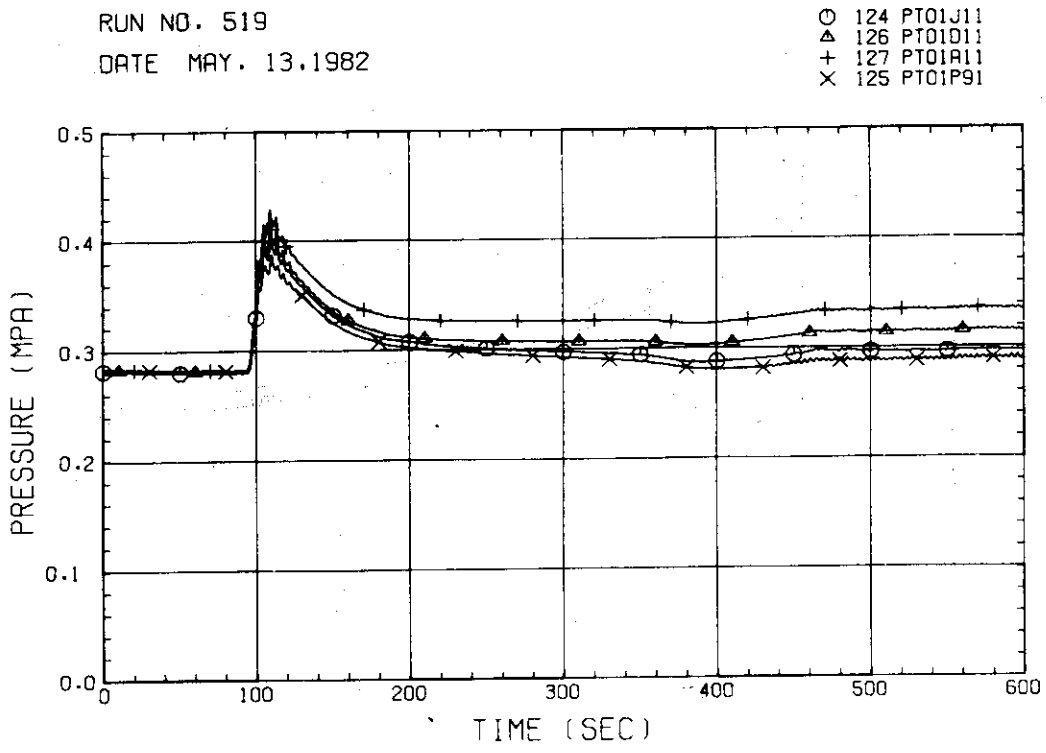

Fig. C-67 PRESSURE IN PV (J - TOP OF PV, D - CORE CENTER, A - CORE INLET, P - BELOW COLD LEG NOZZLE IN DOWNCOMER)

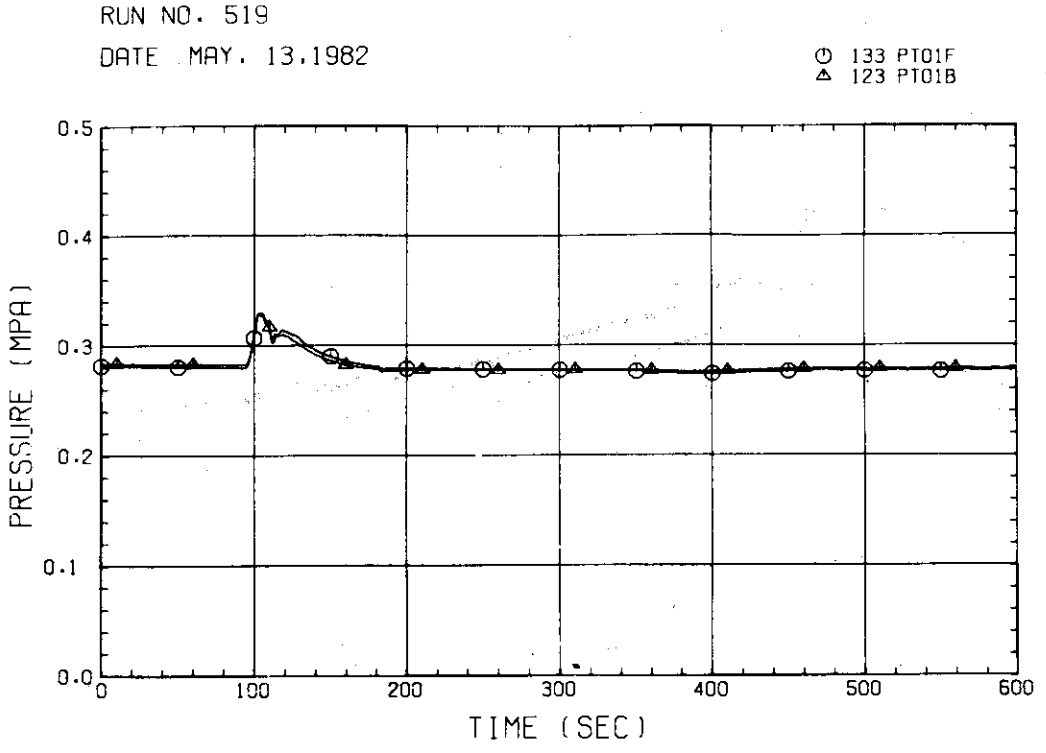

Fig. C-68 PRESSURE AT TOP OF CONTAINMENT TANK-I AND CONTAINMENT TANK-II (F-CONTAINMENT TANK-I, B-CONTAINMENT TANK-II)

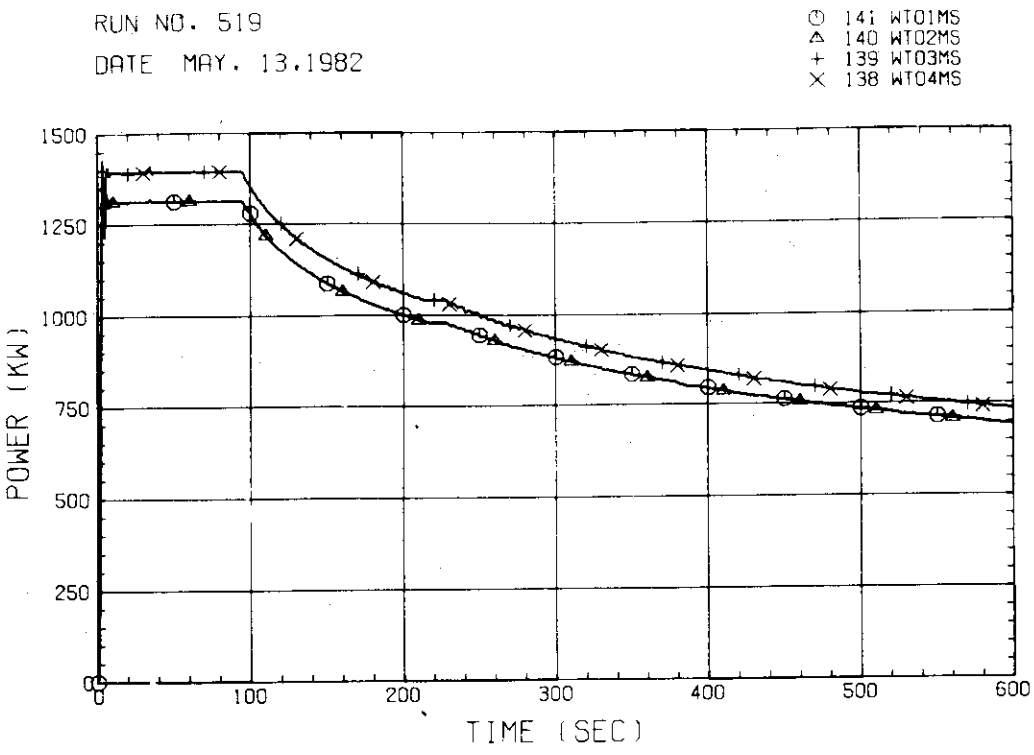

Fig. C-69 BUNDLE POWER (BUNDLE 1.2.3.4)

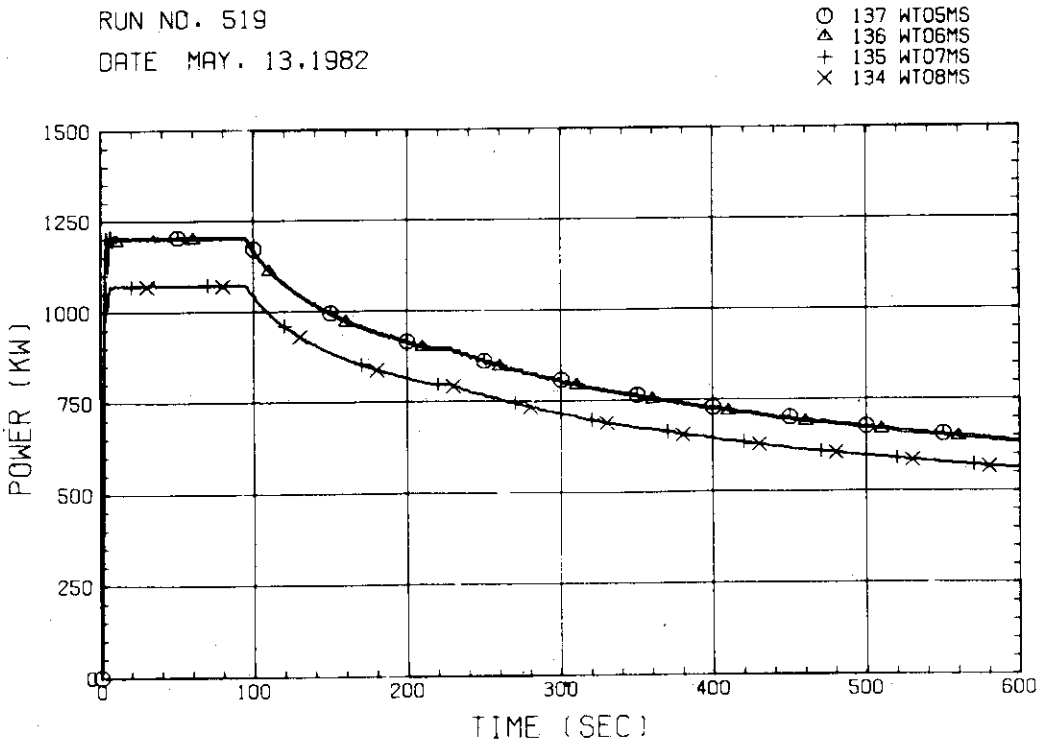

Fig. C-70 BUNDLE POWER (BUNDLE 5.6.7.8)

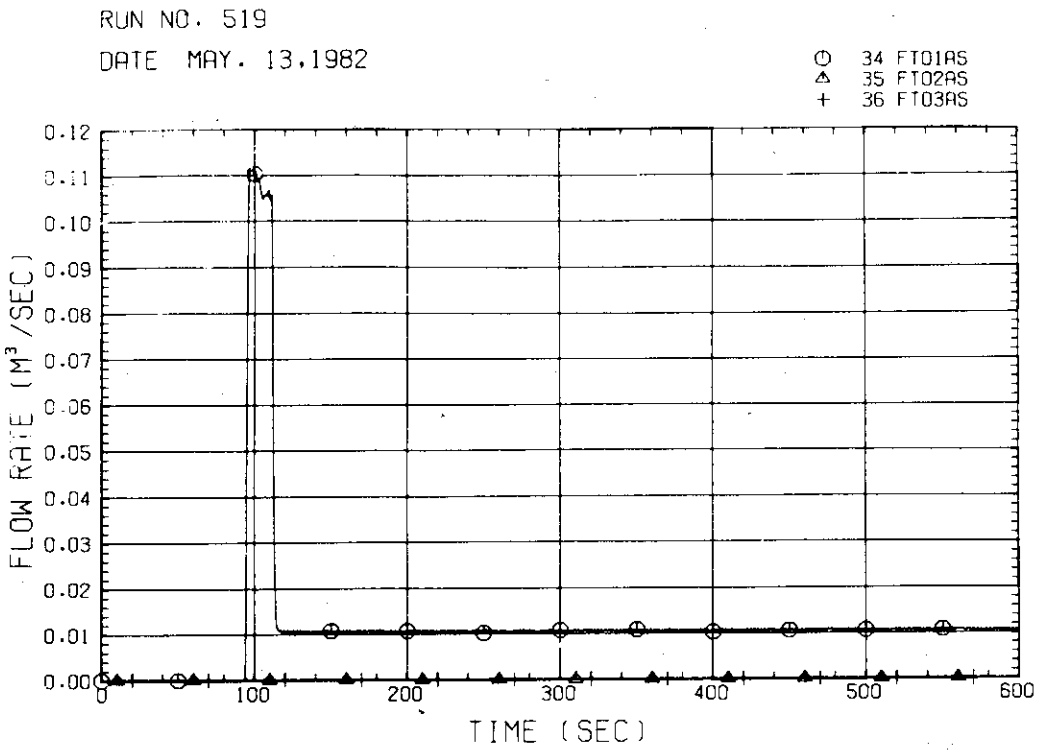

Fig. C-71 FLOW RATE OF ECC WATER (01-DOWNCOMER/LOWER PLENUM/ HOT LEG, 02-INTACT COLD LEG, 03-BROKEN COLD LEG)

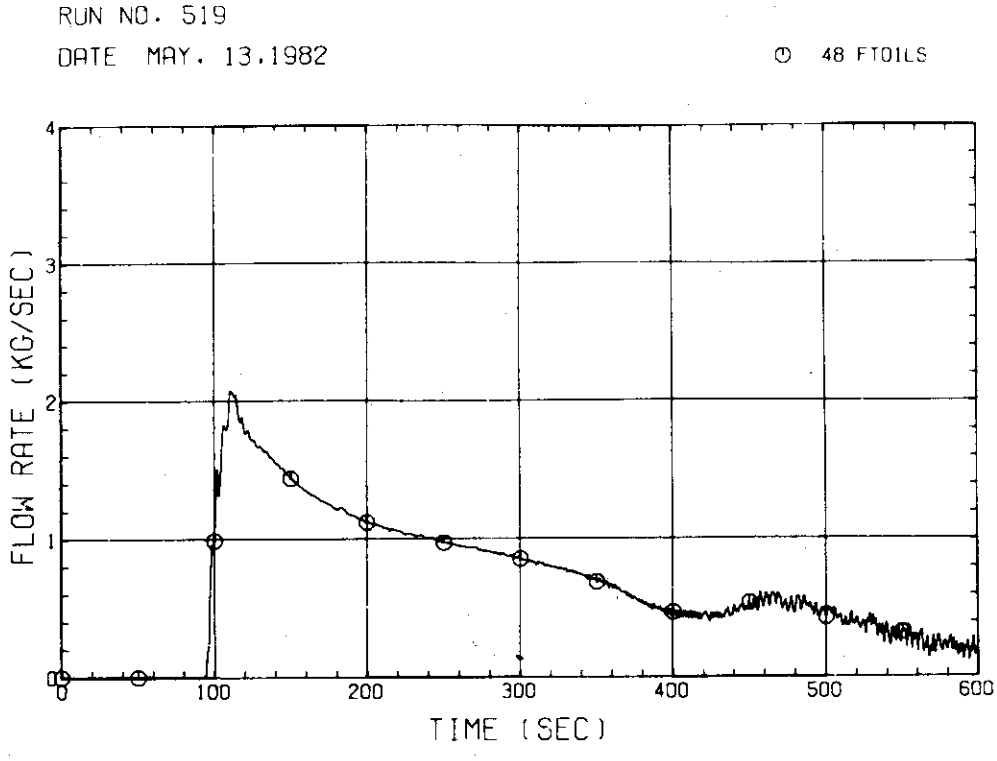

Fig. C-72 MASS FLOW RATE OF BROKEN COLD LEG - STEAM/WATER SEPARATOR SIDE

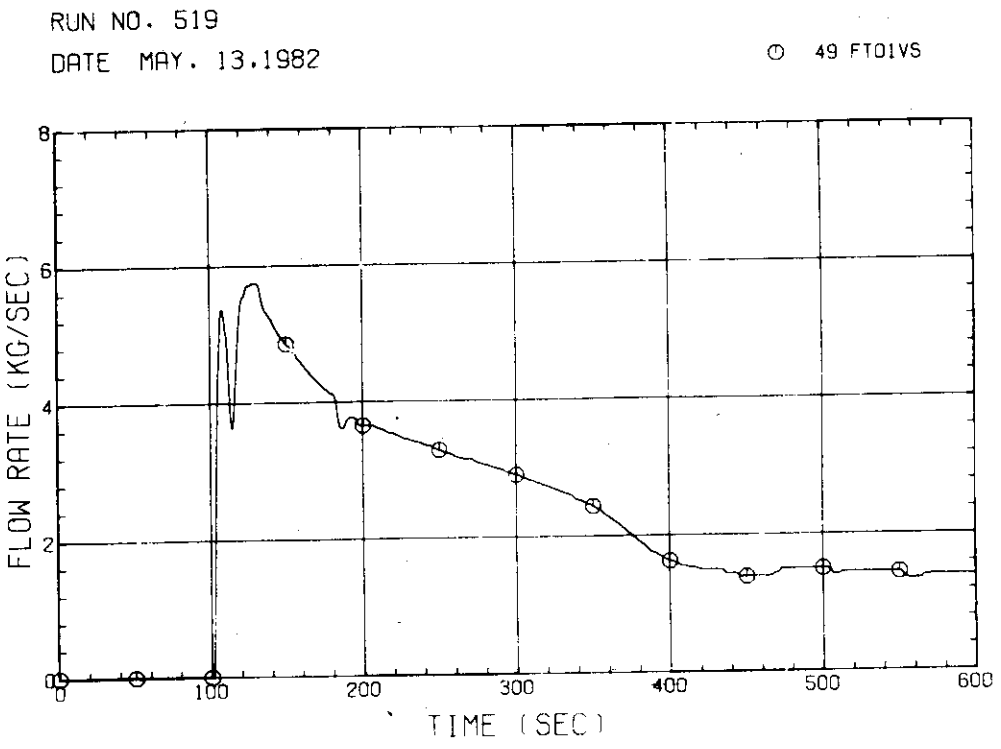

Fig. C-73 STEAM FLOW RATE OF DISCHARGE FROM CONTAINMENT TANK-II

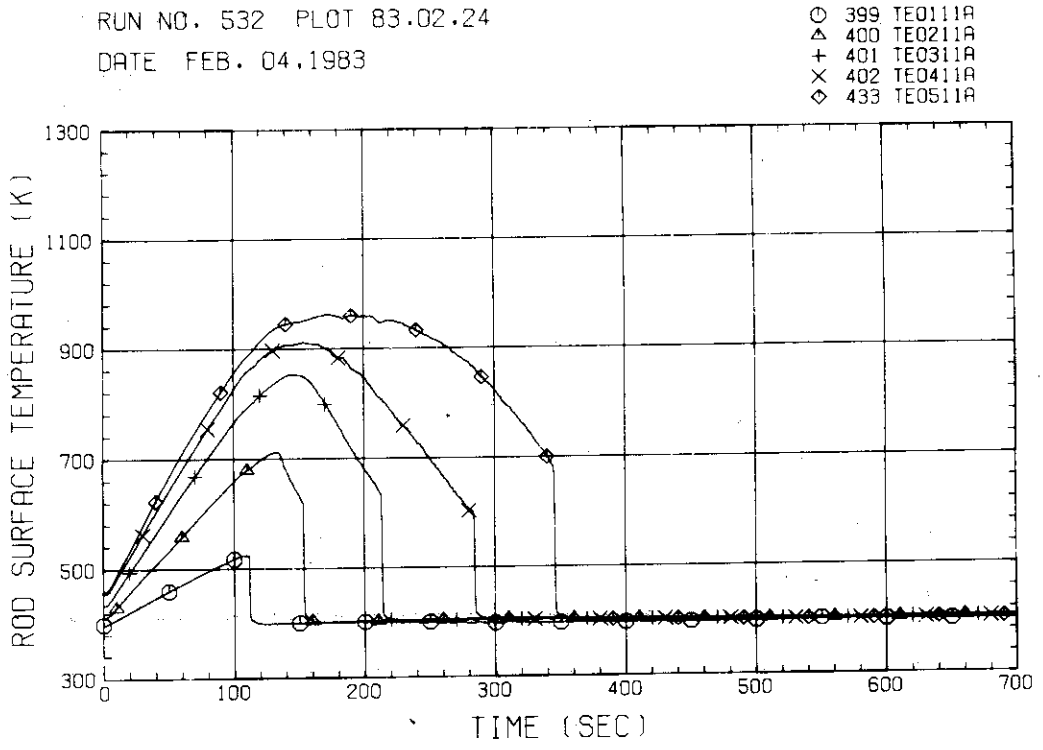

Fig. D-1 HEATER ROD TEMPERATURE (BUNDLE 1-1A, LOWER HALF)

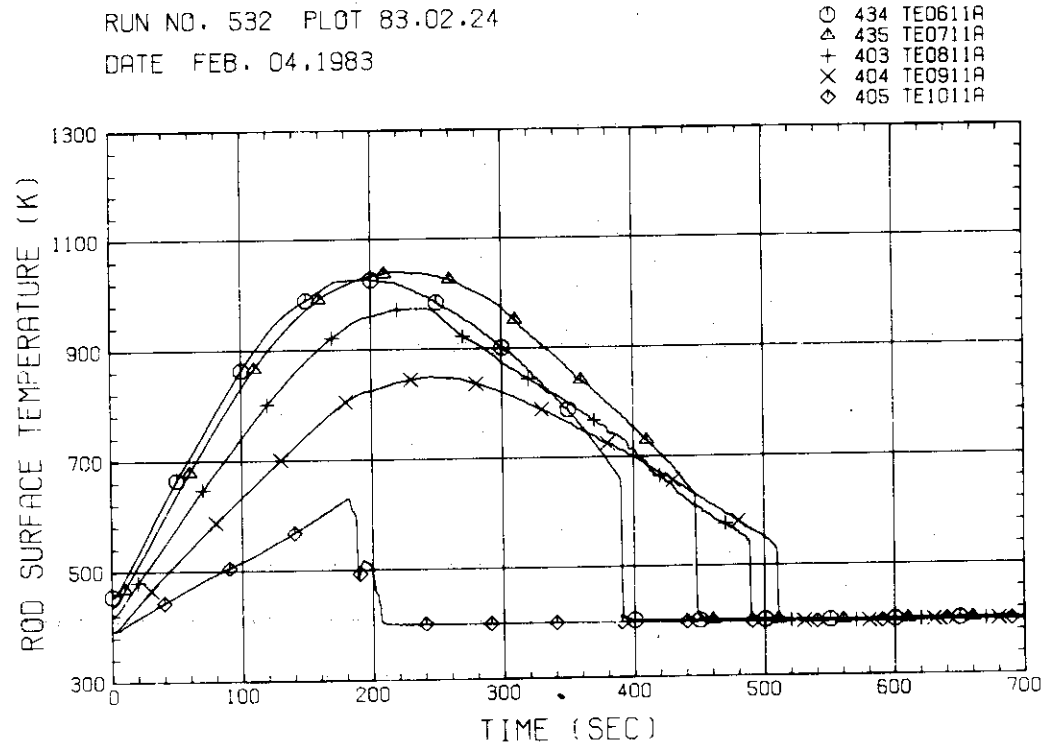

Fig. D-2 HEATER ROD TEMPERATURE (BUNDLE 1-1A, UPPER HALF)

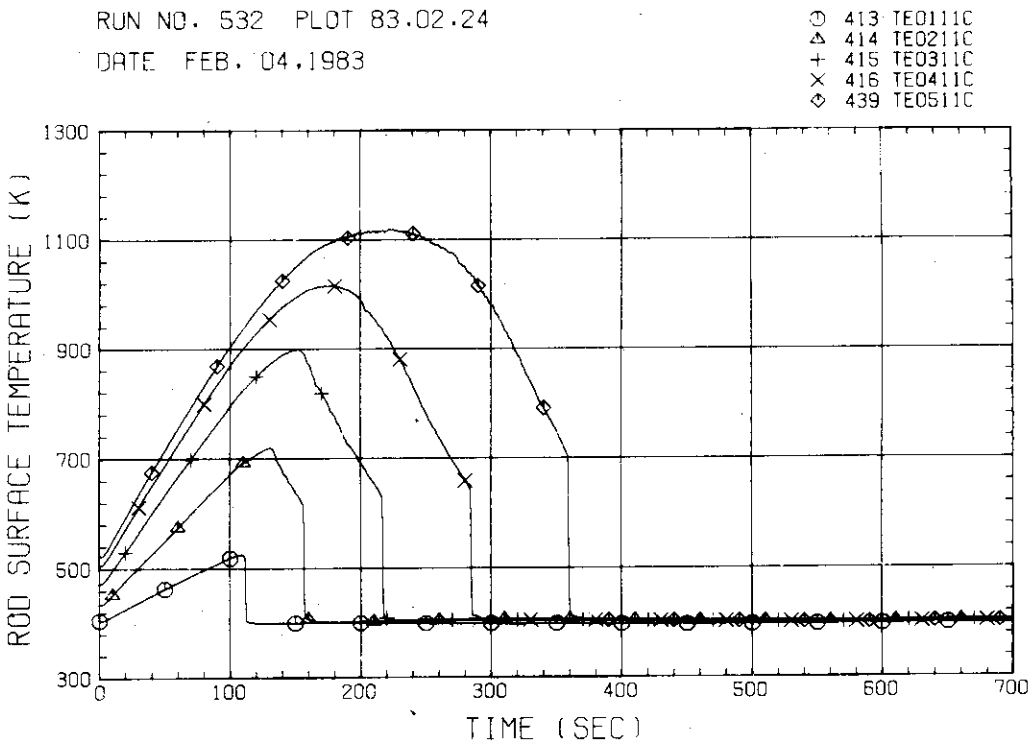

Fig. D-3 HEATER ROD TEMPERATURE (BUNDLE 1-1C, LOWER HALF)

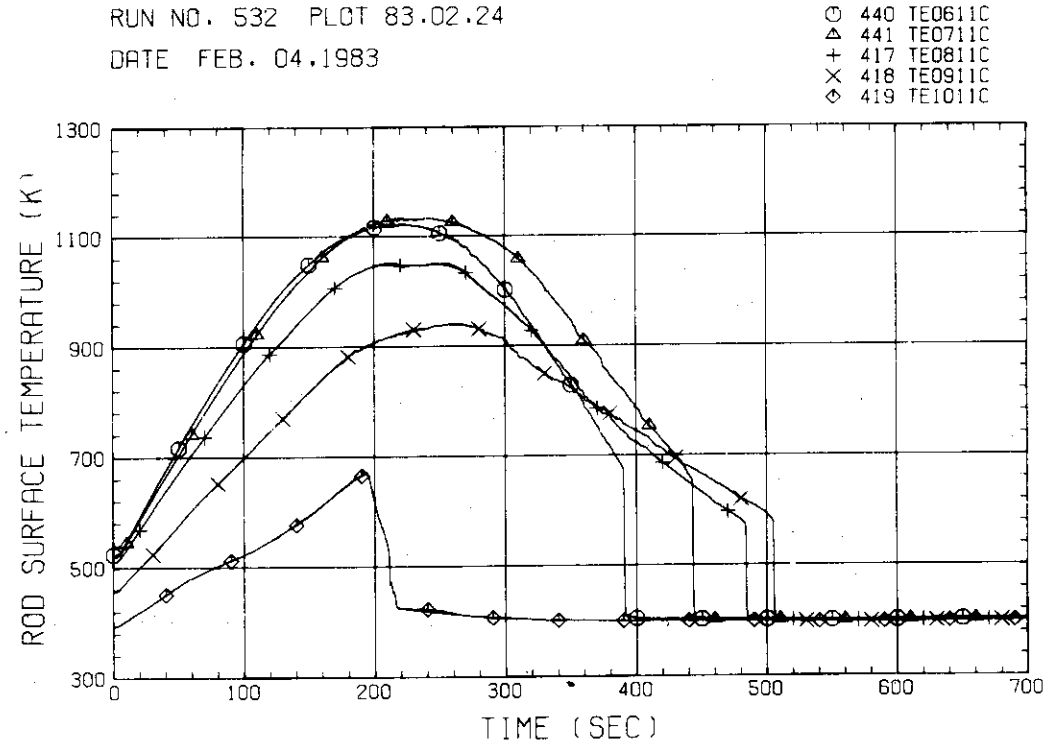

Fig. D-4 HEATER ROD TEMPERATURE (BUNDLE 1-1C, UPPER HALF)

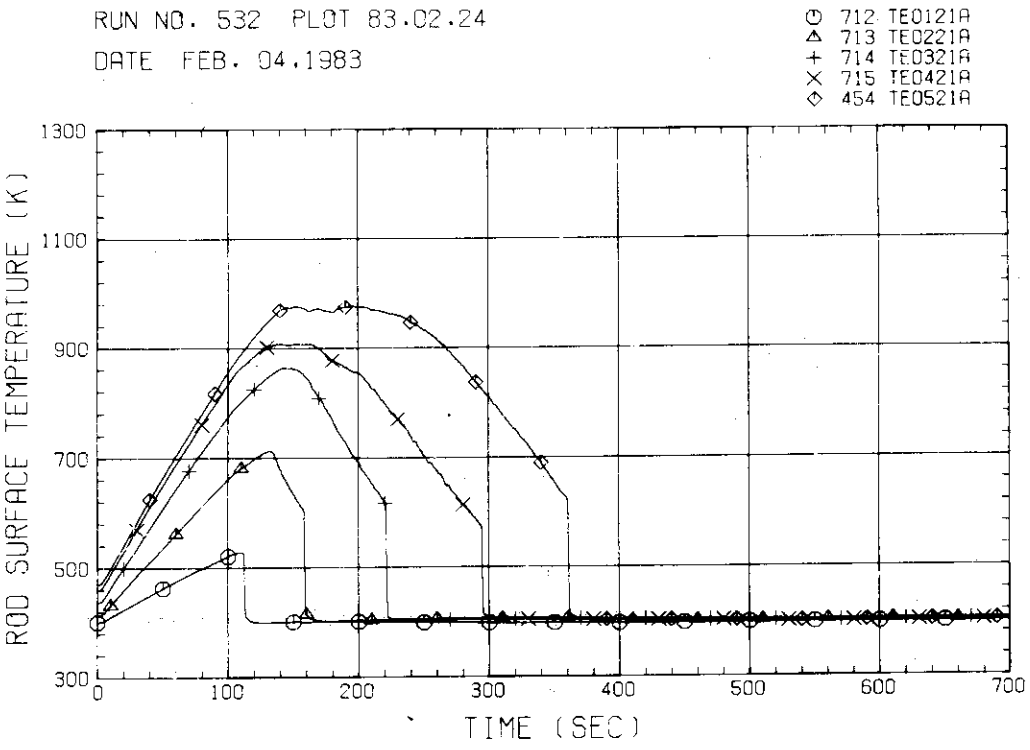

Fig. D-5 HEATER ROD TEMPERATURE (BUNDLE 2-1A, LOWER HALF)

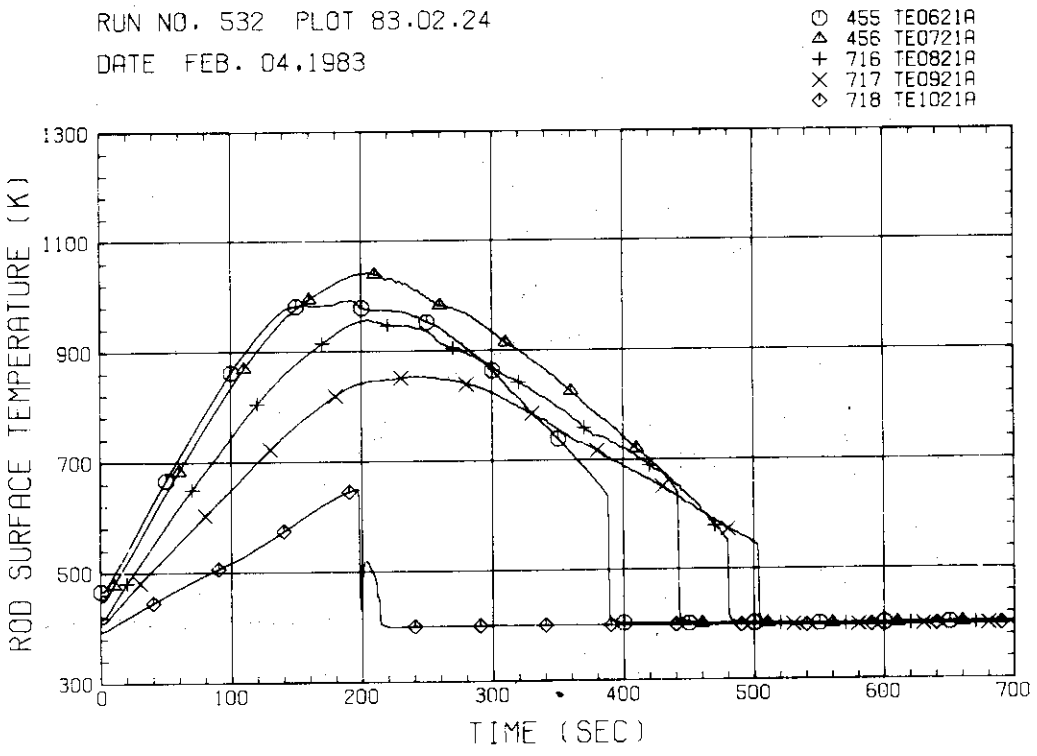

Fig. D-6 HEATER ROD TEMPERATURE (BUNDLE 2-1A, UPPER HALF)

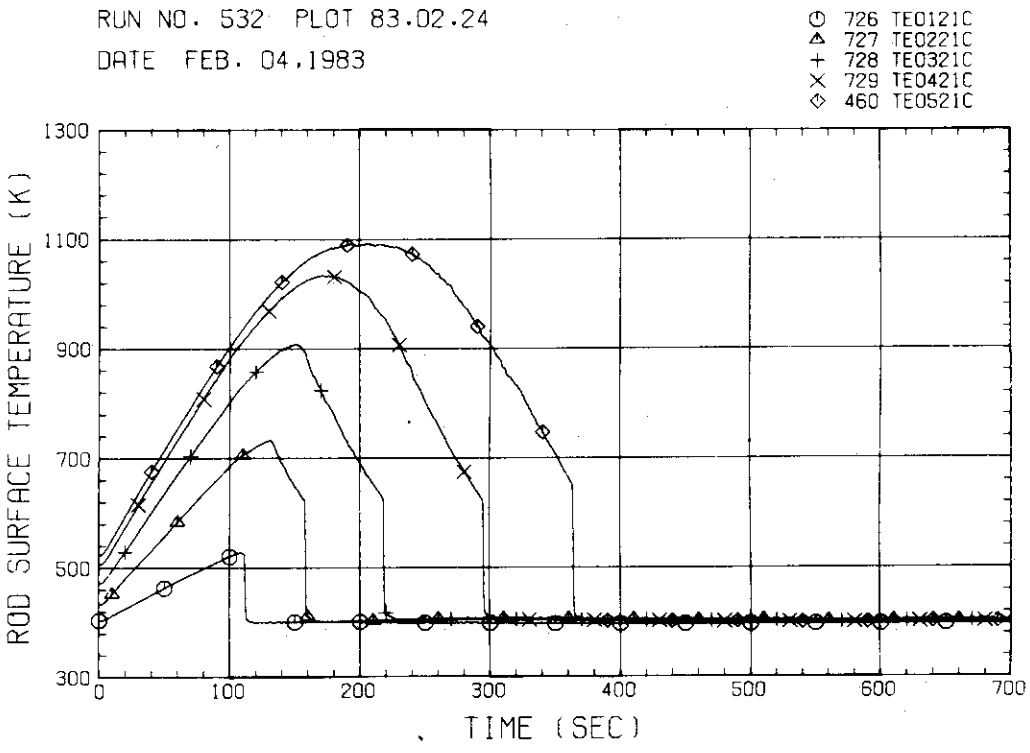

Fig. D-7 HEATER ROD TEMPERATURE (BUNDLE 2-1C, LOWER HALF)

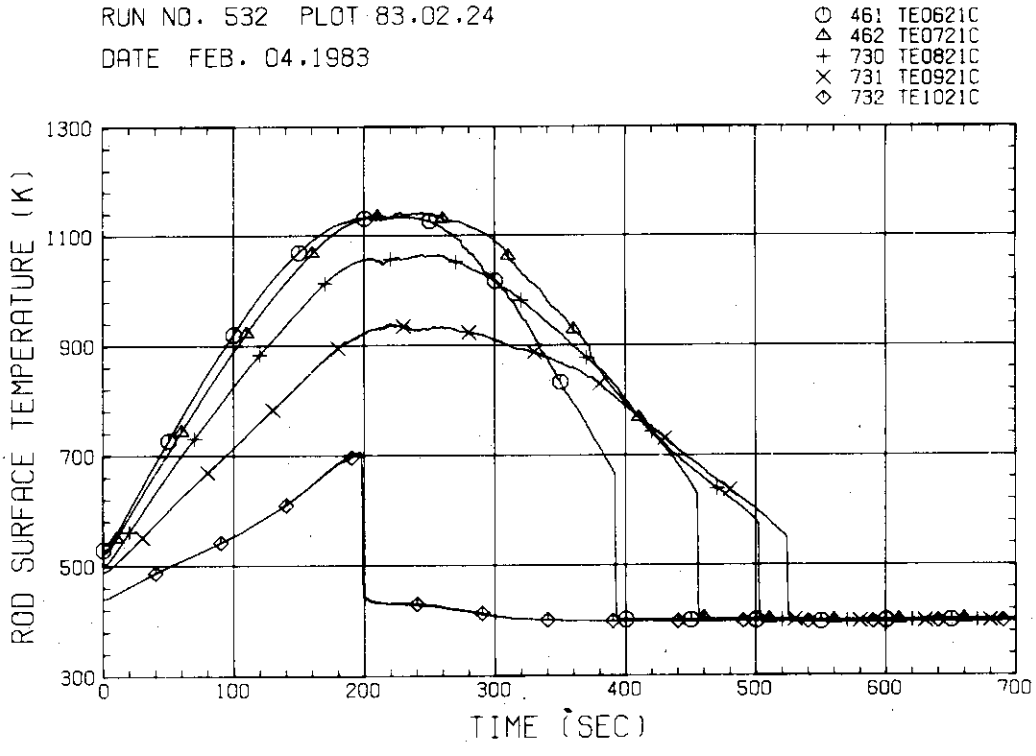

Fig. D-8 HEATER ROD TEMPERATURE (BUNDLE 2-1C, UPPER HALF)

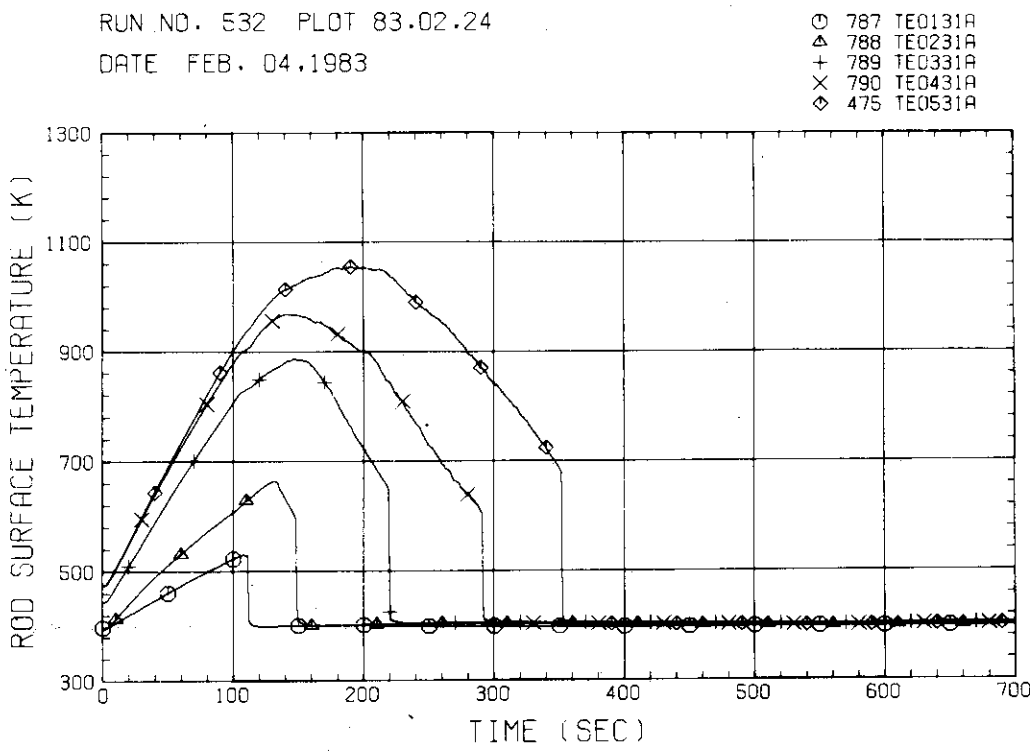

Fig. D-9 HEATER ROD TEMPERATURE (BUNDLE 3-1A, LOWER HALF)

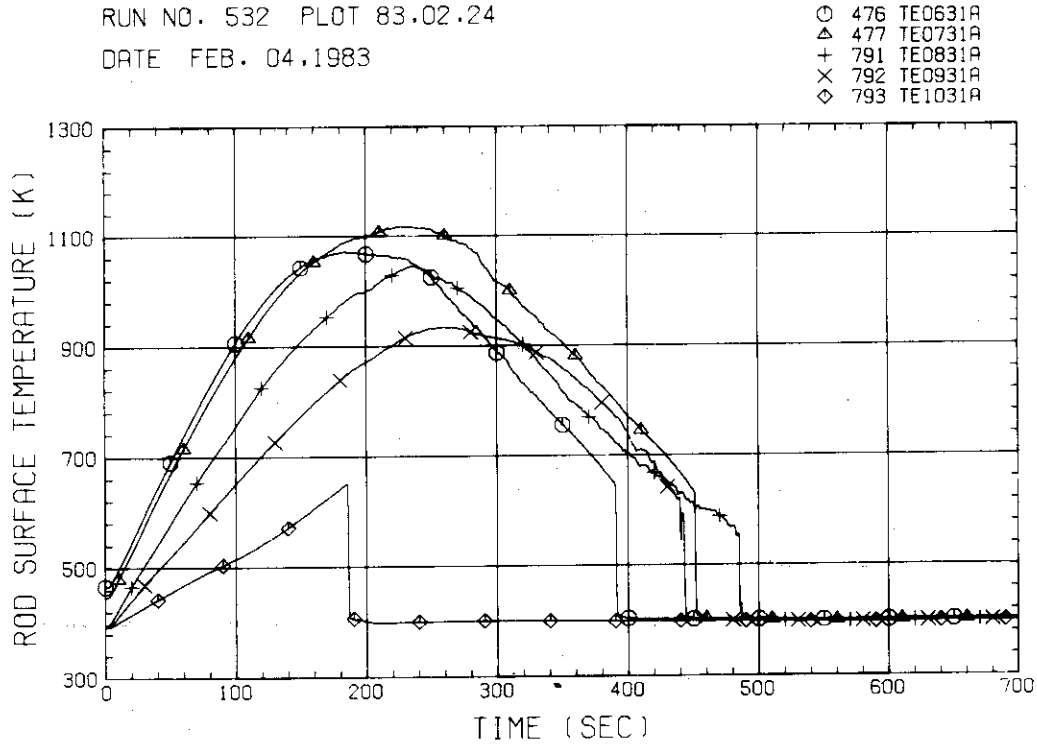

Fig. D-10 HEATER ROD TEMPERATURE (BUNDLE 3-1A, UPPER HALF)

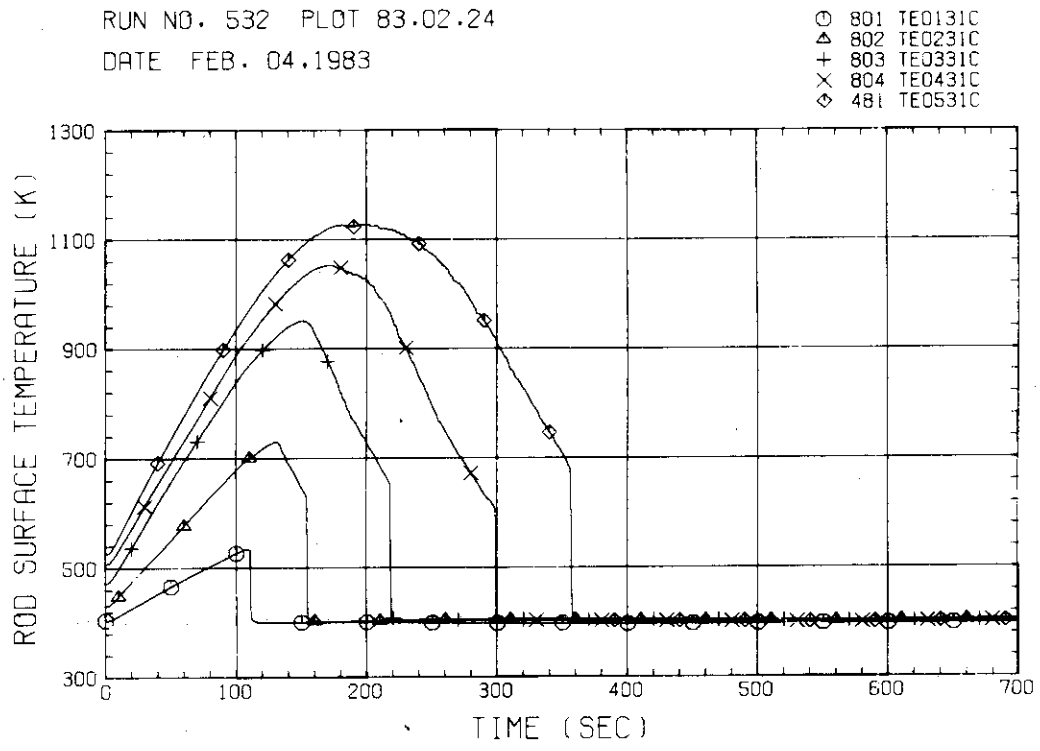

Fig. D-11 HEATER ROD TEMPERATURE (BUNDLE 3-1C, LOWER HALF)

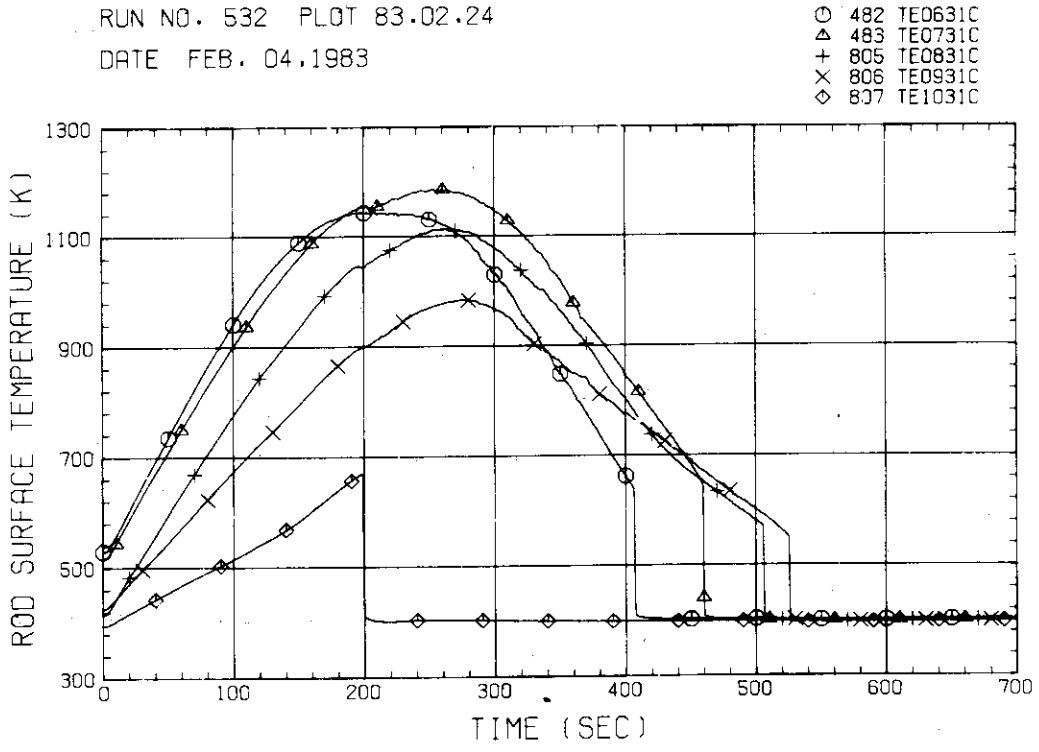

Fig. D-12 HEATER ROD TEMPERATURE (BUNDLE 3-1C, UPPER HALF)

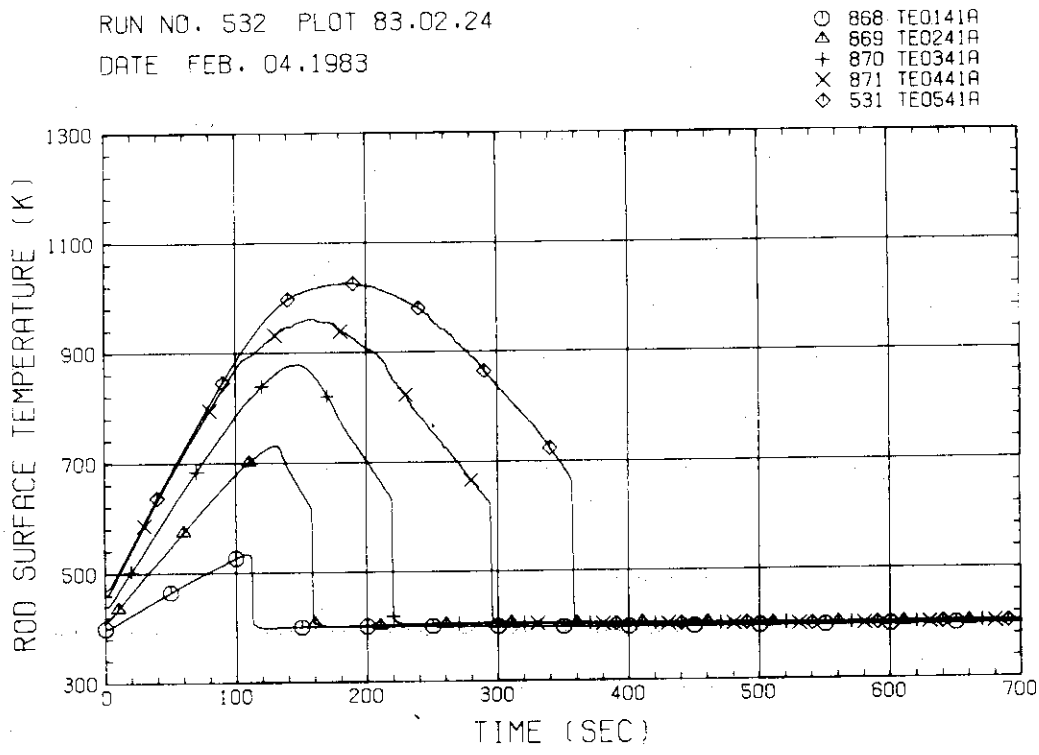

Fig. D-13 HEATER ROD TEMPERATURE (BUNDLE 4-1A, LOWER HALF)

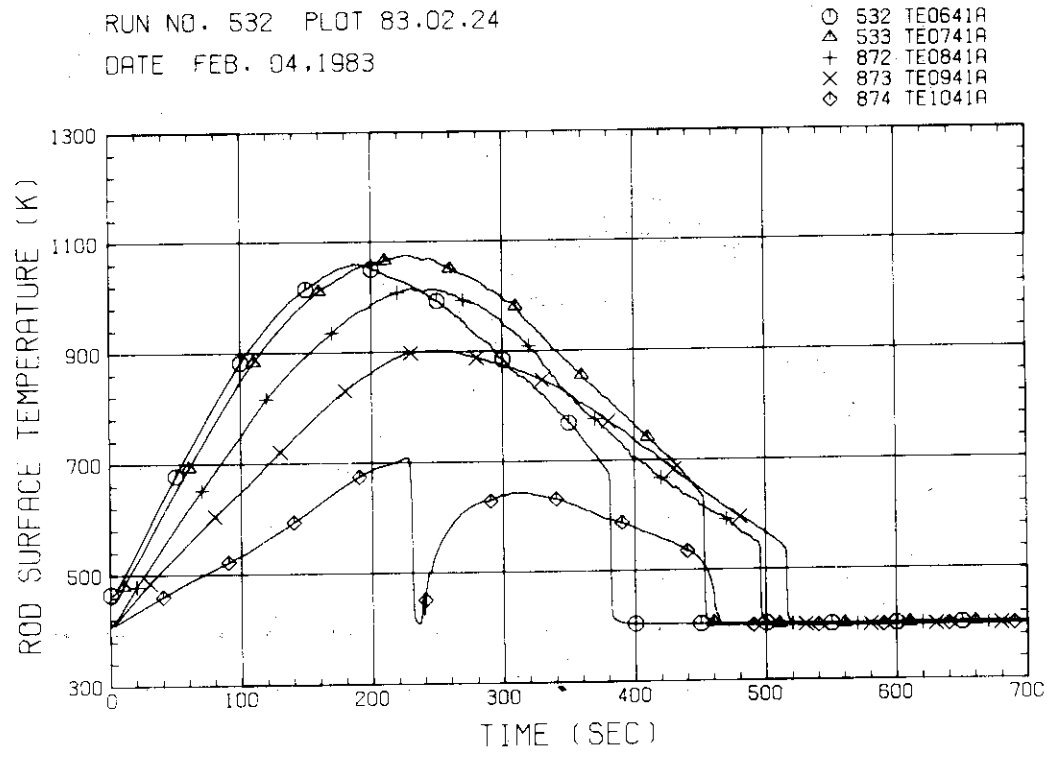

Fig. D-14 HEATER ROD TEMPERATURE (BUNDLE 4-1A, UPPER HALF)

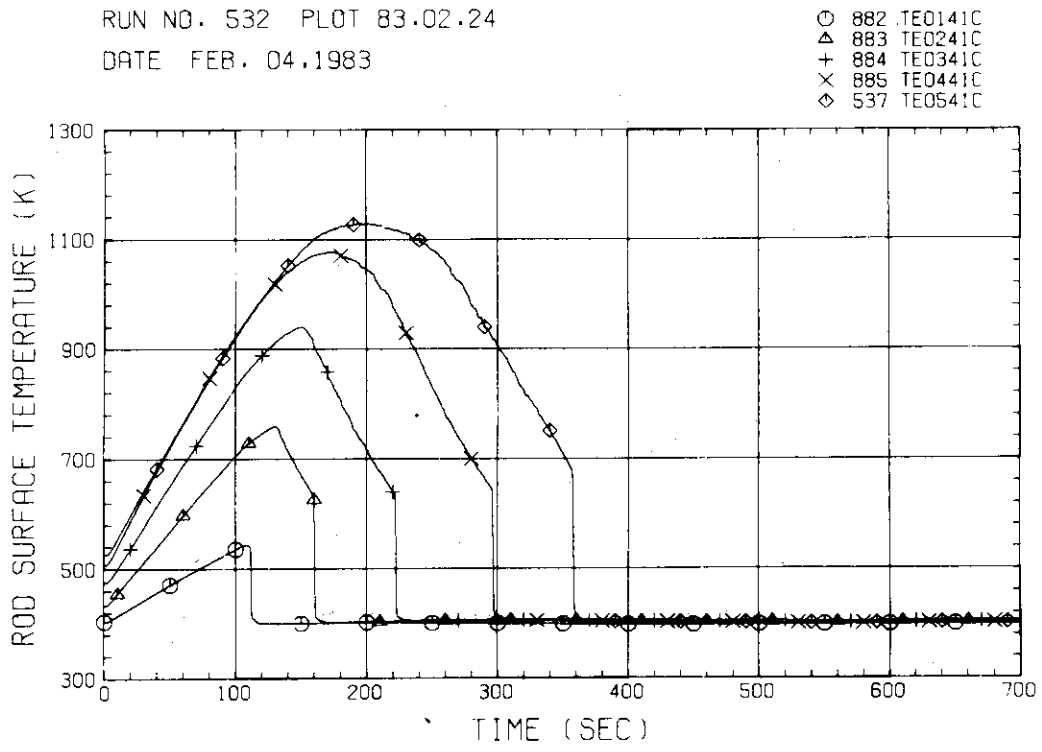

Fig. D-15 HEATER ROD TEMPERATURE (BUNDLE 4-1C, LOWER HALF)

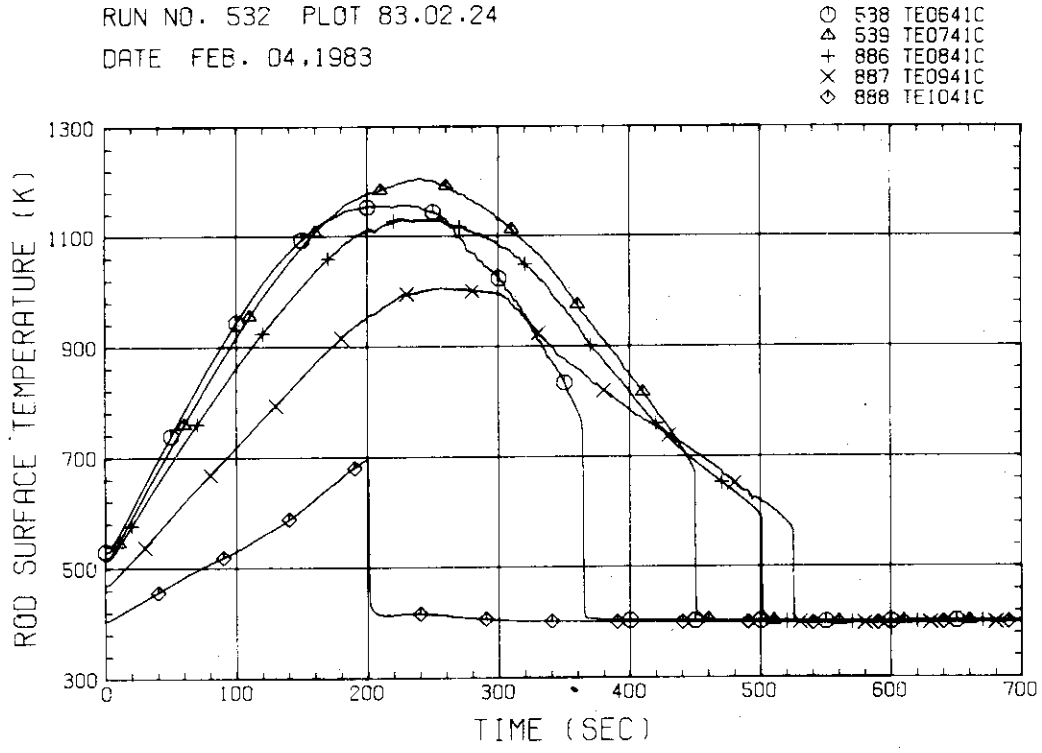

Fig. D-16 HEATER ROD TEMPERATURE (BUNDLE 4-1C, UPPER HALF)

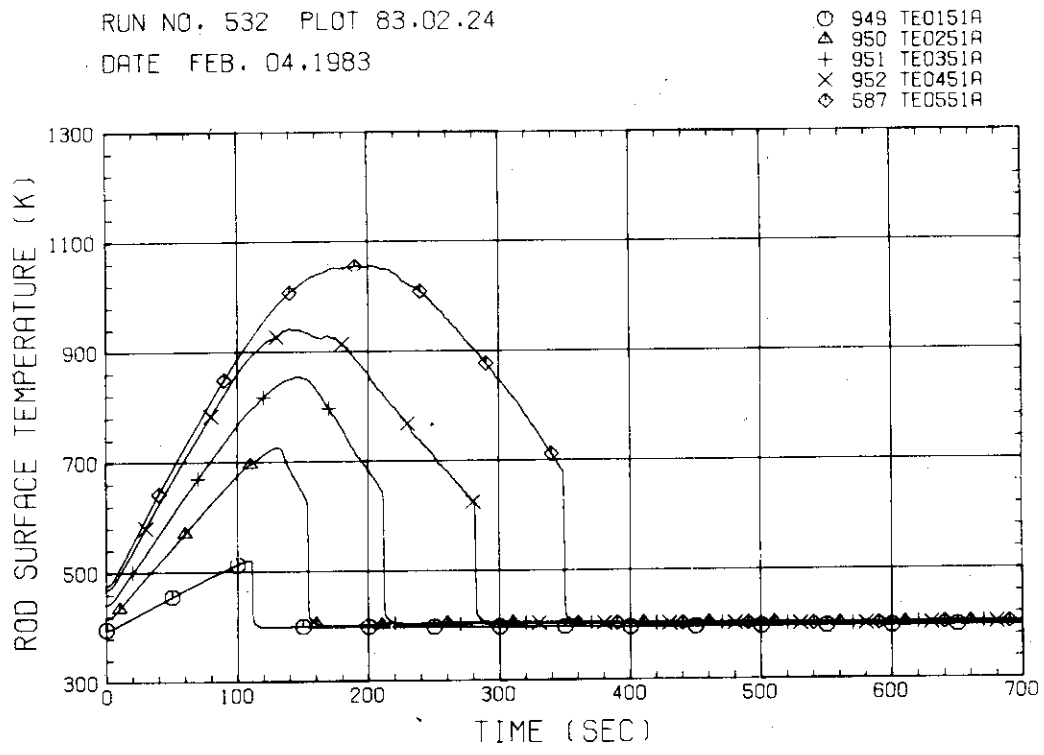

Fig. D-17 HEATER ROD TEMPERATURE (BUNDLE 5-1A, LOWER HALF)

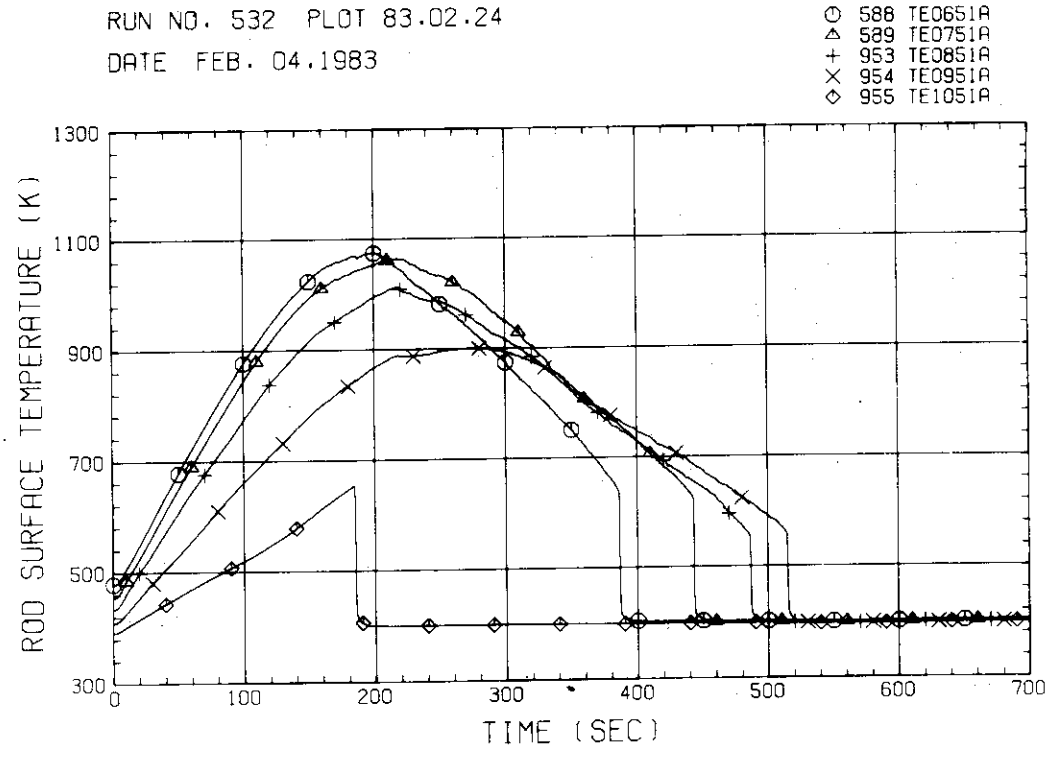

Fig. D-18 HEATER ROD TEMPERATURE (BUNDLE 5-1A, UPPER HALF)

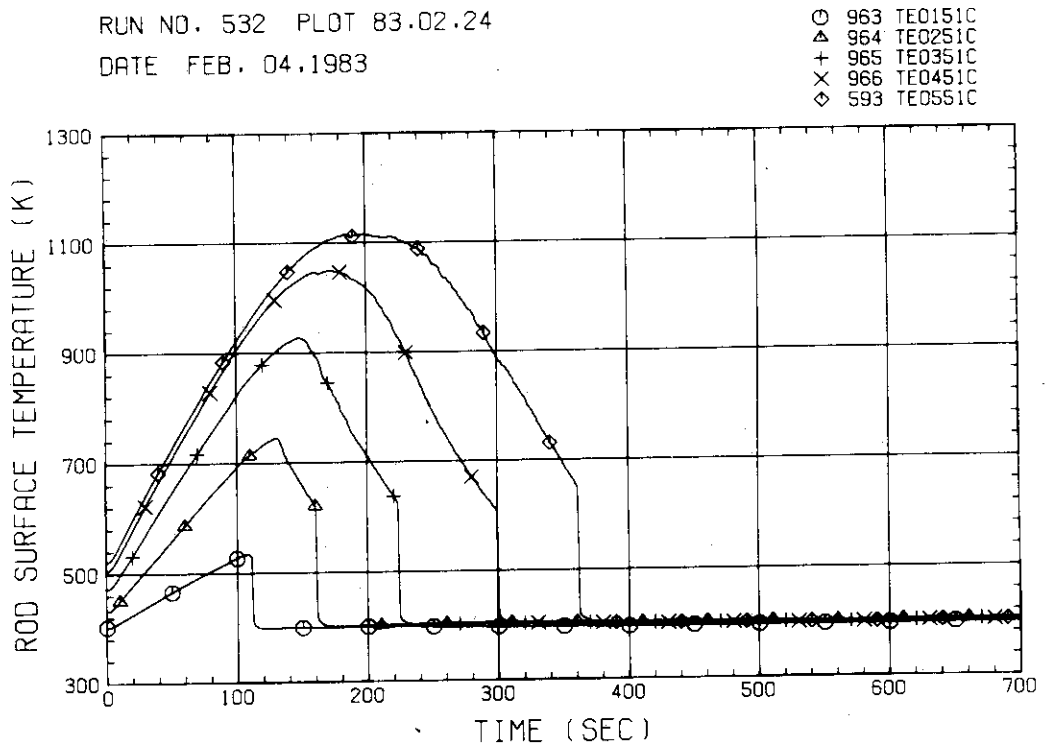

Fig. D-19 HEATER ROD TEMPERATURE (BUNDLE 5-1C, LOWER HALF)

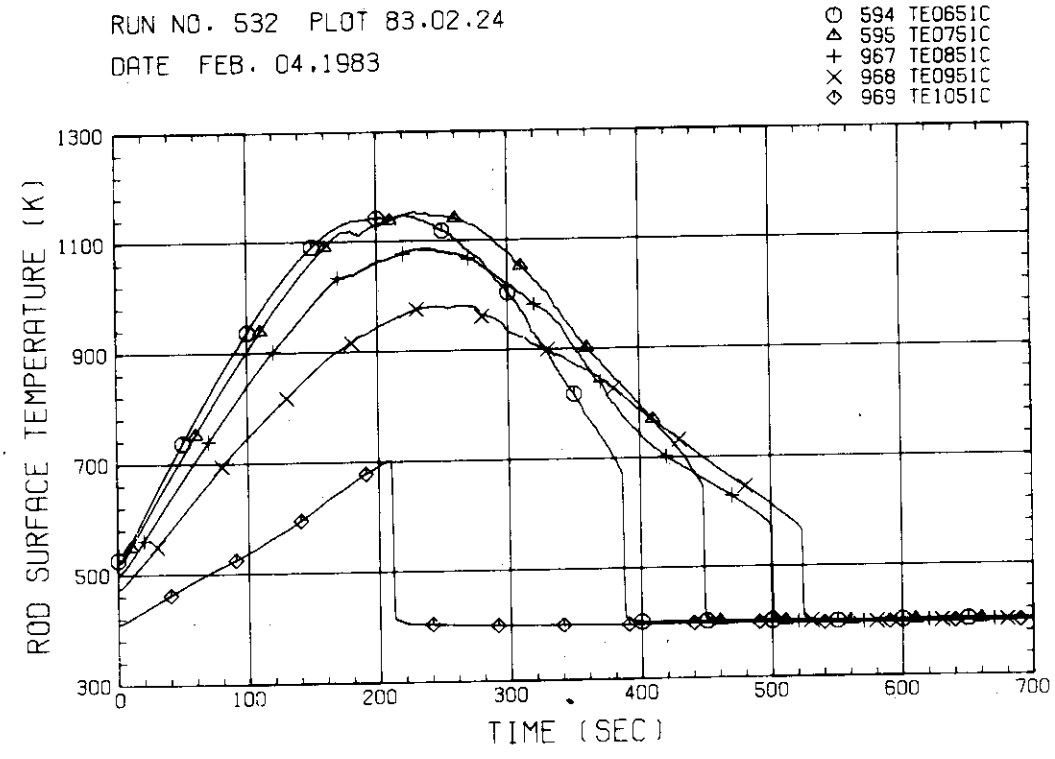

Fig. D-20 HEATER ROD TEMPERATURE (BUNDLE 5-1C, UPPER HALF)

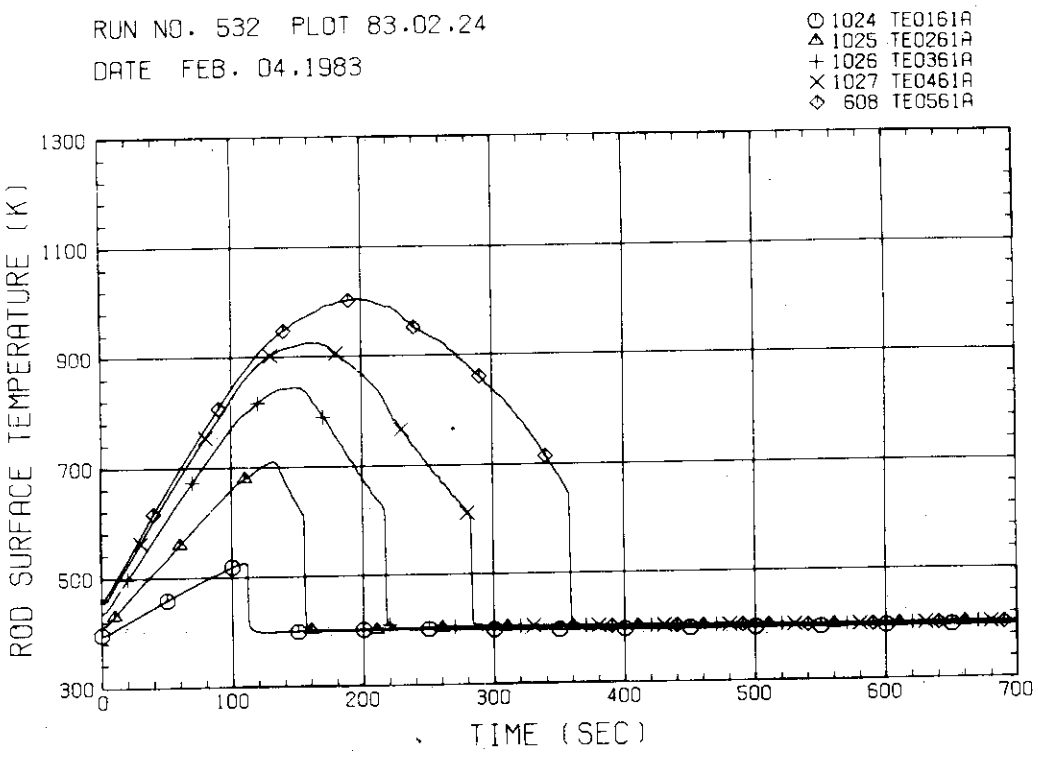

Fig. D-21 HEATER ROD TEMPERATURE (BUNDLE 6-1A, LOWER HALF)

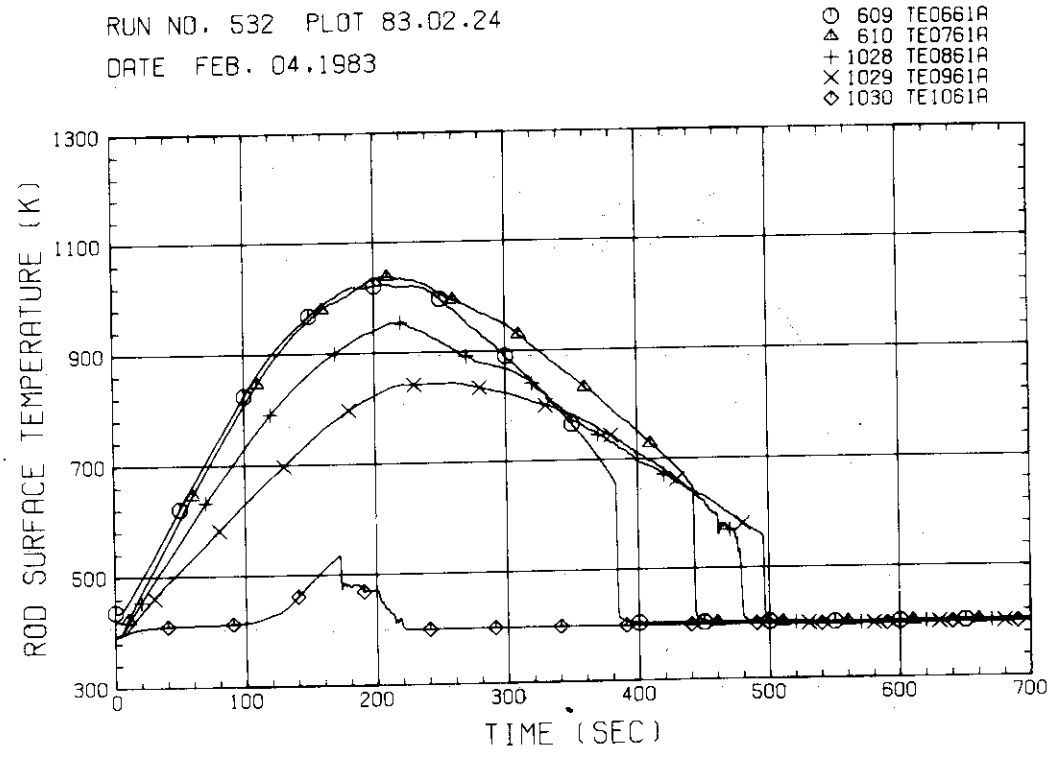

Fig. D-22 HEATER ROD TEMPERATURE (BUNDLE 6-1A, UPPER HALF)

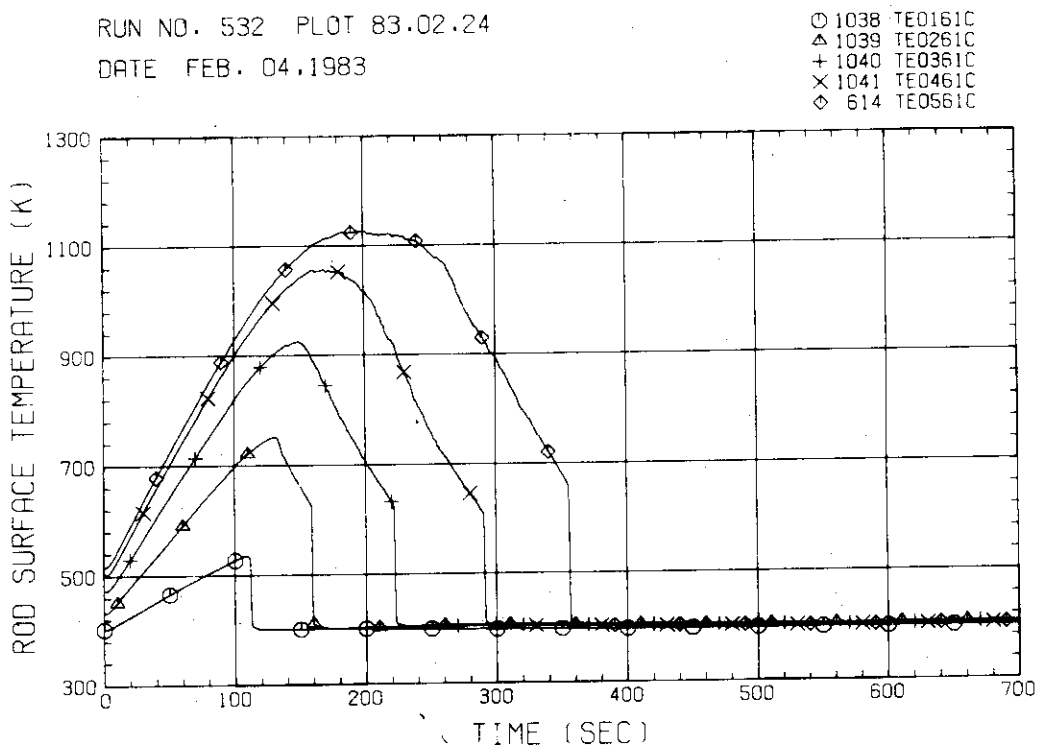

Fig. D-23 HEATER ROD TEMPERATURE (BUNDLE 6-1C, LOWER HALF)

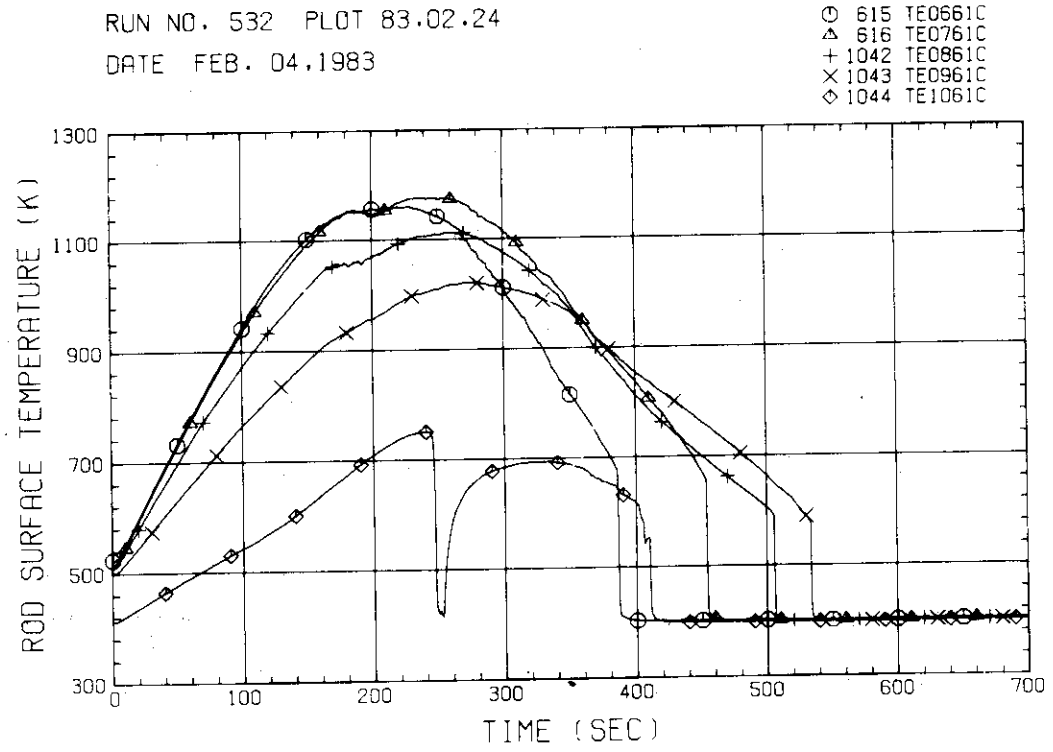

Fig. D-24 HEATER ROD TEMPERATURE (BUNDLE 6-1C, UPPER HALF)

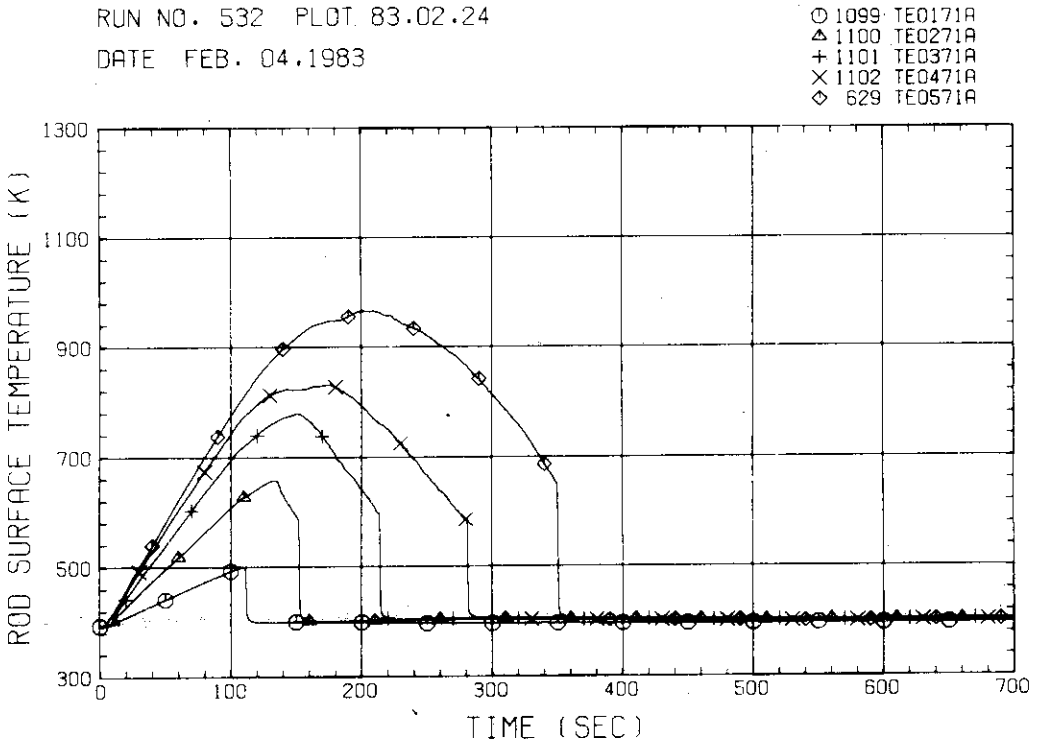

Fig. D-25 HEATER ROD TEMPERATURE (BUNDLE 7-1A, LOWER HALF)

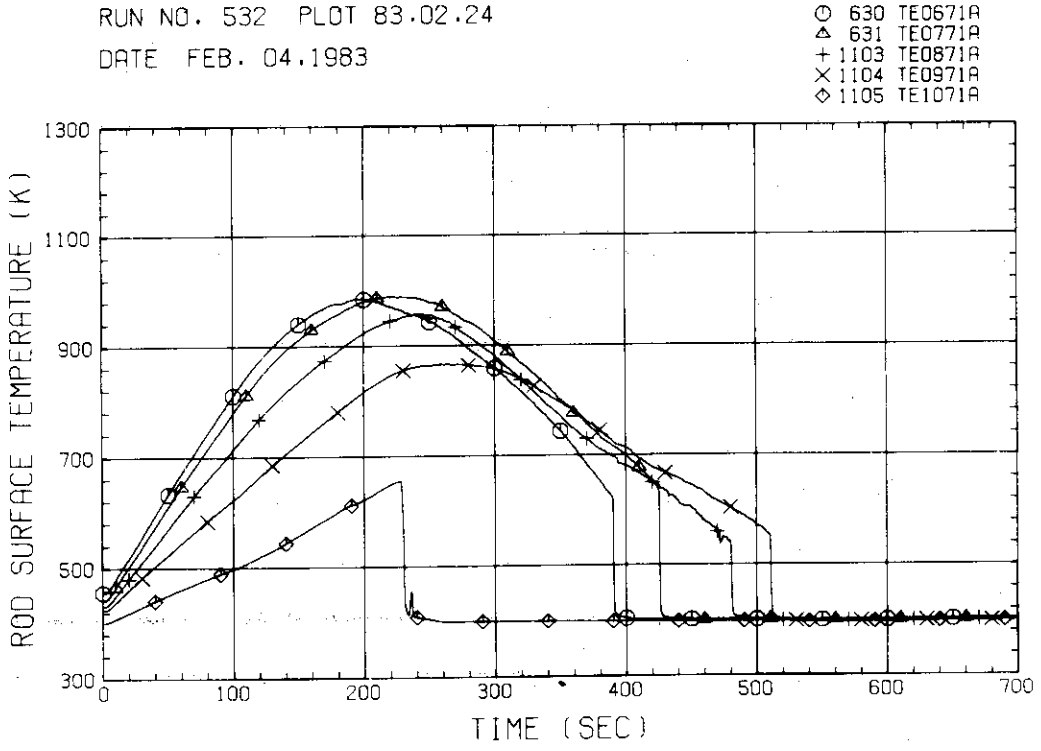

Fig. D-26 HEATER ROD TEMPERATURE (BUNDLE 7-1A, UPPER HALF)

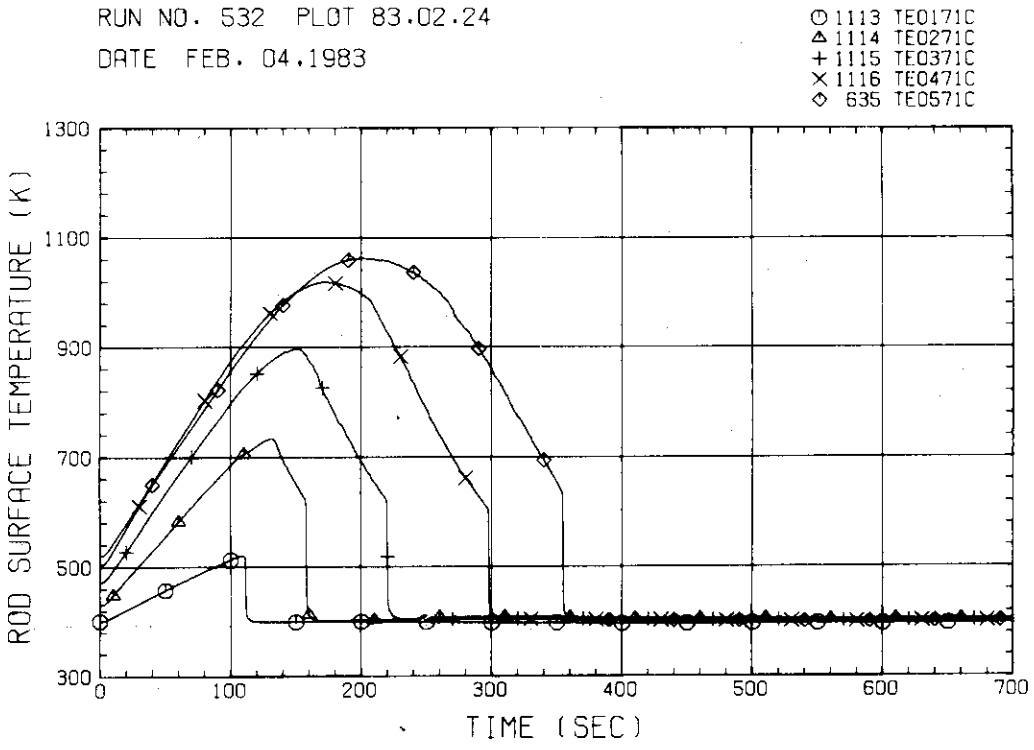

Fig. D-27 HEATER ROD TEMPERATURE (BUNDLE 7-1C, LOWER HALF)

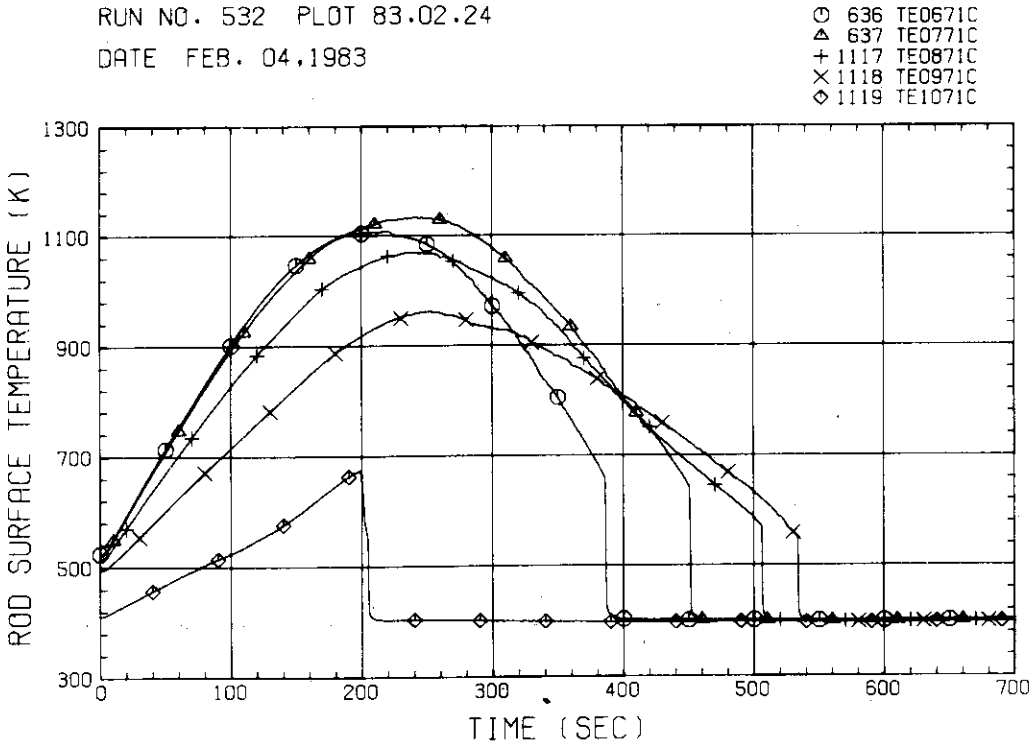

Fig. D-28 HEATER ROD TEMPERATURE (BUNDLE 7-1C, UPPER HALF)

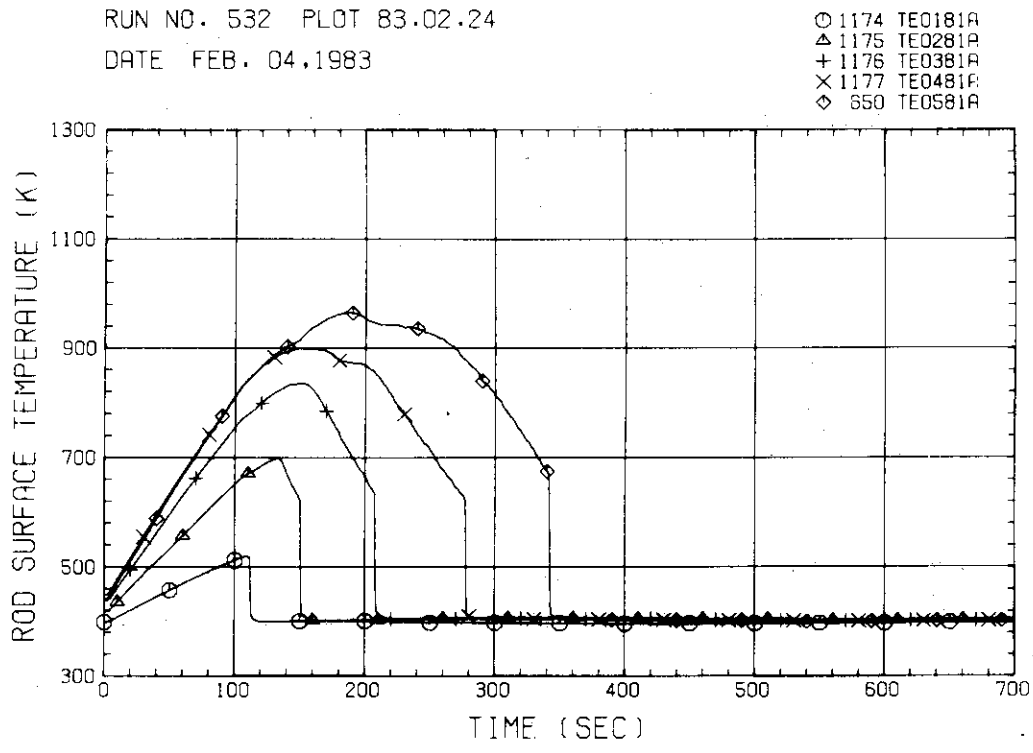

Fig. D-29 HEATER ROD TEMPERATURE (BUNDLE 8-1A, LOWER HALF)

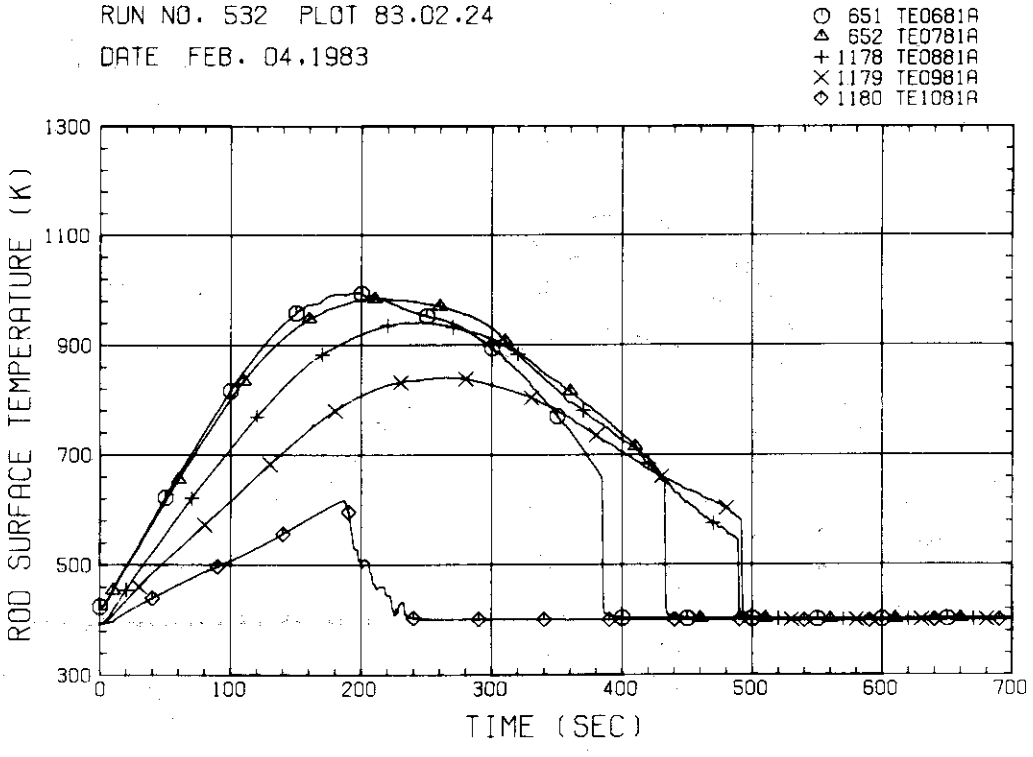

Fig. D-30 HEATER ROD TEMPERATURE (BUNDLE 8-1A, UPPER HALF)

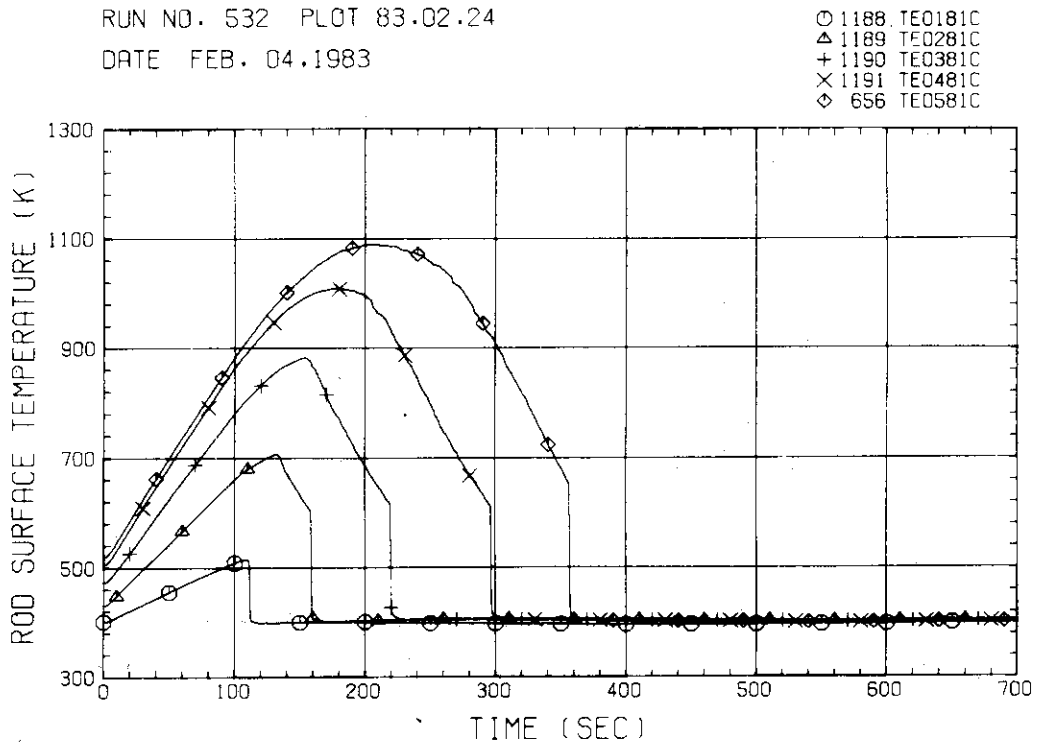

Fig. D-31 HEATER ROD TEMPERATURE (BUNDLE 8-1C, LOWER HALF)

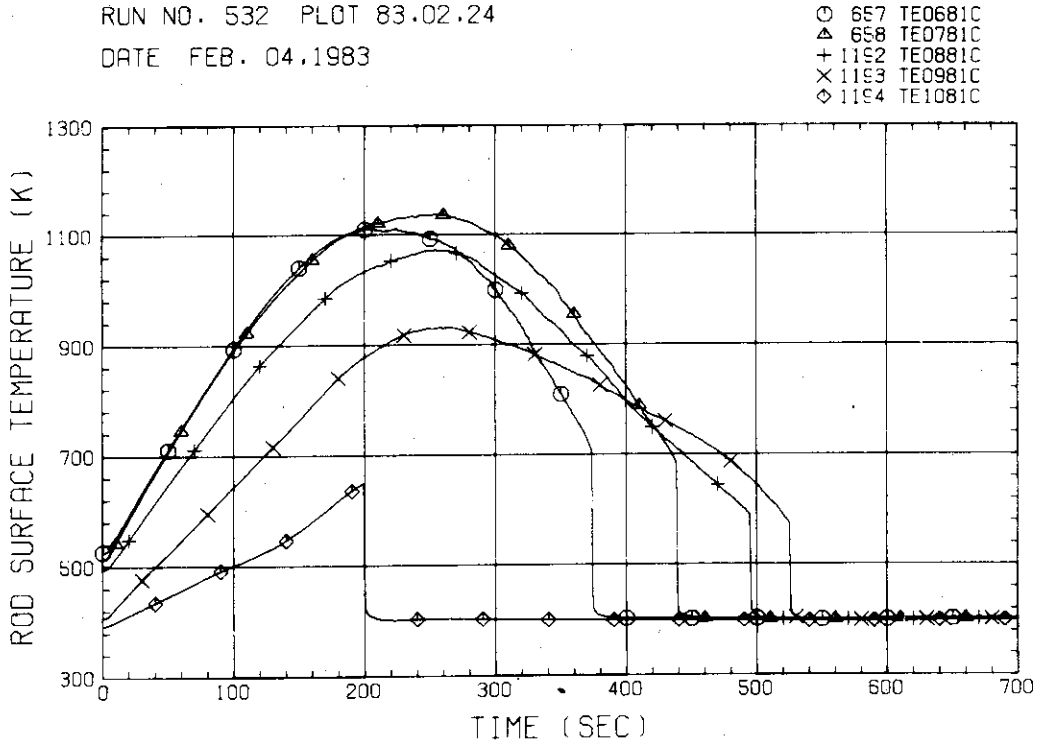

Fig. D-32 HEATER ROD TEMPERATURE (BUNDLE 8-1C, UPPER HALF)

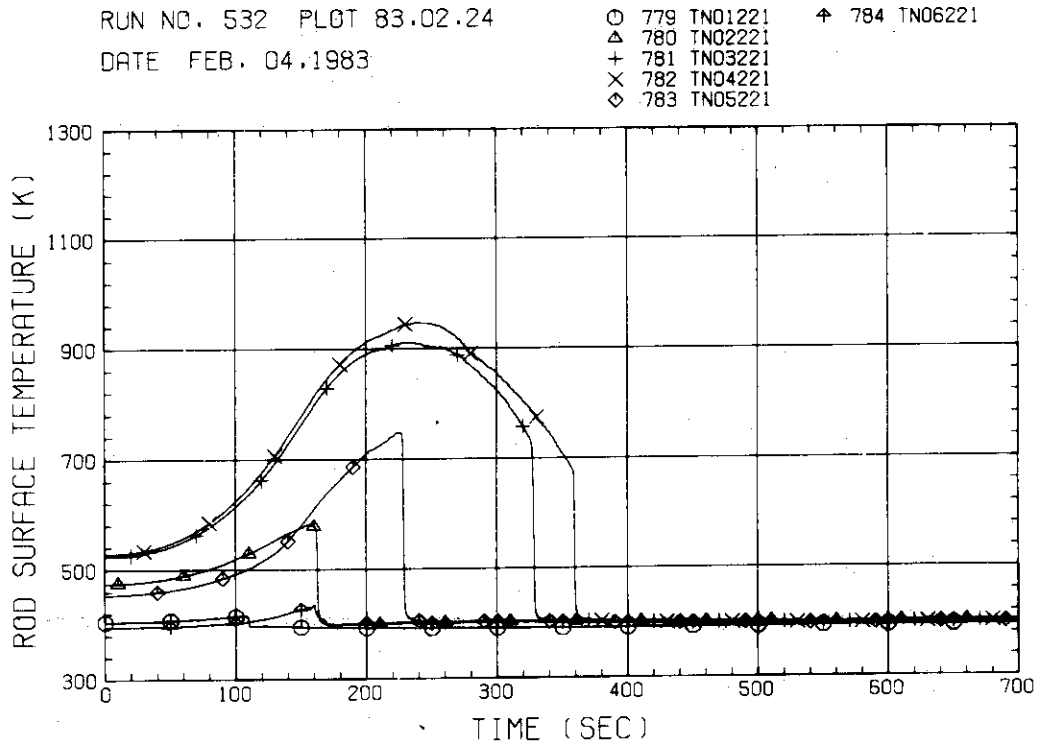

Fig. D-33 NON-HEATED ROD TEMPERATURE (BUNDLE 2-2)

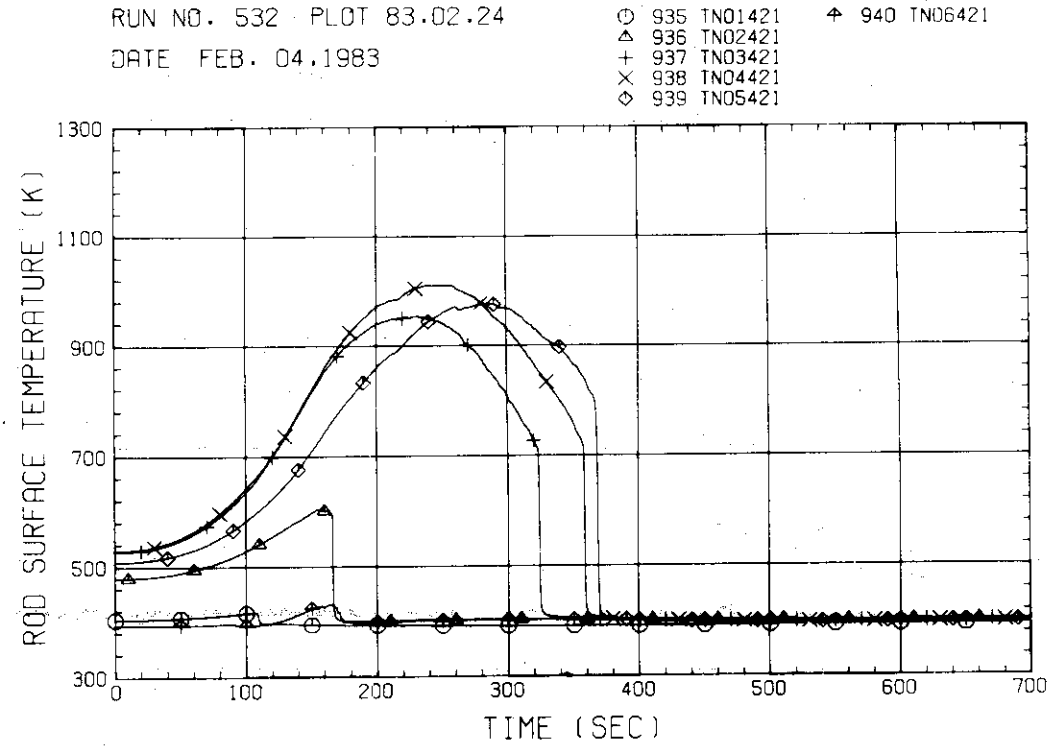

Fig. D-34 NON-HEATED ROD TEMPERATURE (BUNDLE 4-2)

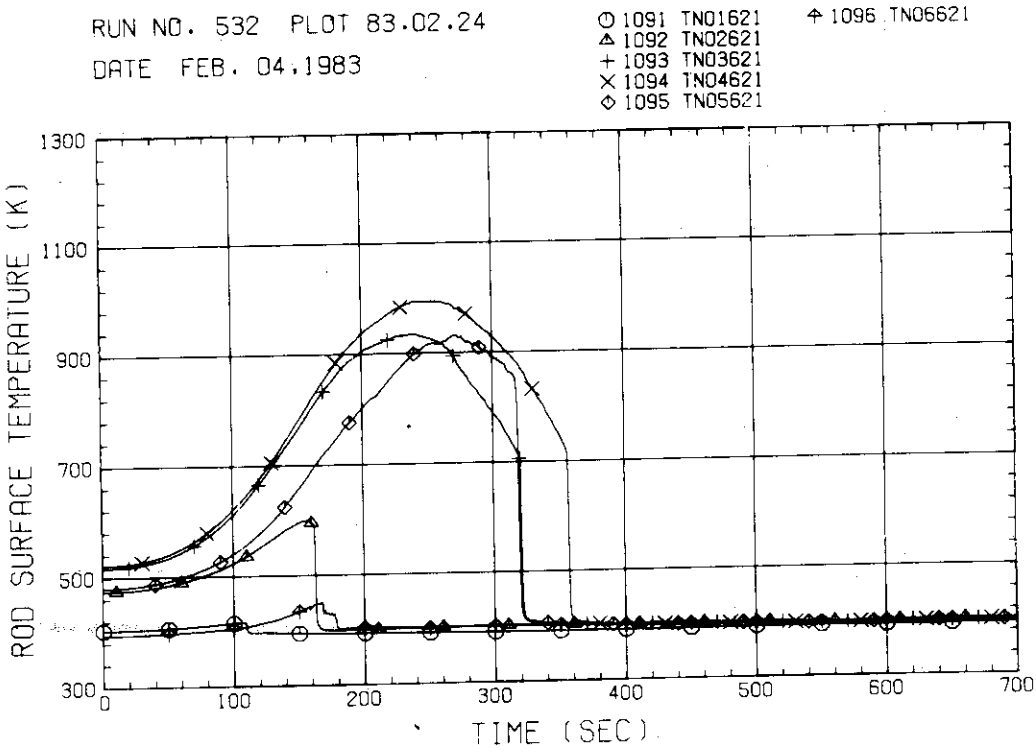

Fig. D-35 NON-HEATED ROD TEMPERATURE (BUNDLE 6-2)

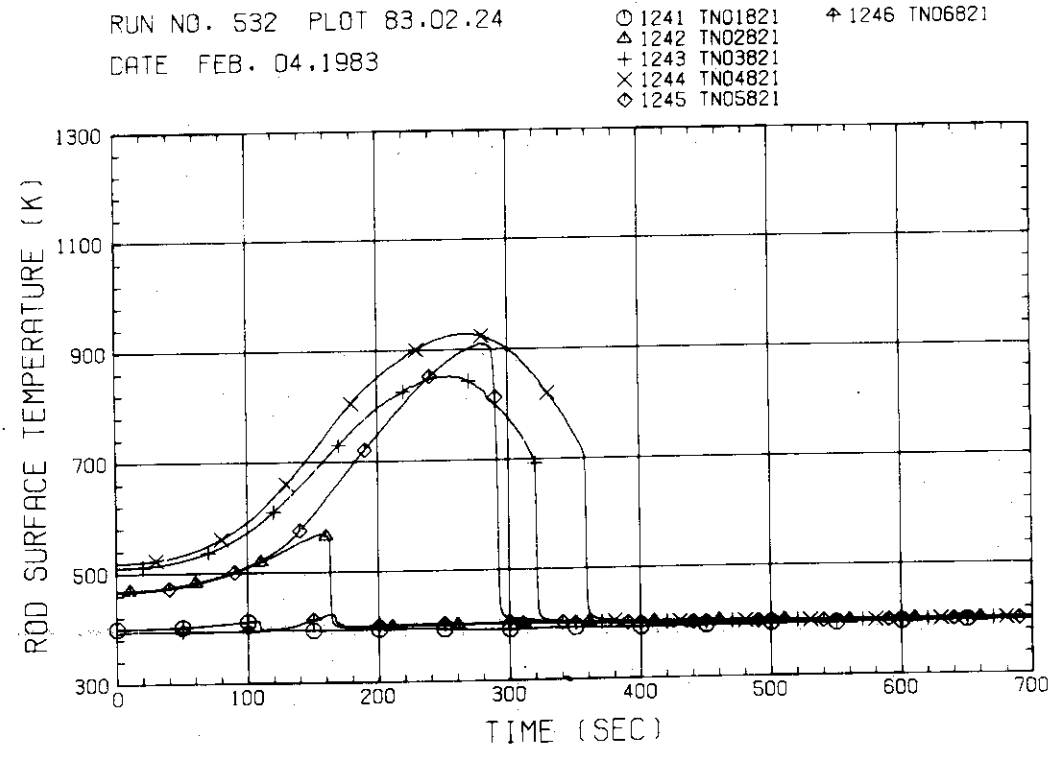

Fig. D-36 NON-HEATED ROD TEMPERATURE (BUNDLE 8-2)

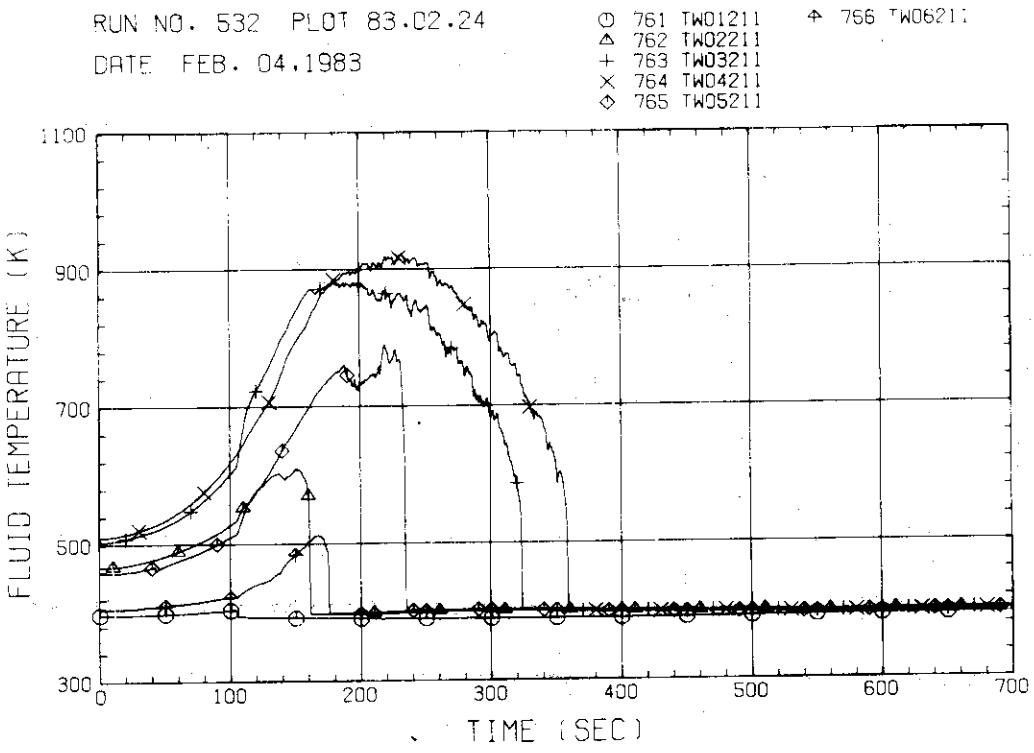

Fig. D-37 FLUID TEMPERATURE IN CORE (BUNDLE 2-1)

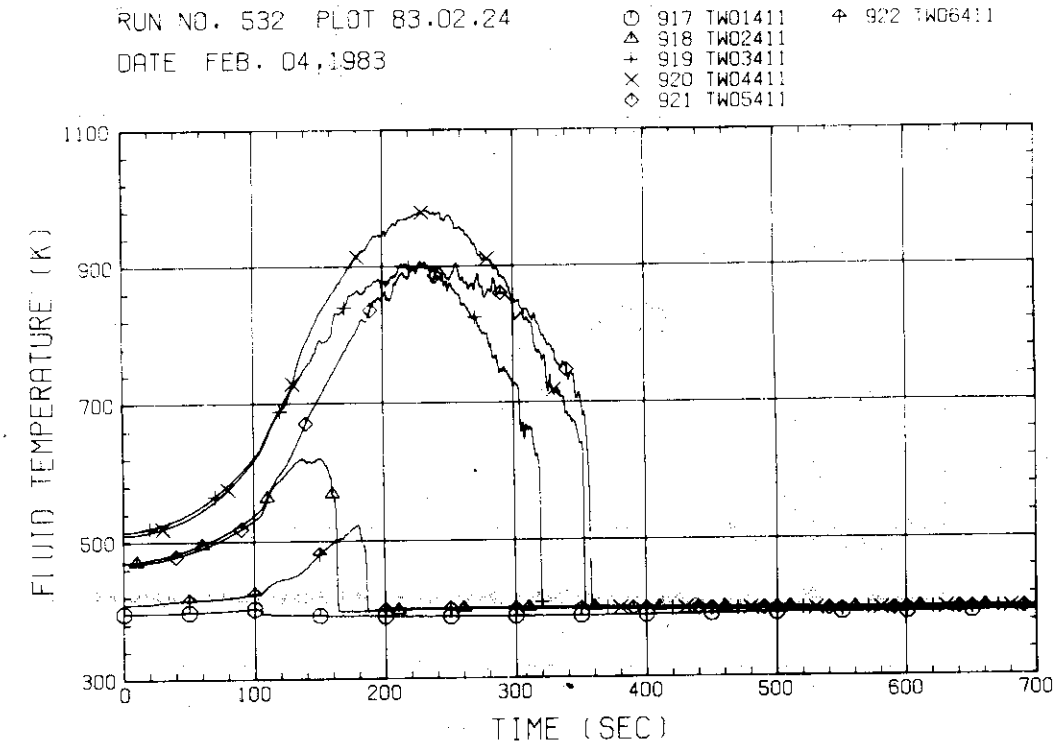

Fig. D-38 FLUID TEMPERATURE IN CORE (BUNDLE 4-1)

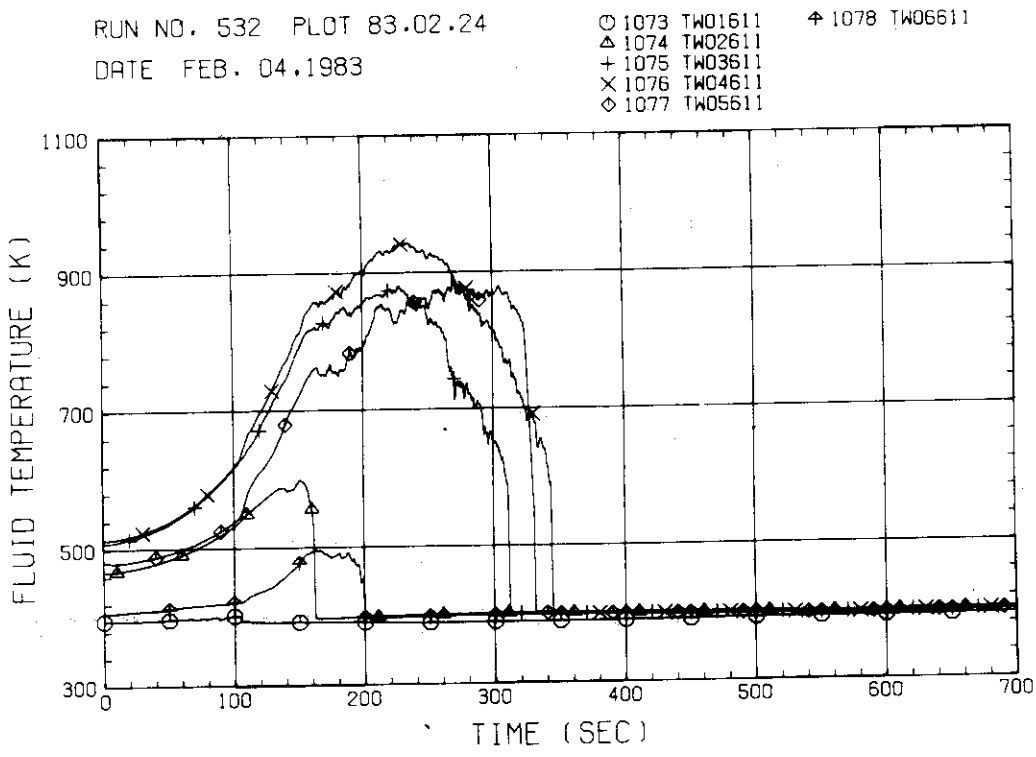

Fig. D-39 FLUID TEMPERATURE IN CORE (BUNDLE 6-1)

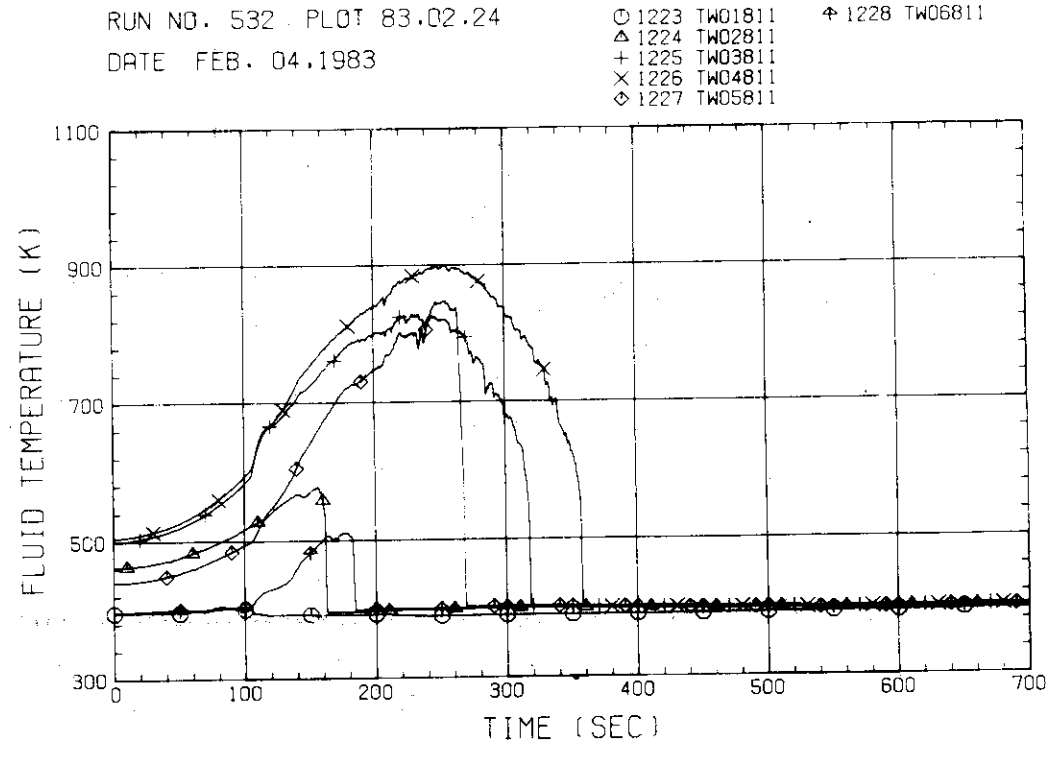

Fig. D-40 FLUID TEMPERATURE IN CORE (BUNDLE 8-1)

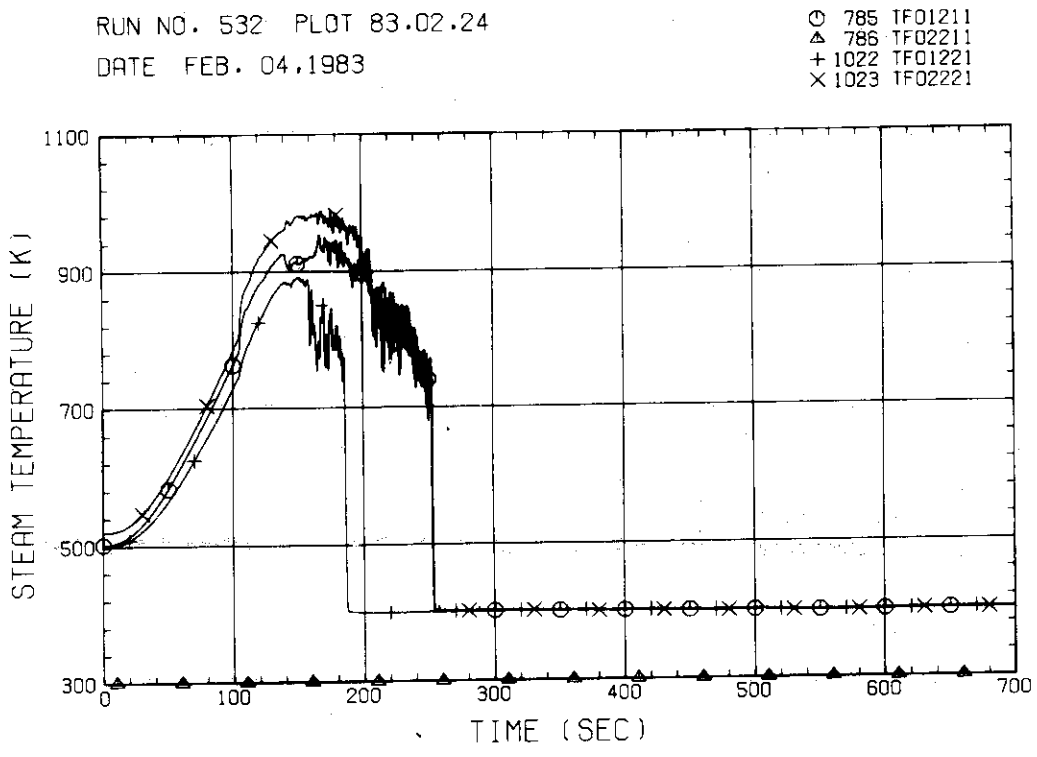

Fig. D-41 STEAM TEMPERATURE IN CORE, BUNDLE 2
(01211-1.735M, 02211-1.875M, 01221-1.38M, 02221-1.915M)

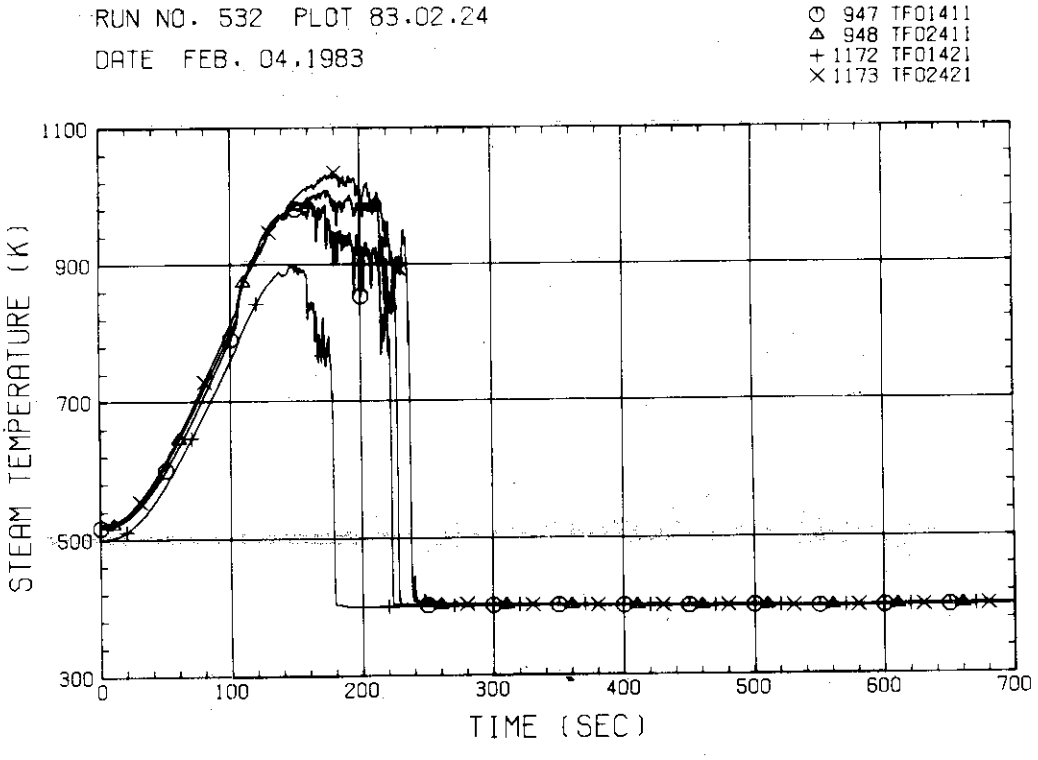

Fig. D-42 STEAM TEMPERATURE IN CORE, BUNDLE 4
(01411-1.735M, 02411-1.875M, 01421-1.38M, 02421-1.915M)

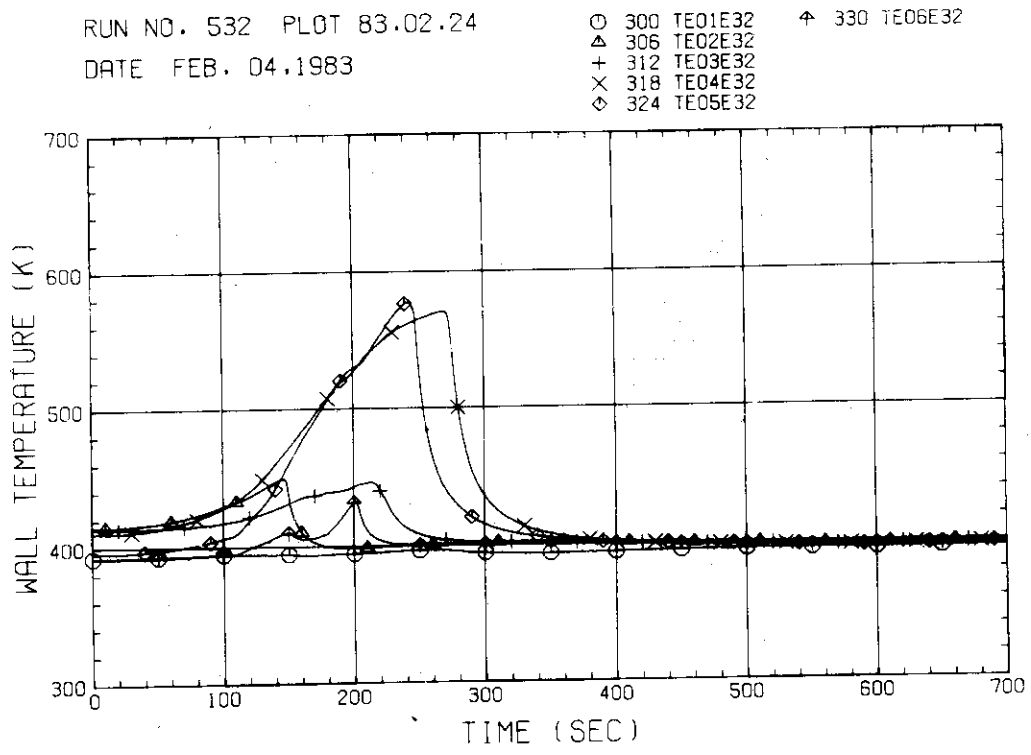

Fig. D-43 SURFACE TEMPERATURE OF CORE SIDE WALL (BUNDLE 3, OPPOSITE SIDE OF COLD LEG, INNER SURFACE)

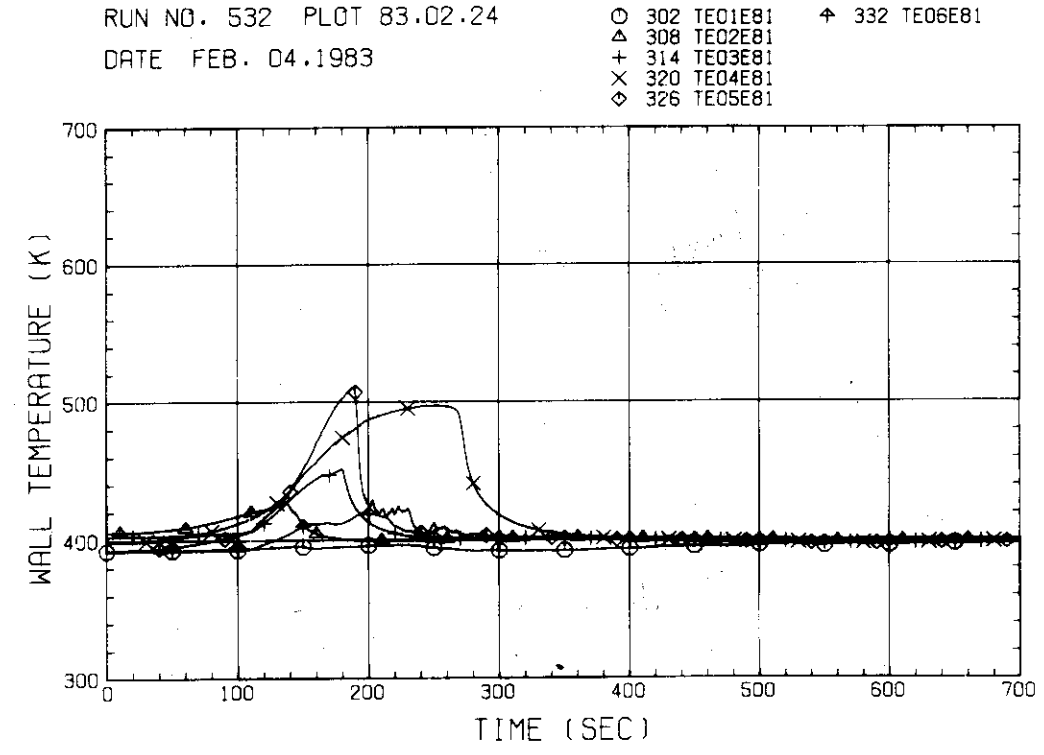

Fig. D-44 SURFACE TEMPERATURE OF CORE SIDE WALL (BUNDLE 8, OPPOSITE SIDE OF COLD LEG, INNER SURFACE)

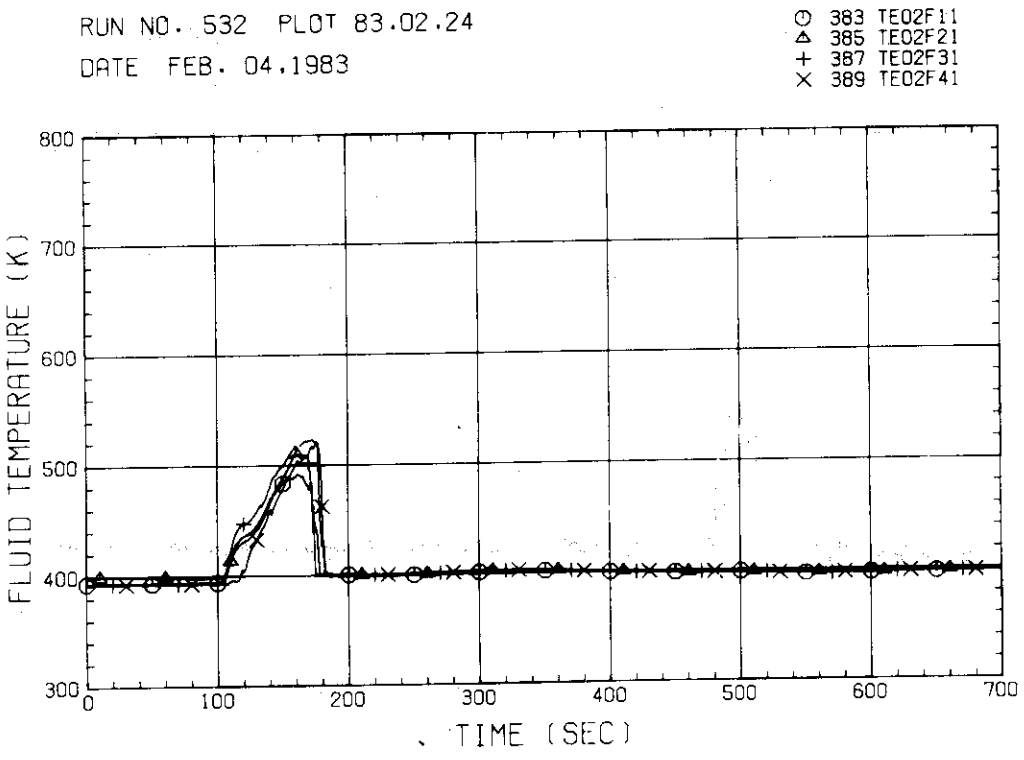

Fig. D-45 FLUID TEMPERATURE JUST ABOVE END BOX TIE PLATE (BUNDLE 1,2,3,4, OPPOSITE SIDE OF COLD LEG)

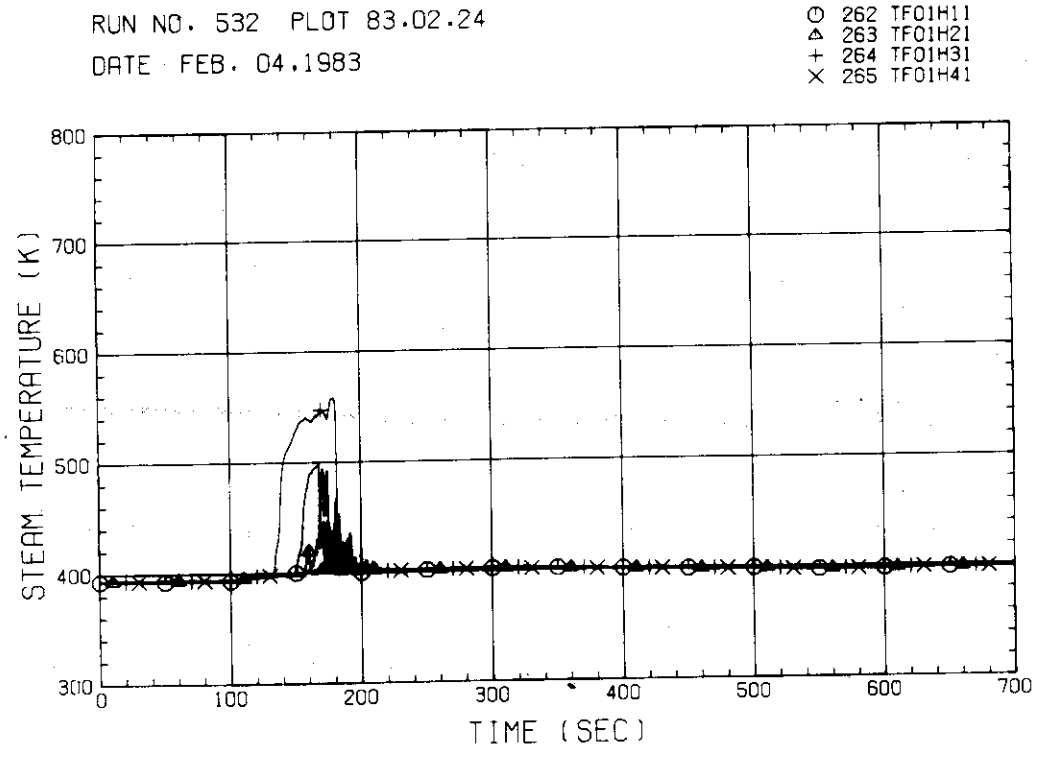

Fig. D-46 STEAM TEMPERATURE ABOVE UCSP HOLE (BUNDLE 1,2,3,4)

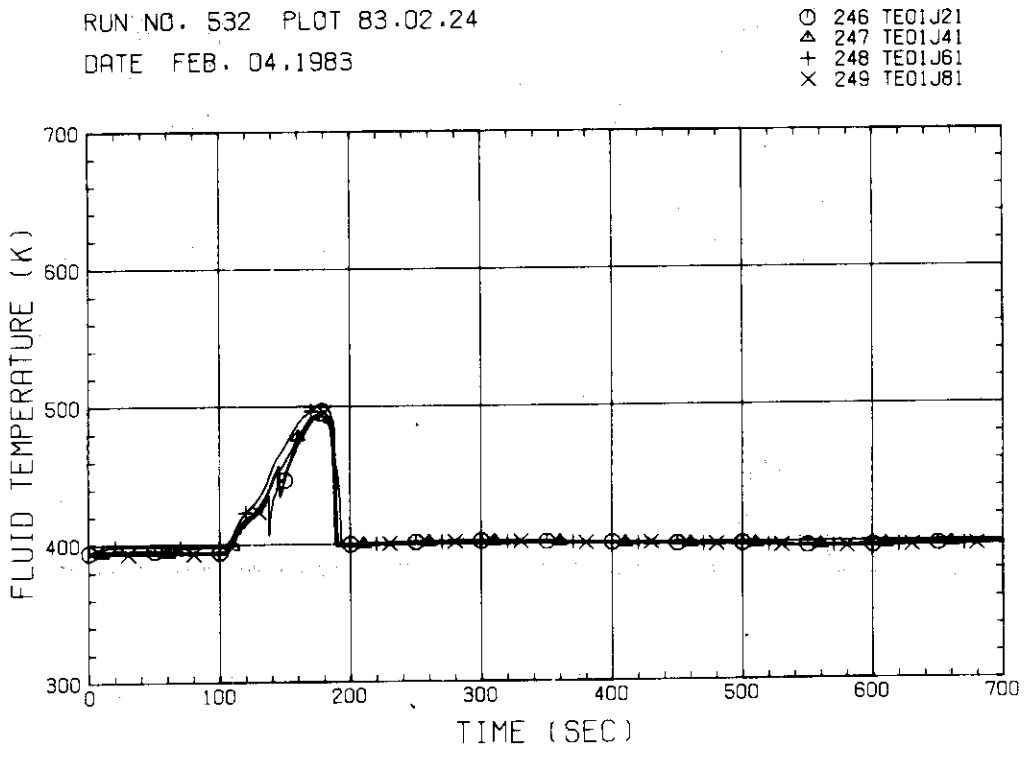

Fig. D-47 FLUID TEMPERATURE ABOVE UCSP (BUNDLE 2,4,6,8, 250MM ABOVE UCSP)

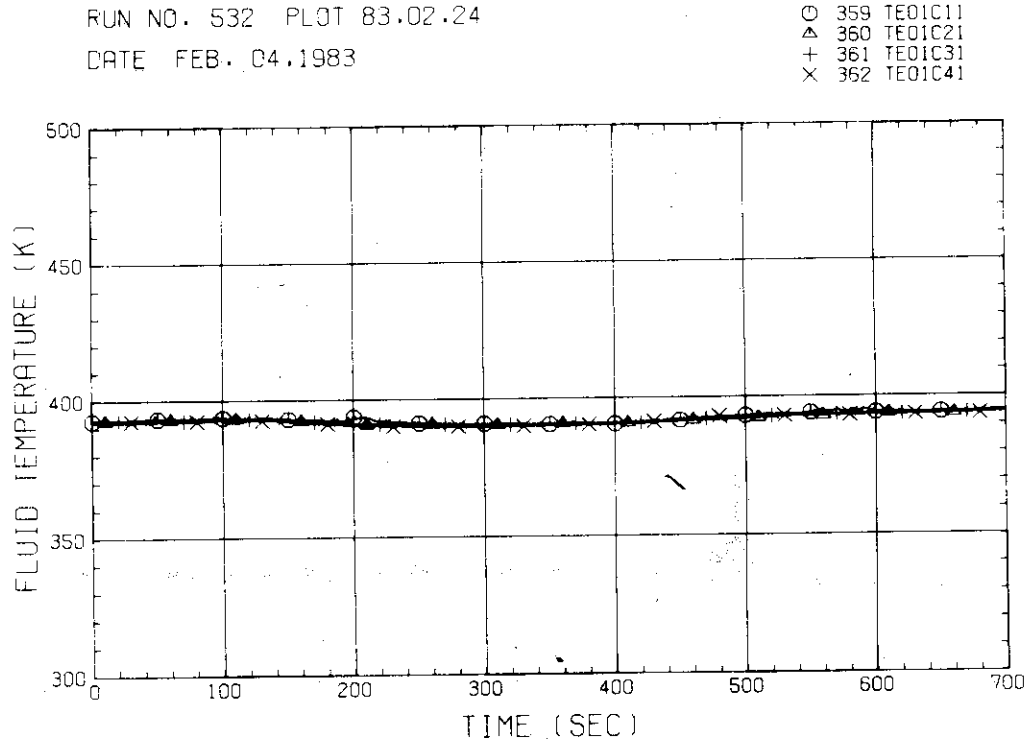

Fig. D-48 FLUID TEMPERATURE AT CORE INLET (BUNDLE 1,2,3,4, 100MM BELOW HEATED PART)

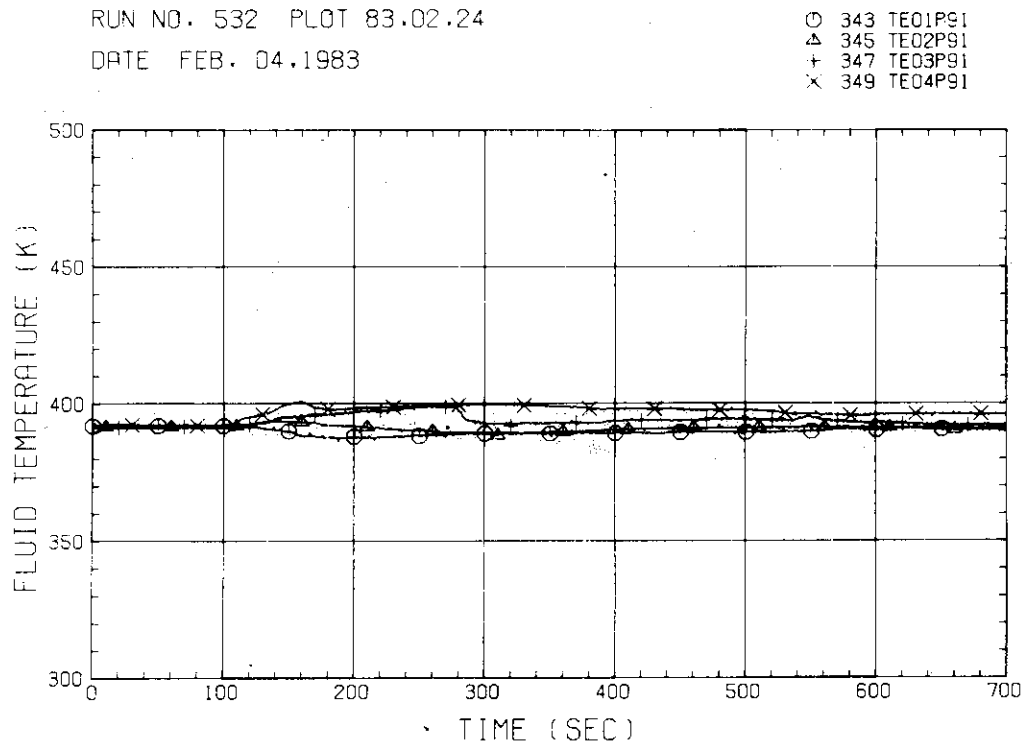

Fig. D-49 FLUID TEMPERATURE IN DOWNCOMER (BELOW INTACT COLD LEG)

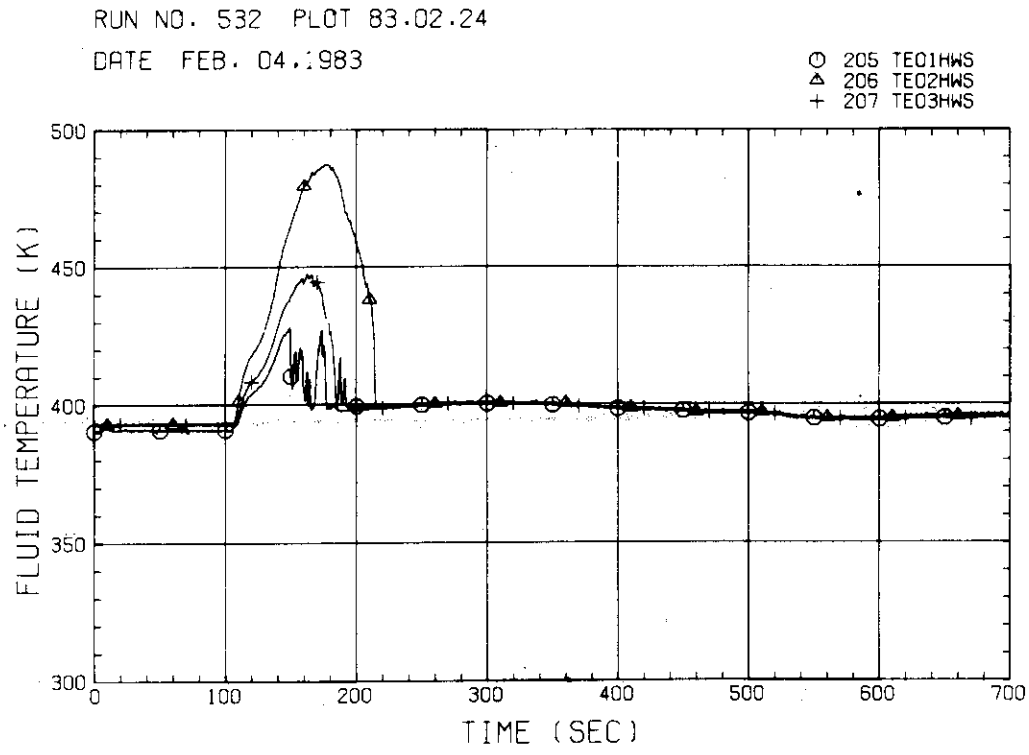

Fig. D-50 FLUID TEMPERATURE IN HOT LEG (01,02,03 - FROM PV TO STEAM/WATER SEPARATOR)

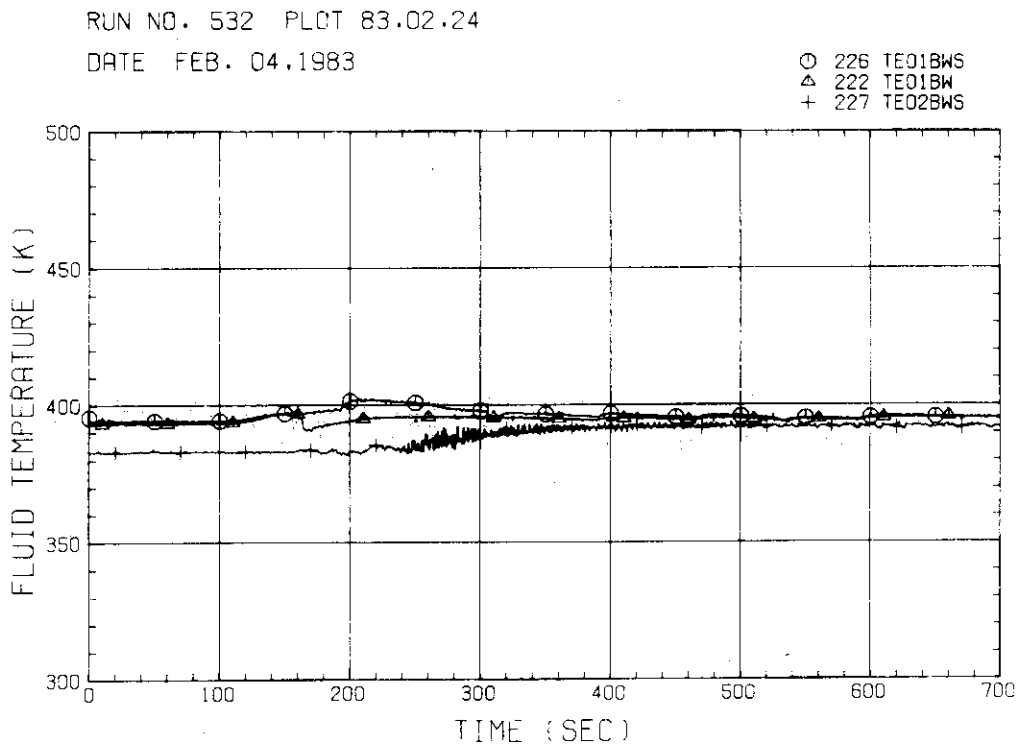

Fig. D-51 FLUID TEMPERATURE IN CONTAINMENT TANK-II
(01BWS - TOP, 01BW - MIDDLE, 02BWS - BOTTOM)

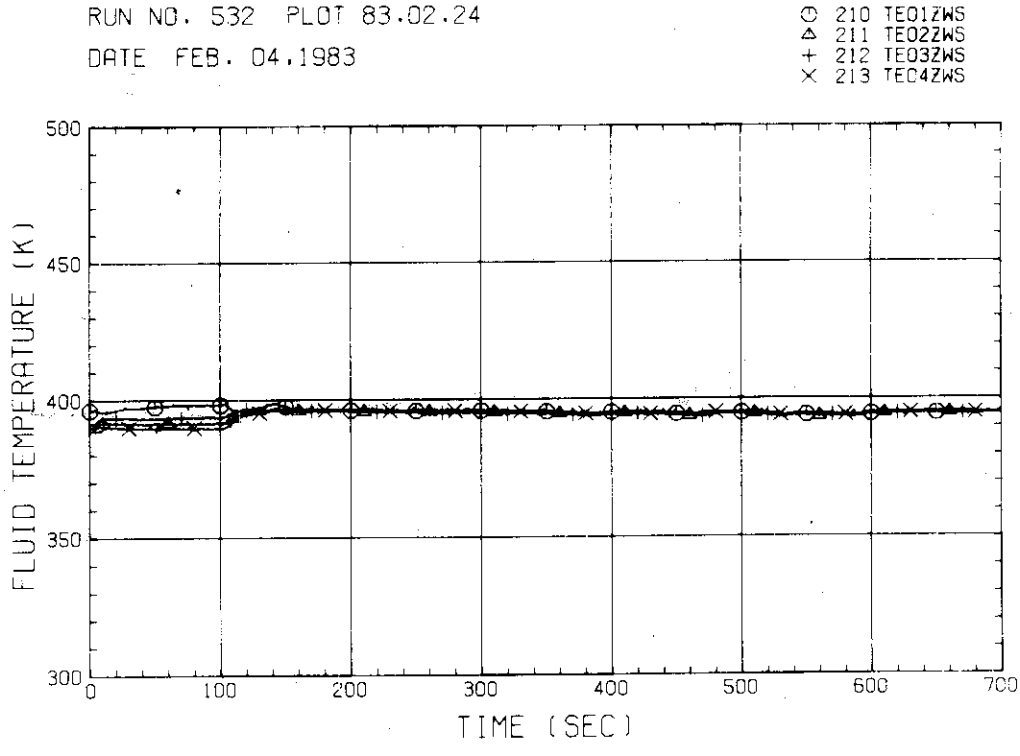

Fig. D-52 FLUID TEMPERATURE IN BROKEN COLD LEG - PV SIDE
(01.02.03.04 - FROM PV TO CONTAINMENT TANK-I)

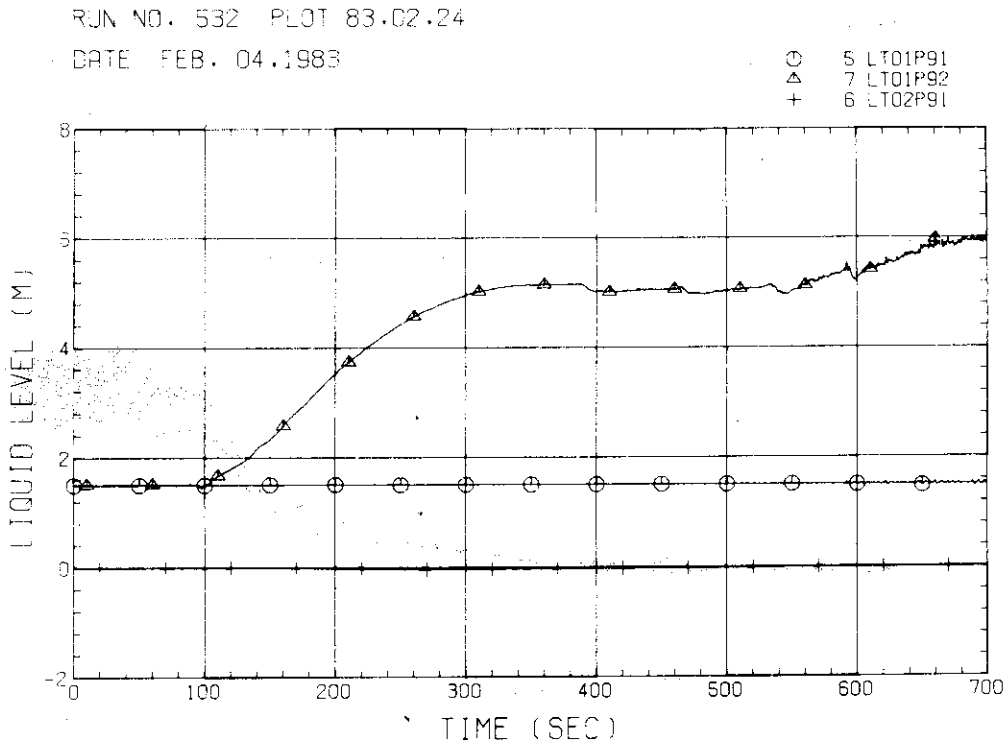

Fig. D-53 LIQUID LEVEL IN DOWNCOMER (01P91-BELOW CORE INLET, 01P92-BOTTOM TO COLD LEG, 02P91-COLD LEG TO TOP OF PV)

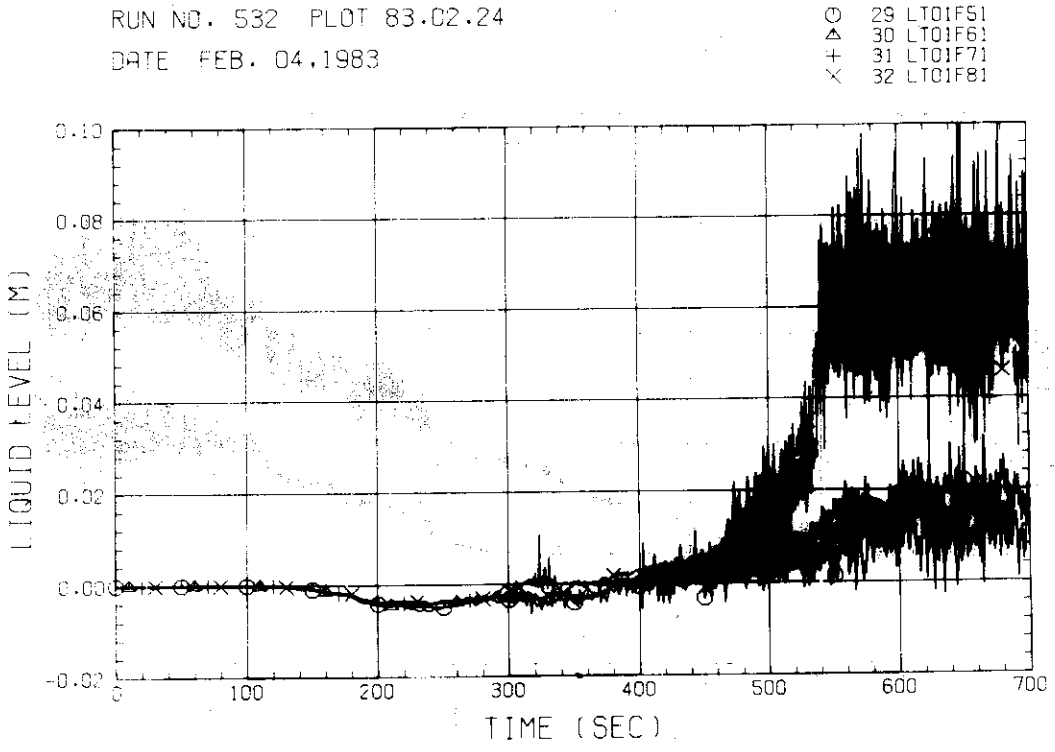

Fig. D-54 LIQUID LEVEL ABOVE END BOX TIE PLATE (BUNDLE 5,6,7,8)

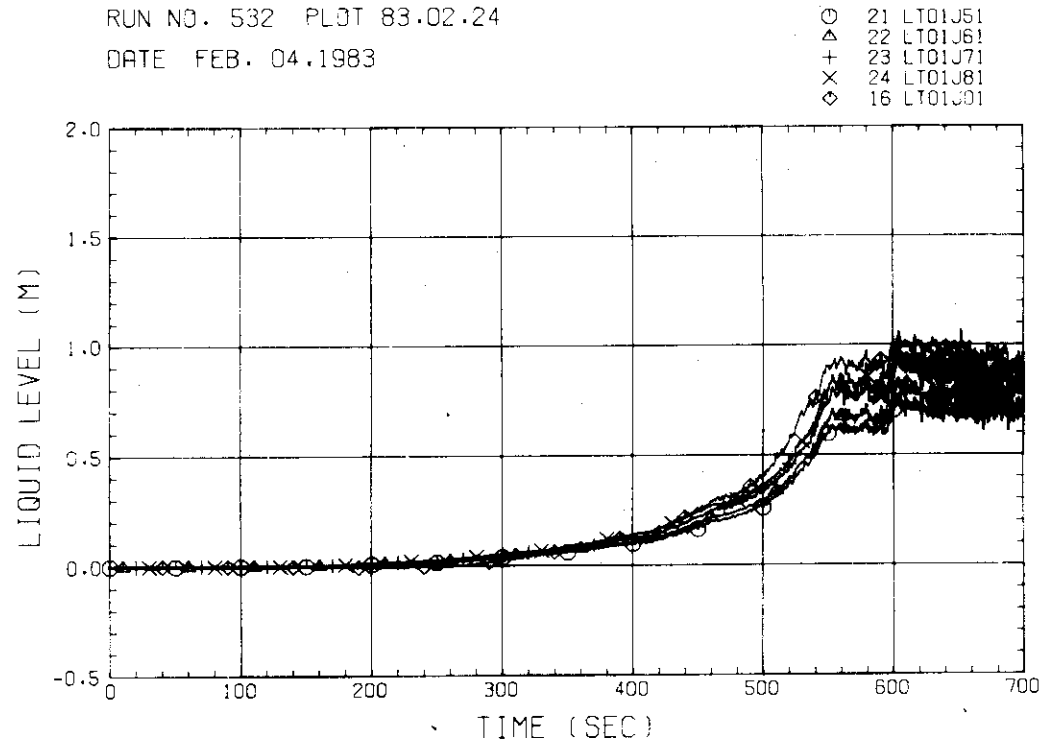

Fig. D-55 LIQUID LEVEL ABOVE UCSP
(BUNDLE 5,6,7,8 AND CORE BAFFLE)

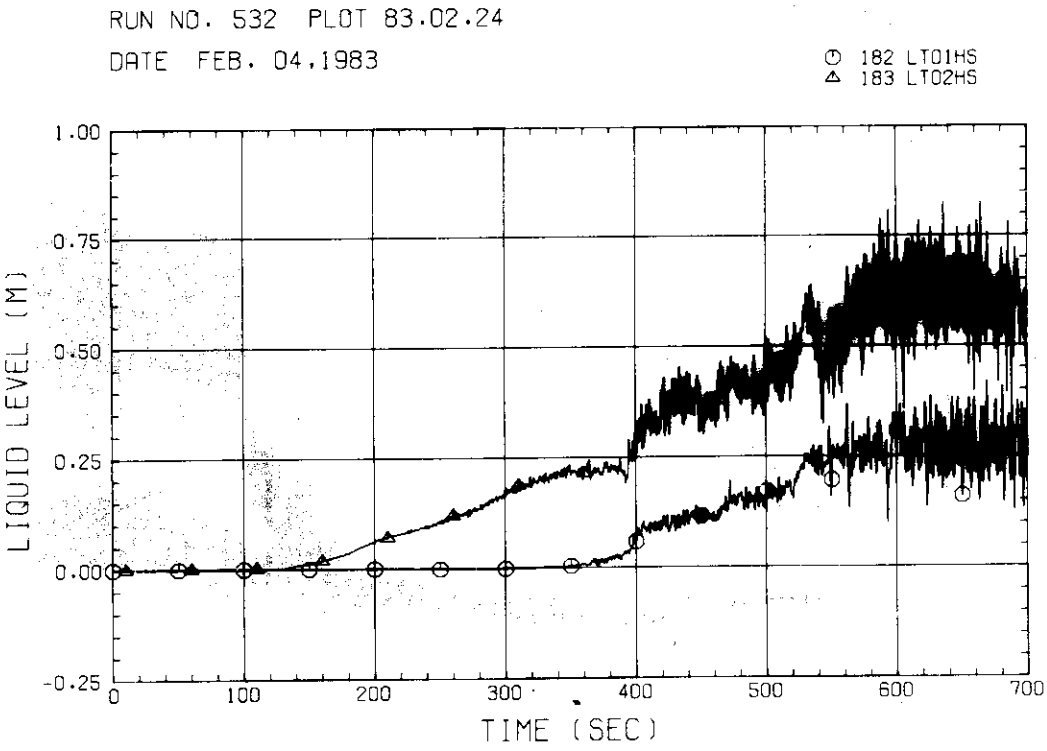

Fig. D-56 LIQUID LEVEL IN HOT LEG
(01HS - PV SIDE, 02HS - STEAM/WATER SEPARATOR SIDE)

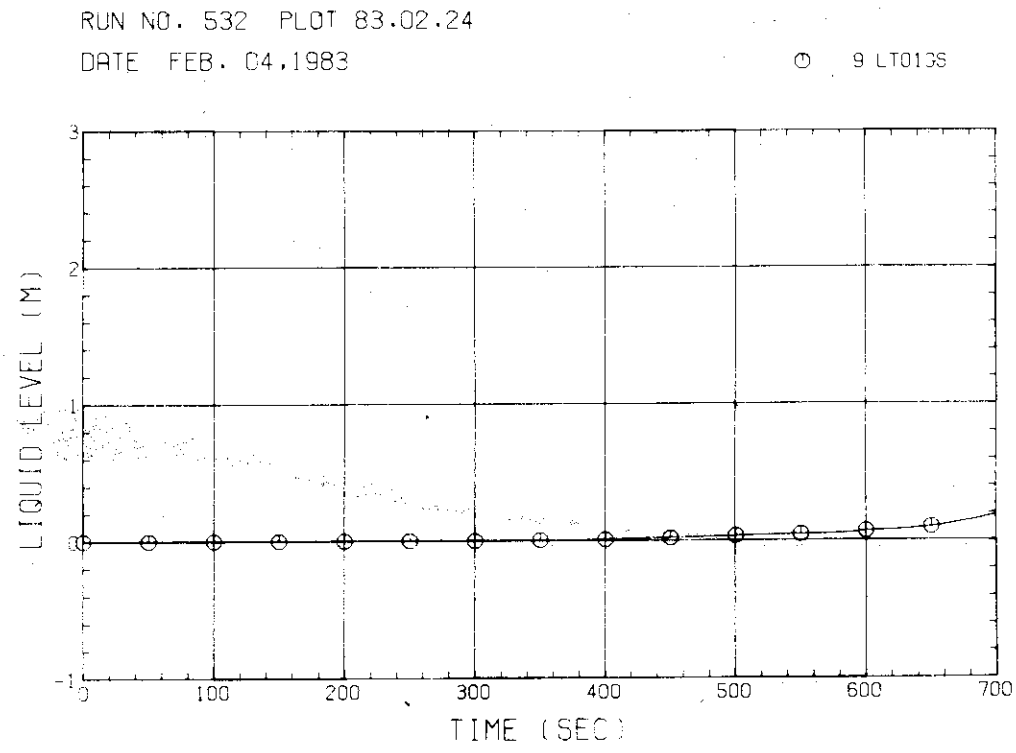

Fig. D-57 LIQUID LEVEL IN STEAM/WATER SEPARATOR

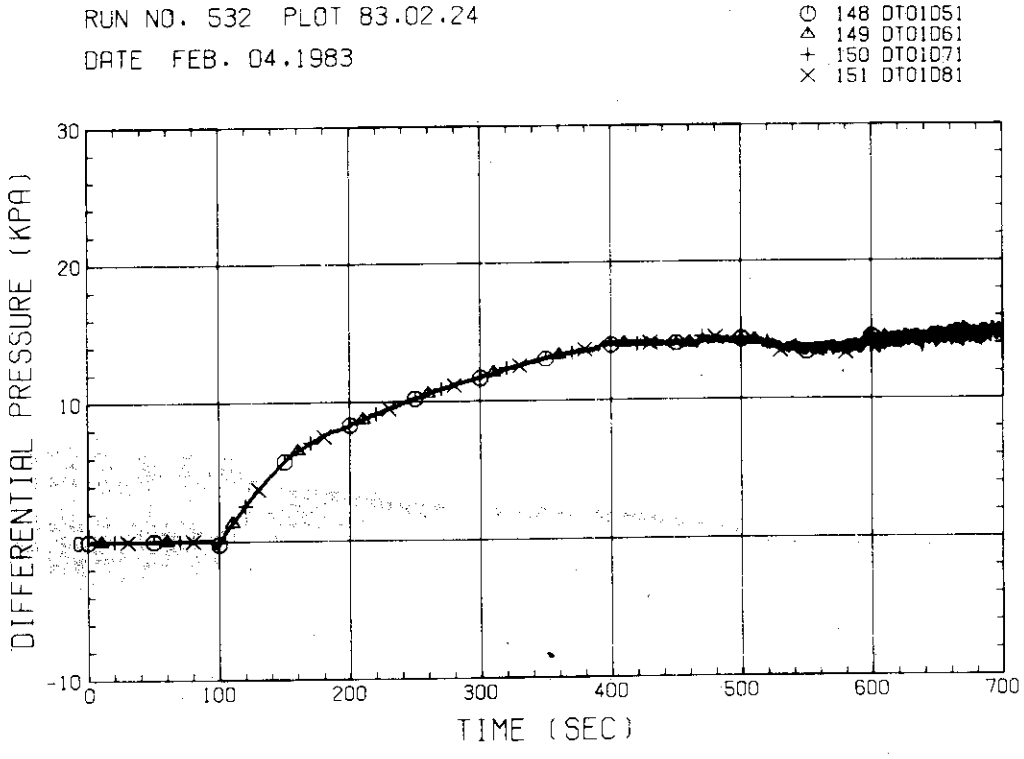

Fig. D-58 DIFFERENTIAL PRESSURE OF CORE LOWER HALF (BUNDLE 5,6,7,8)

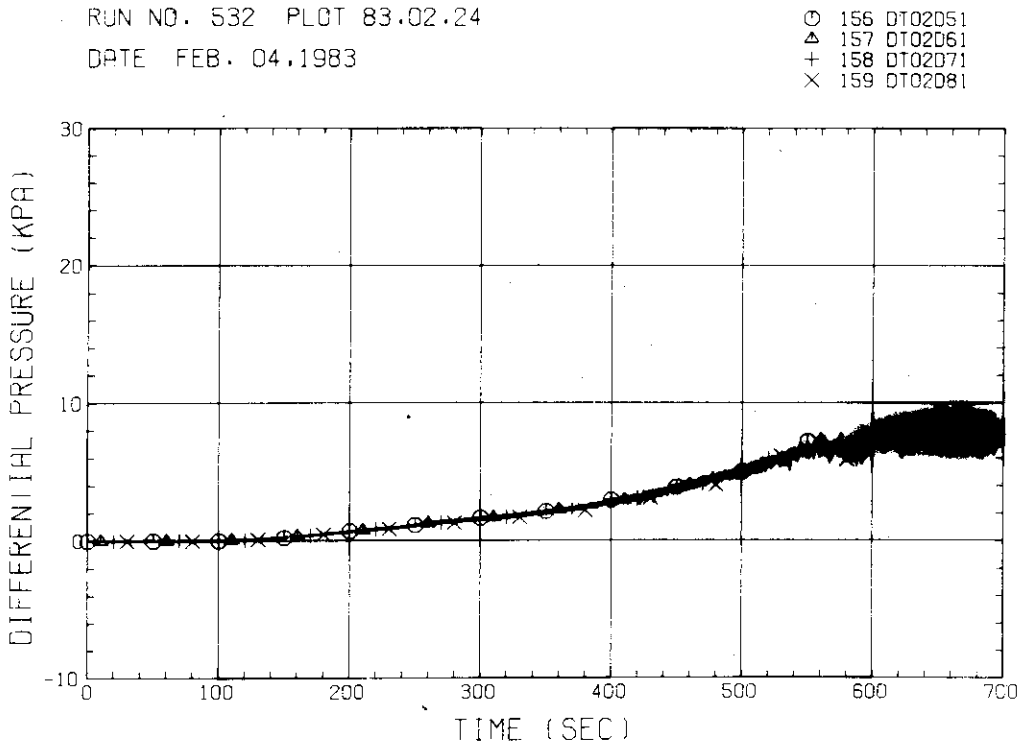

Fig. D-59 DIFFERENTIAL PRESSURE OF CORE UPPER HALF (BUNDLE 5,6,7,8)

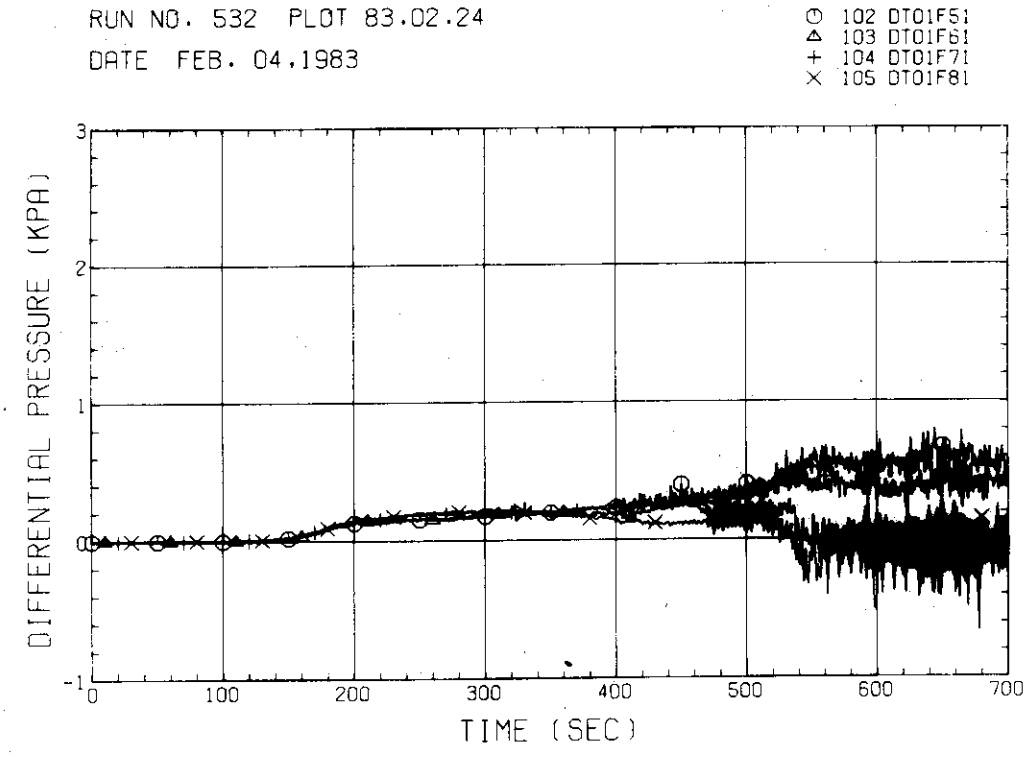

Fig. D-60 DIFFERENTIAL PRESSURE ACROSS END BOX TIE PLATE (BUNDLE 5,6,7,8)

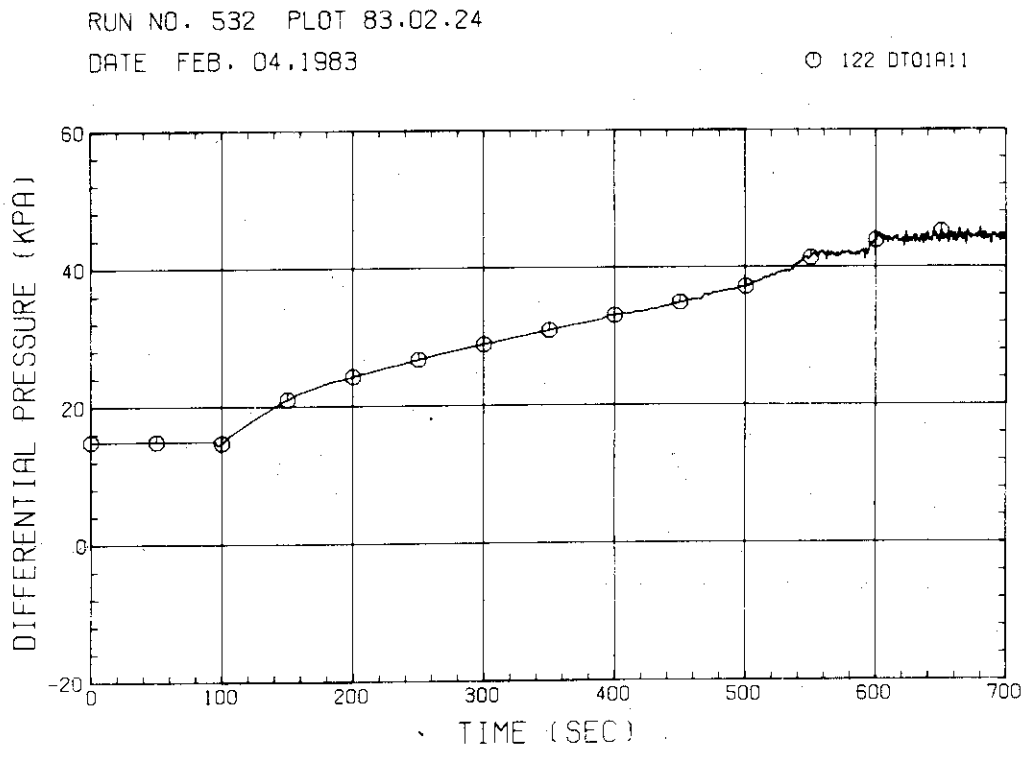

Fig. D-61 DIFFERENTIAL PRESSURE, BOTTOM OF LOWER PLENUM - TOP OF UPPER PLENUM

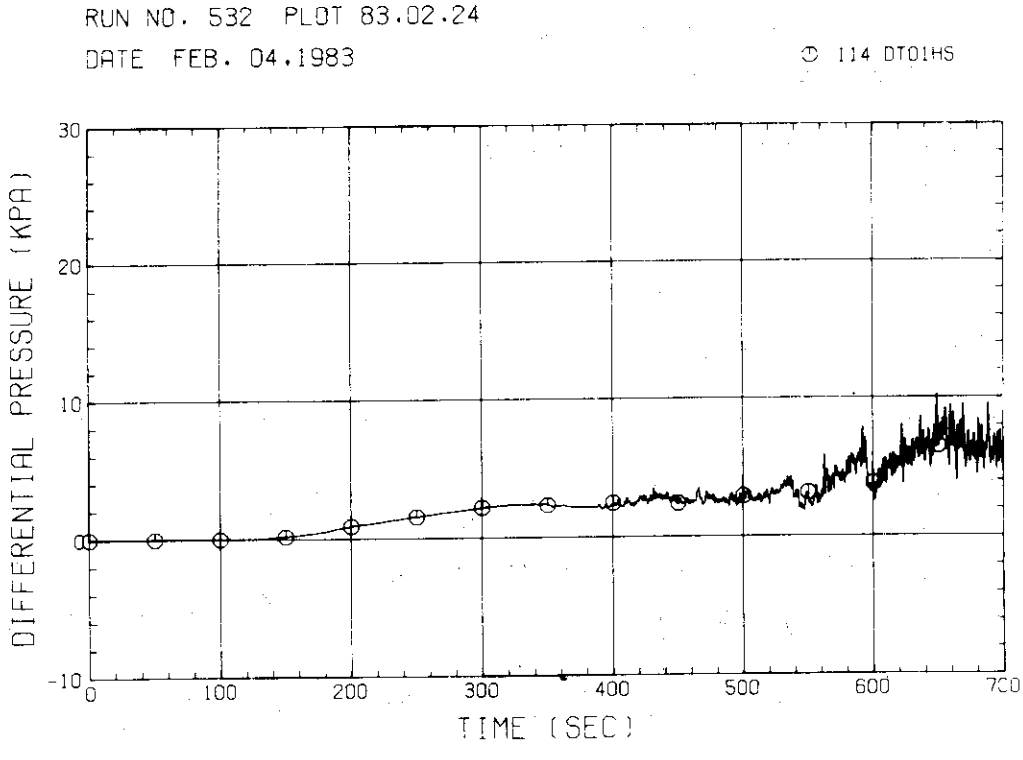

Fig. D-62 DIFFERENTIAL PRESSURE OF HOT LEG.
HOT LEG INLET - STEAM/WATER SEPARATOR INLET

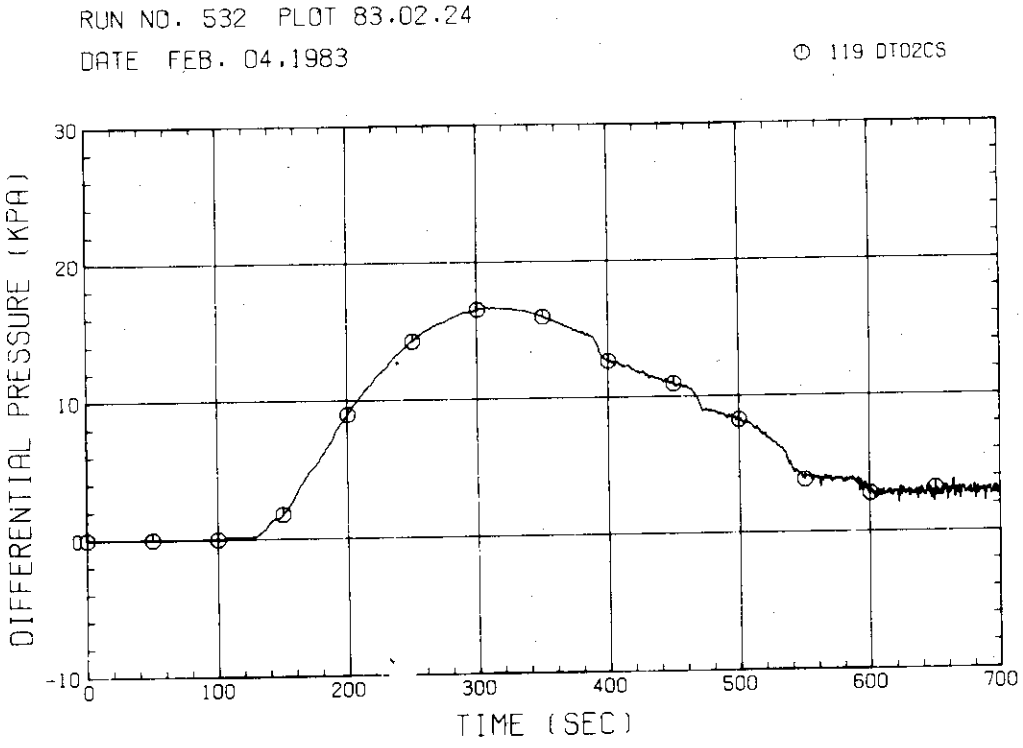

Fig. D-63 DIFFERENTIAL PRESSURE OF INTACT COLD LEG

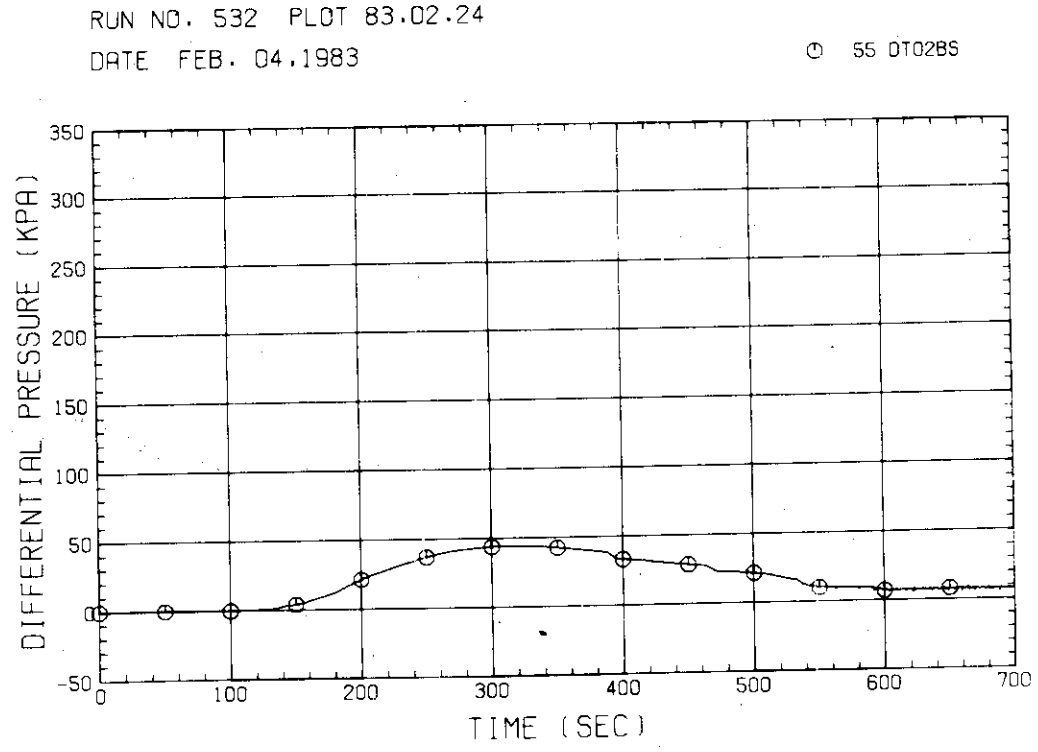

Fig. D-64 DIFFERENTIAL PRESSURE, STEAM/WATER SEPARATOR - CONTAINMENT TANK-II

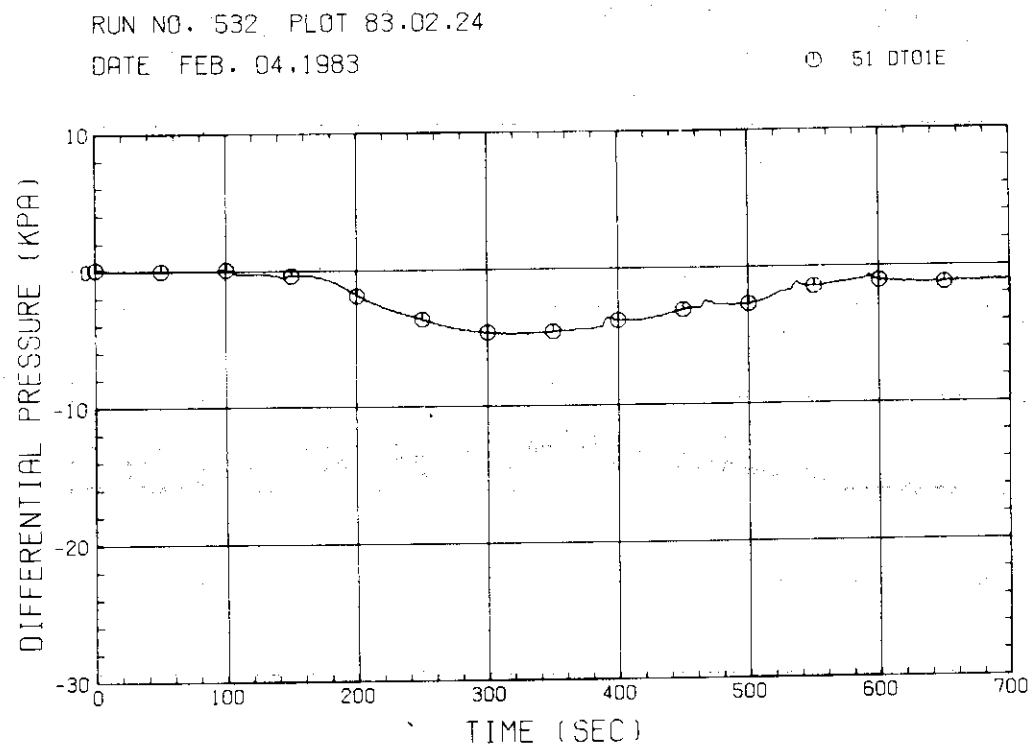

Fig. D-65 DIFFERENTIAL PRESSURE, CONTAINMENT TANK-II - CONTAINMENT TANK-I

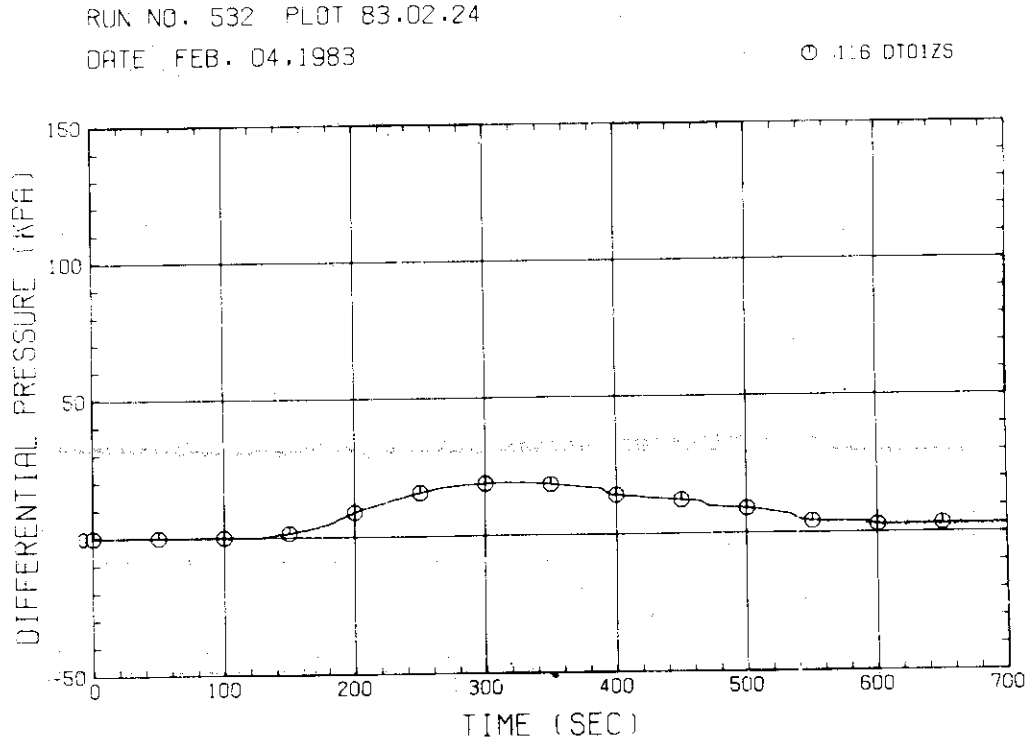

Fig. D-66 DIFFERENTIAL PRESSURE OF BROKEN COLD LEG - PV SIDE, DOWNCOMER - UPSTREAM OF RESISTANCE ORIFICE

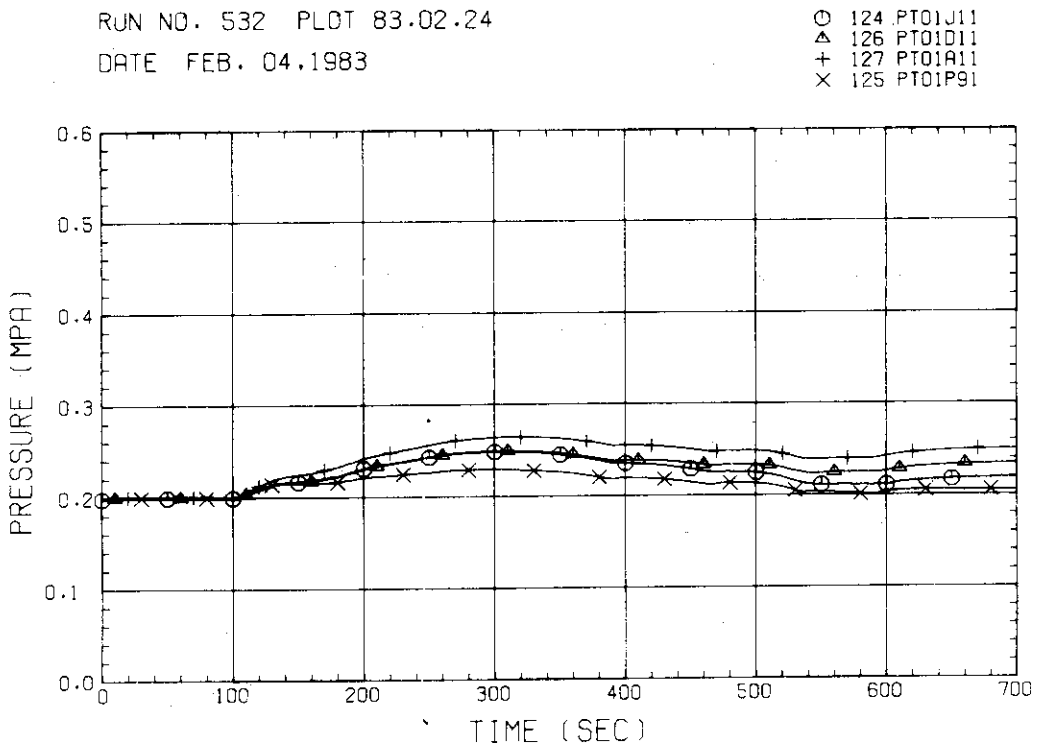

Fig. D-67 PRESSURE IN PV (J - TOP OF PV, D - CORE CENTER, A - CORE INLET, P - BELOW COLD LEG NOZZLE IN DOWNCOMER)

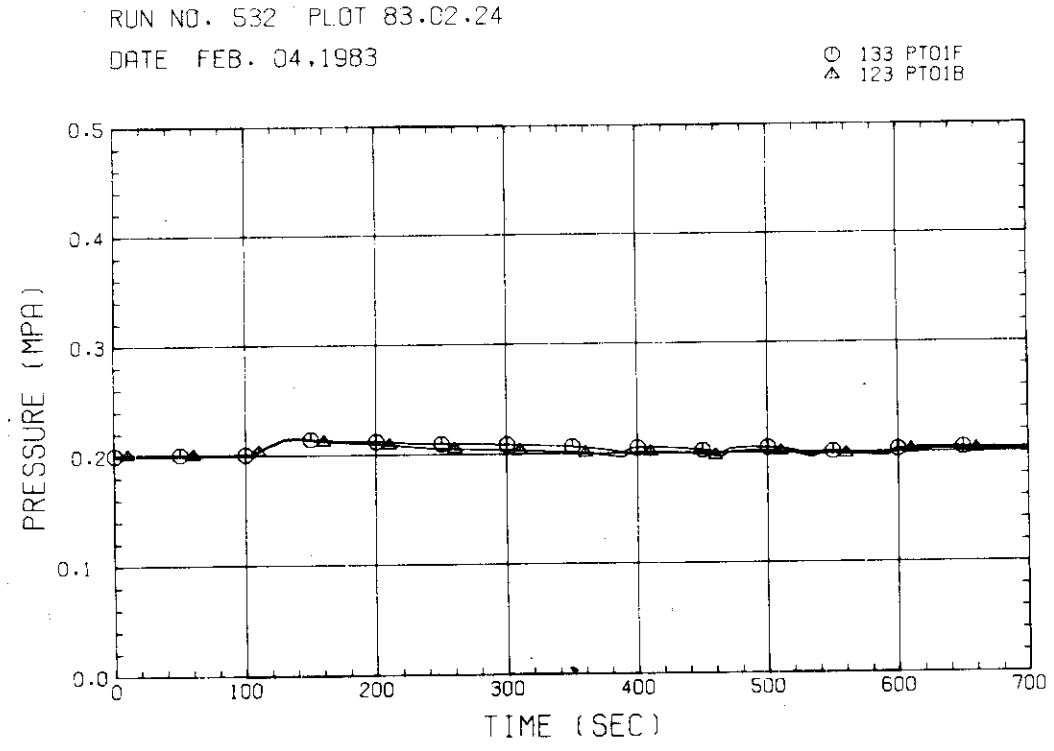

Fig. D-68 PRESSURE AT TOP OF CONTAINMENT TANK-I AND CONTAINMENT TANK-II (F-CONTAINMENT TANK-I, B-CONTAINMENT TANK-II)

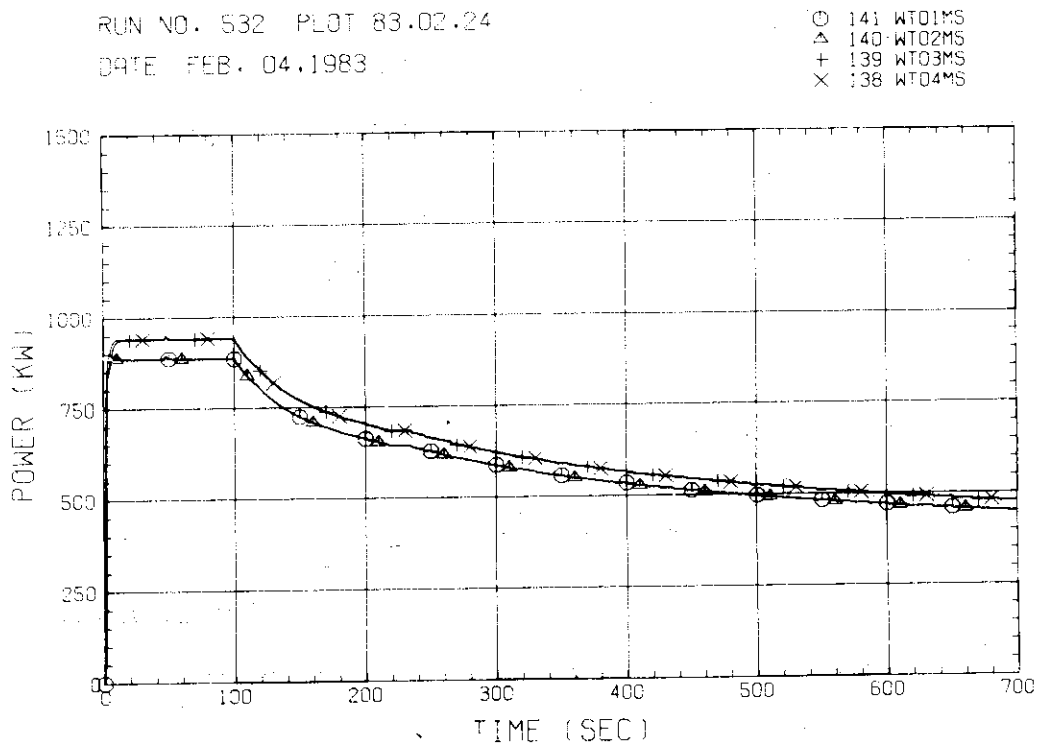

Fig. D-69 BUNDLE POWER (BUNDLE 1,2,3,4)

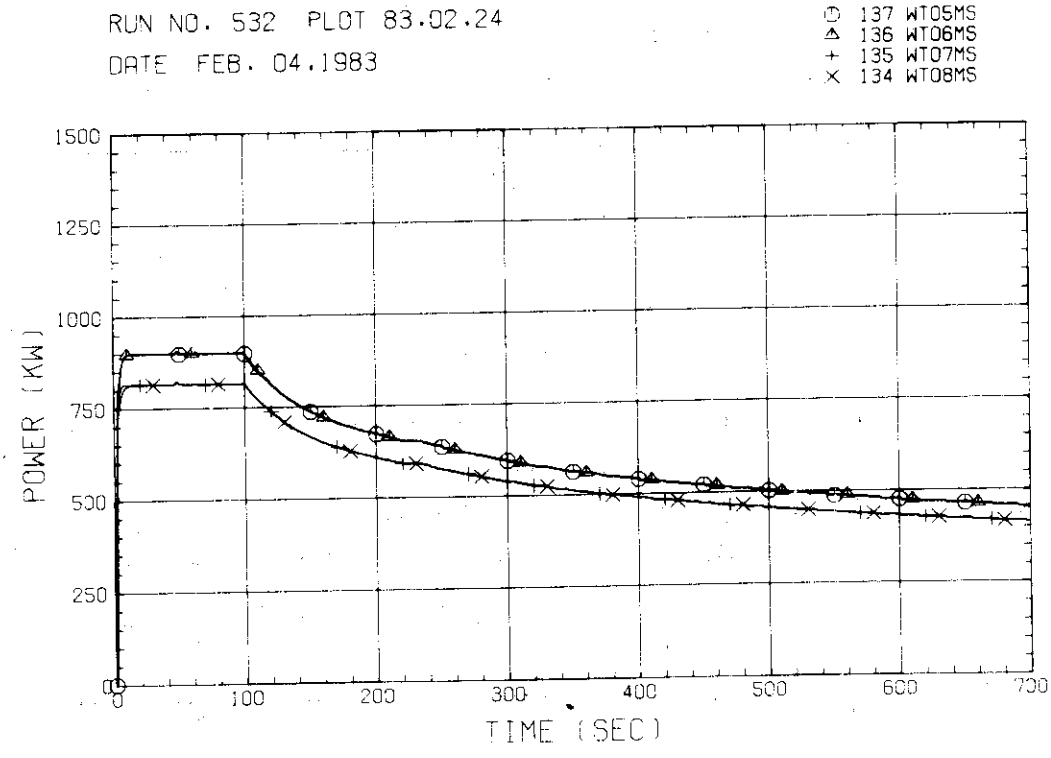

Fig. D-70 BUNDLE POWER (BUNDLE 5,6,7,8)

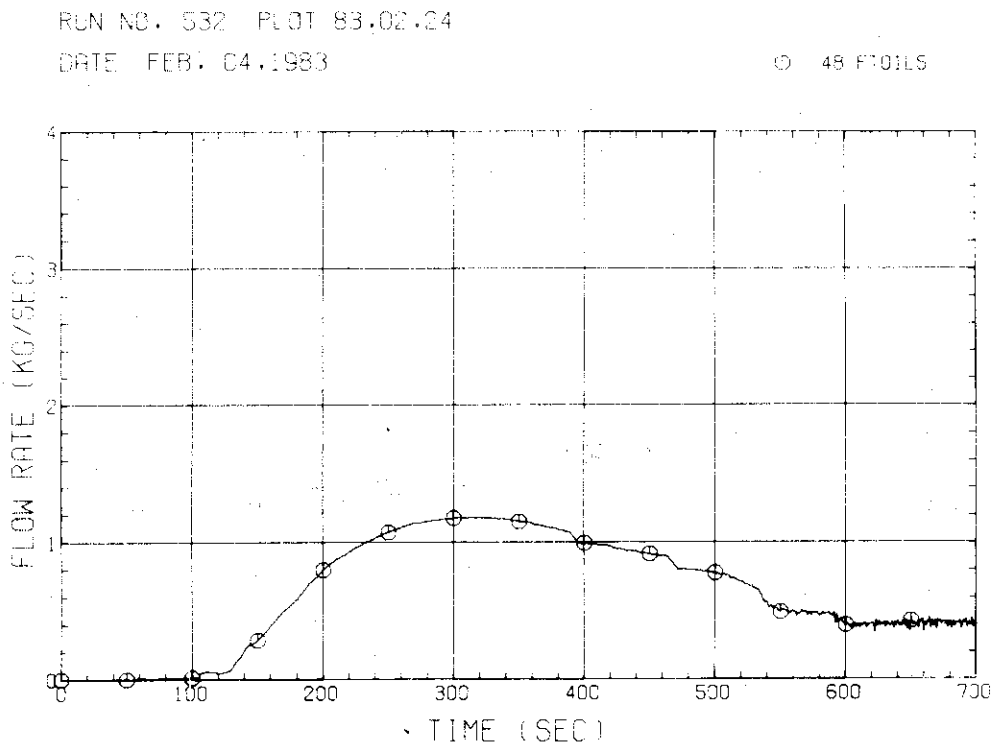

Fig. D-71 MASS FLOW RATE OF BROKEN COLD LEG - STEAM/WATER SEPARATOR SIDE

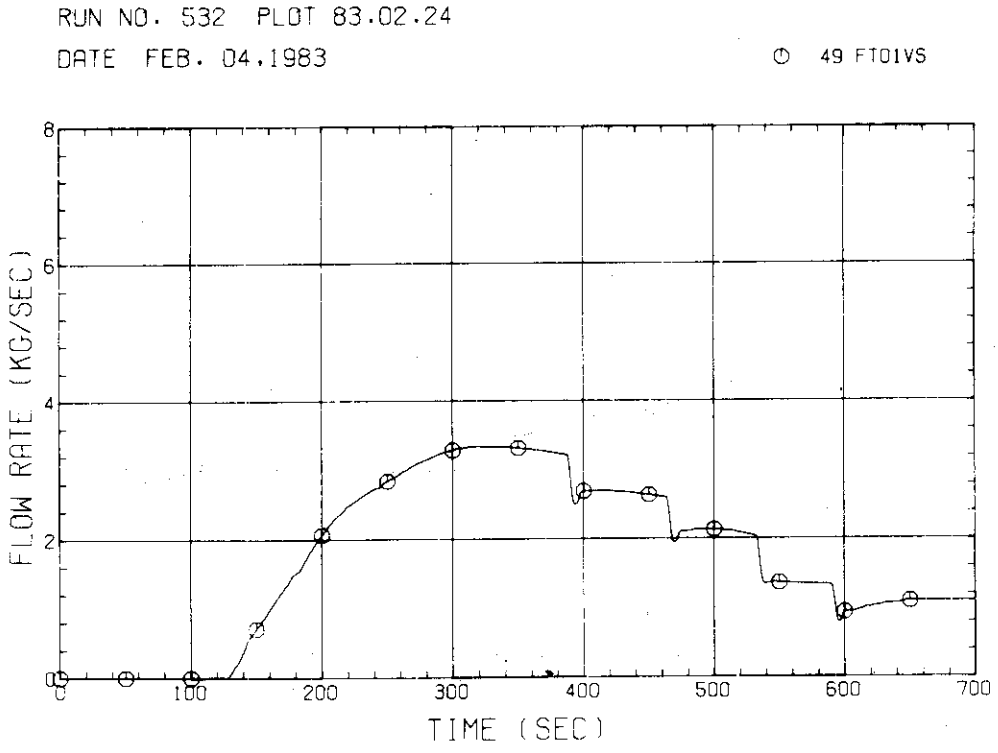

Fig. D-72 STEAM FLOW RATE OF DISCHARGE FROM CONTAINMENT TANK-II